INTRA- SEASONAL OSCILLATORY MODES OF THE SOUTHERN AFRICA SUMMER CIRCULATION

Amos Makarau

The thesis is submitted in fulfilment of

the Degree of Doctor of Philosophy,

Department of Oceanography, University of Cape Town,

South Africa

March 1995

CONTENTS:

Glossary/ Acronyms

The following definitions and acronyms are not universal and serve the purpose of this thesis only. This section has been included to facilitate the reader to view intepretations with the author's perspective.

Southern Africa:
This is defined as the region poleward of 10°S over Africa. The extreme southwest of Africa is excluded for climatological reasons.

Tropical- sub- tropical boundary (TSB):
This is a zone demarcating the tropics from sub- tropics (or extra- tropics) over Africa at 700 hPa. The demarcation occurs in the vicinity of 20°S latitude during austral summer (November to March).

El Niño:
This term is used in the thesis to describe the appearance of warm surface water from time to time in the eastern Pacific region along the coast of Peru. The south- flowing current is quasi- regular annually during February and March

La Nina:
Refers to the appearance of colder- than average sea surface temperatures (SSTs) in the eastern equatorial Pacific region (opposite to conditions during El Niño).

Warm event:
Anomalous warming of SSTs in the central and eastern equatorial Pacific. The term is used to avoid confusion over the use of other terms like ENSO or El Niño. A warming in the regions mentioned is accompanied by a relative cooling in the western equatorial Pacific.

Cold event:
Where the SSTs become anomalously colder compared to the long- term average for the central and eastern equatorial Pacific. (It is the opposite of a warm event in that region.)

The Southern Oscillation (SO):
A seesaw of atmospheric mass (pressure) between the Pacific and Indo- Australian areas. For example, when the pressure is low in the southeast Pacific and high over Indonesia and tropical Australia, the Pacific trade winds weaken. Upwelling of cool water on the Pacific equator and along the Peruvian coast weakens or ceases, and SSTs increase.

The Southern Oscillation Index (SOI):
This index monitors the SO using the difference between sea level pressures at Darwin (Australia) and the Pacific island of Tahiti. Other stations have been used by different scientists. Large negative values of the SOI indicate a warm event, and large positive values indicate a cold event. There is, however, not a one- to- one correspondence between the occurrence of the SO events and El Nino events.

ENSO (El Nino + Southern Oscillation):
Term used to describe the full range of the SO that includes both SST increases (warming) as well as SST decreases when compared to a long- term average. The acronym is composed of El Nino- Southern Oscillation. It is basically an oscillation between a warm and a cold phase, commonly referred to above as El Nino and La Nina, respectively.

Teleconnections:
These refer to atmospheric interactions between widely separated regions which may be identified through statistical correlations in space and time. For example, droughts in southeast Southern Africa, Australia and India have been found to be associated with the Southern Oscillation.

Quasi-Biennial Oscillation (QBO):
The QBO is regarded as a 26- 28- month oscillation (near year- to- year reversal) in equatorial stratospheric (between 30 and 50 hPa) winds whose maximum amplitude is along the Equator. The westerly and easterly wind regimes propagate downwards towards the tropopause at roughly 1 km/ month.

Intra- Seasonal Oscillations (ISO)
These are general descriptions for observed atmospheric convective Kelvin- type waves travelling round the globe at frequencies which range from about 10 to 50 days. The oscillations have been observed to propagate eastward, mainly along the equator, as well as poleward.

Walker circulation

The Walker circulation is a zonal Hadley- type circulation which is assumed to be driven by zonal temperature gradients within the tropics. It is evident over the Atlantic and more, prominently, the Pacific Ocean, associated with a surface easterly and an upper westerly branch. The reverse cell is less certain, but most research mention the tropical Indian Ocean.

Mozambique Channel- Angola Trough (MCAT):

This refers to a semi- permanent feature of Zimbabwe wet spell phases linking low pressure centres over Angola and the Mozambique Channel. The trough oscillates in the vicinity of the TSB.

Botswana Upper High (BUH):

The BUH is an anticyclone over southern Africa centred over Botwana in the 600- 300 hPa layer. The anticyclone is a characteristic feature of dry spells over southern Africa.

Commonly used abbreviations:

AOA	: Atlantic Ocean Anticyclone
IOA	: Indian Ocean Anticylone
EIO	: East Indian Ocean
SWIO	: Southwest Indian Ocean
MCAT	: Mozambique Channel- Angola Trough
TSB	: Tropical- Subtropical Boundary
ISO	: Intra- seasonal Oscillations

Abstract

This thesis gives attention to the circulation of the tropical atmosphere over southern Africa and the immediate oceanic regions on either side at sub- monthly or intra- seasonal oscillation scales (ISOs). Questions about the region include seasonality of summer rains, time variations of wet and dry spells, weather- bearing systems associated with each phase and in the case of wet events, evolution.

The study first touches briefly on monthly and seasonal variations of Zimbabwe rainfall and regional teleconnnections. Summer rainfall in Zimbabwe is declining and weather events are becoming more severe and cyclic. Interannual fluctuations are dominated by the 2.3- year (28- month) cycle. Secondary cycles are found at 18.6 and 3.8 years. The cycles are attributed to the Quasi- Biennial Oscillation (QBO), the luni- solar tidal action and El Nino/ Southern Oscillation (ENSO), respectively. Zimbabwe rainfall can be reasonably predicted as early as six months prior to occurrence and is best correlated with equatorial Indian Ocean SST and equatorial Atlantic Ocean 200 hPa zonal winds.

Intra- seasonal time scale analysis of southern Africa pentad (five- day) summer rainfall indicates cycles ranging from 10- 45 days, the mean frequency being 3- 4 pentads (20 days). The season is composed of 5 wet spells alternating with four dry spells. The rainfall distribution is multi- modal and divided into early (or short rains) and late (long rains) summer separated by a major dry spell from the end of December to mid- January. The 20°S latitude demarcates tropical from extra-tropical circulations. Period mean analysis for varous phases shows systems propagating eastward from the South Atlantic throughout early summer. There is evidence of a monsoon system propagation southwestwards from the central equatorial Indian Ocean in late summer.

Over southern Africa, early summer convective phases are characterised by low- level anticyclonic ridging from the Atlantic Ocean and a mid- level southerly wind circulation. Prior to peak wet spells, low- level easterly anomalies advect moisture from the central Indian Ocean. Upper troughs are transported from the Atlantic Ocean. Late summer wet spells are dictated by the intensity of two low- level troughs, one stretching from the Mozambique Channel to Angola (MCAT) and other from Angola to South Africa on the western flank. Moisture is from two sources; the equatorial Congo basin and the SW Indian Ocean. Rainfall is often triggered internally over southern Africa.

Dry spell frequencies range from 3 in wet years to 5 in dry summers. They are characterised by an anticyclone over Botswana accompanied by subsidence and divergent southeasterlies over southern Africa. Anticyclonic support is from the Atlantic Ocean at low- levels. During this time a dipole is created between drought stricken southern Africa and the western Indian Ocean, where the atmosphere remains convectively unstable. Meteorological variables often exhibit anti- phase patterns between wet and dry spells. The findings of this research demonstrate predictive potential and are of use in agriculture where operations are of the order of ISO time frames.

List of Figures

5.1 Mean 700 hPa geopotential height and temperature for all five phases of summer.

5.2 Mean 700 hPa zonal wind and meridional wind.

5.3 Mean horizontal wind vectors at 700 hPa.

5.4 Mean 700 hPa horizontal divergence and vorticity.

5.5 Mean 500 hPa geopotential height and vorticity.

5.6 Mean 500 hPa meridional wind and zonal wind.

5.7 Mean horizontal wind vectors at 500 hPa.

5.8 Mean 500 hPa vertical velocity for all phases.

5.9 Mean geopotential height for all phases at 200 hPa.

5.10 Mean 200 hPa zonal and meridional wind patterns.

5.11 Mean horizontal wind vectors at 200 hPa.

5.12 Mean 200 hPa horizontal divergence and vorticity .

5.13 Mean stream function and velocity potential at 200 hPa.

5.14 Mean vertically integrated water vapour flux.

5.15 Mean vertically integrated internal energy.

6.1 Horizontal wind vectors at 700 hPa at the peak (Pentad P0) of each major wet spell.

6.2 700 hPa divergence and vorticity for each wet spell at peak activity (Pentad P0).

6.3 500 hPa zonal wind and meridional wind for each wet spell during peak activity.

6.4 Horizontal wind vectors at 500 hPa at the peak (Pentad P0) of each major wet spell.

6.5 500 hPa vertical velocity and vorticity for each wet spell during peak activity.

6.6 200 hPa divergence (a) and vorticity (b) for each wet spell at peak activity (Pentad P0).

7.8 200 hPa total wind field for EFW.

7.9 200 hPa geopotential height anomalies for EFW.

7.10 Divergence and vorticity field anomalies for EFW at 200 hPa.

7.11 700 hPa meridional and zonal eddy temperature covariance anomalies for the life cycle of LSFW.

7.12 700 hPa geopotential height anomalies for LSFW.

7.13 Divergence and vorticity field anomalies for LSFW at 700 hPa.

7.14 500 hPa meridional and zonal wind anomalies for LSFW.

7.15 500 hPa total wind field for LSFW.

7.16 500 hPa geopotential height and vorticity anomalies for LSFW.

7.17 200 hPa geopotential height anomalies for LSFW.

7.18 200 hPa meridional (a) and zonal (b) wind anomalies for LSFW.

7.19 200 hPa total wind field for LSFW.

7.20 Divergence and vorticity field anomalies for LSFW at 200 hPa.

7.21 Water vapour flux for EFW, integrated from the surface to 500 hPa.

7.22 Water vapour flux for LSFW, integrated from the surface to 500 hPa.

7.23 Vertically integrated internal energy for EFW and LSFW. The integration is between 700 and 300 hPa.

8.1 700 hPa temperature (°C), dew point (°C), meridional and zonal temperature transports (°C m s^{-1}) for MSD and LSD.

8.2 700 hPa geopotential height, divergence and vorticity for MSD and LSD.

8.3 MSD horizontal wind vectors at 700, 500 and 200 hPa as well as vertically integrated water vapour flux.

8.4 LSD horizontal wind vectors at 700, 500 and 200 hPa as well as vertically integrated water vapour flux.

List of Tables

Table	Description

Annexures

Acknowledgments

This research was funded by the Water Research Commission, South Africa. Contributions came from many people and some deserve mentioning. Dr. Mark Jury gave constructive criticisms and advice as my supervisor and played a significant role in the interpretation of results. Special thanks are extended to staff in the Oceanography Department, particularly Professor G. Brundrit, who made the working environment more conducive, Shaun Courtney and Roy van Ballegooyen. Sincere gratitude is extended to members of the Climate Research Lab namely, Kevin Levey, Bhawoodien Parker, Abdallah Nassor (from the Madagascar National Meteorological Service), Tiba Kabanda (Tanzania Meteorological Services) and Johan Beyers (Namibia Meteorological Service). The support they provided, from computing to exchanging of ideas was invaluable.

The thesis also acknowledges support from the Zimbabwe Meteorological Department directorate and staff as well as the Drought Monitoring Centre (Harare) who not only provided the data but granted me the study leave. Dr. Caxton Matarira is thanked for faith and encouragement. I am also grateful to support from Messrs. Mucha Musemwa, Kathy Matsika, Thenjiwe Kona and Mrs. Sheila Ntshona for usage of her computer.

Finally, and more important, profound thanks are extended to the Makarau family, my wife, Rita, and daughter, Farai, for their patience and understanding and it is to them that this thesis is dedicated.

Chapter 1

Introduction

1.1 Motivation, hypothesis and layout of chapters

From 1982 to 1992, southern Africa (**Figure 1**) experienced recurring droughts with devastating effects, most notable of which were livestock losses of up to 90% in the 1982-83 drought, reduced harvests, socio-economic hardships, negative economic growth rates and political instability. Since then climatic variability, possibly enhanced by global warming, has been getting a fair share of recognition. The climate is one of the most important factors in determining agricultural potentialities of any region. For the African sub-continent, whose economies are highly dependent upon the success of agriculture, there is an urgent need to focus research on drought, not only for the purpose of understanding its causes, but to be able to predict its occurrence.

Agriculture has become more sophisticated and scientific. Plant growth and yield are strongly dependent upon the weather and climate. Crop yield and farm management can be most effective if cognisance of the effects of climatic variability is taken. In order to achieve more sustainable agricultural production, it is important for policy makers and economists to understand and accept the variability of climate both inter- annually and intra- seasonally in order to efficiently utilise natural resources. The rainfall distribution on monthly and sub-monthly time frames is vastly different and may even vary by two orders of magnitude, as do crop water requirements at different phenological phases. These differences impact differently on farm management techniques, hence crop yields.

The climate of southern Africa and its surrounding oceans is now undergoing rigorous scrutiny. For example, the major rain- bearing weather systems in the region are being identified, isolated and analysed further. These include the Inter- Tropical Convergence Zone (ITCZ), easterly waves and related monsoon circulation, westerly waves and associated incursions of extra- tropical cyclones, frontal systems, cloud bands originating from Namibia and Angola as well as tropical cyclones which pass through the Mozambique Channel. However, most findings to date still have some degree of uncertainty, moreso at regional and local levels where the results have not been operationally useful. This can be attributed to many factors. Firstly, some of the

conclusions reached have been based upon results from general circulation models (GCMs) which are still in developmental phases whose spatial resolutions have yet to be tested for representativeness at sub-grid or station level.

Secondly, the parameterisation and interpolation schemes are not yet universal. The physics and dynamics of the ocean-atmosphere system are not fully known, hence climate variability is not comprehensively represented. There is now sufficient evidence concerning the role, say, of topography in shaping local climate. It is imperative, therefore, that diagnostic research findings at regional and local levels be carried out and incorporated into GCMs. This would complement existing knowledge and provide realistic scenarios of climate, both present and future. This 'bottom- up approach', which has been successfully done in other spheres of research, should be applicable in climate modeling studies.

Thirdly, research to date does not indicate precisely the role played by teleconnections in determining and predicting rainfall patterns over southern Africa, particularly from country to country and at rainfall station level. For example, the El Niño/ Southern Oscillation (ENSO) events have been directly associated with seasonal rainfall in southern Africa. Warm ENSO episodes off the coasts of Peru/ Ecuador have been shown to coincide with drought conditions over this region while cold episodes associate with above normal rainfall. The findings are only beginning to be tested operationally both at regional and national levels and have started to precisely demarcate which areas are more responsive to ENSO, when and how. Inappropriate perceptions of these linkages coupled with inadequate knowledge about the El Niño, have resulted in inaccurate forecasts of seasonal weather being issued with obvious consequences.

Lastly, to date, it is assumed that the austral summer rainfall over most of southern Africa is nearly normally distributed and unimodal centred on January. While that may be true with respect to monthly averaged rainfall, this appears not to be so for daily or pentad (5-day) data. The season is actually composed of alternating wet and dry spells whose duration is of the order of 1- 2 weeks. These spells occur regardless of the outcome of the overall season and determine accumulated rainfall. Thus, it is important to understand the climate of a region through the distribution of the rainfall in a particular season. This variability is equally, if not more, useful compared to that of the inter- annual variability. By dissecting the summer season, subsequent patterns/ characteristics provide more insight into the nature, frequency and behaviour of different weather- bearing regimes influencing southern Africa.

The research approach may shed light on the influence of global phenomena and planetary scale motions on day-to-day weather. In addition, the role played by synoptic scale circulations regarding in- season dry and wet spells can be made clearer as it is currently not adequately represented or accounted for in mean monthly and seasonal time frames. Results of the investigations can be useful in developing conceptual models in pursuit of user- friendly algorithms for predicting weather operationally up to 20 days in advance.

Due the relatively short ECMWF data set (six years), the discussion puts less emphasis on the absolute values of meteorological parameters or their derived products. This is particularly the case regarding anomalies. Rather, the thesis focuses on differences and common features which are operationally useful, especially in the identification of precursors. It should also be worth mentioning here that, since intra- seasonal analyses are relatively new in southern Africa, there are relatively few references or historical analogues to compare the findings with. This is despite the fact that a significant amount of effort has been placed on case studies which have ignored time variations of climate over the region.

This thesis aims to address the above issues. In **Chapter 2**, the thesis provides a background summary of research to date on the climatic variability of southern Africa. The first section discusses notable research carried out using monthly and seasonal periods. The second part is a literature review of efforts worldwide to understand climatic variability in the order of days and weeks as compared to months and years. This type of research is relatively new, moreso in Africa. Practically applied, the research offers useful guidance not only in weather forecasting but in the improvement of our understanding of the physics and dynamics of the atmosphere.

The thesis is divided into two parts. The first part reveals, by exploring further, some aspects of monthly rainfall which have not been clearly observed and noted before. It uses Zimbabwe data as a sample to illustrate discrepancies between observations and current theories about the monthly and seasonal variability of climate in central and southern Africa. Throughout Africa, countries are in the process of establishing mechanisms for monitoring and mitigating the effects of drought through national early warning systems. Seasonal forecasts are being developed and tested. Through **Chapter 3,** the thesis looks for and identifies distinctive patterns and relationships among a time series of Zimbabwe summer season rainfall, other global weather phenomena and spatial teleconnections. Specifically, this chapter investigates associations of sea surface temperatures (SST), the

Southern Oscillation (SO), ENSO, horizontal winds (zonal and meridional), outgoing long wave radiation (OLR) and the Quasi- Biennial Oscillation (QBO) with Zimbabwe rainfall. The statistically determined relationships are investigated at various lags for predictive purposes. Unique relationships between the variables are quantified. Lastly the possible cause and effect, and feedback mechanisms are explored. Noting the controversy within the international community and that the study is not the subject of this thesis, no attempt is made to explain physical mechanisms between regional teleconnections and rainfall. It may be mentioned here that in this chapter, and throughout the thesis, figures are generally at the end of each chapter. In some cases, however, they are inserted within the text.

The second part, the focus of this research, is concerned with predictability of rainfall on the medium scale (of the order of days and weeks) during the course of the summer season which generally extends from mid- October to mid- April (nearly half a year in duration (approximately 182 days). For rain-fed agriculture and maize production in particular, though, the effective season is November- March (about 150 days). The thesis is based upon the hypothesis that the southern African summer rainfall is modulated by low frequency intra-seasonal oscillations ranging from 10 to 50 days. The physics and dynamics of the atmosphere vary as the season progresses. In other words, early and late summer climatic variability may exhibit different characteristics, particularly in the precursor patterns. In addition, it is suggested that tropospheric circulation patterns near 20°S determine the intensity of wet and dry spells over Africa south of the Congo basin. The 20°S latitude effectively demarcates the tropics from the extra- tropics over southern Africa north (south) of which winds are from the east (west). The latitude is sometimes referred to in this thesis as the tropical- sub-tropical boundary, or TSB.

Chapter 4 illustrates intra-seasonal oscillation (ISO) modes in southern African rainfall. It commences by analysing pentad rainfall data from Zimbabwe, Zambia, Botswana and northern South Africa with the objective of verifying the common characteristics over the sub- continent during summer. The analyses are used to identify wet and dry episodes, construct composites and reveal the most probable occurrences of in- season active as well as passive spells, including the most probable onset, cessation and duration of the main season. Additional and supportive information regarding construction of composites is provided in **Annexure 1**.

Chapters 5 through 9 are based on climatic variability at intra- seasonal time frames. They utilise the findings of Chapter 4, noting mean occurrences of wet and dry phases as well as

life cycles of wet events. Data reduction techniques, equations and formulae used for the inter-comparisons are shown in **Annexure 2**.

In **Chapter 5**, the mean circulation patterns of major phases of summer are determined. The analysis is based upon the hypothesis that circulation controls over southern Africa during austral summer are variable. Thus, a period mean approach is used, based upon the life cycles of individual major wet spells. The chapter provides background meteorological information during the 1986/87 -1991/92 period. The meteorological analyses continue in **Chapter 6** but the patterns analysed are for the peaks of wet spells only. The main object is to ascertain unique characteristics of each of the five individual wet spells comprising the summer rainy season.

Chapter 7 looks at life cycles of the first wet spells of early and late summer. Based mostly on anomalies, each cycle is analysed in a four stage process namely initiation (or formation), development, maturity and dissipation (or decay). The cycle lasts four pentads (20 days). The procedure aims at identifying trajectories of air masses, preferred regions of initiation, intensity and decay as well as triggering mechanisms.

Chapter 8 discusses mechanisms associated with intra-seasonal droughts in southern Africa. Droughts, especially in-season dry spells, have not been adequately addressed before. It is necessary to understand them for forecasting purposes. Emphasis is placed on circulation patterns in the mid-troposphere, represented by the 500 hPa pressure level. This level is selected mainly because it represents the middle troposphere and circulation patterns (like vertical velocity) are indicative of tropospheric dynamics.

A 3-D perspective of circulations over southern Africa is completed in **Chapter 9,** using the 20°S latitude. The first section of the chapter discusses summer circulation patterns for each season from 1987 to 1992. By means of hovmoller diagrams along 20°S (longitude versus time diagrams) the mid- tropospheric levels are investigated from 30°W (central Atlantic Ocean) to 90°E (eastern Indian Ocean) to show behaviour of selected meteorological variables across the tropical- subtropical boundary from November to March, inclusive. The second part looks at the vertical sections (longitude- height diagrams) of meteorological parameters along 20°S from the surface to 100 hPa, again between 30°W and 90°E. The analysis is a continuation of Chapter 7, which focuses on wet spells, and Chapter 8, but concentrating on the mid- summer dry spell.

The final chapter, **Chapter 10**, summarises major findings of the thesis, highlighting characteristics of austral summer from the intra- seasonal oscillation perspective. Attention is also given to relationships between local rainfall and regional teleconnections, with particular reference to Zimbabwe.

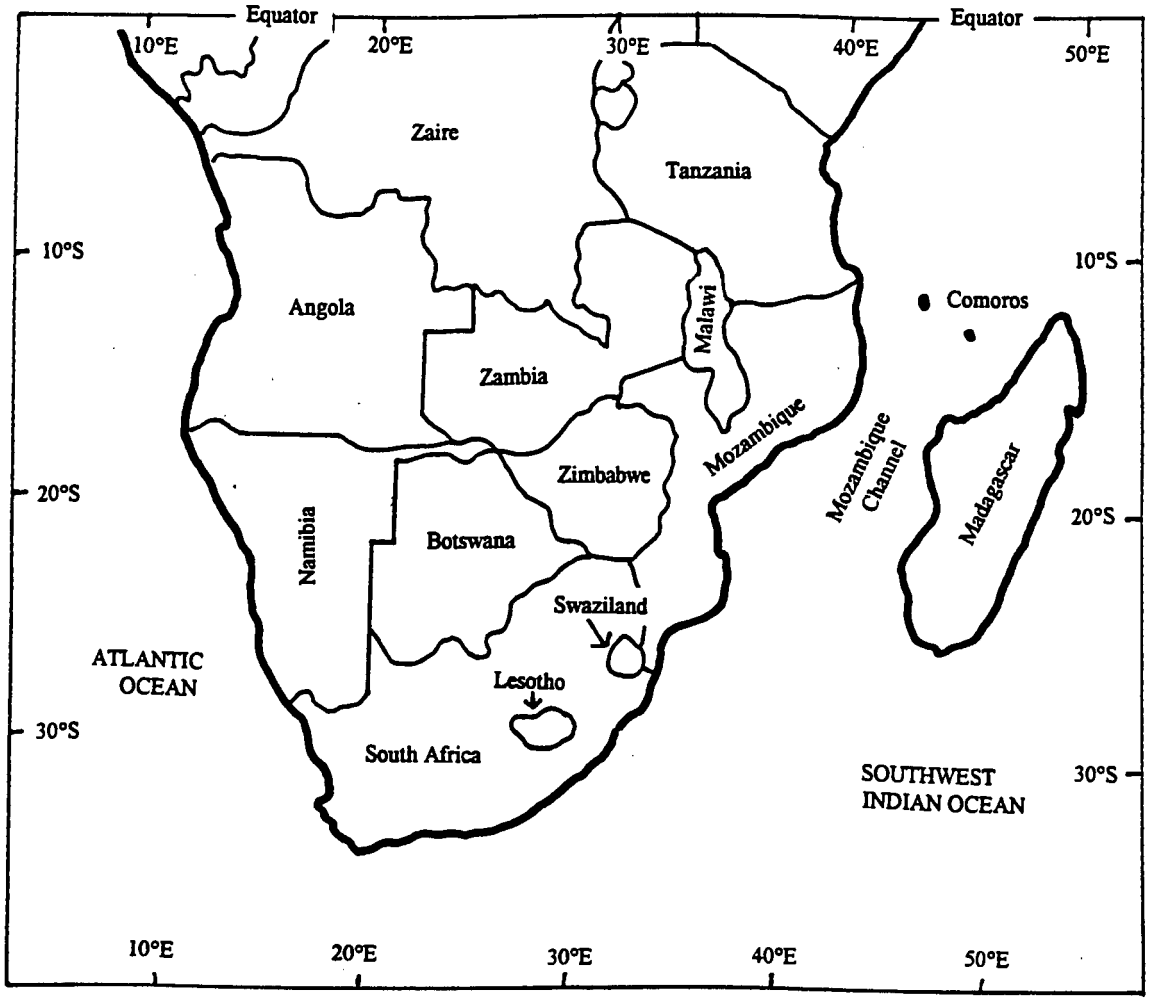

Figure 1 : Southern Africa, with political boundaries.

Chapter 2

Climate Variability of Southern Africa: Literature Review

This chapter provides a summarised literature review of climatic variability in southern Africa. The first section lays emphasis on main weather bearing systems over the region and observed relationships between precipitation and teleconnections. The second is a review of previous research findings pertaining to intra- seasonal oscillations mostly at the event scale. Most of the literature is based on research outside southern Africa, since studies of intra- seasonal oscillations in the sub- continent is relatively new.

2.1 Main rain-bearing systems.

Several studies of rainfall characteristics over southern Africa have been made. These studies have included inter- annual variations (e.g Janowiak, 1988), decadal cycles (Tyson, 1981, 1984, 1987) and more recently, intra-seasonal variations (Lyons, 1991; Matarira and Jury, 1991; Chen and Tzeng, 1991; and Levey, 1993). A detailed account of the causes of rainfall and characteristic circulation patterns on the interannual time scale is not the subject of this thesis. The topic has been relatively extensively covered elsewhere, most notably by Torrance (1981), Rocha (1992), Mason (1992), D'Abreton (1992) and Pathack (1993). However, it is necessary to highlight the major rain- bearing systems influencing southern Africa.

Climate variability in southern Africa at monthly and inter- annual time scales is now generally understood. In the tropics, rainfall is mainly of organised deep cumulus convection embedded in a large- scale disturbance, where a confined area produces most of the rainfall. The daily rainfall can vary greatly within a few hundred kilometres (Jackson, 1977; Sharon, 1981) while long- term means may be similar throughout an area. With the exception of the extreme southwest of South Africa which receives rainfall mainly in winter, the region generally experiences one rainy season usually stretching from late- October to early April. However, areas in the vicinity of the equator (eg., northern Tanzania) experience two rainfall episodes (short rains in November and long rains from March to May) in sympathy with the movement of the ITCZ. The lag period between the latitudinal cycle of the sun and the ITCZ is usually two months (Riehl, 1979), but over

Southern Africa it is only one month (Hsu and Wallace, 1976; Kidson, 1977). This could be due to intense sensible heat fluxes greater than 100 Wm^{-2} at the 850 hPa plateau level. During this period, pressure gradients over the sub- continent are generally weak and the winds normally light and variable.

The primary control on rainfall in the tropical areas are several convergence zones (Acharya and Bhaskara Rao, 1981) the most important of which is the ITCZ, which advances southwards to the northern Kalahari in the austral summer (Nicholson, 1986a). Over land, the ITCZ tends to follow the seasonal march of the sun. According to Jury and Pathack (1991), the convective intensity of the ITCZ, as identified by OLR data, is at its maximum over southern Africa near 10°S, 20- 30°E. In the southwest Indian Ocean, the summer ITCZ is located between 10 and 15°S and is less intense and more variable.

Janowiak (1988) observed that during the Southern Hemisphere summer, the ITCZ reaches its southernmost position at about 12°S in December- January. In addition, during the austral summer the region of maximum rainfall and the ITCZ are nearly co-located with the ITCZ and most active in January, in partial agreement with Nicholson and Chervin (1983). It was proposed that the duration of the dry and rainy season is determined by the oscillation of the ITCZ around the equator. Nicholson and Chervin (1983), however, contended that it is the inter- annual differences in overturning along the ITCZ rather than latitudinal displacements that appear to be the main cause of rainfall and energy release variations over the southern African tropics.

Despite its importance in influencing weather patterns over tropical Africa, the ITCZ remains less understood with regard to the physical mechanisms responsible for its formation, development and movement. This can be partly attributed to the fact that the ITCZ is a confluence of several airmasses (Torrance, 1981) with different origins which have to be in phase to produce effective convergence. Its exact composition, development and role, including characteristic weather sequences, are not essential here, but are documented in Kreft (1972), Kumar (1978), Torrance (1981) and Gadgil and Guruprasad (1990), to name just a few.

During summer, quasi-stationary low- pressure centres occur in the Mozambique Channel and near the Caprivi strip area (Torrance, 1981). They are linked by a semi- permanent trough controlling relatively moist westerlies equatorward of it and drier easterlies to its south. This trough oscillates between about 12 and 16°S, depending upon the dominating

airmass at the time with the latter being more conducive for good falls over most of the region. This feature was similarly observed by Harrison (1984), Lindesay and Harrison (1986) and Lindesay (1988) as part of an anomalous Hadley- type phenomenon.

Tropical cyclones originating from the southwest equatorial Indian Ocean at times contribute significantly to weather patterns over Southern Africa, especially the eastern seaboard and Madagascar. The cyclone season is usually from December to April (Padya, 1989; Matarira, 1990a; Jury 1993; Nassor, 1994). The trajectories and consequent weather effects vary significantly from cyclone to cyclone. While most cyclones remain to the east of Madagascar and thus remain a feature of the Indian Ocean, a sufficient number form or move into the Mozambique Channel. Depending upon their tracks, the cyclones can cause either dry or wet conditions into southern Africa. When in the central Mozambique Channel, hot sunny weather prevails over much of eastern southern Africa (Zimbabwe and Mozambique, mainly). This is attributed to the development of relatively dry upper- level southeasterly winds over the southern African interior possibly due to diffluent and subsident outflow from the cyclone. Torrance (1981), Dunn (1985), Diab (1988), Matarira (1990) and Jury and Pathack (1991) provide more details on these tropical cyclones.

Outside the tropics to the south of 20°S, much of the rainfall has been linked to mid-latitude systems (Kumar, 1978; Harrison, 1983; Harangozo and Harrison, 1983). Cloud bands associated with mid-tropospheric pre-frontal troughs and waves in the upper- level westerlies produce a high proportion of the summer rainfall. Pre- requisites for cloud band formation in the region are a cyclonic vortex situated over central Africa and tropospheric easterlies over southern Africa. According to Harangozo and Harrison (1983) and Harrison (1984a), a tropical- temperate trough, linking areas of convection over tropical and sub- tropical southern Africa with mid- latitude depressions to the southeast of the continent, is the most important late- summer rainfall producing system. Taljaard (1990) proposes that it is an upper- level trough coupled with lower-tropospheric convergence that is essential for the development and intensification of the cloud bands across southern Africa.

In addition to the above, independent research on southern African climate has established the following :

- In the early summer (October- December), heavy rainfall episodes are often associated with cut- off lows (cold- cored baroclinic systems originating in the middle- and upper-level westerlies) over South Africa (Taljaard, 1982, 1985; Tyson, 1986; Lyons, 1991). These are frequently associated with positive geopotential height anomalies to the south of Africa (Tyson, 1986; Taljaard, 1987; Barclay 1992). Webster (1982), supported later by Kuhnel (1989), suggests the rainfall during this period is a consequence of extra- tropical responses to equatorial forcings resulting in equatorward surges of westerly waves. The equatorward penetration occurs through upper- level troughs over the Mozambique Channel and southeast Africa (Lyons, 1991).

- Summer mean rainfall varies in a "see- saw" of drought and flood (Jury and Pathack, 1991). The development of a flood- producing system is characterised by low surface pressures over the interior, moist inflow over the southeast coast by ridging anticyclones and periodically enhanced sub- tropical easterly flow. Drought is induced through sinking motions in a high pressure system centred over Botswana, often reinforced by the Atlantic Ocean Anticyclone and strengthened mid- latitude westerlies with a high zonal index.

- Tropical easterlies are a determinant of rainfall over much of the continent. In southern Africa, particularly in late summer, reduced upper- level easterly flow is associated with drier conditions (Nicholson, 1986). Their importance has been sufficiently documented (Bhalotra, 1973; Kumar, 1978; Taljaard, 1981; Harrison, 1983; Harangozo and Harrison, 1983). They are unusual in the Southern Hemisphere (Riehl, 1979) but seem to occur in the south-west Indian Ocean, affecting the east coast of Africa (Okoola, 1989).

- Rainfall over the central interior of southern Africa is normally nil to light when tropical-temperate troughs (TTTs) overlie Madagascar rather than the sub-continent (Nicholson and Chervin, 1983; Harrison, 1986; Lyons, 1991). Similar east- west "dipole" behaviour is found when tropical cyclones are active east of Madagascar (Jury 1993).

2.2 Observed links between precipitation and teleconnections.

2.2.1 Global Observations

The earlier findings of Walker and Bliss (1932), Bjerknes (1966, 1969) and Namias (1963), among others, have provided evidence of relationships among meteorological variables at remote locations of the world. Most of these relationships have been based on fluctuations of sea surface temperatures and the Southern Oscillation and, more recently, the Quasi- Biennial Oscillation.

2.2.1.1 Sea Surface Temperatures (SST)

Regions of high tropical precipitation have been observed to be well correlated with regions of high SSTs (Bjerknes et.al., 1969; Cornejo-Garrido and Stone, 1977; Liebmann and Hartmann, 1982; Gill and Rasmusson, 1983; Neelin and Held, 1987). Other studies have considered patterns of SST anomalies and their influence on regional climate (Webster, 1981; Rasmusson and Carpenter, 1982; Voice and Hunt, 1984; Yamazaki, 1988). Results to date concur that SST anomalies offer better chances for useful forecasts than most other statistical indices.

As adequately summarised by Ropelewski and Halpert (1987), a problem still exists concerning the physical links between SST anomalies and precipitation anomalies. It is still unclear exactly how anomalies trigger such large scale atmospheric responses. Even the triggers themselves have yet to be successfully explained. It is also unclear whether there are preferred locations, times of the year, areal extents and threshold values involved (e.g. Graham and Barnett, 1987). Without this information, seasonal forecasts will remain uncertain and subjective.

There have been several attempts to link SST and rainfall. Bjerknes (1969), for example, postulated that the link was through enhanced latent and sensible heat fluxes in regions of warm SST, as did Newell et al. (1972) and Boer (1985). A major issue is that direct measurements of sensible heat and moisture fluxes are problematic and scanty and also that tropical surface winds are generally light. According to Neelin and Held (1987), however, warmer surface temperatures create mean upward motion by increasing the low level moisture convergence and thermodynamic instability of the air. Precipitation in the favoured regions is enhanced by convergent moisture transport at the expense of less favoured regions. Agreement is noted in the association between high SST (eg., the

western equatorial Pacific) and heavy rainfall, but changes in heat fluxes into the atmosphere are ambiguous. A critical surface temperature (approximately 28°C; Gadgil et al., 1984) is thought to be necessary for sustained deep convective activity, above which the SST- convection correlation breaks down.

2.2.1.2 The El Nino/ Southern Oscillation (ENSO)

The Southern Oscillation (SO), the "see- saw" of the oscillation of sea-level pressure between tropical regions of the east Indian and east Pacific Oceans, has been extensively studied since the works of Walker and Bliss (1937) and later findings of teleconnections from the Pacific by Bjerknes (1966, 1969). Included are studies linking it with the El Nino, a seasonally recurring oceanic phenomenon in the eastern Pacific off the coasts of Ecuador and Peru, hence ENSO. Some have concentrated solely on understanding the dynamics of the coupled tropical ocean- atmosphere system (e.g., Cane 1986; Deser and Wallace, 1987; Philander, 1990) and others on the predictability of ENSO (notably Chu and Katz, 1985; Graham et al., 1987; Barnett et al., 1988; Fraedrich, 1988; Kappenne and Ghil, 1992). Most research, however, has focussed on the observed association between the phases of ENSO and precipitation on global scales (e.g., Horel and Wallace, 1981; Rasmusson and Carpenter 1982; Ropelewski and Halpert 1987, 1989; Latif et al., 1990; Ropelewski et al., 1992), as well as regionally.

For want of a plausible mechanism, the causes of ENSO episodes are still tentative at this stage. Bjerknes (1969) gave a detailed proposal basing his argument upon the ocean-atmosphere interaction and concluded that the resonance constituted the Southern Oscillation. In other words, the SO was caused by inter-annual variations of SST in the tropical Pacific. Recently, Gray et al. (1991) and Knaff et al. (1991) concluded that there was a strong association between the stratospheric QBO and the onset and maintenance of warm and cold ENSO events.

It is consoling, however, that numerical models are progressively becoming more accurate in predicting the El Nino by identifying those occasions and preferred locations where and when interactions between the ocean and atmosphere are strong. Thus, it is now possible to reasonably anticipate the imminence of ENSO events, but the models currently suffer from serious climatic drift and are still too crude to foretell how these events will evolve and how severe they will become. The predictions are still merely probabilistic in nature and based on historical analogues. Whatever the case, it is now known that the low phase

of the SO (warm event) is generally associated with above-normal central Pacific and Indian Ocean SSTs, while negative SST anomalies occur in conjunction with the high phases (cold events).

It is now acknowledged that year- to- year variability in the tropics is controlled largely by the ENSO phenomenon. However, a review of literature indicates that there is not a single variable or index that can be used to unequivocally define warm and cold events in the tropical Pacific. While there is generally no ambiguity in identifying a particularly strong warm (e.g 1982/83, 1991/92) or cold (e.g 1973/ 74, 1988/89) event, the inclusion or exclusion of moderate events is still highly subjective and depends upon the indices and criteria used as far as forecasting is concerned.

2.2.1.3 Quasi- Biennial Oscillation (QBO)

The QBO is a quasi- periodic alternation of zonally symmetric equatorial westerly and easterly winds observed in the stratosphere. Therefore, it can be predicted as accurately as ocean tides. However, there is some variability in the duration of both the east and west phases (Hamilton, 1990) in that the duration of a particular phase depends on the duration of the preceding phase. In addition, the duration of the phases is coupled to some extent to the annual cycle. Holton and Tan (1980), using 50 hPa equatorial wind, observed the phases were either easterly or westerly in January, implying that the transition from one phase to the next did not occur in January. Studies using zonal wind components between 30 and 50 hPa have produced a reversal period ranging from 2.1 to 2.4 years. Differences of stratospheric meridional winds in the phases of the QBO are relatively too small to be identified (Naujokar, 1986). A comprehensive literature review establishing the presence and characteristics of the QBO can be found in Palmer (1954), Dartt and Belmont (1970), Holton and Lindsen (1972), Ebdon (1975), Brier (1978), Trenberth (1980), Kuma (1990), Gray et al. (1991) and, recently, Ogallo et al. (1993).

2.2.1.4 Outgoing Longwave Radiation (OLR)

The advent of satellite imagery has made it possible to study the variation of large scale (planetary) convection through analyses related to OLR. High values of OLR are usually associated with high radiative temperatures of the earth's surface as well as a lack of deep convective clouds in the free atmosphere. Conversely, low OLR is associated with low radiative temperatures of cold cloud tops (Asnani, 1993). On monthly and seasonal time

scales, major zones of convection can be readily delineated as regions of low OLR in the tropics and summer sub- tropics. The convective anomalies can be driven by teleconnections (Lau and Chan, 1983a; Janowiak et al., 1985; Yoo and Carton, 1988; Arkin and Ardunay, .1989; Gadgil and Gurupsarad, 1990).

Caution must be exercised when utilising OLR as proxy for convection. High level clouds (cirrus), which are nonconvective, can contaminate data as they also have low OLR (Morrisey, 1986; Gadgil and Guruprasad, 1990). This results in a poor correlation between precipitation and OLR. Thus, the data must be calibrated to filter out cirrus contamination first. A threshold technique has been applied in several studies. Gadgil and Guruprasad (1990) used 180- 210 W m^{-2} to remove stratocumulus and middle- level cloud and an albedo of 0.5 for cirrus clouds. Richards and Arkin (1981) used a brightness temperature of 240°K, while Gruber and Krueger (1984) utilised an OLR threshold of 190 W m^{-2}. It must be emphasised here, also, that strong convective instability does not necessarily imply a lot of precipitation will occur. It merely suggests that if a mechanism is present for organised lifting of air parcels and if ambient air is sufficiently moist, then clouds are likely to attain considerable depth.

2.2.2 Southern Africa and regional teleconnections

In sub- equatorial Africa, climatic patterns especially rainfall, have been linked to spatial anomalies of SST (Lough, 1986; Rocha, 1992; Pathack, 1993), the phase of the QBO (Mason and Tyson, 1992; Ogallo, 1993), inter- hemispheric teleconnections (Nicholson and Chervin, 1983; Nicholson, 1986), the phase of ENSO (Lindesay, 1988; Ogallo, 1988, Matarira, 1990; Rocha, 1992) and parameterised using OLR (Lyons, 1991; Jury et al., 1992; Pathack, 1993).

Dyer (1979), Nicholson (1986), Lindsey (1988), Ogallo, (1988), Matarira (1990), Hutchinson (1992) and Rocha (1992) have attained the general consensus that high (low) phases of the SO, or cold (warm) El Nino events, are generally associated with excess (deficient) rainfall over southern Africa.

The research is extensive. For brevity, the following are some of the major findings to date:

- Weak onset of Indian NW monsoon outflow and reduced penetration across the equator is associated with above normal rainfall over southern Africa. Lag correlations between the southern Africa rainfall index and surface winds in the monsoon region peak at +0.91 near 5°S, 55°E in the spring (Jury et al., 1991). Similarly Pathack (1993) has noted correlations between a summer South African rainfall index and spring OLR fields of +0.88 at 5°S, 70°E. Both results highlight the onset of monsoon outflow as a climatic determinant possibly through the re- direction of water vapour fluxes in the northern Hadley Cell.

- Halpert and Ropelewksi (1992) observed that cold event (La Nina) temperature composites for southern Africa indicated below- normal surface temperatures occurring June through August prior to the onset of the good summer rains. The series showed that only 1 in 17 high- phase years had above- normal temperatures in the preceding winter. It was then concluded that the observed cooler (warmer) winter temperatures in southern Africa are associated with the increased (decreased) cloudiness and above (below) normal rainfall the following summer.

- Ogallo et al. (1993) investigated the QBO over tropical eastern Africa using Kenya upper wind data and determined its relationship with seasonal rainfall. Successive recurrences of the easterly and westerly wind phases appeared at 30 hPa (in agreement with observed characteristics over Singapore (Plumb, 1984) and propagate downwards at an average rate of 1.2 km/ month, as was found by Plumb (1984) and Holton and Lindzen (1972). Dominant spectral peaks which were discernable from spectral analysis were centred around 28 months. Above normal rainfall during the long rainy season and stratospheric westerly winds had a probability of 80%. The probability of below normal rainfall associated with easterly winds were 75% and 71% for the long and short rains, respectively. Simple and cross- correlation analyses could not reveal statistically significant associations between rainfall and the various stratospheric zonal wind phases although Jury et al. (1993) has shown a prominant negative correlation between OLR over east Africa in November and QBO in the following summer.

- Central Indian Ocean SSTs in the domain 0-10°S, 60-80°E are significantly negatively correlated with the southern African rainfall index (-0.60 at lags of -3 to -4 months; Pathack, 1993). Relationships between SSTs and convection (OLR) indicate that a cooling of waters within this cyclogenesis region (NE of Madagascar) brings about increased rainfall to SE Africa (Jury and Pathack, 1991). Rocha (1992) also suggests that anomalously warm SST in the tropical Indian Ocean are the most direct cause of dry summers over southern Africa. This sustains a low- level cyclonic circulation east of Madagascar (increasing moisture convergence over the central Indian Ocean) which weakens southeasterly trade winds and northeast monsoons over Southern Africa. The overall result is reduced precipitation over the African sub- continent in favour of the SW Indian Ocean.

- Increased low- level easterly anomalies off the northern tip of Madagascar promote the inflow of moisture and subsequent rainfall over southern Africa (Jury et al., 1991). Similarly, low- level westerly anomalies south of Madagascar in the region 25- 35°S, 40- 55°E enhance rainfall and act as an outflow channel for convection. The overall pattern is one of an anticyclone centred on Madagascar in wet summers over southern Africa. Research on wet and dry spells using ECMWF data sets (D'Abreton, 1992) are in close agreement, confirming the role of the low level anticyclonic anomaly centred on Madagascar as a mechanism for moist inflow to southern Africa.

According to Jury at al., (1992), above- normal convective activity across equatorial eastern Africa, NE Madagascar and the SW Indian Ocean coincides with below- normal convective activity across southern Africa. Circulation anomalies may provide simultaneous centres of descent over Botswana and ascent over the Mauritius region. Lag correlations of 700-hPa zonal winds indicate a maximum correlation of +0.71 at 15°S, 50° E (NE Madagascar) two months prior to southern Africa rainfall departures. A standing wave across southeast Africa and the Mozambique Channel is critical to the positioning of clouds bands and other tropical- mid- latitude interactions which provide much of the summer rainfall, confirming the suggestion by Lyons (1991).

2.3 Intra- seasonal research

Intra-seasonal oscillations (ISO) in the atmosphere are generally defined as fluctuations with frequencies much shorter than the seasonal cycle. They are mostly of the order of 10-60 days. The most studied of these are 30-60 day oscillations, sometimes called Madden-Julian oscillations (hereafter referred to as MJO). They were first discovered by Madden and Julian (1971, 1972) in time series of zonal winds at Canton Island in the tropical Pacific and other individual tropical rawinsonde stations. Since then, they have been extensively analysed (for example, Weickmann 1983; Lorenc 1984; Krishnamurti et al. 1985; Lau and Chan 1985; Weickmann et al. 1985, Vincent et al. 1990).

A 40-50-day spectral peak has also been observed in coupled fluctuations of the angular momentum of the atmosphere and solid earth (Anderson and Rosen, 1983; Rosen and Salstein, 1983). Anderson and Rosen (1983) showed that the largest coherences between 40-50- day fluctuations of zonally averaged zonal winds and global relative angular momentum were found in the tropical latitudes. They also observed that the oscillations were in phase with "wave- like motions" at upper levels of the tropical troposphere which were propagating poleward and downward. This was also confirmed by Benedict and Haney (1988). Mysak and Mertz (1984) detected a 40- 60- day oscillation of longshore ocean currents and ocean temperatures in the western Indian Ocean.

According to Chen et al. (1988b), the ISO and the annual cycle each can explain about 40% of the variance of daily global divergent circulation's departure from its annual mean, in addition to being the most significant short-term climate signals of planetary-scale divergent circulation. In short, they appear to be global in extent (wavenumber one or two), eastward propagating and fully developed during the southern hemisphere summer. Indeed, Wang and Rui (1990b) find the December- February period to exhibit the highest amplitude of the ISO, particularly in the central Indian Ocean region.

Murakami et al. (1985) detected 40- day oscillations travelling in a SW- NE direction in the southern Hemisphere. The perturbation seemed to commence in the mid- latitudes and moved north- eastward crossing the sub- tropics in the vicinities of 30°S, 160°W, 15°S, 150°W to the equatorial regions (5°S, 120°W). In addition, another 40- day wave was noted originating in the South West Indian Ocean off the coast of South Africa and propagating towards the north Pacific Ocean. As they seem to start outside the tropics and undergo changes in coriolis, these waves cannot be Kelvin waves.

There is also evidence of the existence of 10- to 30- day oscillations. It is believed (Asnani, 1993) that a 16- day globally travelling wave was first detected by Kuboto and Iida (1954). Madden (1978, 1979), while studying Rossby waves, observed "16-day" waves that were also global in nature. Lazante (1990) found intra- monthly modes lasting between 10 and 30 days in the vicinity of the Rocky mountains (USA). Ghil and Mo (1991) observed that in the southern hemisphere, the dominant mode of 500 hPa geopotential height had a period of 23 days, followed by one of 40 days. A 16- day oscillation was also apparent, but was relatively weak. Branstator (1987) found a weak 23-day westward travelling wave in a S. Hemisphere (SH) nine-year dataset. Anyamba (1992), observed a 20-30 day oscillation in global OLR data over the Indian and Pacific oceans.

Studies of Asian summer monsoons have indicated a relationship with the tropical circulation with a period of about 15 days (Krishnamurti and Bhalme, 1976; Murakami, 1976; Krishnamurti and Ardunay, 1980), especially the active and break epochs (Asnani, 1993). Yasunari (1981), using geopotential height field, also detected an association between a 40- day oscillation and the summer monsoon. Murakami et al. (1983) studied 850 hPa zonal and meridional wind perturbations in 1979 and noted pronounced 40- 45 day spectral peaks over the monsoon region (0- 20°N, 60- 150°E) in the zonal wind and shorter than 10- day peaks for meridional wind. Krishnamurti et al. (1985) also found a 30- 50 day wave originating at the Equator and moving to the Himalayas, phase- locked with another 10- 20 day wave in a westward- travelling mode. Murakami and Nakazawa (1985) documented an association between the south Asia monsoon and a 45- day oscillation in the intensity of the Walker circulation. During active monsoons, the Walker circulation was stronger than normal, and vice versa.

More recently, Shapiro and Goldenberg (1993) studied intraseasonal oscillations that included 13- 29 day bands (with average periods of 16-18 days) "to correspond to the time scales for which zonally oriented mobile wave trains appear" with reference to Blackmon et al.'s (1984a) short period oscillations. Hartmann et al. (1993) also observed 25- 30- day oscillations in the Pacific. Levey (1993), observed a 20- 30 day oscillation, in addition to that of 40- 60 days, in the precipitation and evaporation data for central South Africa during austral summer. Through compositing pentad data, a tropically initiated signal of the 20- 30 day oscillation was identified in the water vapour flux anomaly field just south of the Equator in the central Indian Ocean.

A five- day periodicity was detected in tropical weather systems towards the end of the 19th century. Eliot (1895) observed stationary quasi- periodic pressure oscillations in the Indian tropical monsoon region. Frolow (1942) detected pressure oscillations over the entire tropical region from central Africa across the Atlantic to central America with a mean period of 5- 6 days. The wave was also noticed by Madden and Julian (1972), Tsay (1974) and Madden (1978) in wind and pressure fields. Ngara and Asnani (1978) reported 5- day oscillations in the intensity of the low- level jet over the Kenyan coast.

Since their discovery, there has been interest in elucidating the essential mechanisms responsible for the ISO. Parker (1973) proposed an equatorially trapped Kelvin wave mechanism. Blackmon et al. (1984a, b) found differences in the oscillations ranging between 10 and 30 days and those greater than 30 days. The former were mostly zonal in nature, originating near jet stream entrances and traversing the jets to the southeast. They had wavelengths of approximately 6000 km, were quasi-stationary and with no evidence of preferred positions. The latter, on the other hand, were dominated by meridional wind components and geographically fixed in the vicinity of exits of subtropical upper-tropospheric jet streams. Observational work of Madden (1986) and simulation studies of Hayashi and Sumi (1986) and Lau and Lau (1986) also indicate that the oscillations possess a substantial meridional wind response, suggesting a mixed mode characteristic which is not solely Kelvin wave. Hayashi and Sumi (1986) further contend that equatorial Rossby modes are a major determinant in shaping horizontal structures of intra-seasonal disturbances.

Emanuel (1987) and Neelin et al., (1987) independently proposed a mechanism for the generation of the MJO involving a feedback between the zonal wind perturbation and evaporation. However, their mechanism depends on the assumption of a basic state with westward flow, which is not valid everywhere in the tropics (Wang 1988b). Lau et al., (1988) suggested that the intraseasonal oscillation is associated with a Kelvin wave- CISK mode. Frederiksen and Frederiksen (1993), argue that a Kelvin wave with observed vertical structure, corresponding to the first internal mode would have a period closer to 10 days than to the observed 30-60 days. Also, the phase speeds are far greater than observed ones. They also point out that observed oscillations are not only confined to the tropics (unlike those of Wang and Rui, 1990a), but include extra-tropical responses, as noted by Knutson and Weickmann (1987), Hendon and Liebmann (1990) and Schubert and Park (1991).

To date, there is still controversy regarding horizontal and vertical structures of ISOs. Murakami et al. (1983) concluded that the monsoon region represented the major source for the 40- 50 day oscillations. The proposal was that potential energy was converted to kinetic energy mostly in the upper tropospheric levels (between 500 and 200 hPa). The energy flux was directed downward to maintain the MJO at lower levels, opposing the effects of friction. Madden (1986), using station wind and OLR data, showed that eastward moving regions of convection force a Kelvin- like wave to the east and anticyclonic, Rossby- like waves to the west. He emphasized asymmetric response in solstice seasons; with dominant anticyclonic eddies occurring during the summer hemisphere.

Knutson and Weickmann (1987), by analysing the spatial relationship between eastward-propagating divergent circulation and OLR anomalies of 30- 60 day oscillation, found good agreement between centres of upper- level divergence and areas of convection inferred from OLR data. They found upper tropospheric cyclones to the east of the convection and anticyclones alongside or west of convection. Murakami (1987, 1988), investigating teleconnection patterns during eastward propagation phase, indicated that a succession of upper level cyclonic and anticyclonic disturbances develop over both the northern and southern subtropics mainly downstream of the convection anomalies, while at 850mb, strong 30- 60 day meridional wind anomalies surge from cold mid- latitudes.

According to Chen and Tzeng (1990), for intraseasonal oscillations to occur, positive (negative) precipitable water anomalies and negative (positive) OLR couple with the convergent (divergent) centre of the potential function of the water vapour transport anomalies and the divergent (convergent) centre of the upper- level divergent circulation anomalies. Chen and Yen (1990) also obtained similar results between centres of upper-level divergence and vertical differential heating anomalies of intraseasonal oscillations.

Composite ISO life cycle studies suggest that the equatorial Indian Ocean is the most favourable geographic location for the development of low- frequency convection anomalies. Besides the warm ocean surface condition, the interaction between Walker circulation and transient intraseasonal disturbance and the interaction between monsoon circulation and equatorial intraseasonal mode may be important factors in determining favoured locations for convective development. Interaction between the tropics and extratropics, evidenced by equatorward meridional flow, may activate equatorial convection in those favoured regions (Murakami 1987, 1988).

Wang and Rui (1990b) observed that the development of an intra- seasonal OLR minimum (a measure of deep convective activity) occurs in the equatorial Indian Ocean and Western Pacific with a composite rate of intensification of about 15 W m^{-2} $pentad^{-1}$, corresponding to an e- folding (collapsing) time of the order of 5 days (Rui and Wang, 1990a). After crossing the date line where the SST drops below 27.5°C, the intraseasonal convection anomalies tend to decay rapidly. 28°C is a plausible critical (threshold) SST for the development of tropical intra- seasonal modes.

Jury et al. (1991), identified transient convective waves in the SW Indian Ocean that moved westwards (eg. 1970, 1972, 1974, 1976, 1977, 1981), were quasi- stationary (eg. 1971, 1975, 1978, 1979, 1982, 1983, 1984) and eastwards propagating (eg. 1980). Subsequent climatological statistics for 47 transient convective waves in the 10- 20°S latitude band indicated a lack of homogeneous zonal propagation, implying a wide range of convective structures. They also noted that convective systems from hovmoller INSAT IR imagery composites in the subtropical latitude bands, for February 1986 and 1988, appeared to be patchy, short- lived and quasi- stationary. In Lindesay and Jury (1991), Meteosat composites indicated three westward moving convective waves crossed into southern Africa from the Indian Ocean and dissipated near 20°E, 25°S causing extensive flooding. The tropical convective disturbances were steered westwards by the subtropical ridge located to the southeast of Africa near 40°E, 35°S .

Recently, Levey (1993), studied hovmoller patterns of some tropical meteorological variables between 1987 and 1992, inclusive. Of the systems either extending at least 60° of longitude or whose anomalies lasted at least 20 days, 50% propagated eastwards, 21% were stationary, 18% had ambiguous patterns and the rest (12%) were propagating westward. This implied a 4:1 ratio of eastward versus westward movement in the tropics. The results partially agreed with the findings of Wang and Rui (1990) who observed 63% of systems travelling eastward as compared to 12% going westwards.

Regarding vertical structure, fluctuations of the zonal wind at 850 hPa are nearly out of phase with that at 200 hPa. This confirms conclusions derived from previous cross-spectral and EOF analyses (e.g., Madden and Julian, 1972). Also, amplitudes of zonal wind fluctuation are unequal at upper and lower levels: rather, the amplitude at 200 hPa is about twice that at 850 hPa. The zonal wind fluctuation in the mid-troposphere is asymmetric, with the upper- level fluctuations dominating and determining mid-tropospheric vertical motion. Since rising motions in the tropics are nearly coincident with

negative OLR anomalies, the anomalous rising motion is nearly in phase with 200 hPa divergence and convection anomalies. At the same time, the low- level convergence centre is not found directly underneath the upper-level divergence. Instead, it is either located at the leading edge of the convection region or there is significant low- level convergence to the east of the convection centre. The convection is situated in the low-level westerlies with maximum westerly winds behind it. Lau et al. (1988) made composites of the structure of the intra-seasonal mode based upon primary EOF components that shows a general tendency of westward tilt of the upward motion. Wang (1988a), Wang and Chen (1989) and Hayashi and Golder (1993) attributed this feature to boundary layer convergence due to frictional effects.

Other important findings include the following;

- Madden and Julian (1971, 1972) observed that, in the tropics, the 30- 60- day zonal wind anomalies in the lower troposphere were completely out of phase with those in the upper levels. Mobile Walker cell anomalies were implicated.

- Lau et al. (1990) found that the low latitude zonal wind and OLR have strong spectral peaks in the 30- 60 day time scale range. They found that strong zonal wind fluctuations at 50 days are associated with the expansion and contraction of low level sub- tropical easterlies and the north/ south migration of upper level subtropical jet streams.

- A seesaw -like phenomenon exists in the 30-60 day oscillation between the Indian and Pacific Oceans (Lau and Chan, 1986; Weickmann and Khalsa, 1990; Zhu and Wang, 1993). Lau and Chan (1986), analysing OLR data between 1974 and 1984, noted that 40- 50 day oscillations appeared as a family of waves pulsating eastward and originating from the western Indian Ocean. The waves moved towards the central Pacific Ocean where they "vanished" upon reaching the International date- line. In other words, there appears to be a shift in the convection from the eastern Indian Ocean to the western Pacific. How this occurs is still being debated upon. However, according to Zhu and Wang (1993), the convective systems originate and amplify in the equatorial Indian Ocean, propagate slowly eastwards and terminate in the South Pacific. During this process, it is observed that Mexican and South Asian anticyclones experience fluctuations in sympathy with the oscillation (Magana and Yanai, 1990).

It is apparent from the above that there is as yet no generally accepted explanation for the generation of the ISO. The research is often subjective and selective. It is still unclear whether the ISOs are only of tropical origin or whether they show extratropical variability and forcing as well. Momentum studies (Lau and Phillips, 1986; Risbey and Stone, 1988; Dickey et al., 1991; Ghil and Mo, 1991; Gutzler and Madden, 1993) indicate the meridional nature of the oscillations, implying tropical-extratropical energy transfer. The role of the oceans (upwelling and thermocline effects, for example) and the ocean-atmosphere interface has not yet been thoroughly investigated. This may explain and account for some of the problems of incompatibility between observations and proposed theories.

Hayashi and Golder (1993) provide a detailed review of some of the theories of ISOs stating problems associated with their applications. These include viscous gravity-wave theory with regard to the vertical structure (Chang, 1977), thermal-forcing theory (horizontal structure and propagation), wave-CISK theory (periodicity and wavenumber structure through conditional heating) and evaporation-wind feedback instability theory (Neelin et al., 1987; and Emanuel, 1987) which indicates that convective heating is proportional to both moisture convergence and evaporation.

Inferences on ISO causation have been based upon statistical studies with less effort on the physical mechanisms to substantiate them. Therefore, these analyses have difficulties in, for example, describing characteristics of the oscillations in their formative, developmental, mature and dissipative stages (Rui and Wang, 1990a). More theoretical studies accompanied by numerical models with realistic parameterisation schemes are needed. These should consider the effect of differential heating due to land-sea distribution and topography, and diabatic as well as diurnal heating on the thermodynamics of the boundary layer. They should take into consideration that circulation systems associated with ENSO episodes can significantly influence characteristics of selected case studies leading to varied conclusions. Kuma (1990) observed that the strength of the 40- 50 day oscillation was modulated by the stratospheric QBO in that it was strongest (weakest) during the east (west) phase of the QBO. The QBO variation has also been hypothesised as a plausible mechanism for the onset of ENSO events (e.g. Lau and Chan, 1988; Knaff et al., 1991; Gray et al., 1991).

In spite of diverse theories currently offered, there is general unanimity that ISOs are part and parcel of tropical general circulation and tropical- temperate linkage. The ISOs dominate tropical variability (Schubert and Park, 1991). This thesis has refrained from considering theories of ISOs as they are deemed to be beyond its scope. Instead, it recognises their existence and investigates the roles ISOs play in shaping the seasonal cycle of southern African rainfall. The evidence that ISO preferred locations include the equatorial Indian Ocean (which has been found to be directly linked to the Southern African summer rainfall) necessitates the need for further research, this time at synoptic scale time frames.

Chapter 3

Temporal and Spatial Aspects of Zimbabwe Summer Rainfall

3.1 Introduction

This chapter focuses on climatic variability with respect to Zimbabwe. Current perceptions and scenarios of southern Africa climate are largely based upon regional analyses. While this has merit, the area- averaged rainfall used (Matarira, 1990; Rocha, 1992, for example) has not been assessed or tested for representativeness at national levels. This is especially the case with regard to teleconnectivity studies, where conclusions have often not been substantiated by observations at sub- regional levels. Consequently, not being country-specific, the results have not been utilised for operational medium- or long- range weather forecasting in the countries comprising the region of study, including Zimbabwe.

To address the above concerns, Zimbabwe data is used as a sample for southern Africa. Similar work has already been done for South Africa (Lindesay, 1988; Walker, 1989; Rocha, 1992; Pathack, 1993). Procedurally, the process firstly looks for and identifies distinctive features of Zimbabwe summer rainfall, e.g. trends, cycles, periodicities, seasonal patterns. It then reviews relationships between Zimbabwe seasonal rainfall and other phenomena, revealing and quantifying, where possible, relationships between the variables: El Nino, SOI, SST, QBO, OLR and horizontal wind. Finally, the chapter proposes a conceptual model for operational long- range weather prediction, a model which can be adopted and adapted by the rest of Southern Africa.

It is not essential to the goals of this chapter to attempt to explain the mechanisms responsible for the observed links between the regional teleconnections and Zimbabwe summer rainfall. The mechanisms are not peculiar to Zimbabwe alone and research in this area is continuing. Therefore, unless absolutely necessary and to avoid duplication, emphasis on cause and effect amongst the parameters under study is minimised.

Zimbabwe is a landlocked country extending from approximately 16 to 22°S, a north-south extent of about 750 km. The east- west extent is 25 to 33°E. The eastern boundary is just under 200 km from the Mozambique Channel. The lowest areas of the country are in the extreme south where the elevation is less than 300 m above sea level. Along the

eastern border are mountains which exceed 2 000 m in places. The central parts of the country are comprised of a central watershed divide, oriented SW- NE with an average height of nearly 1 400 m. Another ridge, oriented NW- SE, extends from the eastern highlands and meets the central ridge in the vicinity of Harare, the capital city of Zimbabwe.

3.2 Data and sources of data

The summer season in Zimbabwe is defined as occurring from October of one calendar year to April of the next. This period is not only significant to Zimbabwe, but the whole sub-region (Lindesay, 1988; Lyons, 1991; Rocha, 1992; Jury et al., 1992).

3.2.1 Rainfall data

To understand the temporal behaviour of rainfall in southern Africa, monthly totals from November to March were obtained from 30 Zimbabwe stations. The rainfall data were quality controlled using standard WMO procedures. Thus, all stations had a continuous record, used the same type of raingauge and most sites remained unchanged. A rainfall index was computed by averaging time series of standardised departures for each month for each station and then obtaining the seasonal (summer) departure from sum of the monthly departure values. The anomalies so obtained had the season removed to enable corresponding periods to be compared. For purposes of temporal analysis, 15 stations were available over the period 1900- 1992. For spatial correlation analyses, all 30 stations with data from 1951 were used. The station rainfall data were inter- correlated and from the cluster analysis, 9 stations in the north of the country were selected. These lie in the main agricultural districts of the country. The 9 individual station time series were inter-correlated at values above +0.8 and so can be considered to lie in a relatively homogeneous climatic zone. In addition, the 9, 15, 30 station area indices were highly correlated and may be considered intrechangeable. Hereafter, these area averaged seasonal rainfall indices are referred to as the Zimbabwe Rainfall Index (ZRI).

3.2.2 EL Nino/ Southern Oscillation (ENSO) data

ENSO data were extracted from Ropelewski and Jones (1987), where high (low) ENSO years were defined as those years during which the Tahiti-Darwin SOI remained in the upper (lower) 25% of the distribution for five months or longer.

High (or warm) ENSO years were identified (according to the onset year) as

1888 1896 1900 1905 1911 1912 1914 1918 1919 1923 1925 1930 1932 1940 1941 1946 1951 1953 1957 1965 1969 1972 1977 1982 1987

Conversely, low (cold) ENSO years were defined as those years during which the SOI remained in the lower 25%. These were

1886 1889 1892 1904 1909 1910 1915 1917 1924 1928 1938 1950 1955 1956 1964 1970 1971 1973 1975

The dataset was then upgraded to include the period 1988- 1992. In this regard, the 1991 summer was incorporated into the high ENSO category.

3.2.3 Sea- surface temperatures (SST)

SST data were utilised from the Comprehensive Ocean-Atmosphere Data Set (COADS) as monthly averages on a 2x2 degree grid globally for the period 1951- 1989. This data set was used despite having a non-uniform data density in the southern oceans, including the Indian Ocean. Details pertaining to the methods of and criteria for the compilation of COADS data have been discussed at length by Barnett (1984), Slutz et al. (1985) and Jones et al. (1986). Woodruff et al. (1987) indicates that the preparation and quality control of COADS makes it as representative as possible.

Some pre- processing of the SST data was carried out. The procedure is described in detail by Rocha (1992). First- order statistics (means, standard deviations, etc) were computed at each grid point for monthly data of the period in question. Monthly anomalies were next determined, again at every grid point, using standard procedures (as algebraic differences between the individual months and the climatological monthly mean). Any missing values were replaced by simple arithmetical averaging of neighbouring grid points. To further reduce noise, some smoothing was carried out at each grid point by, firstly, averaging as many non- missing values in a 6°x6° box (ie, up to 9) as available and then replacing the centre value with the smoothed one. Seasonal values of the SST were created by averaging three- monthly data at each grid point, i.e., December, January and February (DJF), etc. The objective was to create SST fields at lag periods of -9, -6, -3 and 0 months in relation to summer rainfall, where 0 lag refers to January.

3.2.4 SOI, Wind, OLR and QBO

SOI data were provided by the Australian Bureau of Meteorology as algebraic differences in pressure between Darwin (12.5°S, 131°E) and the Pacific island of Tahiti (17.5°S, 210.4°E). Pressure is used as it is sensitive to relatively basin- scale fluctuations of climate. This data set is operationally used by its National Climate Centre. The index is a useful indicator of ENSO variability (Chen, 1982) and has been applied in southern African studies (Lindesay, 1988; Matarira, 1990; Rocha, 1992). The data prior to 1933 were suspect and eliminated during quality controlling.

The remaining data (wind, OLR and QBO) were obtained from the Climate Analysis Centre (CAC), Washington DC, USA. The horizontal wind data were available as zonal (u) and meridional (v) components at 1000, 850, 700, 500, 300 and 200 hPa. The time series varied, with the lowest levels having comparatively shorter periods. Data for 1000 hPa (850 hPa) was available from December 1975 (1974) to February 1987. The data for remaining pressure levels is from March 1968 to February 1987. Details regarding the determination of raw wind data, quality control and interpolation schemes are not deemed essential here but are available in Pathack (1993). The resolved wind components were produced on a Mercator grid projection.

OLR data were also provided by CAC in the same format as wind, obtained originally from the Advanced Very High Resolution Radiometer (AVHRR) on NOAA satellites. The period covered by the data was June 1974 to February 1987. There was missing data in 1978 between March and December due to satellite failure. It was indicated in Chapter 2 (and by Heddinghaus and Krueger, 1981; Liebmann and Hartmann, 1982, among others) that OLR can be used to infer convective regions in the tropics and is assumed to be related to cloud- top temperatures. Section 2.2.1.4 also noted situations when the proxy fails to hold and specifically in areas where there is cirrus (upper level cloud) contamination. For example, at high latitudes where the mid- latitude jet stream is strong, high level cloud persists.

The stratospheric Quasi- Biennial Oscillation (QBO) data was available as 30 hPa zonal wind departure over Singapore. More details about the QBO have been discussed in Chapter 2 (Section 2.2.1.3).

3.3 Methods of Analyses

The rainfall data and the temporal indices were all normalised appropriately with respect to the means and standard deviations, a usual procedure to remove annual and seasonal cycles. The rainfall time series was adjusted according to period of data availability of the other parameters. The parameters were firstly subjected to time series analyses using the Statgraphics package version 4.0. Regarding rainfall, an area- averaged rainfall was determined using 15 stations with data from 1900/01 summer season as previously outlined. Inter- comparisons were then made between rainfall and the other indices. A contingency table was made using the Zimbabwe seasonal rainfall and ENSO years from 1901 to present. For this, the 1991/92 drought year was added to the Ropelewski and Jones (1987) ENSO data. The ENSO years were classified into three categories, namely high ENSO (El Nino), low ENSO (La Nina) and neither (remaining years). The rainfall had a similar classification: excess rainfall, drought and normal seasons. A drought (wet) season was defined as when seasonal rainfall was below (above) one standard deviation from the long-term mean. Otherwise the season would be classified as normal.

The SST field and SOI monthly anomalies were grouped into three-monthly overlapping averages. Preliminary analyses included all the months of the year. Spatial point-to- field correlation maps were computed with Zimbabwe rainfall at lags from years to months using the Statgraphics PC Version 4 package. The Pearson's product moment linear regression technique was applied. Correlations were analysed for the entire global domain, but results are presented for key areas surrounding Africa. For the SST, SOI and QBO, correlations greater than ±0.3 are significant at the 95% confidence limit. Regarding the CAC wind and OLR correlations, the limited degrees of freedom necessitate that coefficients should exceed ±0.4 and ±0.5, respectively, to be considered statistically significant. The correlation maps were contoured using objective analysis, except for winds, where the coefficients for u and v were re- combined to form vectors (**see annexure 2**) for easier interpretation.

3.4 Results

3.4.1 Cyclic signals in Zimbabwe seasonal rainfall data

Figure 3.1 shows a time series analysis of Zimbabwe's area- averaged seasonal rainfall from 1901/02 to 1991/92, inclusive. The linear trend is superimposed. The pattern illustrates a high year to year variability. Drought years, defined as when the Zimbabwean summer rainfall is $\leq$ 1 times the standard deviation below the long-term mean include 1912, 1914, 1916, 1922, 1924, 1947, 1960, 1964, 1968, 1973, 1982, 1983, 1984, 1987 and 1992 (In this case, the year in question is centred on January). Of these, the 1991/92 rainfall season was the worst, followed by the drought of 1946/47. During the same period, and by using the converse definition of the above for abnormal rainfall, the country had excess rainfall in 1901, 1914, 1917, 1922, 1924, 1928, 1938, 1952, 1954, 1973, 1977 and 1980. The return interval is more widely spaced compared to drought years, especially since the middle of this century.

Visual inspection of the pattern indicates a cyclic fluctuation from the 1920's with troughs around 1931, 1946, 1964 and 1983 and peaks in 1937, 1954 and 1974. This suggests a cycle periodicity of 17- 19 years, implying roughly a 9- year change from peak to trough. Also significant is the apparent increase in the amplitude of the interannual cycle, implying that floods and droughts are becoming more severe. This is in partial agreement with the findings of Jury et al. (1992) who observed that wet summers over South Africa and Botswana were getting wetter.

The trend analysis of 91 years of areally averaged summer rainfall shows that, apart from large interannual variability, Zimbabwe rainfall is on the decline. The linear equation of change is given by:

$$\mathbf{R = 698.0 - 0.8*T},$$

where R is the rainfall (mm) and T is the number of years after 1901.

The trend indicates a reduction of approximately 100 mm since the turn of the century, a result confirmed by quadratic and exponential analyses (not shown). The reduction is more pronounced at station level.

Spectral analysis of summer rainfall time series (**Figure 3.2**) reveals, in order of decreasing spectral power, periodicities of 2.3 years closely followed by the 18.0 year cycle. Two

other significant modes can be noted, namely 2.7 and 3.8 years. A number of other periodicities are noted in the two to five year range. The 2.3- year cycle has only recently been identified in southern Africa rainfall and linked with the quasi-biennial oscillation (QBO) of stratospheric zonal winds (Mason, 1992) and to the tropospheric biennial variability of the Southern Oscillation (Ropelewski et al., 1992). Several studies (eg., Rasmusson and Carpenter, 1982; van Loon and Shea, 1985; Deser and Wallace, 1987; Ropelewski and Halpert, 1987, 1989) have identified a roughly 2- year cycle within the El Niño/ Southern Oscillation (ENSO). The biennial cycle influences Zimbabwe summer rainfall (**Figure 3.1**), especially during relatively wet periods as evidenced by the frequent 'M' shape of the unsmoothed area- rainfall time series.

The presence of the 18- year cycle confirms previous research findings regarding southern Africa rainfall. Tyson (1986) cited many papers giving evidence of 18- and 10- 11- year oscillations in rainfall and other parameters. Jury et al. (1992), using spectral analysis of the Southern Africa Rainfall Index (including Zimbabwe data), showed a major peak at 18.8 years with minor peaks at 2.3 and 4 years. In the Zimbabwe spectra (**Figure 3.2**), the 18-year cycle is subordinate to the 2.3- year cycle. Currie and O'Brien (1988) have cited literature on the 18- year cycle and contend that it is due to a resonant, quasi-standing wave in the atmosphere as a consequence of luni- solar tidal action. The tide is due to the moon's plane of motion inclined at a mean angle of 5° 09' to the elliptic at approximately 0.053° per mean solar day, thus making a complete revolution in 18.61 years (Doodson and Warburg, 1941; Pugh, 1987). Currie (1993), using South Africa rainfall at various locations, also observed the forcing functions of luni- solar tidal influence with periodicities of 18.6 and solar- flux sunspot cycle at 10- 11 years.

According to Currie and O'Brien (1988), epochs/ dates of tidal maxima in this century were 1917.5, 1936.1, 1954.7 and 1973.3. These dates were approximately coincident with tree- ring data of Hameed and Currie (1986) in the USA. When compared with seasonal rainfall in Zimbabwe, these epochs coincided with periods of heavy rainfall (**Figure 3.1**). Thus, it can be inferred that, barring the effects of other weather parameters, the next peak is in the early to mid 1990s (1992/93- 1994/95 seasons), implying increased rainfall over southern Africa, especially Zimbabwe, during this period. The 3.8- year cycle, also observed in South Africa rainfall, can be attributed in part to the El Nino (**Section 3.2**). The SOI, for example, exhibits similar spectral peaks at 4 and 18 years.

3.4.2 El Nino/ Southern Oscillation (ENSO) and Zimbabwe Rainfall

Table 3.1 is a contingency table indicating the association between extreme ENSO years according to Ropelewski and Jones (1987) and extreme rainfall years in Zimbabwe. High (low) ENSO years were defined as those years in which the Tahiti- Darwin SOI remained in the upper (lower) 25% of the distribution for five months or longer. Statistically, extreme ENSO years (either high or low) recurred every 4 years. Successive years of extreme ENSO events are rare. Reference to Table 3.1 shows that, among other observations:

- Droughts in Zimbabwe are more associated with high ENSO (El Nino) events than with low events. This is in agreement with previous research findings for south-eastern Africa. They occur simultaneously with high ENSO years in 53% of the cases compared to only 14% with low ENSO years. Also droughts and extreme ENSO (both high and low) episodes are related in 67% of cases.

- At the same time, years with excess seasonal rainfall coincided more with low phases of ENSO (La Nina events) than with the high phases. However, the association was just 50% of the total cases compared to 33% with high ENSO years.

- In 33% of cases, droughts in the country have occurred in the absence of both high and low ENSO events. Hence, other factors play significant roles in determining the rainfall patterns in Zimbabwe.

- The association between high ENSO events and extreme rainfall occurrences (both excess rainfall and drought seasons) accounts for 12 out of 25 cases (48%). Even more significant is the observation that El Nino events have coincided with normal rainfall seasons in 52% of the cases.

- Similarly, low ENSO episodes appear to be related to extreme rainfall events in 44% of the cases, and to 56% of the cases during normal rainfall seasons.

	Wet Season	Drought Season	Normal season
El Nino Year	1914, 1922	1911, 1923, 1946	1912, 1918, 1919, 1925
(High ENSO)	1952, 1977	1972, 1981, 1982	1930, 1932, 1940, 1941
		1986, 1991	1951, 1957, 1965, 1969
La Nina	1917, 1924	1915, 1963	1904, 1909, 1950, 1956
(Low ENSO)	1928, 1938		1964, 1970, 1971, 1975
	1954, 1973		1988
Neither	1901, 1980	1913, 1921, 1959	Remaining Years (44)
		1967, 1983	

Table 3.1: Contingency Table showing occurrences of extreme rainfall in Zimbabwe, El Nino (High ENSO) and La Nina (Low ENSO) events from 1901 to 1992. All dates are according to onset year.

3.4.3 The Southern Oscillation Index (SOI) vs Zimbabwe rainfall

Regressions between normalised seasonal rainfall in Zimbabwe and SOI on monthly and annual bases, including lags, yielded weak relationships. Correlations were then carried out between the seasonal rainfall and 3-month average SOI values. The results are shown in Table 3.2. The greatest correlation between rainfall over Zimbabwe and SOI is only +0.33 and for the August- October period. This period is approximately two months prior to the onset of the main rains. September-November and October-December SOI values are almost equally related to the rainfall. The correlations account for about 11% of the variance, suggesting that other precursor indices and phenomena, collectively more important than the SOI, should be investigated to determine factors governing the variability of Zimbabwe rainfall.

SOI Period	r^2 x 100	Corr Coeff	Lag (mths)
January - March	10.5	0.32	- 11
February - April	2.5	0.158	- 10
March - May	2.7	0.164	- 9
April - June	3.7	0.192	- 8
May - July	5.4	0.232	- 7
June - August	8.3	0.254	- 6
July - September	10.1	0.318	- 5
August - October	10.9	0.330	- 4
September - November	10.5	0.324	- 3
October - December	10.5	0.324	- 2
November - January	10.0	0.316	- 1
December - February	9.1	0.302	0

Table 3.2 : Lag correlations between seasonal rainfall in Zimbabwe and period-averaged SOI for the period 1951-1992, inclusive.

3.4.4 Station Rainfall versus August- October (ASO) SOI

The August-October averaged SOI were correlated with mean monthly (from October to April) rainfall and seasonal (October- April mean) rainfall for 26 stations in Zimbabwe. The objective was to demarcate those areas according to their responses to the fluctuations of the SOI both in time and space, results of which are shown in **Figure 3.3**. Summer rainfall in the country is more related to the SOI along and to the north of the central watershed than anywhere else in the country. The two parameters were least correlated over the extreme west.

Halpert, 1987; Lindesay, 1988; Matarira, 1990; and Rocha, 1992) which generally indicated that the strongest correlations were over the southern parts of Mozambique and Zimbabwe, as well as northern South Africa. The difference can be attributed to many factors: period of study, data resolution, data selection (number of rainfall stations) and SOI format, all which have a bearing on representativeness. To substantiate this point, SOI averages for ASO (August, September, October), SON, OND and NDJ periods were analysed for periodicities for the period 1933-1992. The results are tabulated in **Table 3.3**

Period	Major cycles of period- averaged SOI (in order of decreasing importance)		
ASO	**4.14 yrs**	**2.42 yrs**	**6.44 yrs**
SON	**4.14 yrs**	**2.42 yrs**	**19.3 yrs**
OND	**19.3 yrs**	**4.14 yrs**	**2.5 yrs**
NDJ	**5.8 yrs**	**19.3 yrs**	**4.14 yrs**

Table 3.3: Major periodicities of the period- averaged SOI between August and January from 1933 to 1992, inclusive.

The 4.14 -year (49.7- month) cycle of the SOI carries most weight as regards inter-annual variability of rainfall. The next cycle in importance is that of 2.4 years (29 months). The first cycle could be attributed to the ENSO phenomena while the later could be its quasi-biennial oscillation similar to that of Ropelewski and Halpert (1992). A minor cycle of 2.2 months or its multiple was also apparent. Though minor, it has a noticeable impact on the spatial distribution of the correlations between monthly rainfall and the SOI. The spatial correlation patterns are oriented SW-NE across Zimbabwe and propagate from the southeast of the country to the northwest as the season progresses.

The relationships between the SOI and rainfall in the region have been studied before. Lindsey (1988), for example, using South Africa rainfall, found correlations of +0.3 at zero lag at different times of the year at different stations. The correlations were highest in a NW- SE band extending across 25- 30°E. The research also confirmed that the high phase of the SOI was associated with increased rainfall. Torrance (1990), comparing SOI anomalies with Zimbabwe seasonal rainfall, noted that positive values of the SOI coincided with rainfall of 101- 125% of normal. Negative values occurred generally with rainfall below normal. These observations are in agreement with those mentioned in **Section 3.2.1**, that high (low) ENSO events and above (below) normal rainfall occurrences were associated about half the time. Matarira (1990) used area- averaged rainfall for Zimbabwe, Zambia, Botswana, Mozambique, Northern South Africa, Malawi, Angola and Namibia. Zero to +1 year lag correlations (SOI leading) were +0.3 to +0.42, respectively, suggesting droughts occurred in years during and after the El Nino. Rocha (1992), investigating rainfall for Southeast Africa, observed that only the southern- most areas (which included the extreme southeast Zimbabwe) correlated significantly with SOI (+0.4). Elsewhere, the correlations were +0.2 or less. The study also indicated that stronger associations were found when the SOI led rainfall by about four to five months.

3.4.5 Sea Surface Temperature vs Zimbabwe rainfall

Figures 3.4 and **3.5** are correlations between seasonal rainfall in Zimbabwe and Indian Ocean SSTs at lags from -9, -6, -3, and 0 months, which refer to MJJ (May/June/July), JAS, SON and DJF, prior to the onset of and during the rainy season. The correlation structure is dominated by negative (positive) values in the central (south) Indian Ocean. At -9 months (**Figure 3.4a**) rainfall is positively correlated with SSTs in the South Indian Ocean ($r = +0.42$ near 5-10°S, 70°E) and negatively correlated ($r = -0.39$ in the region 20-25°S, 70-75°E) in the central Indian Ocean. The N- S dipole in the Indian Ocean is maintained at -6 months lag with negative anomalies in the equatorial regions and positive anomalies to the south. The correlation values increase relative to -9 month lag, and values of -0.53 are found in the central basin. The correlation values in the preceding July reach statistical significance at the 95% confidence limit within the region 5°N-20°S, 50-90°E.

At -3 month lag (**Figure 3.5a**), the highest correlations are in the central Indian Ocean (with r = -0.56 at about 8°S, 60°E), covering a much wider area compared to previous months. A small region of positive correlations is found near Indonesia (+0.52, 10°S, 100 °E) and a larger one in the southwest Indian Ocean. By zero lag, the negative association between Zimbabwe rainfall and SST in the central equatorial Indian Ocean has weakened. The zone of positive correlations in the sub-tropics to the south of Madagascar has moved westwards towards the southeast African coast and strengthened ($r > +0.40$) over the area 10-35°S, 30-50°E.

From the correlation analyses, SST in the Indian Ocean from the Equator to 10°S between 60 and 70°E, some 3 to 6 months prior to the austral summer, offer useful forecast guidance. Pathack (1993), using a southern Africa rainfall index, obtained r = -0.6 at lags -3 to -4 months with central equatorial Indian Ocean SSTs. The correlation implies that negative (positive) SST anomalies foreshadow seasons of above (below) normal rainfall in Zimbabwe. How the teleconnections occur is still unclear, although thermocline perturbations, upwelling and ocean currents linked with atmospheric circulation and convection as well as the ENSO phenomena are implicated.

Correlations between Zimbabwe seasonal rainfall and SST in other basins are relatively weak. This suggests that the Atlantic and Pacific Ocean SST have little bearing on rainfall in Zimbabwe. Mason (1992) analysed sea surface temperatures in the Atlantic Ocean and southern African rainfall, reached a similar conclusion, as did Rocha (1992), and confirmed earlier results of Walker (1989, 1990). Pathack (1993) determined that central Atlantic SST are positively correlated only with early summer (November) rainfall over central South Africa. The Atlantic Ocean SST correlation changes sign for late summer rainfall.

3.4.6 Rainfall and Outgoing Longwave Radiation (OLR)

Major zones of convection in the tropics, hence regions of potential precipitation, have been associated with low OLR (Riehl, 1979; Gadgil and Guruprasad, 1990). Jury et al. (1993) have determined that summer rainfall anomalies over southern Africa are -0.93 correlated with OLR over the period 1975- 1987. This implies that OLR may be a useful

proxy for summer convection. It has also been observed that regions of high precipitation, hence low OLR, are associated with regions of above normal SST (Bjerknes, 1969; Liebmann and Hartmann, 1982; Gill and Rasmusson, 1983; Neelin and Held, 1987), although the relationship varies from place to place (Jury and Pathack, 1991). In the tropics (and during summer in the sub- tropics), OLR values are strongly influenced by cloudiness and vary directly with cloud- top temperature and cloud depth. Regions of intense and/ or frequent convection, such as those associated with the ITCZ appear as regions of low OLR. At the same time, cloudless sub- tropical trade wind regions, which are characterised mainly by subsidence activity, are associated with relatively high OLR values. Because of these properties of OLR data, precipitation estimates have been made over otherwise data- sparce tropical oceans (Arkin 1983; Yoo and Carton 1988).

Figures 3.6a,b,c illustrate the correlation of rainfall and OLR at lags -4 (September), -2 (November) and 0 months, respectively. **Figure 3.6a** shows negative correlations over Africa, with higher magnitudes over southern Africa. A northwest- southeast band of negative correlations stretching from the Benguela region to the southwest Indian Ocean is apparent. The -4 month lag (September) pattern suggests sympathy between spring and summer periods. The -2 month lag pattern (**Figure 3.6b**) reveals a positively correlated area in the central Indian Ocean monsoon region roughly along 70°E. Hence, positive OLR anomalies and cooler SST correspond with reduced cloud depth in the central Indian Ocean, and anticipate wet conditions over Zimbabwe. Negative OLR anomalies in the central South Atlantic Ocean also have a bearing on rainfall ($r > -0.6$). The pattern implies a weakening of the Atlantic Ocean Anticyclone and a possible source region for cloud bands responsible for early summer rainfall in western southern Africa, confirming earlier findings (Harrison, 1986; Walker, 1989; Barclay, 1992; Mason, 1992; Pathack, 1993). The 0 lag pattern (**Figure 3.6c**) illustrates a configuration similar to that at lag -4 months over southern Africa. The centre of maximum correlation shifts from the central interior (25°S 20-25°E) in September to the western south Atlantic off the Namibian coast at 0 lag (January). Sympathy with the ZRI is also noted reflecting the deeper nature of convection. Also of note is a negative OLR correlation over the bulge of West Africa. The NW- SE orientation suggests that baroclinic cloud bands contribute significantly to summer rainfall.

3.4.7 Rainfall and horizontal wind

Some of the correlations performed between Zimbabwe rainfall and wind anomalies are shown in **Figures 3.7** and **3.8** for upper (200 hPa) and lower (700 hPa) levels, respectively. At the upper level, highest correlations ($r > 0.7$) are over the equatorial Atlantic and refer to easterly vector anomalies in the preceding spring (September, lag -4, **Figure 3.7a**). These patterns are consistent with the influence of the Southern Oscillation (Section 3.2.2). Hence, a La Nina event is associated with a reduced equatorial penetration of the Atlantic westerly wave in spring, prior to rainy summers over Zimbabwe. The easterly vector anomalies persist until November (lag -2 months, **Figure 3.7b**). In the meantime, southerly vectors across central southern Africa in September are replaced by a cyclonic gyre with westerly vectors between 10 and 20°S and northerly vectors from the south Mozambique Channel polewards. The highest correlations shift to the Indian Ocean where, two months prior to southern wet summer, an anticyclonic gyre to the SE Madagascar controls a southerly wind flow along 70-80°E from about 30°S northwards to the northern hemisphere. Thus, wet summers in Zimbabwe can also be predicted in November by upper level west- southwesterly wind along the Equator to the south of India.

At the 700 hPa level, where moisture transport is a key element, easterly wind anomalies in the south Atlantic poleward of 30°S from 10°W to about 10°E offer another useful forecast reference at lag -4 (**Figure 3.8a**). However, easterly vectors along the Equator between 10°W and the African west coast as well as southerly winds to the southeast of South Africa in November (**Figure 3.8b**) are better indicators of Zimbabwe summer rainfall. At lag 0, (January, **Figure 3.8c**), northwestward wind anomalies are pronounced along the entire eastern seaboard of equatorial Africa, probably inferring that cross-equatorial flow is weaker in rainy years. An anticyclonic anomaly appears just to the south of Madagascar. This circulation gyre yields a poleward flux of surface moist, unstable warm air on its western flank over Zimbabwe, and equatorward fluxes in the South Indian Ocean. Easterly anomalies in wet years are maintained over the south Atlantic.

3.4.8 Rainfall and QBO

Figure 3.9 shows correlations between lagged QBO and the Zimbabwe Rainfall Index using data from 1955- 1990, inclusive. It shows a positive but weak relationship between the two parameters throughout summer. The best correlations are in late summer, the highest being +0.22 for Fberuary to April QBO value. This coincides with a time when the ITCZ and tropical barotropic systems influence Zimbabwe rainfall. Thus, despite the relatively low correlation, the QBO should enhance rainfall when the stratospheric winds are westerly. This is supported by Nicholson (1989) who showed a greater than 90% coherence between Zimbabwe rainfall and the 2.3- year cycle. This relationship is consistent with that found by Ogallo et al. (1993) in comparison with Kenya rainfall. His rainfall contingencies demonstrated that probabilities of large deviations of seasonal rainfall were of the order of 70- 80% when the QBO was in phase with the main rainy season. Recent research by Jury et al. (1994) has determined that upper tropospheric winds are in phase and well correlated with the QBO over southern Africa with a cyclonic gyre over Zimbabwe (20°S, 25- 30°E) and an anticyclonic gyre SW of South Africa.

3.5 Discussion and summary

Significant issues have emerged from this investigation. Firstly, the seasonal rainfall in Zimbabwe is declining and droughts appear ever- more frequent and severe. Analyses of rainfall data at station level has revealed a more rapid decline, implying an inevitable need to review current agricultural practices as well as water conservation and management.

Seasons of extreme weather in Zimbabwe (that is, excess rainfall and droughts) are associated with extreme ENSO years (high and low phases, according to the classification of Ropelewski and Jones, 1987) in 74% of the years of simultaneous occurrence. However, extreme ENSO events have also occurred even when the country was experiencing normal rainfall (52% for high ENSO and 53% for low ENSO). High ENSO is associated more with drought more than otherwise. Conversely, low ENSO years are linked more to those seasons with excess rainfall in Zimbabwe.

Correlations, both lagged and simultaneous, between Zimbabwe's seasonal rainfall and monthly- as well as seasonally- averaged SOI were low and may be unreliable operationally. This implies that the climatic variability of Zimbabwe rainfall cannot be predicted or accounted for solely by fluctuations of the SOI. Other factors, presumably even more significant, should be used. Lagged correlations, the August-September-October (ASO) period being the most signficant, are stronger than simultaneous ones. Regressions (not shown) between ASO and SON SOI values and monthly and seasonal rainfall for selected stations in the country yielded useful results during different months of the year.

Even more revealing is the observation that the correlations vary across Zimbabwe from one month to the next and from station to station. Thus, the response is not confined to areas in the southeastern parts of Zimbabwe. In fact, the greatest responses of seasonal rainfall to the Southern Oscillation are found in the north. During the course of each rainy season regions of high and low correlations progress northwestwards like ripples. This can be attributed to a 2.2- month cycle in the SOI which, in turn, is likely the result of intra- seasonal oscillation influences.

For prediction purposes, the correlation between Zimbabwe rainfall and QBO is too low to produce usable relationships. The forecast contribution of the QBO is, however, more useful when it is combined with spring time values of the SOI and correlated with Zimbabwe rainfall. The correlation coefficient is +0.58. The QBO displays a singular period of 2.3 years (28 months), suggesting a non- stationary relationship with the summer season. Thus, it will only reach an optimum amplitude which is in phase with austral summer about half the time (ie., 3 years on, 3 years off). The positive aspect of the QBO is that it is rhythmic and predictable. Moreover, it is reproduced as the largest peak in the Zimbabwe rainfall spectra, as previously mentioned.

While the apparent cyclicity in rainfall is acknowledged and now well supported, the physical, precursor and triggering mechanisms responsible for linking rainfall with solar and lunar tides, the SST, QBO or SOI, for example, remain to be explained. It is still unclear what ocean- atmosphere coupling processes cause the anomalies. The answer lies in investigating preferred locations, spatial and temporal extents as well as threshold values, as proposed by Graham and Barnett (1987) and Ropelewski et al. (1987). Unique relationships, whether by individual or collective contributions, for precise weather forecasting purposes still have to be determined. Research has shown that, while there is

some form of association between rainfall and regional teleconnections, they may conflict rather than conspire.

Despite the above, summer rainfall in Zimbabwe may be still be predicted using SOI values but with input from the QBO improving the correlation. Present models are sufficiently accurate to anticipate an El Nino episode, although still too crude to predict evolution, intensity and duration. Even if the El Nino were to be predicted, its impact on summer rainfall in Zimbabwe is not consistent but may operate more efficiently once a threshold is exceeded. That threshold needs to be determined.

3.5.1 Predictability of Zimbabwe summer rainfall

Figure 3.10 indicates lagged correlations between standardised departures of Zimbabwe summer rainfall and upper level zonal wind (200 hPa) in the Atlantic Ocean and between rainfall and SST in the central Indian Ocean (Jury, 1994, personal communication). The regions under study are bounded by 5°N, 35°W and 10°S, 5°W in the Atlantic Ocean for the winds and 0°S, 60°E and 10°S, 80°E for SST. The two regions have been found to be best related to Zimbawe rainfall, as mentioned previously. Reference to the figure shows that correlations between the two parameters and Zimbabwe rainfall increase as summer approaches. However, the correlation with Atlantic Ocean upper level zonal wind peaks at lag -3 (around October) while that of the SST does not change appreciably until October before increasing rapidly to -0.6 in November (lag -2). In addition, prior to summer (whose onset normally occurs at the end of November (Chapter 4)), the winds are better correlated with Zimbabwe rainfall than SST.

SST in the central equatorial Indian Ocean remain useful predictors of seasonal precipitation in Zimbabwe. All lag correlations exceed statistical significance in the area 5° N-20°S, 50-90°E. The findings are in agreement with those of Rocha (1992) and Jury et al. (1992). Thus, prior to the onset of a drought in Zimbabwe, warm anomalies occur in the equatorial waters of the Indian Ocean. This was indeed the case in the devastating drought of 1991/92. Jury and Pathack (1993) have indicated that changes in SST in the central Indian Ocean are highly correlated with the eastern Pacific as well as with SOI.

In addition to Indian Ocean SST and equatorial Atlantic upper zonal winds, other climatic determinants include:

- OLR anomalies during September over central interior of southern Africa (centred near 25°S, 23°E),
- September 700 zonal wind anomalies in the south Atlantic Ocean,
- the strength and penetration of the Monsoon over the western Indian Ocean, as found in lag -2 (November) OLR anomalies in the central Indian Ocean, and,
- the phase of the QBO. Westerly (easterly) phase favours (suppresses) rainfall over southern Africa.

Given real-time climatic anomalies, it is possible to predict over half the variance of summer rains in Zimbabwe as early as four months prior to their occurrence. Operationally though, the relationship between Zimbabwe rainfall and regional teleconnections warrants more study. Research has indicated that Zimbabwe rainfall's association with the combined influence of the SOI and QBO is weaker than for central South Africa (Mason, 1992). Using central Indian Ocean SST, Zimbabwe rainfall is more predictable than areas to the southwest. The implication of these differences in predictive potential is that further consideration should be given to spatial variations across southern Africa; after which more realistic advisories can be offered. Further research will be also be necessary to explain the mechanisms of global forcings (i.e., ENSO) and regional teleconnections.

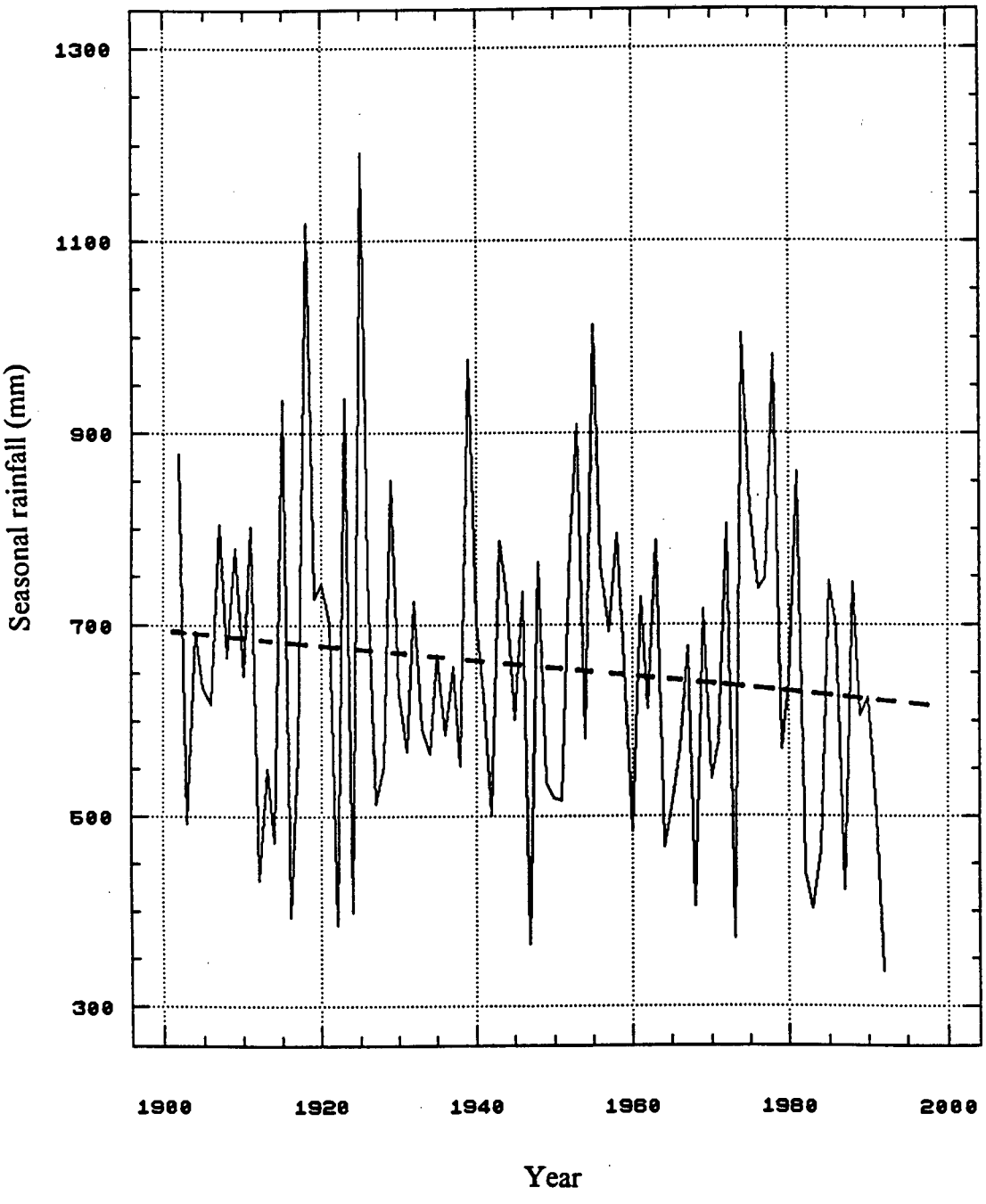

Figure 3.1 : Time series analysis of Zimbabwe's rainfall departures from 1901 to 1992. The linear trend of the rainfall is superimposed.

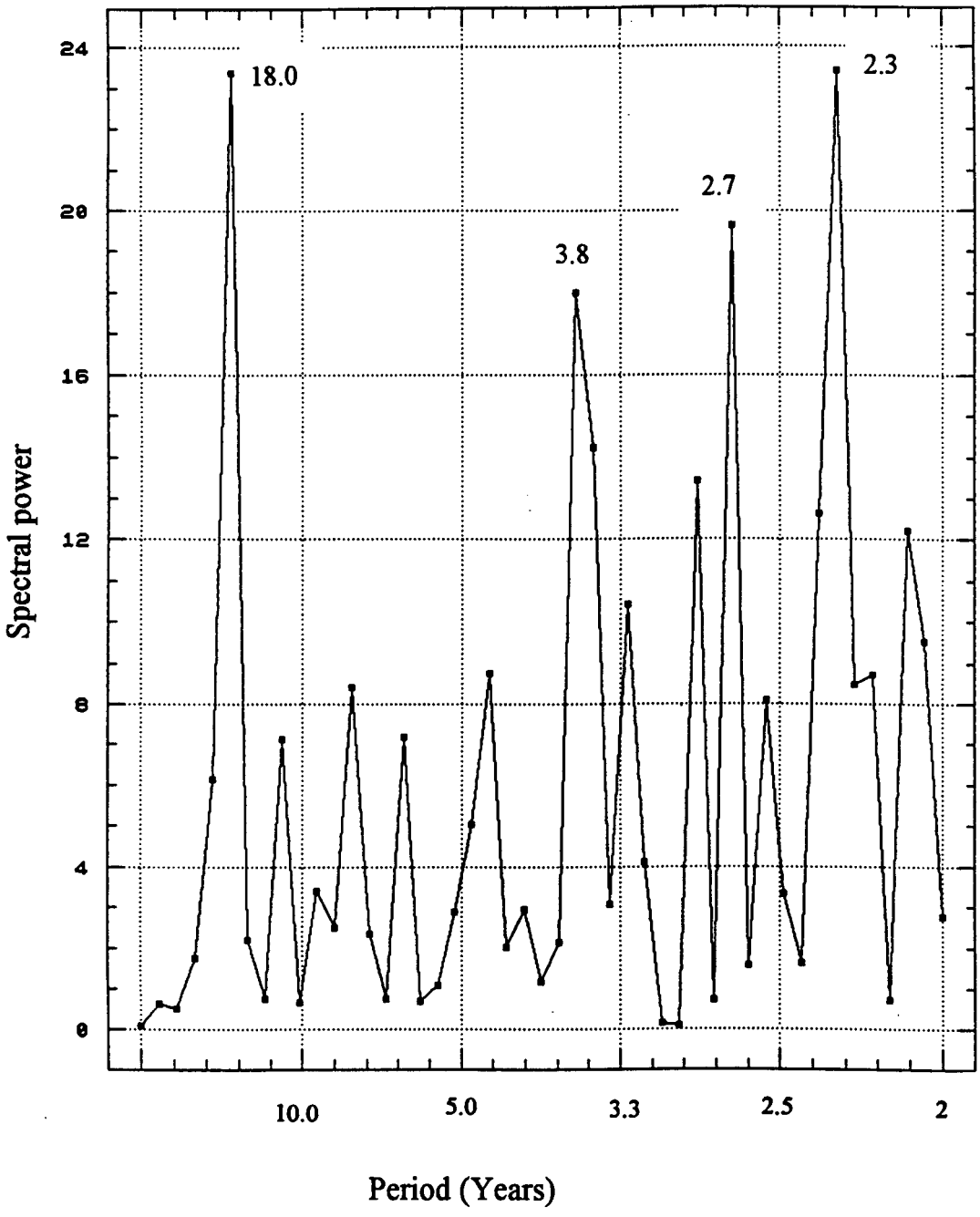

Figure 3.2 : Spectral analysis of Zimbabwe summer rainfall time series. The period is 1901- 1992.

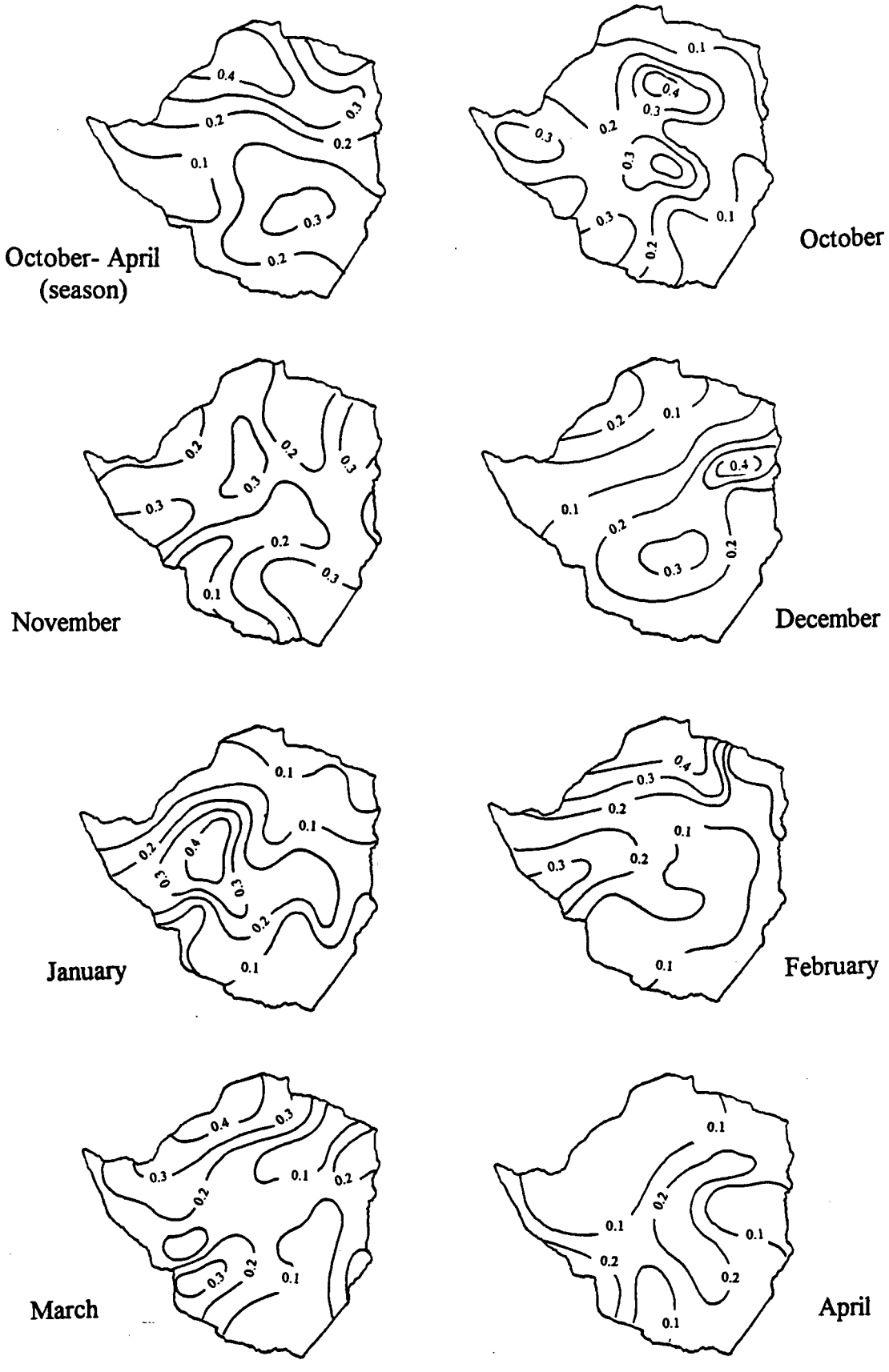

Figure 3.3 : Correlation coefficients between August- October SOI and monthly summer rainfall in Zimbabwe.

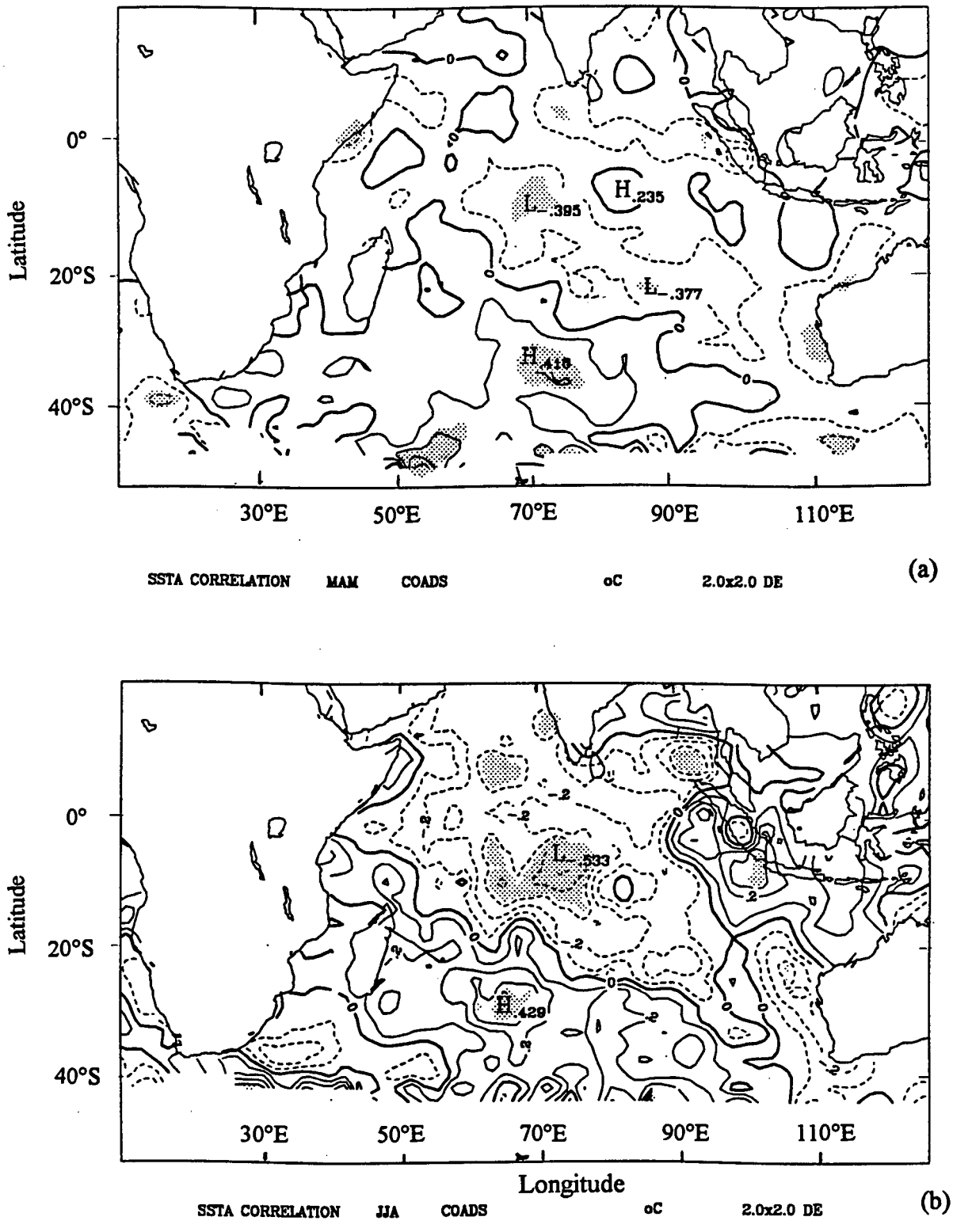

Figure 3.4 : Correlations between November- March Zimbabwe rainfall and the Indian Ocean SSTs at lags -9 (a) and -6 (b) months. Contour interval is 0.1°C. Stipling illustrates correlations significant at 5 significance level.

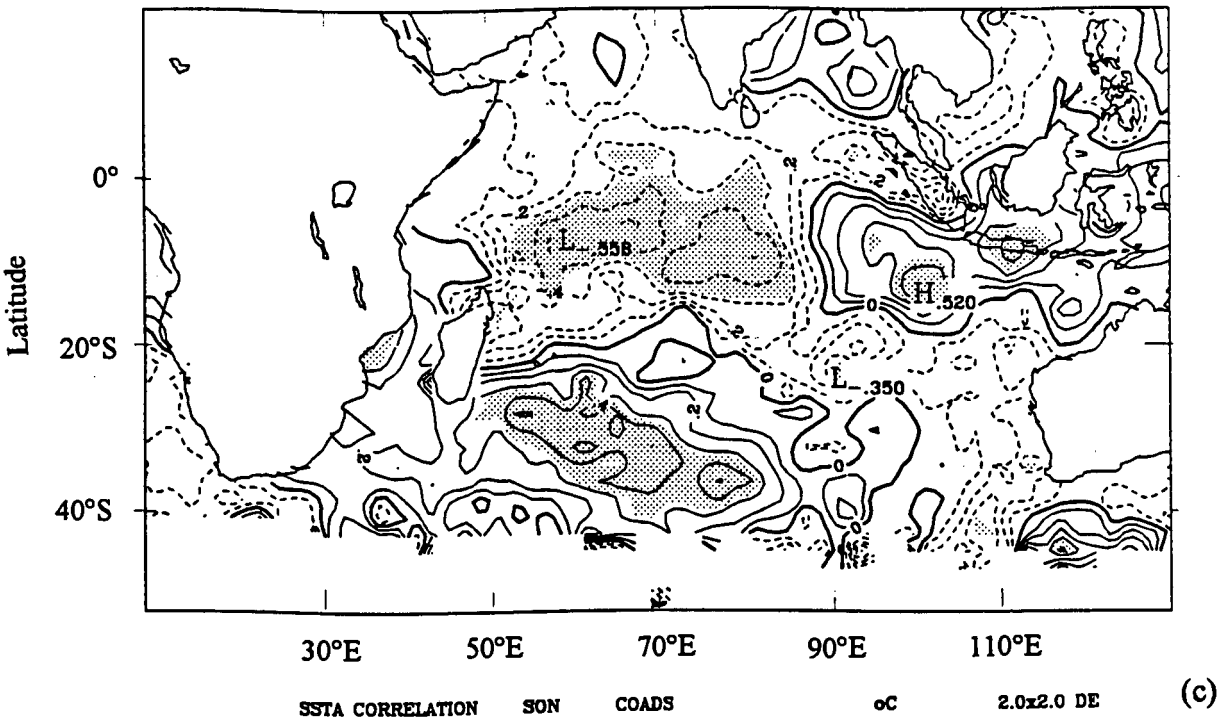

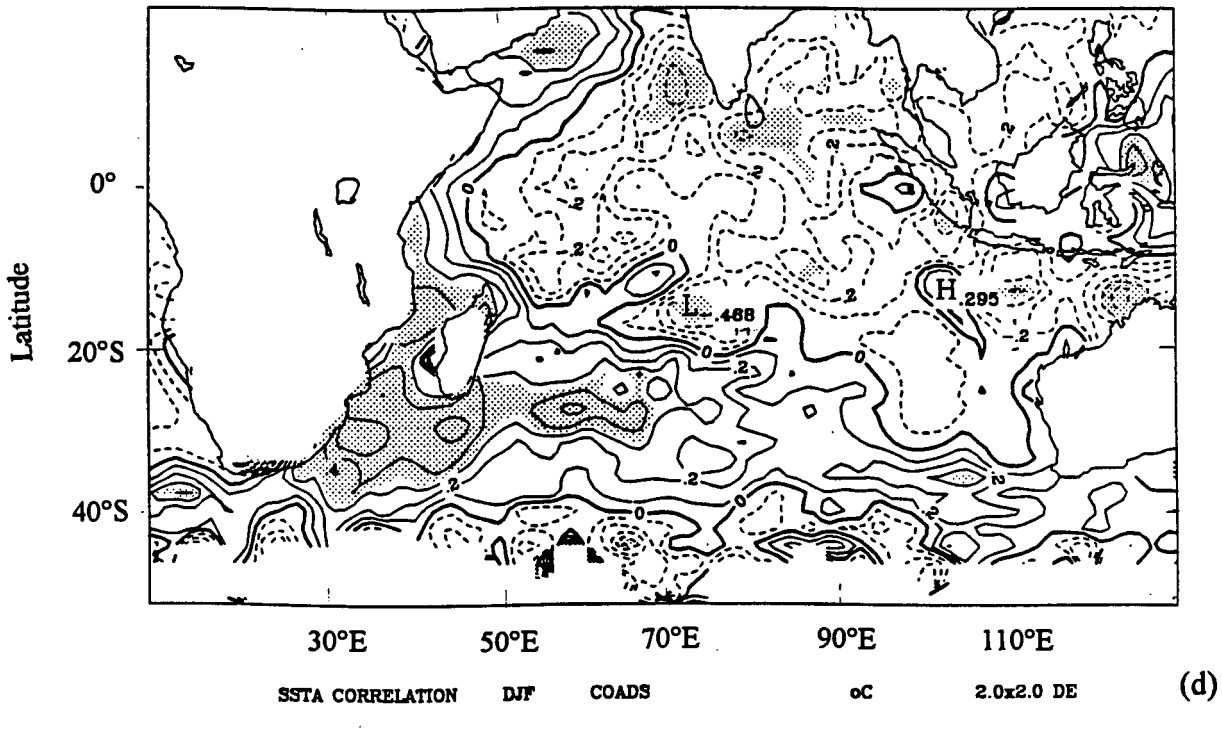

Figure 3.5 : Same as Figure 3.4, but for lags -3 (c), and 0 (d) months.

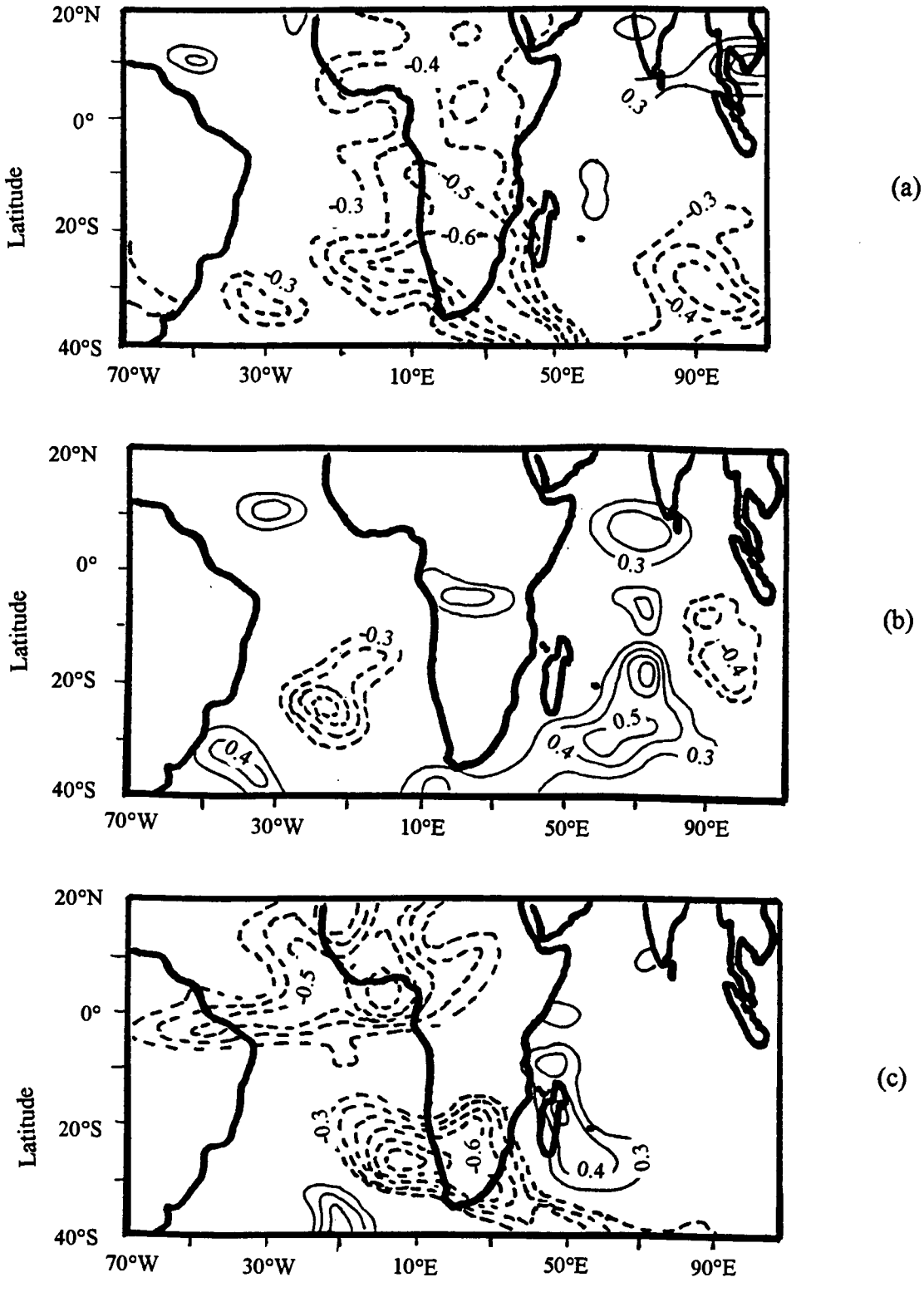

Figure 3.6 : Correlations between the Zimbabwe Rainfall Index (ZRI) and Outgoing Longwave Radiation (OLR) at lags -4 (a), -2 (b) and 0 (c) months.

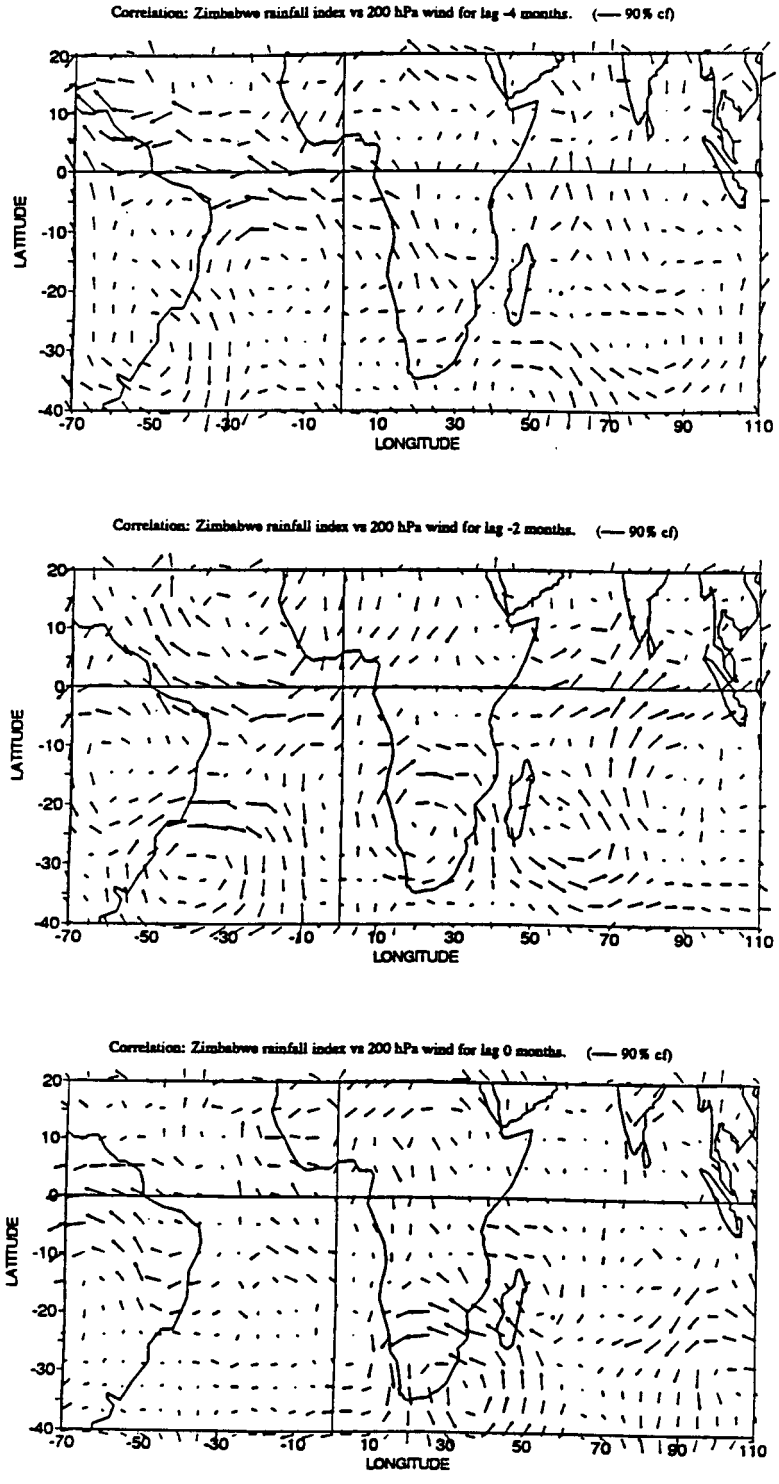

Figure 3.7 : Correlations between ZRI and wind at 200 hPa at lags -4 (a), -2 (b) and 0 (c) months. The length of the longest correlation vector corresponds to 0.65 at 99% confidence level.

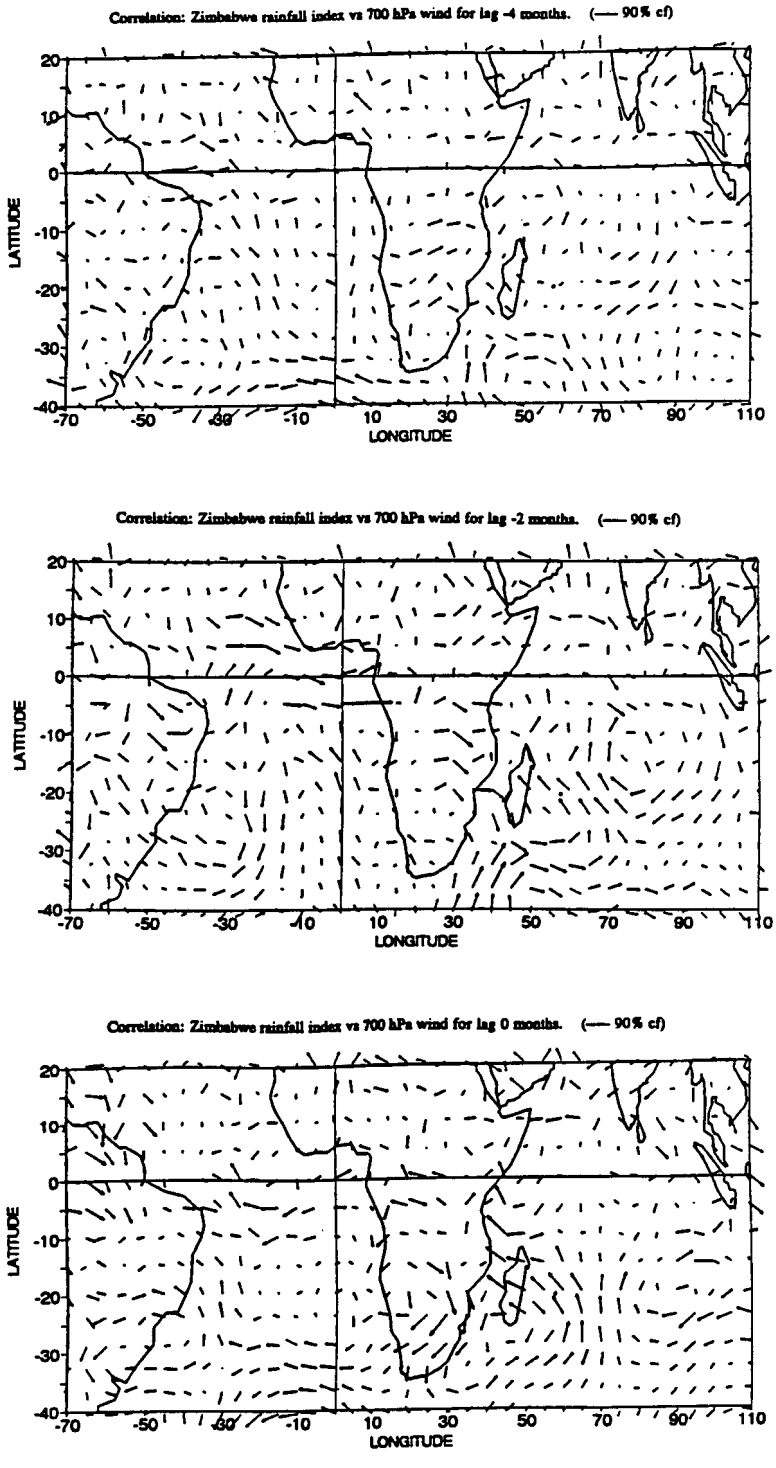

Figure 3.8: Correlations between ZRI and wind at 700 hPa at lags -4 (a), -2 (b) and 0 (c) months. The length of the longest correlation vector corresponds to 0.65 at 99% confidence level.

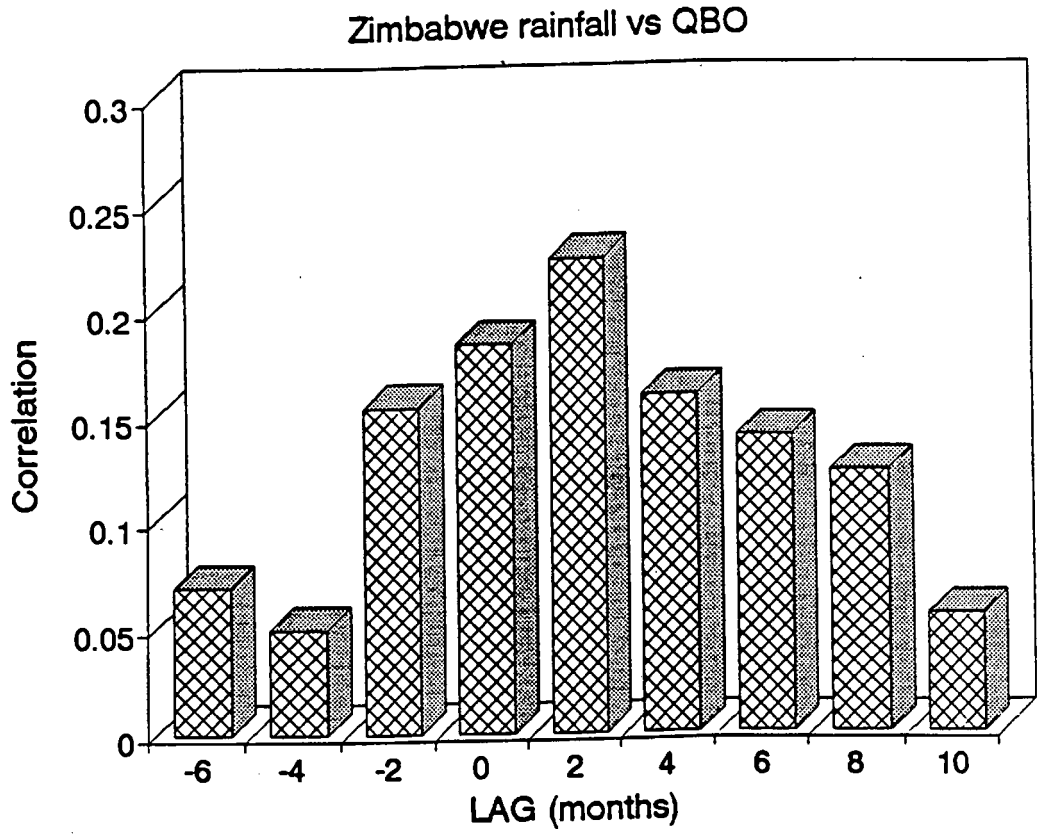

Figure 3.9 : Lagged correlations between the ZRI and QBO from 1955 to 1990. Zero refers to QBO value for DJF, +2 for FMA, etc.

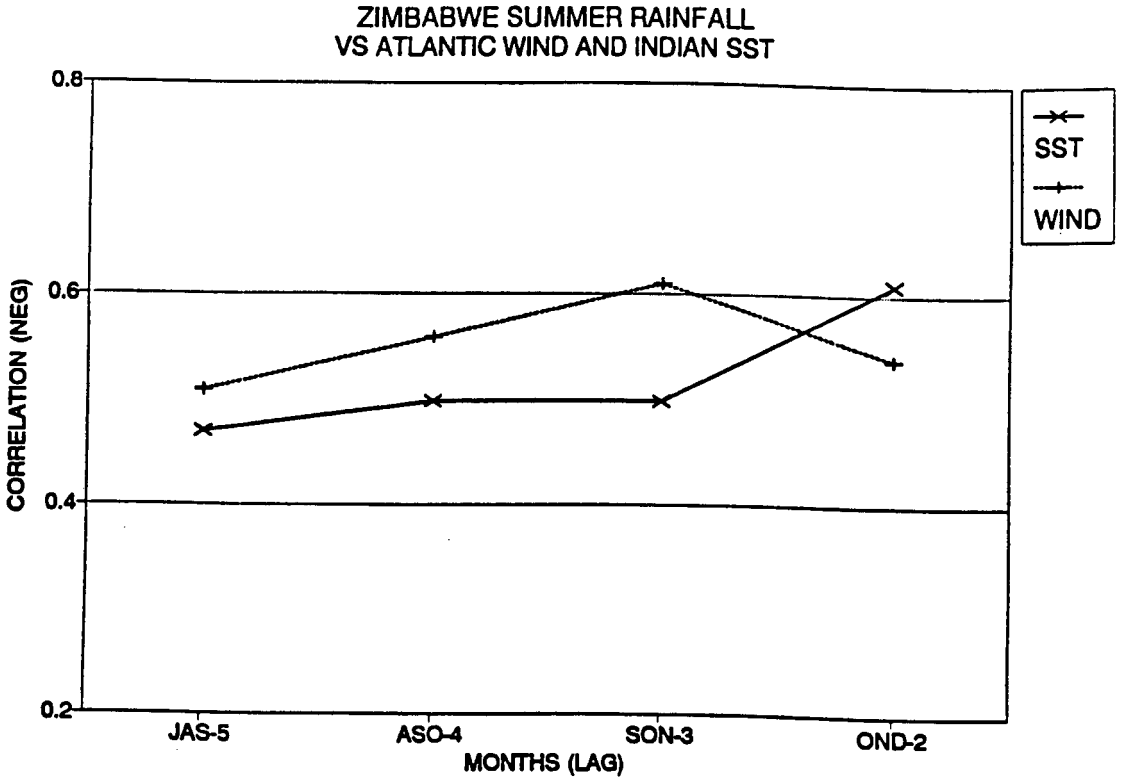

Figure 3.10 : Lagged correlations between ZRI and equatorial Atlantic upper zonal winds and between ZRI and central Indian Ocean SST. (Source : Jury, 1994, personal communication)

Chapter 4

Intra- Seasonal Phases of Southern African Rainfall

4.1 Introduction

The inter- annual variability of summer climate over southern Africa is primarily expressed as intra- seasonal wet and dry events with varying characteristics. Much of this knowledge has been gained from ensemble analyses of events composed of sub- monthly periods (Tyson, 1981, 1984; Miron and Tyson, 1984; Taljaard, 1986b; Matarira and Flocas, 1989) where emphasis has been on excessive rainfall situations. Recently, Barclay (1992) investigated differences between composite wet and dry troughs over southern Africa during October and November using data from 1985 to 1989. Features prominent in the two troughs were identified, including their precursors and triggering mechanisms. Matarira and Jury (1992), studied wet and dry spells for south-eastern Africa, as identified by Zimbabwe daily rainfall data, for 1980 and 1981 December- January periods. Wet and dry spells were defined and meteorological analyses carried out on 5- 15- day composites.

More recently, Levey (1993) examined intra- seasonal rainfall variability over South Africa during summer (October- March) using a water balance index: rainfall minus evaporation over the Western Transvaal. Case studies of wet events were selected from the entire summer for the 1986 to 1992 period. From these 16 cases, a series of composite pentads and composite anomalies was established to represent any wet spell during summer. The life cycle, from initiation through maturity to dissipation, of the final composite was investigated through spatial synoptic analyses of selected observed and derived meteorological parameters

The above approaches assume that climatic controls over southern Africa are invariable throughout the season. Emphasis is placed on common events with greatest anomalies. Little consideration is given to the stage of the season. A drawback with this procedure is its inadequacy to explain why similar synoptic systems produce different weather and precipitation. The analysis also falls short in understanding the physics, dynamics and climatology that characterise summer patterns over southern Africa because the composites cannot describe interaction of the ISO and the seasonal cycle.

This thesis, unlike the approach of Miron and Tyson (1984), Matarira and Jury (1990) and others, is based upon a sequential life- cycle approach rather than an ensemble approach. The objective is not to predict precisely the spatial distribution of meteorological parameters, but to "time" the occurrence of common features of wet and dry episodes. This approach is based upon the assumption that, while the presence of wet and dry spells during the season is beyond question, their causes are not the same throughout the season. By tracking the season, the method aims to analyse each wet spell in chronological order so as to understand the dominant modulating factors. Through this technique, one is able to identify corresponding synoptic circulation structures, sources and sinks of moisture and energy as well dynamic and thermodynamic variables and mechanisms associated with the progression of summer. Thus, apart from its academic implications, this knowledge has practical importance in that it is potentially invaluable for in-season weather monitoring as it enables appropriate preparations to be made and contingency plans to be effected. It offers statistical objective criteria for medium- range weather forecasting.

This chapter looks at southern African rainfall characteristics at sub-monthly time scales by analysing data from selected stations in Zimbabwe, Zambia, Botswana and northern South Africa. To avoid duplication of efforts, the analysis takes advantage of results from previous studies stressing similarities of interannual rainfall patterns in the region. It uses the rainfall data, with major emphasis on Zimbabwe, to make composites over periods denoting the different aspects or characteristics of a typical summer season. Composites, with respect to phases of identified episodes, provide an orderly sequence of snapshots of the mean systems' past evolution. This procedure has been used before and has become accepted (Rasmusson and Carpenter, 1983; Lindesay, 1988; Murakami, 1988; Chen and Tzeng, 1990; Matarira and Jury, 1990; Wang and Rui, 1990a, and more recently, Levey, 1993). Only the events with the most conspicuous signals are used to construct composite structures with regard to the stage of summer. Weather parameters associated with strong convective episodes are expected to produce clear signals. Thus, the composite dynamic structure of these outstanding events should be identifiable and statistically significant (Rui and Wang, 1990). Ultimately, the chapter will reveal the major wet and dry spells comprising southern Africa summer convection, probable onset, cessation and duration of the main season, and lastly, objectively- averaged times of occurrences of in- season spells.

4.2 Data sources and Processing and Analysis Techniques

4.2.1 Sources of Data

The basic data used in this study consists of surface station rainfall and gridded data from the European Centre for Medium- Range Weather Forecasting (ECMWF).

4.2.1.1 Rainfall data:

Initially, 41 years (1951-1992) of summer daily rainfall data were extracted from 30 stations in Zimbabwe, 6 in Zambia, 4 in Botswana and 3 in NW Madagascar. The summer season in Zimbabwe is from 1 October to the first week of April (Torrance 1981). The Zimbabwe data were provided by the Department of Meteorological Services, Harare while that for Zambia and Botswana were kindly supplied by the SADC Sub-Regional Drought Monitoring Centre, Harare. Rainfall data for Madagascar was kindly provided by Nassor (1994). All the stations had continuous records and had quality control specifications consistent with the World Meteorological Organisation (WMO). Data records were inspected briefly and it was deemed unnecessary to adopt further quality control procedures.

4.2.1.2 ECMWF data:

The ECMWF data were extracted for the summers of 1986/87 to 1991/92 in the area 20°N- 40°S, 30°W- 90°E for the months October to March. Data prior to June 1986 are deemed less accurate owing to poor moisture fields (ECMWF, 1989) and therefore are not utilised. The data is the upper air, standard level IIIb, uninitialised, 12 UT (1400 local) product at 2.5° resolution and is displayed at regular latitude- longitude grids. The basic parameters used consist of geopotential height, temperature, horizontal meridional and zonal wind, vertical wind velocity and relative humidity. Some derived kinematic and thermodynamic products were added. All meteorological variable computations which are utilised are summarised in **Annexure 2**. The ECMWF data are used in the following chapters to elucidate meteorological structure.

4.2.2 Methodology

For each season, the rainfall and ECMWF data are converted from daily to 5-day averages (hereafter referred to as pentads), to reduce noise associated with day-to-day variability. The final summer period of investigation is from 3 October to 31 March, making 36 pentads. Because of leap year considerations, some of the pentads at the end of February had data for six days. These pentad divisions are also in accordance with WMO devised format. Using pentad data, a seasonal average is determined, from which anomalies are calculated by subtracting the seasonal value from pentad values. The resulting rainfall perturbations are then normalised by dividing them by the standard deviation, the mathematical procedure of which is in **Annexure 2**. The final product is free of seasonal cycles and is a trend time series for each point. Anomalies are employed to better illustrate intra- seasonal variability. This technique has been employed widely (Dole, 1989; Reinhold and Yang, 1993). Rui and Wang (1990a) used 5- day mean anomaly (pentad analyses) of OLR, to investigate intra- seasonal variations with time scales from 10 days to 3 months. Levey (1993), used pentad anomalies to study intra- seasonal oscillations of convection over southern Africa.

Cross-correlation analyses are performed using Statgraphics version 4 package on the thirty Zimbabwe stations. Based upon resulting correlation coefficients, a subset index is developed comprising nine rainfall stations in the most agriculturally productive region of Zimbabwe. They are intercorrelated at 0.8 at 95% significance level. This index, hereafter referred to as the Zimbabwe Rainfall Index (ZRI), is used as a basis for subsequent pentad analyses. The location of the area in question, is indicated in **Figure 4.1**. The rainfall in this index region is the most reliable (less erratic) from an agricultural perspective compared to the rest of Zimbabwe.

The ZRI is inter- correlated with anomalies of Bulawayo (southwest Zimbabwe), Lusaka (Zambia), Maun (Botswana), Western Transvaal (South Africa) and NW Madagascar. Western Transvaal (South Africa) data were extracted from Levey (1993), comprising area-averaged rainfall from 16 stations near Gaborone, Botswana. Data from NW Madagascar is a three- station area average on the west coast (Maintirano, Mahajanga and Nosy-Be). All the pentad anomalies were obtained for the period 1970-1991.

4.2.3 Composite methodology:

Composites are made to identify wet and dry spells comprising southern African summer from the ZRI. Time series of other pentad rainfall index regions are used to check for consistency with the ZRI patterns, particularly the timing of outstanding events. The following criteria are applied to determine the timing of the strongest cases, thereby defining the crucial spells:

Wet episodes

- pentad rainfall anomalies should be ≥ 1 standard deviation from the long-term mean. Successive wet spells should be separated by at least three pentads. This separation in phase space between two regime states is large enough to make it easy for graphical displays to be made without any filtering (Reinhold and Yang, 1993). By so doing, destructive interference is minimised.

Dry episodes

- either single pentad anomalies should be ≤ -0.7 standard deviation from the long-term mean, or at least three consecutive anomalies are ≤ -0.5 standard deviation. Dry spells which occur before the first major wet spell (early November), are not taken into consideration as they have no impact as far as rain- fed agriculture is concerned.

Cut- off times

The cut- off times are based upon crop water requirements at various crop phenological phases. Traditional rain- fed varieties of maize generally require 60- 90 days from the time of planting to maturity and harvesting stages. Crop yield is a function of not only rainfall amounts, but temporal distribution of rain days throughout the season. On- farm operations, planting dates and successful harvests depend upon the occurrence and duration of wet and dry spells. Cut- offs are therefore essential in order for appropriate contingency measures to be implemented. Early and late summer crop requirements are different so, mid- summer dry spell is used to separate early and late summer rains. The occurrence of this dry spell fluctuates from season to season but should last at least two successive pentads, beginning not earlier than pentad 17-21 December and ending not later than pentad 11-15 January.

Pentad composites are constructed for life cycles of various wet spells. The objective is to investigate characteristics associated with wet spells from formative to decay stages so as to determine predictability in various phases of summer. The life cycle composites are in 4 stages namely initiation (2 pentads before prior to wet spell peak occurrence, or P-2), development (P-1), maturity (P0) and dissipation (P+1). The rest of this thesis is based upon these composites. More detailed procedures used in investigating these wet and dry spells are discussed in appropriate sections of the following chapters.

4.3 Results of the pentad rainfall analyses

Table 4.1 summaries inter- correlations among the rainfall indices selected to represent southern Africa (the ZRI, Maun, Bulawayo, Lusaka and Western Transvaal) and NW Madagascar. These are historical mean pentad anomalies for the period 1970- 1991. Positive correlations exist among the anomalies, with correlation coefficients ranging from 0.66 (between Maun and Bulawayo) to 0.92 (between ZRI and Lusaka anomalies), all at the 99% significance level using 36 pentads per season. Another important feature is the high correlation between the rainfall anomalies over southern Africa and NW Madagascar.

	Bulawayo	**NW Tvl**	**ZRI**	**Lusaka**	**Maun**	**NW Mgr**
Bulawayo	1	0.69	0.74	0.70	0.66	0.66
NW Tvl		1	0.75	0.68	0.74	0.74
ZRI			1	0.92	0.76	0.86
Lusaka				1	0.72	0.81
Maun					1	0.77
NW Mgr						1

Table 4.1 : Inter- correlations of pentad rainfall anomalies for representative regions of central southern Africa and Madagascar. Correlations are at 99.9% confidence limit.

The mean seasonal distribution of rainfall from pentad analyses for five countries, namely Zimbabwe (ZRI and Bulawayo), Zambia (Lusaka), South Africa (Western Transvaal), Botswana (Maun) and Madagascar (NW region) is presented in **Figure 4.2**. The base mean is 1970- 1991, inclusive and each season comprises 36 pentads beginning from 3 October. There are similarities in the patterns. The most conspicuous of all that the summer rainfall season in the region is not unimodal in its distribution, unlike monthly mean patterns. From pentad 1 (3-7 October) until approximately pentad 11 (November 22-26), the entire region is under dry conditions, suggesting that any convective activity during this period cannot be reliable as far as rainfed agriculture is concerned. The onset of effective summer rains is similar for all except the Western Transvaal, whose season is not well established until late January. Cessation times are similar with an uncertainty of two pentads and a mean around pentad 31 (March 2-6). Inspection shows that the pentad mean rainfall is highly variable, implying large amplitude synoptic "pulsing" of convection throughout the season. Maun's (northern Botswana) rainfall is the only exception, within one standard deviation from the long- term mean. Its seasonal standard deviation pattern (not shown) shows greater variability, moreso in late summer, suggesting that ISO over northern Botswana vary significantly each season "cancelling" each other when a long-term mean is determined.

The mean rainfall distribution patterns for ZRI, Lusaka and NW Madagascar are quite similar, as evidenced by the high correlation coefficient between them (**Table 4.1**). The onset of rains is typically pentad 12 (November 27- December 1) $\pm$ 1 pentad. The rainy season lasts until pentad 30 (February 25- March 1) $\pm$ 1 pentad. This similarity suggests that the seasonal cycle and associated climatic controls over the three countries are similar. It appears, though, that the rainy season over Madagascar is delayed by about two pentads. Another interesting feature are differences in the rainfall distribution across Zimbabwe. The ZRI is more similar to Lusaka's than Bulawayo's, which exhibits a bimodal distribution. Peak rainfall is in December for Bulawayo but in late January for the northern regions of Zimbabwe. This discrepancy has useful applications in intra- seasonal (medium-range) weather forecasting for Zimbabwe. Further inspection, also, reveals there must be a demarcation zone, possibly oriented NNW- SSE, through southern Africa separating the east from the west. The trajectories of the airmasses and varying SSTs on east and west coasts can account for some of the differences in the intensity and timing of events from pentad to pentad within the season.

Considering the period between the onset and cessation of main rains (for example, between pentads 12 and 30) is more useful because drier spells prior to and at the end of the season mask in- season dry spells. Contrasts between wet and dry phases also become more distinct. For example, the first wet spell around pentads 13 and 14 is quite pronounced and so is the dry spell in mid summer. For all the countries, the late summer wet spells are of longer duration but with two main peaks which are centred on pentads 23 (January 21-25) and 27 (February 10-14) ± 1 pentad.

Table 4.2 summarises the results of spectral analysis of the ZRI pentad anomalies from 1970- 71 to 1991- 92 summers carried out for each season. The equivalence in days is also shown. For brevity, spectral figures for individual seasons are excluded here. Generally, a flat (white- noise) spectrum is potrayed. With the ordinate ranging from 0- 12, a threshold spectral power of 3 is applied with only higher values being considered. Visual inspection of the analysis indicates the 45- day cycle and its harmonic (22.5 days) as the most dominant, detected almost every other season. Other prominent periodicities include 10- 20 days. Prominent ISOs are identified better by clustering them as illustrated in **Figure 4.3**, which summarises **Table 4.2.** The figure shows a frequency distribution pattern of the cycles in **Table 4.2** at various ranges in days. The frequency distribution shows that the 40- 50 day ISOs are most frequent followed by those in the 21-25 day category, then 15- 20 days. The 21- 25 day ISOs may include harmonics of the 45- day cycles and so should be treated with caution. However, this figure confirms the existence of two major oscillations over southern Africa, namely 10- 25 days and 40- 50 days, partially in agreement with the findings of Levey (1993) for central South African rainfall. Collectively, these oscillations account for approximately 91% of all oscillations detected in the 21- year ZRI rainfall data. The 10- 25 day mode is broader due to higher climatic variability associated with different synoptic patterns while the latter cycle is externally (globally) influenced. More filtering may result in these two modes being more pronounced.

The ZRI's pentad anomalies for each summer season for the period October 1986 to March 1992 (coinciding with the limited ECMWF data) are illustrated in **Figure 4.4**. The anomalies display features not represented in the mean pattern of **Figure 4.2.** Wet and dry spells, plus their durations are more evident. The onset and cessation of the rainy season varies from year to year. The occurrences of spells are non- stationary with respect to the season. More important, temporal and intra- seasonal characteristics of summer can be investigated in more detail than from mean patterns. During the dry summers of 1987 and

1992, there were only two major wet spells which occurred in December and January; about 45 days apart in 1987 and 20-25 days in 1992. Relatively wet years (for example, 1989 and 1990) show continuously wet periods in January and February.

Season	Periodicity
	Pentad (**days**)
1970 - 71	9 (**45**)
1971 - 72	5.15 (**25.8**), 12 (**60**), 7.2 (**37.5**), 3.3 (**16.5**)
1972 - 73	4.5 (**22.5**), 3.3 (**16.5**), 2.3 (**11.5**)
1973 - 74	9 (**45**)
1974 - 75	6 (**30**)
1975 - 76	2.1 (**10.5**), 2.6 (**13**)
1976 - 77	3.3 (**16.5**), 9 (**45**)
1977 - 78	No dominant cycle apart from seasonal peak
1978 - 79	9 (**45**), 4.5 (**22.5**), 3.6 (**18**), 2 (**10**)
1979 - 80	9 (**45**), 2.3 (**11.5**), 5.14 (**25.7**)
1980 - 81	4.5 (**22.5**)
1981 - 82	8.7 (**43.5**), 4 (**20**)
1982 - 83	9 (**45**), 6 (**30**), 4.5 (**22.5**)
1983 - 84	5.14(**25.7**), 3.6 (**18**), 3 (**15**)
1984 - 85	4.5 (**22.5**)
1985 - 86	9 (**45**)
1986 - 87	9 (**45**), 4.5 (**22.5**)
1987 - 88	9.1 (**45.5**), 2.7 (**13.5**)
1988 - 89	2.57 (**12.9**)
1989 - 90	2.77 (**13.9**)
1990 - 91	6.67 (**33.4**)
1991 - 92	7.1 (**35.5**), 3.6 (**18**), 2.9 (**14.5**)

Table 4.2 : Periodicities of pentad (equivalent days are bracketed and bold) precipitation for summer in Zimbabwe. The spectral peaks are listed in descending power separated by commas (see text for threshold criteria).

The initial compositing of wet and dry spells is indicated in **Table 4.3**. From the pentad results, the season is divided into two distinct sub-seasons; early (Ew) and late (Lw). The early season (or short rainy season) occurs anytime between the middle of November and the end of December. However, in 1989 and 1990, the early summer convective spells extended well into the middle of January, a situation regarded as unusual as later analyses will reveal. The late season rainfall starts generally in the middle of January and can last until the end of March. The two seasons are separated by a relatively dry period. Like wet events, the occurrence of the dry spell is non-stationary with respect to each season. For example, it occurred as early as the end of November in 1990 and 1991 and continued into the second week of January in 1987 and 1992, coincidentally El Nino years.

Summer Season	**Early**		**Late**	
	Wet	**Dry**	**Wet**	**Dry**
1986 - 87	11 - 14	15 - 18	20 - 23	28 - 31
1987 - 88	11 - 15	17 - 19	21 - 23, 27 - 29,32	25 - 26
1988 - 89	11 - 13	16 - 19	23 - 26, 28 - 30	33 - 34
1989 - 90	17- 21	16	26	30 - 34
1990 - 91	11, 16 - 17, 20	12, 15	25 - 28, 33	34
1991 - 92	9 - 10, 17	12 - 13, 21	23, 35	24 - 30

Table 4.3 Observed wet and dry episodes based upon pentad precipitation for the period 1986- 1992. The numbers denote pentads (Annexure 1).

The observations of rainfall cycles provide a general guideline of summer patterns. They are used by the farming community to define the onset and cessation of the main rains. However, a reliable timing of events is not yet offered. Thus, an objective tool to evaluate and predict the state of the seasonal rainfall at any time would be useful so that appropriate and effective contingency plans can be put into practice. By knowing the rainy season distribution each year, one is able to assist in optimising agricultural activity and water resources.

Using the ZRI anomaly, pentads of peak convective activity enable the selection of cases for the composite procedure as indicated in **Table 4.4.** Ew0 and Lw0 represent early and late wet spells, respectively, while Ed0 and Ld0 denote early and late summer dry spells. During the 6- year period, early summer wet spells peaked as early as November 17 (in 1991) and as late as January 10 (1991). Late summer spells commenced from January 21 for most years and lasted until March 27 (1987 and 1992). It is also evident that the peak of the mid-summer dry spell is variable and is generally experienced between December 7 and January 15.

Season	Ew0	Ed0	Lw0	Ld0
1986 - 87	14	15 -17, 20	23, 25	24, 29, 31, 34
1987 - 88	12, 15	17, 20	23, 29, 32	26, 35
1988 - 89	12	14, 17	23, 25, 28, 30	22, 33, 34
1989 - 90	12	17 - 21	24, 26, 29	30 - 33
1990 - 91	11, 16, 17, 20	12, 15	27, 33	31
1991 - 92	10, 17	12, 21	23, 35	24, 27 - 29

Table 4.4: Pentad of peak activity. Ew0, for example, refers to early summer wet spell peak, etc.

From further analysis using the compositing criteria, it becomes clear that the summer season is pulsed with three main wet and two main dry periods, each period on average lasting up to three pentads. The peak pentad for the first wet period is around pentad 12, that is 27 November- 1 December, hereafter referred to as early summer first wet spell (EFW). There is a minor wet spell (ESW) which occurs around 12- 16 December. Late summer has three pronounced wet spells, namely LSFW (with a peak around 21- 25 January), LSSW (10-14 February) and LSTW (22- 26 March). The LSTW effectively defines the end of the season as far as rain-fed agriculture is concerned. The major dry periods extend from 27 December to 11 January, the mid-summer dry spell (MSD) and from 25 February to 16 March, the late summer dry spell (LSD). In addition, there are two minor dry periods of 1- 2 pentad's duration just after EFW and LSFW.

Despite the above criteria, pentads defining wet spells contain days which are non-convective. **Annexure 1** illustrates this fact better. In other words, the relatively dry "start" and "end" pentads of wet spell life cycles (P-2 and P+1) fit the criteria for dry spells. Hence, the mean wet spell phases are characterised by a significant percentage of dry days. The major difference with "exclusively" dry spells is the duration and intensity of the dry pentads.

4.4 Discussion

Chapter 4 has provided an overview of intra- seasonal climatic variability over southern Africa during austral summer. Using area- averaged rainfall over agriculturally important northern Zimbabwe (an index referred to as the ZRI), inter- correlations with other areas in southern Africa as well as NW Madagascar were assessed in terms of compatibility. For historical mean pentad rainfall distribution, there was good agreement (**Table 4.1**). The time series analyses also identified closer similarities among eastern areas (the ZRI and Lusaka) and NW Madagascar than for the western areas. This was particularly the situation in early summer.

The relative differences in the mean pentad rainfall distributions during early summer between western (evidenced by Maun, Bulawayo and Western Transvaal) and eastern central Africa (ZRI, Lusaka and NW Madagascar) suggests different climatic factors in operation. A possible demarcation should divide Zimbabwe in a NNW- SSE orientation.

This configuration partially supports observed patterns and behaviour of cloud bands emanating from Namibia/ Angola which mainly affect the southwest of Zimbabwe and rarely reach the north. The bands have been observed to intensify as they propagate southeastwards in association with pre-frontal troughs. This can be explained by the seasonal rainfall phase lags and intensity between Maun and Bulawayo. Detailed circulation patterns to explain the seasonal anomaly patterns are not of relevance here.

Composites are constructed with regard to pentad rainfall data between 1986 and 1991 summers, the period deemed suitable for ECMWF data quality. The patterns are non-stationary in time from year to year, hence the dates (pentads) of peak activity were variable. Wet and dry spells are composited differently. Composites of life cycles of wet spells are constructed and these provide the basis of Chapters 5 through 7 as well as vertical sections in Chapter 9. Dry spells, and in-season droughts in particular, are the subject of Chapter 8, where their diagnostic patterns are investigated. The composites consist of dry pentads meeting the criteria set above and precursor symptoms are not considered.

Another important result from this chapter is the intra- seasonal nature of precipitation patterns in southern Africa and Zimbabwe. The summer rainfall distribution consists of an alternating sequence of wet and dry weather. The accumulation of rainfall depends upon the intensity and duration of the wet spells. Despite the fact that the period under investigation is relatively short, inspection reveals a sustained periodic behaviour of wet and dry episodes. The major peaks occur around pentads 12, 15-17, 19-21, 23, 26-27, 29-31 and 33-35, indicating oscillations of approximately 3-4 pentads (15-20 days). This pattern is not the same every year, but the intervals of the spells are either of that order or their multiples. The result substantiate periodicities detected in **Figure 4.3**. The ISOs therefore, recur in approximately two phases, namely every 15 ± 5 days and 50 ± 10 days. Any lower frequencies are within the seasonal cycle range and no longer intra- seasonal. These results concur with Ghil and Mo (1991) who detected a principal 23- day mode followed by another at 40 days and a weak 16- day wave in the southern hemisphere. The 15- day oscillation is also consistent with the mean 16- 18- day cycles detected by Shapiro and Goldenberg (1993).

As far as wet spells are concerned, emphasis is on life cycles (from evolution to dissipation), prediction and early warning. The composites are determined with respect to the pentad of peak activity (P0). The approach of Rui and Wang (1990a) is used to

investigate further the intra- seasonal anomalies. To do this, a four-stage life cycle was adopted: initiation (P-2), unstable intensification or development (P-1), maturity (P0) and dissipation or decay (P+1). Thus, each wet episode has a build- up and assumed duration of 20 days. The individual pentads used in constructing the composites are illustrated in **Annexure 1.** The final composites from long term ZRI rainfall analyses, are shown in **Table 4.5**, the corresponding organogram of which is presented in **Figure 4.5**.

Pentad	EFW	ESW	LSFW	LSSW	LSTW
P-2	17-21 Nov	7-11 Dec	11-15 Jan	31 Jan-4 Feb	12-16 Mar
P-1	22-26 Nov	12-16 Dec	16-20 Jan	5-9 Feb	7-21 Mar
P0	27 Nov-1 Dec	17-21 Dec	21-25 Jan	10-14 Feb	22-26 Mar
P+1	2-6 Dec	22-26 Dec	26-30 Jan	15-19 Feb	27-31 Mar

Table 4.5 : Mean dates of prominent wet spells during southern African summer as identified by the ZRI .

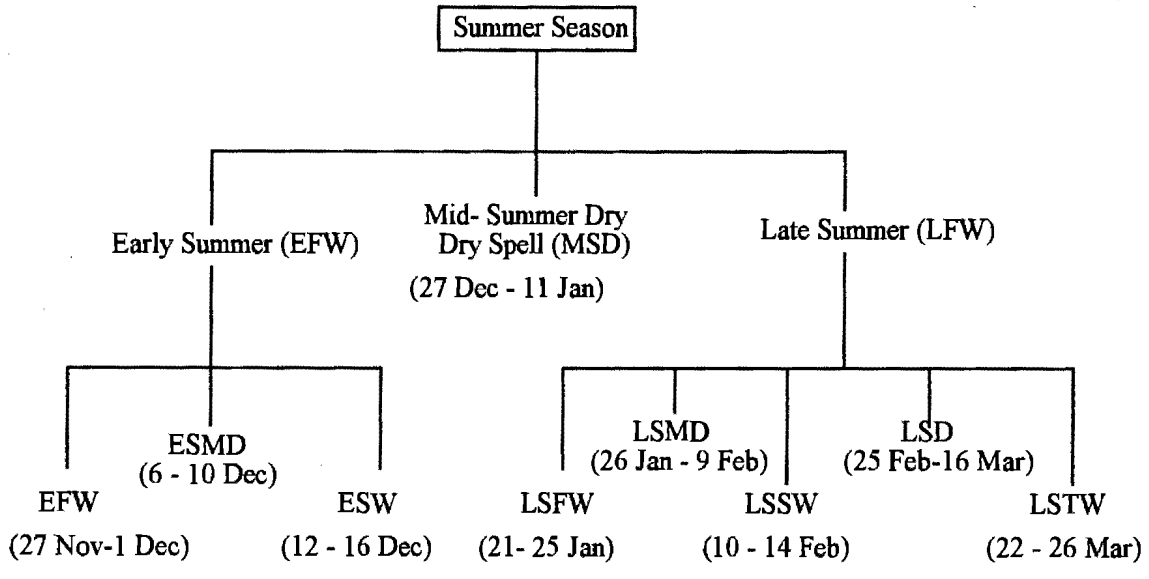

Figure 4.5 : Observed wet and dry spells occurring over Zimbabwe during summer

It is evident that, in the long- term, approximately 30 days lapse between the last peak of early summer (ESW) and the first peak of late summer (LSFW). A similar period also exists between the LSSW and LSTW (in other words between the February and March wet spells).

Finally, it must be noted that, like any other objective technique, the analysis procedure has its flaws. For example, while the chapter has identified the most probable occurrences of wet and dry spells, the regional atmospheric structure is not necessarily consistent with the criteria applied to surface data. With regard to wet spells, progression from initiation to dissipation is not always gradual and systematic. The relatively short period of analysis (six years) may show the vulnerability of the compositing procedure. Identifying the peak is less problematic than the determination of pentads immediately before and after. These are necessary to appropriately define development and dissipation. This is the case when wet spells prolong their duration above the threshold criteria. To avert this, in a few cases, the P-1 was designated to be up to two pentads prior to P0.

In summary, the findings in this chapter have useful applications, particularly as regards agriculture. Crop planning requires accurate definition of the growing season, critical stages of crop development and time of occurrence of such critical stages (Pereira, 1982). The critical stages include germination, flowering and grain filling. Crop success or failure is largely dependent upon adjustment of the life cycle of the crop to the sequence of seasonal climatic conditions. The growing season is governed by the onset and cessation dates of the summer season. The crop requirements vary throughout the growing season and for annual crops like maize which take three to four months to reach maturity, the most critical stages are defined largely by presence, absence and timing of EFW and LSTW. Secondly, dry spells are necessary for agriculture by facilitating opportunities for cultivating, spraying and weeding, in addition to providing the heating degree days necessary during different phases of crop phenology. This chapter has objectively determined the characteristics of the summer rainfall distribution over southern Africa. By tracking the season, the analysis has revealed spatial and temporal patterns over the region, a significant contribution to existing knowledge about the climatic variability of the southern Africa. The results introduce a novel dimension to understanding weather patterns over this region at sub- monthly time frames. The rest of this thesis will elaborate on these aspects.

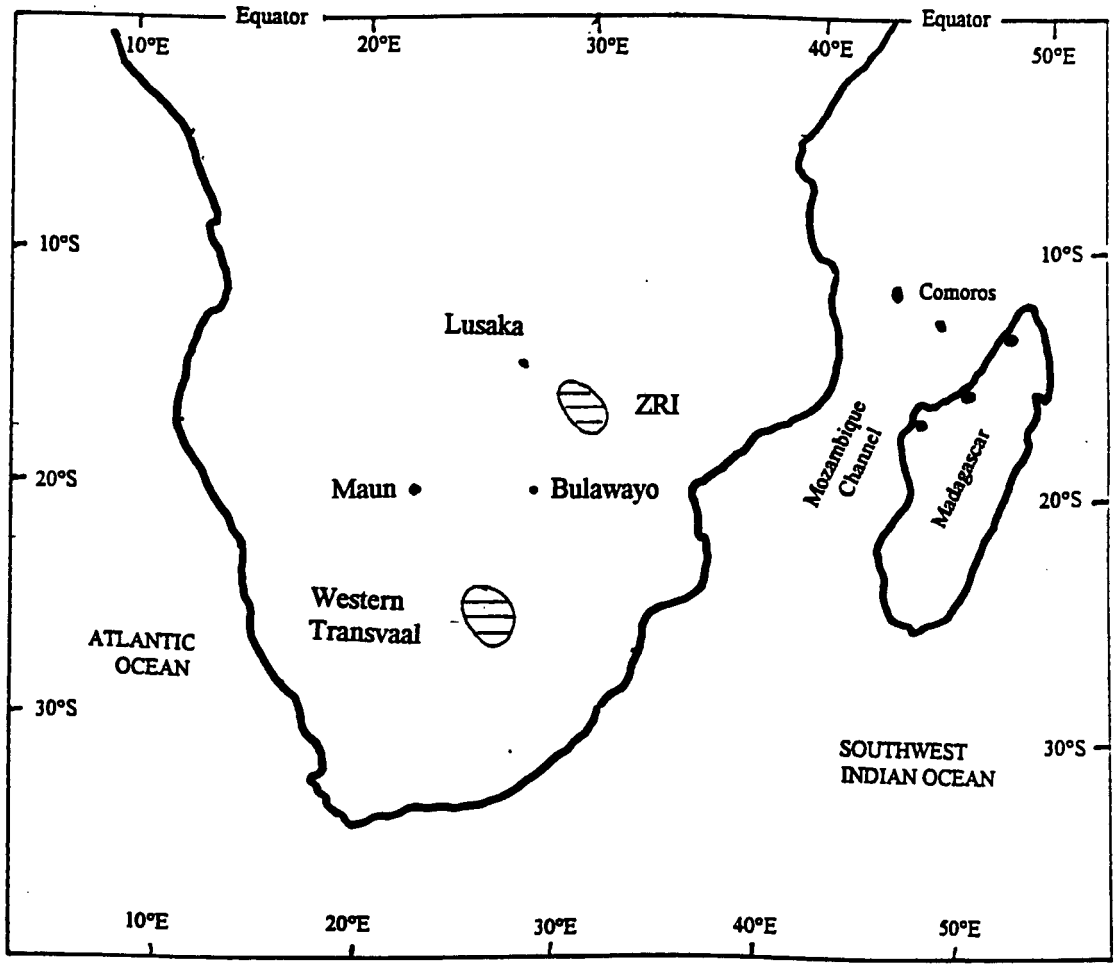

Figure 4.1 : Southern Africa and rainfall index stations. The Madagascar index is represented by three stations along the NW coast.

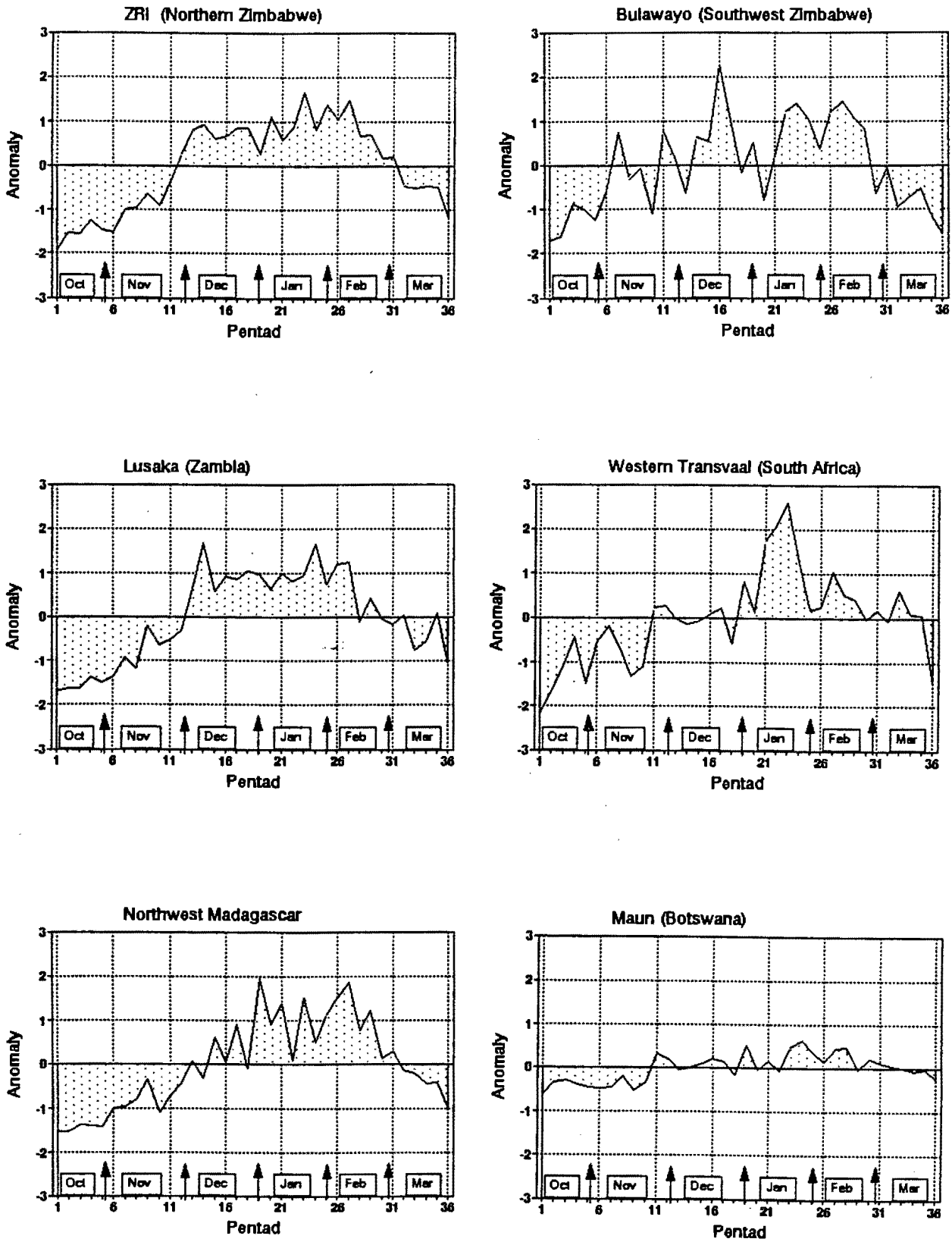

Figure 4.2 : Time series analysis of mean (1970- 1991) seasonal pentad rainfall for selected stations. The data is normalised with respect to the standard deviation.

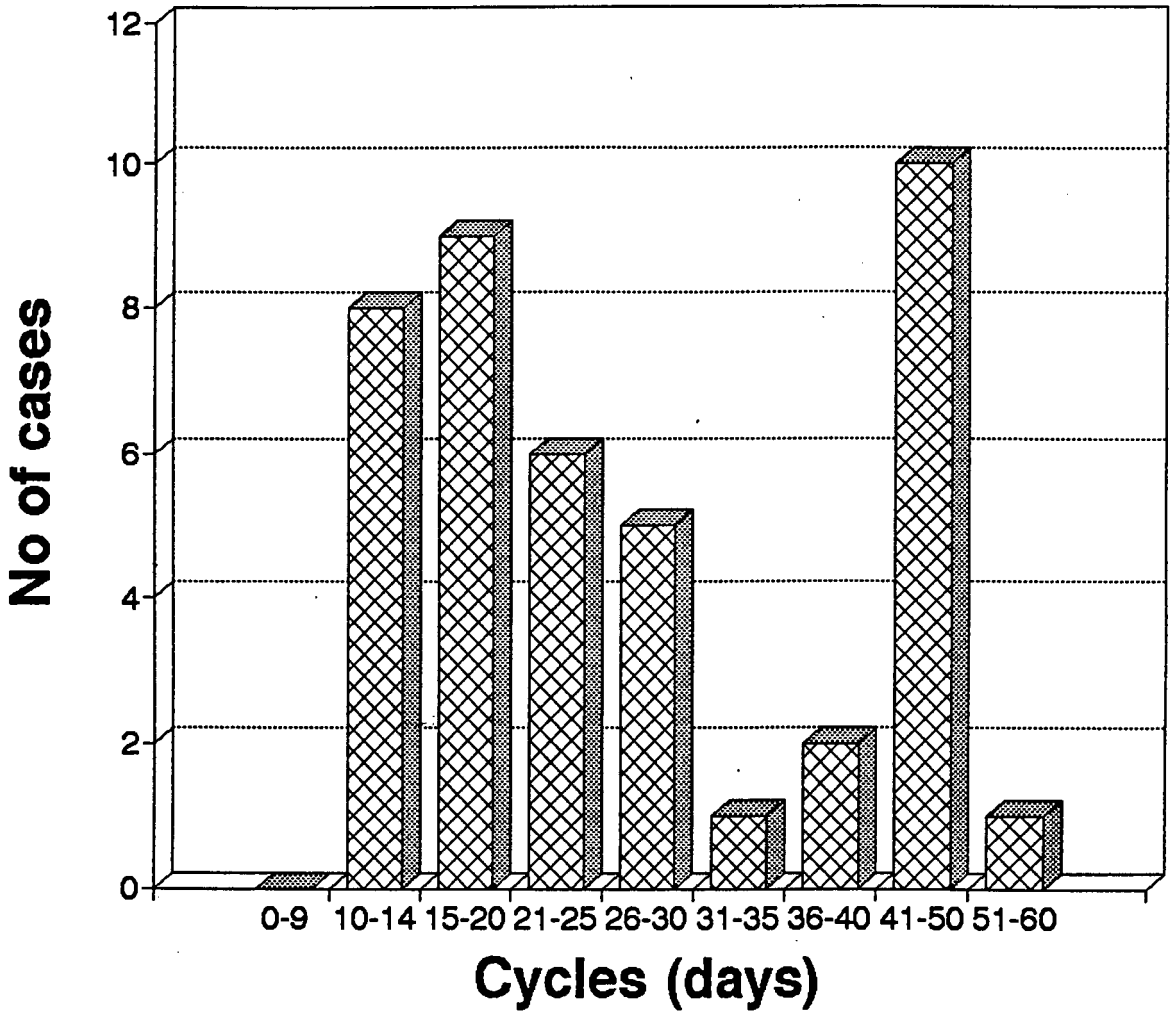

Figure 4.3 : Frequency distribution of intra- seasonal oscillations detected in the ZRI rainfall from 1970- 1991, inclusive.

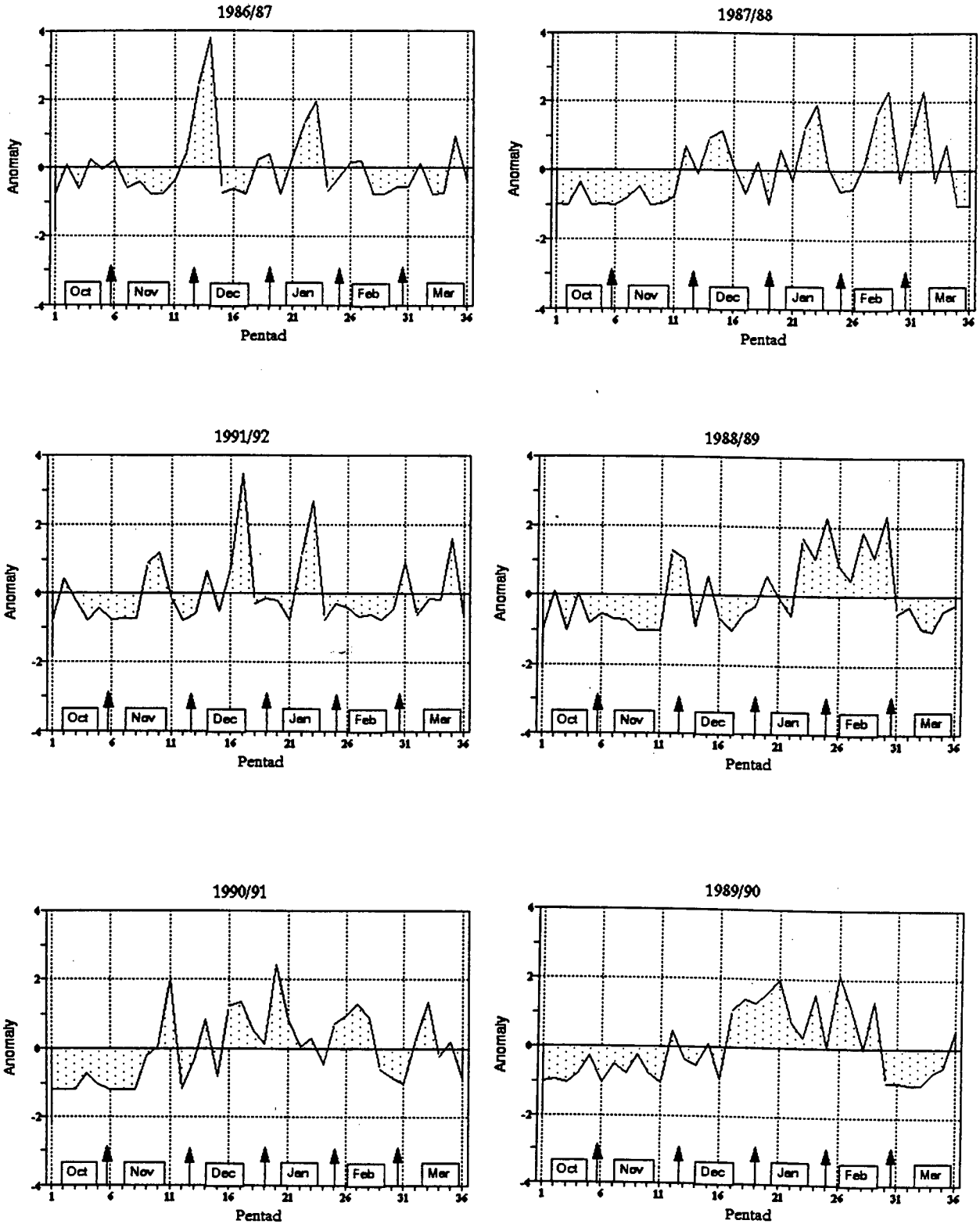

Figure 4.4 : Time series analysis of ZRI pentad rainfall during the overlapping ECMWF period 1986- 1992. The seasons are arranged in a clockwise pattern.

Chapter 5

Phases of southern African summer : Mean Circulation patterns

5.1 Introduction

This chapter looks at mean characteristics of selected meteorological fields comprising each part of the summer rainy season defined according to the wet spell onset and cessation as in Chapter 4. The underlying assumption is that the controlling circulations vary as a function of time during the summer. The mean circulation patterns are computed from a six- year dataset, due to significant improvements in ECMWF data after 1985. Despite representing a relatively short period in terms of years, the composite means are calculated from vast amount of daily data. A wide range of weather characteristics occurred during the period in question (from drought to wet as well as "normal" years).

5.2. Methodology

For each major wet spell, determined from standardised area- rainfall departures from 1986/87 to 1991/92 summers, the duration was identified from the time of initiation through development and maturity to dissipation, a period lasting 20 days. A mean was then determined by averaging ECMWF data for all days comprising each phase, results of which are indicated below (**Table 5.1**).

Phase	Period of mean
EFW	**7 November - 6 December**
ESW	**12 December - 11 January**
LSFW	**6 January - 9 February**
LSSW	**31 January - 11 March**
LSTW	**25 February - 31 March**

Table 5.1: Periods utilised in the determination of phases

To be as inclusive as possible, the onset (cessation) of each phase is determined from the earliest (last) date of occurrence of the spell from all individual cases between 1986 and 1992. Reference to Table 5.1 shows that the periods in some cases overlap (for example, ESW and LSFW, LSFW and LSSW). This is so because the occurrences of the individual phases of summer in which the wet spells occur are non- stationary with respect to the season.

This "period- mean" method of analysis has been utilised before, most notably by Tyson (1981, 1984) and Miron and Lindesay (1983), whereby pre- selected episodes are composited. The method has some advantages which include a reduction in data volume minimisation of noise (filtering) associated with individual synoptic events and provision of "a blanket" description of climatological features for a given period. Inferences thereof carry more weight than individual case studies. Like any other technique, there are some flaws in the approach. For instance, the results are general and diagnostic. Equally critical are the criteria for selecting cut- off times identifying periods whose means are to be deemed representative. There is an element of subjectivity with slight differences in interpretations.

Considering that the effective summer season as defined in this thesis is approximately 182 days' duration, the base periods used here for calculating the means for each phase of summer range from approximately 25 to 45 days. Selected meteorological variables were then analysed with a view to obtaining prevailing conditions during each wet spell. It should be noted that these fields are computed from about half of relatively passive days (P-2 and P+1 pentads) and half convective days and are representative of the mean and not wet spells per se. Chapter 6 will look at the active convective stages in isolation, whereas here, the emphasis is on changes in the background circulation as the summer season progresses. These reference means will be used to compute intra- seasonal oscillation lifecycle departures in Chapter 7.

5.3 Characteristic circulations

5.3.1 Lower- troposphere : 700 hPa

5.3.1.1 Geopotential height

At the beginning of summer (**Figure 5.1**, EFW), there is ridging from the Atlantic Ocean Anticyclone into southern Africa with axis along 22.5 - 25°S. A trough of low heights is also apparent along the Equator over Africa stretching from the Indian Ocean. The trough spreads southeastwards in December to NE Madagascar. Simultaneously, the sub-tropical high pressure belt increases in strength, evidenced by the increasing heights in the preferred location. During the entire late summer, the low- level circulation is characterised by the ridging of the Atlantic Ocean Anticyclone (AOA) into Southern Africa with its axis oscillating between 20 and 30°S. The sub- tropical ridge is evident in January (LSFW) linking the AOA and the relatively weak Indian Ocean Anticyclone (IOA). At the same time, a broad trough extends from the central Indian Ocean into equatorial Africa. The trough penetrates deepest in the February wet spell (LSSW). By the end of March (LSTW), the pattern resembles that in January.

5.3.1.2 Mean temperature field

The mean temperature gradient is slack in tropical areas throughout summer (**Figure 5.1b**), as expected. Outside the tropics, isotherms are zonal and decreasing systematically towards higher latitudes. At EFW, a tongue of highest temperatures extends from the central equatorial Atlantic Ocean to western southern Africa (Angola region). The tropical Indian Ocean also displays relatively high temperature. The temperatures increase as austral summer progresses, more rapidly from January onwards near 20-25°S, 20°E (over Namibia). The 10°C isotherm spreads to cover the tropical areas and northeast Africa by the time of LSTW. Significantly, the mid- latitudes gradually warm throughout summer. Also worthy of note, is the difference in the temperature budgets between the land mass of southern Africa and adjacent oceans, particularly the tropical Indian Ocean. There is a two month lag (Indian Ocean temperatures are warmest in March compared to January for southern Africa). Harrison (1986) also detected the lag using SSTs.

5.3.1.3 Mean zonal (u-) wind

The low level wind is predominantly westerly south of about 20°S and easterly north of it during early summer (**Figure 5.2a,** EFW and ESW). There is a weak band of monsoon westerlies around the Equator in the Indian Ocean in November (EFW). The band shifts southeastwards in December (ESW) to lie between 0 and 10°S. The easterlies are relatively strong in November with the greatest intensity in the eastern Atlantic Ocean equatorial region. The flow pattern changes little during late summer. The easterly flow is greatest over the tropical Atlantic Ocean south of West Africa. However, a well defined belt of weak westerly winds is also evident stretching from the equatorial Indian Ocean into east Africa along 10°S in January and February (LSFW and LSSW) while in March it has receded to the central regions of the ocean. The 700 hPa mean zonal winds everywhere are relatively strongest in January and decrease in intensity as the season progresses compared to the later periods.

5.3.1.4 Mean meridional (v-) wind

The patterns (**Figure 5.2b**) over Africa consist of a predominantly northerly flow with poleward motion along the Equator as well as over the western regions of southern Africa (Namibia and Botswana, particularly). From 10°S polewards, a standing wave pattern is apparent and composed of alternating regions of northerly and southerly wind regimes, with the latter flow over oceanic areas in the immediate vicinity of southern Africa. This configuration is maintained in December, although the flow over southern Africa has weakened considerably. During this period, also, the northerly winds in the SW Indian Ocean have spread westwards as far as eastern Zimbabwe.

The standing wave pattern remains evident throughout late summer, with southerly flow over the southeast Atlantic, the Mozambique Channel, Mozambique and Zimbabwe) areas as well as over the Indian Ocean. In addition, northerly flow prevails over equatorial Africa and oceanic areas to the SSE of the sub- continent. During the course of the season, these two link up through the western parts of southern Africa (Namibia, Botswana and Angola) and shift the southerly winds in the Mozambique Channel northwards to include Madagascar. The northerlies over the central interior of South Africa intensify in the process, possibly due to meridional confluence from adjacent waters. This configuration is conducive for moisture advection from equatorial regions resulting in the formation of tropical- temperate troughs (Harrison, 1986) and cloud bands

mentioned earlier in Chapter 2. A most interesting feature is the sympathetic flow over the western Congo in late summer.

5.3.1.5 Horizontal wind vectors

At EFW, easterly wind vectors are evident over tropical Africa (**Figure 5.3**). Part of this air stream comes from the east Indian Ocean between 10 and 20°S. The flow across southern Africa is controlled by a weak anti clockwise system to the SE of the region. There is little evidence of cross- equatorial flow. There is more meridional motion during ESW, particularly over tropical Africa, where the winds have a northerly bias. The winds from the central Indian Ocean are weaker and extend westwards as far as Madagascar. The anticylonic system over South Africa is more pronounced near 25°S, 30°E and is responsible for easterly winds along 20°S (all the way from southern Mozambique to Namibia). During January (LSFW), the northerly flow over the interior of tropical Africa intensifies, increasing zonal convergence in the vicinity of 20°S. Further north, equatorial easterlies from the Indian Ocean veer southwards over Africa when they cross the Equator from the northern Hemisphere. Some of these winds recurve over east Africa to NNW across northern Zambia and return towards the Indian Ocean via southern Tanzania. The rest continue westwards across Africa, increasing in intensity to reach a maximum in the eastern Atlantic around the Equator. Over the Indian Ocean, the wind pattern is somewhat systematic and zonally organised, especially east of 50°E with anti- clockwise circulation along 25°S (continuation of the sub- tropical belt) and along the Equator. Between them is a region of clockwise flow along 10°S (which may delineate the position of the ITCZ). The resulting pattern is one belt of westerly winds along 5°S and another belt of easterlies between 15 and 22°S, both terminating at approximately 50°E.

The patterns over Africa and the Atlantic Ocean remain unchanged in February (LSSW). However, the tropical easterly- northeasterly winds are stronger than in January. Patterns in the west Indian ocean have generally moved southwards such that the belt of westerlies is now along 10°S, thus displacing the easterlies 10° polewards SE of Madagscar. During the March wet spell (LSTW), the only significant changes occur over tropical southern Africa, where the winds are all easterly. Once again, as during January, the winds between 10 and 20°S in the Indian Ocean have turned easterly. This may suggest that lower tropospheric winds in the tropical Indian ocean undergo a reversal of motion approximately every 20- 30 days. This change terminates off the east coast of Africa.

5.3.1.6 Mean horizontal divergence

Figure 5.4a indicates mean low- level tropospheric divergence during all five phases of summer. For the November wet spell (EFW), apart from areas of significant convergence just south of the equator over Zaire/ Congo and the eastern coast of South Africa, southern Africa experiences a generally divergent flow with a local maximum over Botswana (near 20°S, 20°E). The divergent flow is linked to patterns in the tropical regions of the eastern Atlantic as well as the Indian Ocean. The pattern over Africa changes somewhat during December (ESW). The link between divergent areas in the two oceans through southern Africa in November has been severed by convergent flow which has spread from Madagascar in November northwestwards to link with that over Zaire. The divergence over southern Africa has weakened slightly (but still in evidence) possibly due to an increase in and eastward movement of convergence in the south Atlantic. The flow in the Indian Ocean has changed to become mostly convergent, very weak though.

Except along the extreme southeast coast, virtually the whole of southern Africa is under divergent flow throughout late summer. This is not surprising, since the mean patterns are composed of mostly dry days when the anticyclonic ridging from the Atlantic Ocean prevails. The divergence is linked to that just north of the Equator via the Atlantic Ocean. Another area of divergence extends south from the northern hemisphere down the east African coast as the late summer progresses. Simultaneously, a zone of convergent motion is evident stretching from the Indian Ocean through Madagascar into and across Africa between 10 and 20°S. It is apparent that this convergence is being drawn westwards from the Indian Ocean such that by the end of March (LSTW), confluent motion is confined to western equatorial Africa with an axis roughly along 5°S.

5.3.1.7 Mean vorticity

The mean 700 hPa vorticity fields are displayed in **Figure 5.4b**. The peak of EFW is characterised by anticyclonic flow over most of the region. However, there exists a cyclonic pattern between the Equator and 10°S in the Indian Ocean as well as over a small area off the west coast of southern Africa. The area of cyclonic flow spreads rapidly between 10 and 20°S from Africa westwards and between the equator and 20°S in the Indian Ocean during ESW. Development of this band of cyclonic vorticity decouples equatorial from extra- tropical anticyclonic flows. During January and February wet spells (LSFW and LSSW, respectively), there is a 10-15° wide belt of cyclonic activity covering central southern Africa from the Indian Ocean through Madagascar into the Atlantic with

anticyclonic flow to the north and south of it. The anticyclonic area south of 20°S is relatively stronger in February than in January. In March (LSTW), the pattern breaks down between the Equator and 30°S, resulting in a mainly anticyclonic circulation over the sub- continent with isolated weak cyclonic vorticity off the west coast and in the equatorial Indian Ocean.

5.3.2 Middle- troposphere : 500 hPa

5.3.2.1 Geopotential height

A rather slack gradient exists in tropical regions when summer commences (**Figure 5.5a**). However, there are higher values of the geopotential height in the tropical Atlantic Ocean, tilted equatorward with height from the lower troposphere. These extend into southern Africa as in the low levels, leaving only the equatorial regions of Africa under the effect of low values from the Indian Ocean. Late summer begins with a zonal pattern poleward of about 25°S, a geopotential ridge extending from the Atlantic Ocean into Africa with axis along 20°S and a broad trough along the Equator emanating from the Indian Ocean across Africa (LSFW). The geopotential heights generally increase from the west with time (LSSW and LSTW), while those in the Atlantic are gradually displaced northwards, filling up the equatorial trough in the process. The south Indian Ocean undergoes some change with increased troughiness in the vicinity of Mauritius as noted at 700 hPa.

5.3.2.2 Mean vorticity field

The mid- level vortivity patterns closely resemble those at 700 hPa. However, at 500 hPa the narrow belt of cyclonic circulation in the equatorial Indian Ocean is discontinuous as it migrates towards Africa. It appears to dissipate off the NE of Madagascar and re-establish across Africa along 15°S in January (**LSFW, Figure 5.5b**). In February, the area of cyclonicity has shifted eastwards to lie across eastern central Africa and Madagascar and collapses in March. Anticyclonic flow poleward of 20°S weakens from January to March and shows eastward progression to the South Indian Ocean.

5.3.2.3 Mean meridional (v-) and zonal (u-) wind

The mean 500 hPa meridional pattern over southern Africa in November (**Figure 5.6a**) shows a dipole- like structure with northerlies covering the western and southern flanks (centred near 20- 25°S, 15°E) while weak southerlies cover the east with a centre around 22°S, 35°E. This structure is "carried" into December (ESW), but southerly winds are stronger in relation to those in November and have become more dominant in the region by spreading westwards across the continent at the expense of the northerlies. The tropical easterlies have also linked up with those in the Indian Ocean. The centres of both regimes have also shifted southwards and lie along 25- 30°S. While changes are taking place over Africa and the SW Indian Ocean, equatorial Africa and the Atlantic Ocean south of the Equator are under a northerly wind component. The central Indian Ocean exhibits a southerly component.

In January (LSFW), the 500 hPa mean meridional pattern is dominated by a northerly wind component over the South Atlantic, most of Africa and western Indian Ocean. The strongest poleward (negative) winds are to the south of the continent and over the central Atlantic. However, there are strong southerlies over southeast Africa with a centre near Durban (25°S, 30°E) and covering a radius of approximately 10° of latitude. Another area of relatively strong southerly flow is apparent over the equatorial Atlantic. By February (LSSW), the southerly components in the South Atlantic have spread northwards at the expense of the northerly winds in the central basin. At the same time, southerly winds in the vicinity of Durban have linked up with those in the south Indian Ocean (which have increased in intensity) through Madagascar. The region of northerly flow south of South Africa has shown some displacement northwestwards. The February trend is maintained through March to an extent that the eastern South Atlantic is experiencing southerly winds nearly all the way to the Equator. Simultaneously, the belt of southerlies from the south Indian Ocean to SE Africa has receded so that the whole of southern Africa is under a predominantly northerly flow. The overall pattern over the southern African region in February and March suggests the intensification of the AOA as its centre moves equatorwards. There is also some evidence of standing wave patterns poleward of 20°S.

For the mean zonal circulation, the tropical easterly winds are separated from the westerlies at the 12.5°S latitude in November (**Figure 5.6b**, EFW). Three weeks later (ESW), the easterlies have spread southwards so that the zone of demarcation is now along 20°S (though along 15°S in the Indian Ocean). The pattern is maintained into late

summer. However, it is temporarily disturbed during the February wet spell (LSSW), when the westerlies in the SW Indian Ocean spread equatorwards as far north as 10°S. The zonal pattern also indicates a southwestward propagation of easterly winds from the northern hemisphere over Africa to the equatorial Atlantic Ocean from November. The easterly belt reaches its furthest position in January after which it retreats to be centred again over the central interior of equatorial Africa. This behaviour, suggesting a seasonal cycle, is apparent in the vorticity patterns.

5.3.2.4 Mean horizontal wind vectors

In the mean, during November (**Figure** 5.7, EFW), the windflow is basically strong westerly south of about 20°S from the Atlantic right across Africa to the Indian Ocean. The flow is easterly from 10°S towards the Equator. The wind regimes are separated by light and variable winds, indicating the mean mid- level position of the sub- tropical high pressure belt. Over southern Africa, the anticyclone is centred near 25°E along 17.5°S, controlling a northwesterly airflow over the south west. The pattern is generally unchanged in December. However, the axis of the sub- tropical anticyclonic belt has shifted southwards to about 22.5°S and extends from the Atlantic to across southern Africa, with westerly flow poleward of it. The easterly flow covers the whole of tropical southern Africa. There is evidence of slight troughing in the south Mozambique Channel.

In January, (LSFW) a narrow zone of anti- clockwise circulation with an axis along 20-25°S straddles the Atlantic Ocean and southern Africa. The zone separates strong westerlies from tropical easterlies. The easterlies between 15 and 20°S from Mozambique to Namibia seem to have recurved from the westerly belt. However, there is evidence of a weak merger through Zambia, with the easterlies from equatorial east Africa. In the same period, the band of tropical easterlies from the Indian Ocean proceeds westwards across Africa to the Atlantic, intensifying as they go. Also worthy of note are easterly winds approaching Madagascar between 10 and 15°S which recurve southwards along the east coast before returning to the Indian Ocean as westerlies south of 25°S.

In February (LSSW), the Atlantic Ocean- southern Africa anti- clockwise system is still in evidence and has remained quasi- stationary. The easterly flow from the northern hemispheric region of the Indian Ocean becomes more northeasterly as the winds approach east Africa. The 500 hPa winds veer again to easterly as they cross the continent. The link between these easterlies and those from the sub- tropics is restricted

to a mininum The trough located in the south Mozambique Channel in January has moved about 20 degrees of longitude eastwards to 40°E. By the end of March (LSTW), the ridge across southern Africa has weakened, leaving two separate centres of local maxima in the Atlantic (near 20°S,12.5°W) and along 20°S from southern Zimbabwe to the Mozambique Channel. Also, during this period, northeasterly winds into NE Africa have spread southwards to about 12.5°S before veering to easterlies over Africa. Some of the winds recurve over southern Tanzania to return to the Indian Ocean as westerlies between 10 and 15°S.

5.3.2.5 Vertical velocity

Figure 5.8 illustrates vertical wind patterns in the middle- levels. Negative values (upward motion) prevail over much of the domain throughout summer. For early summer, there are primarily two centres of relatively greater uplift; along the Equator over western Africa and eastern Madagscar/ Reunion Island region. The centre of maximum uplift shifts southeastwards from the Equator at EFW to Madagascar region during ESW. The January pattern (LSFW) shows an area of significant rising motion stretching from Madagascar to northern Mozambique, Malawi and Zambia and linked to a similar area over the Congo and Zaire. This link is maintained (though weaker) in February (LSSW) during which the equatorial regions become more active. By March, the link is severed such that there are two zonally oriented and distinct regions; one with an axis along 15°S and the other around the Equator.

5.3.3 Upper- troposphere : 200 hPa

A rather tight geopotential height gradient exists poleward of the TSB (20°S) in the upper- troposphere. An anticyclone is centred on the equatorial regions of Africa at the onset of summer. This anticyclone is located across tropical southern Africa in December with a centre along 12°S, increasing the meridional gradient of geopotential height over the rest of southern Africa. The southeastward displacement of the continental anticyclone ceases in January (LSFW, **Figure 5.9**) when the centre is along 15- 18°S, afterwhich the anticyclone becomes quasi- stationary (near 15°S) with a slight northward displacement with time. This could be the upper-level outflow of convective cells of the ITCZ. As the season progresses, the heights generally increase in magnitude, more obviously over the tropics due to diabatic heating.

The mean upper horizontal zonal wind is basically westerly over southern Africa and adjacent sub- tropical oceans, and the equatorial Atlantic Ocean. There are areas of light easterly wind around the Equator in the Indian Ocean and over west equatorial Africa. The easterly flow regions become linked in December (**Figure 5.10a**, EFW) with a local maximum over Africa along 5-10°S. Elsewhere, the pattern remains westerly. The patterns do not show major changes between January and March (LSFW, LSSW and LSTW). They show easterly winds stretching from the Indian Ocean through Africa to just off the west coast of Angola between 5°N and 15°S, with westerly winds elsewhere. The winds, in general, decrease in intensity with time. The strongest easterly winds are over the central regions of Africa, at LSFW and LSSW compared to over the eastern equatorial Atlantic Ocean at lower levels.

The mean meridional wind pattern during the first wet spell of summer (**Figure 5.10b**, EFW) shows a northerly component over the eastern Atlantic with a jet- like configuration extending from equatorial regions southeastwards through southwest Africa. Another broad region of northerly airflow exists in the central Indian Ocean encompassing northeastern Madagascar and northeast Africa, with a local maximum near 20°S between 60 and 70°E. Sandwiched between the two maritime northerly flow regions are strong southerly winds which stretch from the south Indian Ocean, through southeast Africa (where they are strongest) to the northern hemisphere. The general configuration is maintained over the Atlantic and Africa during the December spell (ESW). However, the systems appear to have moved slightly southeastwards. The northerly airflow in the central Indian Ocean has decreased appreciably and has receded westwards (to cease near Mauritius) so much that the southerly airflow now covers the western Indian Ocean with a local centre in the south Mozambique Channel.

Thoughout late summer, the dominating influence over southern Africa is from the SE Atlantic Ocean where the winds are northerly. These winds are confined to the ocean and the western coastline of southern Africa in January (LSFW) but spread southeastwards to the south of Africa as the season progresses such that by the end of March (LSTW), most of southern Africa is under the influence of a northerly airflow, with an axis through Namibia and central South Africa. At the same time, in the central Indian ocean, northerly winds evident between 10 and 30°S in January spread outwards with time and intensify in the process. Throughout late summer, a link is maintained between the southerly wind regimes in the SW Indian Ocean and equatorial Atlantic via Madagascar and eastern parts of southern Africa (northern Mozambique and Tanzania, for example). The overall picture

shows meridional systems oriented NW- SE composed of alternating northerly and southerly winds. This indicates a marked and organised exchange of moisture and energy between the tropics and higher latitude regions, probably controlled by a sub- tropical wave train.

The upper- level total wind structure (vector field) in November (**Figure 5.11**, EFW) shows a northwesterly airflow stretching from the equatorial Atlantic southeastwards to southern Africa. An anticlockwise circulation cell is centred over the central interior of Africa along 10°S; the flow becomes westerly in the Indian Ocean. The equatorial airflow over Africa illustrates a trough off the east coast to Madagascar. In December, the pattern over the region becomes dominated by an anticyclonic system (upper- level anticyclone, ESW) centred along 17.5°S across Africa (having moved about 8- 10° southwards in 15-20 days). Consequently, an east- southeasterly flow covers tropical Africa while the northwesterly flow poleward of 20°S has been maintained. The northwesterlies from the equatorial Atlantic are still in evidence, but are now weaker. The trough off east Africa has also decayed. Instead, a belt of light and variable winds with an axis along 10°S now separates the equatorial easterlies from the sub- tropical westerly winds.

The continental anticyclone continues its southeastward progression to be centred along 20°S, the tropical- sub-tropical boundary (TSB) in January (LSFW). Together with narrower anticyclonic cells along the TSB in the Indian Ocean, the anticyclone controls a southeasterly windflow across tropics of central and east Africa. The flow then veers to northeast in the northern hemisphere. The anticyclone also causes the equatorial westerlies from the Atlantic Ocean to split resulting in the southern hemispheric portion of the flow redirected southward to become part of the extra- tropical westerly winds. The TSB also demarcates tropical easterlies from extra- tropical westerlies. The pattern is maintained in February (LSSW). The tropical southerly winds in the western Indian Ocean are relatively stronger than during LSFW. In March, flow around the Equator is clockwise in the Indian Ocean and northeast Africa. Further south, the anticyclonic belt along the TSB remains intact. The overall pattern includes a narrow zone of easterly winds in the Indian Ocean between 5 and 10°S. Winds across tropical Africa are easterly. Deformation of the winds occurs in the eastern equatorial Atlantic. The extra- tropical winds across southern Africa have backed to predominant northwesterly.

The corresponding upper- level divergence pattern over Africa is dominated by largely divergent flow covering virtually the whole sub- continent (**Figure 5.12a**). In the South Indian Ocean through the Mozambique Channel, weak convergence is present. There is also convergence over most of the eastern Atlantic Ocean, relatively greater just to the south of the Equator off the African coast. During December (ESW), divergence over the tropical Indian Ocean has spread southwards, displacing the convergence areas poleward of 20°S. The divergence over the central interior of Africa has also increased. The pattern in the Atlantic Ocean has remained basically unaffected.

In January (LSFW), the upper divergence pattern consists of convergence motion in the eastern Atlantic Ocean and south of 25°S across Africa and the Indian Ocean. Elsewhere, there is divergence with the strongest activity over tropical southern Africa (near 12°S, 25- 30°E) and northern Madagascar stretching zonally into the equatorial Indian Ocean. During February, there is evidence of westward movement of the upper- level divergence, although the axis of major activity has remained quasi- stationary. The divergence over Africa is linked to that over Madagascar and the equatorial Atlantic. A tongue of convergent motion is protruding southwards along the northeast coast of Africa from the northern hemisphere.

By the end of March (LSTW), the divergent motion has generally spread further westwards and southwards over Africa, completely separating convergence over the sub-tropical Indian and Atlantic Oceans. Throughout late summer, the divergence pattern over Madagascar has remained strong. Over Africa, the shift in the centres of maximum activity from central Africa northwestwards to equatorial regions suggests the role of differential heating associated with the movement of the sun. The pattern illustrates the regions of upper- level outflow from deep convective activity of the ITCZ. The convergence area off the northeast coast of Africa is still in evidence.

The southern hemispheric mean vorticity circulation at 200 hPa is primarily anticyclonic, with reference to **Figure 5.12b**. The circulation is strongest in November (EFW). Local centres of activity are in the central Indian Ocean and central southern Africa (both along 20°S). The pattern does not change over Africa (though the values increase) but the local maximum in the Indian Ocean is displaced further south (to along 25- 30°S). The beginning of late summer (LSFW) is characterised by an anticyclonic pattern over southern Africa and the Indian Ocean south of about 10°S. The anticyclicity becomes generally stronger, especially across central southern Africa in February (LSSW). In

March (LSTW), though, the pattern is more zonal. A zone of cyclonic motion is evident in the south Indian Ocean along 30°S and is exerting some influence westwards across the southern tip of Africa, thus disecting the anticyclonic flow into two branches. The overall configuration is a well- defined ridge of anticyclonic motion with an axis along 20°S with local centres of maximum activity over southern Africa and in the central Indian Ocean.

Stream functions are isolines akin to a large- scale view of the vorticity field. More details regarding the concepts of stream functions are illustrated in **Annexure 2**. In short, negative (positive) anomalies of the stream function correspond to large- scale cyclocinicity (anticyclonicity) in the southern hemisphere. The closer the isolines, the greater the rotational velocity, directed perpendicular to the lines. According to **Figure 5.13a,** the whole southern hemisphere surrounding Africa has a positive stream function in November (EFW) at upper levels, with a centre along 20°S near 50°E. By the end of December, a negative area has spread into the southern hemisphere as far as 10°S in the equatorial east Atlantic with its centre of maximum activity over West Africa. Positive stream function across central southern Africa has increased in magnitude and gradient. The centre of activity has been displaced slightly southwestwards by about 5-8°. During the course of late summer, the centre of highest positive values continues to spread westwards, reaches 30°S in January before retreating equatorward slightly in February to be along 25°S in March (LSTW).

Like stream function, the velocity potential is derived from the continuity equation. In this case, the motion is irrotational (implying that the vorticity at all points in the domain is zero). Its mathematical determination and sign convention are also shown is **Annexure 2**. At the onset of summer (EFW, **Figure 5.13b**), there is negative velocity potential (large-scale upper divergence) over equatorial Africa and the tropical Indian Ocean while weak positive potential (large- scale convergence) covers most of the central south Atlantic. By December (ESW), the systems have shown southeastward displacement to along 10°S in the vicinity of northern Madagascar east of 20°E in January (LSFW). Positive values in the Atlantic advance and retreat by the end of the season (LSTW). The process indicates a five- month cycle when the maximum large- scale upper- level divergence is temporarily shifted from equatorial Africa in November to the Indian Ocean NE of Madagascar during January and February. The negative velocity potential axis is more meridional over Africa in early summer and towards the end of summer. In mid- summer, the patterns are more zonal and overlie the SW Indian Ocean (SWIO) monsoon region.

5.4 Vertically integrated water vapour Flux

In early summer, there is very little moisture advection over southern Africa, south of 15° S. The moisture into tropical Africa is from the Indian Ocean, sourced from the northern hemisphere as well as the central waters advected between 10 and 25°S. During November (EFW, **Figure 5.14**), there is little evidence of cross- equatorial flow. It appears the monsoon winds towards Africa are in their infancy. Some of the water vapour is re- directed back to the Indian Ocean along the Equator. In the meantime, the Atlantic Ocean fluxes are largely confined to the Ocean with only the coastal regions of western Africa being affected. In December (ESW), the moisture from the northern hemisphere has spread southwards along the east African coast and even as far south as the Comoros Islands. Some of this moisture, though, still returns to the Indian Ocean, but this time further south (between 5 and 10°S). At the same time, the advection of moisture westwards in the south Indian Ocean still takes place between 10 and 25°S. The advection, though, is strong to the south of 20°S and moisture crosses the south Mozambique Channel to southern Africa, increasing low- level moisture in the source regions of Angola and the Mozambique Channel.

In January (LSFW), the water vapour flux field shows the moisture in the Atlantic restricted to the ocean and advected from the sub- tropics equatorward. The pattern also illustrates cross- equatorial moisture advection in the Indian Ocean with some moisture returning to the central waters of the Ocean just south of the Equator. The rest is channelled towards and down the east African coast and even southwards to the Mozambique Channel. At the same time, a broad band of water vapour flux in the Indian Ocean between 10 and 30°S is advected westwards, part of which ends up in the Mozambique Channel/ Madagascar region, while the poleward component of it proceeds westwards into and across southern Africa between 17.5 and 25°S.

During February, the moisture flux in the Atlantic has remained unchanged from January. Major changes are apparent in the Indian Ocean where, firstly, the moisture from the northern hemisphere has advanced further southwards with the return flow to the central waters along 10°S. A well- defined anti- clockwise system with centre along 35°S between 50 and 70°E has developed. The system is contributing moisture towards Madagascar and the southeast quadrant of southern Africa (mainly Mozambique and Zimbabwe). By March (LSTW), the flux field has undergone marked changes over Africa. This time, virtually all water vapour in the western Indian Ocean is directed westwards,

spilling into Africa, especially the eastern segment of the sub- continent from 25°S northwards. As in January and February, the Atlantic Ocean moisture has remained a largely maritime affair with only the coastal areas being affected. This is due to the shallow boundary layer over the cold upwelling waters of the northern Benguela Current.

A major feature of the vertically integrated water vapour flux is the blocking effect of Madagascar with respect to trade wind sources over the warm Indian Ocean. At the onset of summer, the island "re- directs" westward fluxes to equatorial Africa (Tanzania). As the westward stream displaces poleward as part of the seasonal cycle, almost all the moisture from the Indian Ocean is deposited on the island in December and January. The moisture eventually reaches southern Africa in late summer being from the SWIO. Madagascar also "attracts" moisture associated with the monsoon from December to February, the moisture otherwise intended for eastern regions of Africa.

5.5 Mean vertically integrated internal Energy

The importance of internal energy is shown in **Annexure 2**. From the first law of thermodynamics regarding conservation of energy, diabatic effects (radiative heating from solar and infrared sources, latent heating, frictional heating, and turbulent and conductive heating at the ocean- atmosphere boundary) constitute the sources and sinks of internal energy for the atmosphere (Peixoto and Oort, 1992). They play major roles in determining degrees of convective activity, CISK (Conditional Instability of the Second Kind), frontal development and maintenance as well as energy conversion, particularly the generation and destruction of available potential energy. Generation of kinetic energy requires vertical motions whose prerequisites include expansion (hence, uplift) of lighter air and compression of denser air.

The effects of solar insolation and terrestrial heating are evident throughout summer in the mean maximum internal energy over tropical southern Africa (**Figure 5.15**). The centre moves slowly southwards from about 15°S in late November (EFW) to be at the TSB in January and February before weakening towards the end of the season (LSTW). The behaviour is attributed to the movement of the sun and associated sensible heat fluxes during Austral summer. Also evident in the January analysis is the relative increase in the internal energy in the western Indian Ocean in the Madagascar region where mean SST exceed 28°C. This coincides with the mean position of the ITCZ in the Indian Ocean,

indicating the intensity and depth of convective systems at this time. The main contribution or source of internal energy is the latent heat released during the cloud- forming processes and associated convective precipitation in the ITCZ.

5.6 Discussion and Inferences

The mean circulation patterns for various phases of summer were analysed for southern Africa and adjacent oceans from daily ECMWF data in the period 1986- 1992. Meteorological patterns revealed changes taking place as summer progessed, particularly the seasonal cycle due to heating budgets between land and ocean, sources of moisture over southern Africa, and spatial distribution patterns of the different phases. The analyses have demonstrated the need to view summer in stages rather than encompass all the characteristics into one mean. The following summarise major points observed from the analyses.

The tropical/ extra- tropical circulation boundary is demarcated by the 20°S latitude, in partial agreement with the findings of Harrison and Harangozo (1983). A trough in the vicinity of this latitude, evidenced by the low- level total wind field and water vapour flux from December, indicates a potential zone of convection, hence energy and momentum, over southern Africa. The intenisty of convection is a function of the interaction between the tropical easterlies and sub- tropical westerlies. The appearance of this trough (MCAT) in the mean patterns which consist of mostly dry days also demonstates its importance in the region. The TSB should be located poleward at the surface, where kinematic patterns like wind conflunce play a significant role in initiating convective episodes. At the time of writing this thesis no detailed study has given the TSB its relevance to southern Africa. Harrison (1986), however, refers to a thermal low along 20°S also from which convection develops. Chapter 9 of this thesis discusses the TSB in greater detail.

At low levels, the sub- tropical high pressure belt exerts its influence throughout summer with its axis roughly along 25°S at 700 hPa. The Atlantic Ocean Anticyclone remains relatively strong and quasi- stationary, extending a ridge into southern Africa. The Indian Ocean Anticyclone, on the other hand is weakened and displaced further east as low geopotential heights propagate southwestwards from the equatorial Indian Ocean to be at their highest latitude (20°S) in February.

Throughout summer, there is low- tropospheric convergence along and just off the east coast of South Africa. The convergence is greatest in early summer. This can be attributed to the coastal low pressure systems which form ahead of cold fronts passing through the region (Harrison, 1984, Estie, 1984). These coastal depressions often bring cloudiness and across South Africa (Gill, 1977; Bannon, 1981) and have been detected to have a frequency of about seven days throughout the year (Preston- White and Tyson, 1973). Other important factors producing convergence include the Agulhas Current and the steep escarpment near Durban (Jury et al., 1993).

The mean low- level flow over southern Africa is largely divergent along and to the south of 20°S, extending from the tropical eastern Atlantic Ocean. As the season progresses, a zone of convergence becomes more established and continuous from the SWIO through Madagascar across Africa to the equatorial east Atlantic. The divergence pattern also exhibits a Hadley- cell like structure over the African continent with positive values over most of southern Africa and convergence in equatorial regions. The zero line is in the vicinity of the Tropical -Sub- tropical Boundary (20°S latitude). This dipole weakens as the season progresses when the convergence intensifies at the expense of increasing divergence in the northern hemisphere. Mean rising motion over tropical regions and descending motion in the sub- tropics is observed. In late summer, most convergence is due to cross- equatorial flow from the northern hemisphere.

The tropospheric flow is predominantly anticyclonic. However, negative vorticity (cyclonic motion) exists between the Equator and 10°S at the onset of summer. This zone, accompanied by low- level geopotential heights, makes rapid southwestward progression to traverse Africa along 15°S. The zone is a quasi- permanent feature of low- level circulation until the end of the season when it disintegrates, leaving remnants in the adjacent tropical oceans. The cyclonic vorticity zone indirectly indicates the mean position of the ITCZ in the Indian Ocean. Over Africa, the cyclonicity exhibits the mean position of the Mozambique Channel- Angola Trough (MCAT). The ITCZ, which is usually meridionally oriented across the continent, plays a secondary role.

There is evidence of gradual westward propagation of circulation systems in the equatorial regions of the Indian Ocean, as evidenced by low- level geopotential height, vorticity and zonal wind. The westward extent of equatorial westerly winds shifts southwestwards from the Indian Ocean during early summer to central tropical southern Africa (across Zambia

and Angola) in January and February. The westward movement is checked by ridging of the Atlantic Ocean Anticyclone into the western regions of Southern Africa. This is supported by quasi- stationary wind patterns in the east Atlantic Ocean.

The meridional wind patterns show a standing wave train feature of about 35° longitude wavelength across southern Africa oriented SW-NE. In the mean, northerly flow stretches from the northern hemisphere through the Congo to higher latitudes via the western flank of southern Africa. The return flow from higher to lower latitudes takes place mostly in the Indian Ocean where the flow is predominantly southerly. However, some southerly winds are generated in the immediate environs of southern Africa - in the southeast Atlantic as well as in the Mozambique Channel. The combined influence of these two areas provides the necessary eddy effects as it strengthens and enhances the advection of warm equatorial moisture and energy towards extra- tropical regions.

As at low levels, mid- tropospheric geopotential heights are highest in January and February. The sub- tropical anticyclonic ridge is absent. A trough through Mauritius in the SWIO replaces the Indian Ocean Anticyclone, implying an increase in cyclogenesis in the region after January. The Atlantic Ocean anticyclone, on the other hand, remains strong with its axis located near 15-20°S, having tilted equatorward with height compared to its low- level position. There is little evidence of a trough across southern Africa. This indicates that the middle tropospheric climatological structure over the sub- region is dominated by ridging of the AOA into western southern Africa, a condition which naturally suppresses deep convection.

The mean mid level meridional flow, like at lower levels, shows a standing wave across the domain. There is no vertical tilt with height but there is evidence of vertical wind shear, paricularly poleward of the TSB. Southern Africa is dominated by southerly winds which spread westwards from the south Mozambique Channel in November to cover eastern southern Africa in January. Thereafter, a northerly component of the wind prevails, resulting in the retreat of southerly winds back to the SWIO. This is consistent with the existence of a seasonal cycle, detected by Harangozo (1989), where the equatorward components describe the returning part of the cycle. Elsewhere in the Atlantic Ocean, the winds progressively change from being entirely northerly in early summer to mostly southerly by the end of March. Thus, the tropical to extra- tropical flow of warm equatorial air takes place through western southern Africa. Most of the return flow takes place in the eastern Atlantic Ocean with the SWIO providing the

remainder. The mean zonal wind patterns distinguish the equatorward limit of the westerly wind regime compared to the lower- troposphere. An equatorial westerly belt in the Indian Ocean is apparent but weak at 500 hPa, except in January. It remains a feature of the central waters, implying an eastward tilt with height from the surface. In February, the belt merges with the extra- tropical westerly regime such that westerlies in the western Indian Ocean extend as far equatorward as 10°S.

The vector field illustrates the separation between equatorial easterlies and extra- tropical westerlies taking place between 10 and 20°S over the oceans at the onset of summer. From December onwards the demarcation zone is along the TSB in the Atlantic and across southern Africa. There is more disorganisation in the Indian Ocean. Firstly, transequatorial flow at 500 hPa does not take place in earnest until February, when the northeast monsoons influence the east coast of Tanzania. Vortices (cyclonic and anticyclonic) are evident resulting in relatively weak flow in the region. Despite this, the 500 hPa winds between 10 and 20°S reverse direction from one phase to the next.

An upper- level anticyclone exists over tropical Africa, having moved from the equator in November to around 15°S by the end of the summer (compared to about 25°S at low levels). This southward propagation was also observed by Taljaard et al. (1969) and Taljaard (1981) who noted the migration from winter to summer reaching the southernmost location in January. The implication is a seasonal cycle in the weather patterns over southern Africa, largely attributed to solar insolation angle. In the process, equatorial easterly winds propagate westwards from the Indian Ocean, rapidly between November and December to form a continuous and characteristic upper-level feature of tropical circulation thereafter. The mean 200 hPa meridional motion throughout summer consists of a northerly flow emanating from the equatorial Atlantic Ocean through western southern Africa to the south of the continent. The rest of Africa is under a southerly wind regime which is acting as the returning arm of the flow. The southerly wind is steadily displaced eastward during the course of the season. Elsewhere, northerly flow dominates the central Indian Ocean.

Upper- level convergence is confined to the Atlantic Ocean as well as poleward of 25°S in the Indian Ocean, leaving the divergence mainly over Africa and the tropical Indian Ocean. The centre of divergence in the Indian Ocean moves southward from the Equator in early summer to the TSB by March. The airflow is predominantly anticyclonic throughout the southern hemisphere all summer. This is well illustrated in the upper- level stream function

patterns. A local maximum is located over central southern Africa along the TSB. A zone of cyclonic upper flow is experienced between 30 and 40°S in the east Indian Ocean, particularly in November. The anticyclonic flow regime is "spun up" in the early summer by a southeastward stream over the Atlantic and maintained in the mid- summer by tropical easterlies.

In the mean, trans-equatorial advection of moisture does not occur until December. The change takes place in the Indian Ocean, down the east coast of Africa (Tanzania region) up to the northwest of Madagascar. A zone of moisture convergence is present and quasi-stationary throughout the summer season over the western half of southern Africa extending from Angola to South Africa. This is called a west coast trough by Taljaard (1981), Harrison (1986) and Harangozo (1989). Similar troughs in western sides of continents, and the dynamics of their development, have been discussed in detail by Bell (1986). Another zone of moisture convergence exists between Angola and the central Mozambique Channel. However, it weakens towards the end of the season. This configuration is also evident in the middle levels as evidenced by the 500 hPa wind vectors between 12 and 17°S. The "blocking" effect of Madagascar is clearly illustrated in the water vapour flux fields.

In January and February, most of the moisture flux is confined to the Indian Ocean, where in the tropical regions, only the coastal areas of east Africa are affected while the rest of the moisture is re- directed back to the ocean. Moisture in the sub- tropics is supplied from the eastern Indian Ocean by the trade winds between 15 and 25°S and is advected to Madagascar and SE Africa between 20 and 30°S. The fluxes from the warm Mozambique Channel also contribute to the moisture across the sub- continent. In March, moisture in the western Indian Ocean is directed towards Africa and across the eastern escarpment. The transport is stronger in the vicinity of the Equator.

The Atlantic Ocean does not supply much moisture to southern Africa. Water vapour fluxes are confined to coastal regions. However, their influence is in reinforcing an anticyclone centred near 25°S, 30°E throughout summer. This anticyclonic system enhances the moisture advection to the north of it as well as increasing meridional convergence associated with the trough behind it. Its influence becomes more pronounced as the season progresses. Lindesay (1992) also detected the anticyclone as a bud- off from the South Atlantic Ocean. Tyson (1984), using principal component analyses of low-

tropospheric pressure and rainfall, documented that anticyclonic ridging through South Africa accounted for up to 25% of the variance in their correlations.

Monsoonal effects on southern Africa are pronounced over northern Mozambique and northwest Madagascar in January and February. The monsoon winds do not come down far enough to influence the plateau of southern Africa. In the mean, they spread as far south as 12°S over east Africa at low levels and contribute little in terms of moisture. The observation is in partial agreement with the findings of Critchfield (1974) and Tyson (1988). The moisture over the rest of southern Africa is concentrated around the low pressure areas over Angola (near 15°S, 20°E) and in the central Mozambique Channel. Thus, precipitation in the region owes a lot to both kinematic affects (divergence) as well as thermodynamic changes. These properties are interelated through and depend upon convection, also noted by Harangozo (1989), which, in turn, is a function of the internal energy of the prevailing synoptic system over the region. Towards the end of the season, in response to the changing pattern of solar heating of the earth, the moisture associated with the monsoons is restricted to equatorside of 12°S.

It must be stressed, however, that while mean circulation patterns describe and identify atmospheric controls which determine the general climate of southern Africa, they do not represent active convective wet spells at sub- monthly scales. The mean patterns mask characteristics of synoptic- scale weather regimes (eg., Reinhold and Pierrehumbert, 1982), perstistent anomalies (Dole, 1982), blocking activity, and transient waves (Jury et al. 1993) which are themselves perturbations or departures from the mean. As already mentioned in the methodology section of this chapter, the climatological patterns are not intended for forecasting, but provide useful background. They cannot be used for agricultural planning which is vulnerable to weather fluctuations of the order of weeks, the subject of the next chapter.

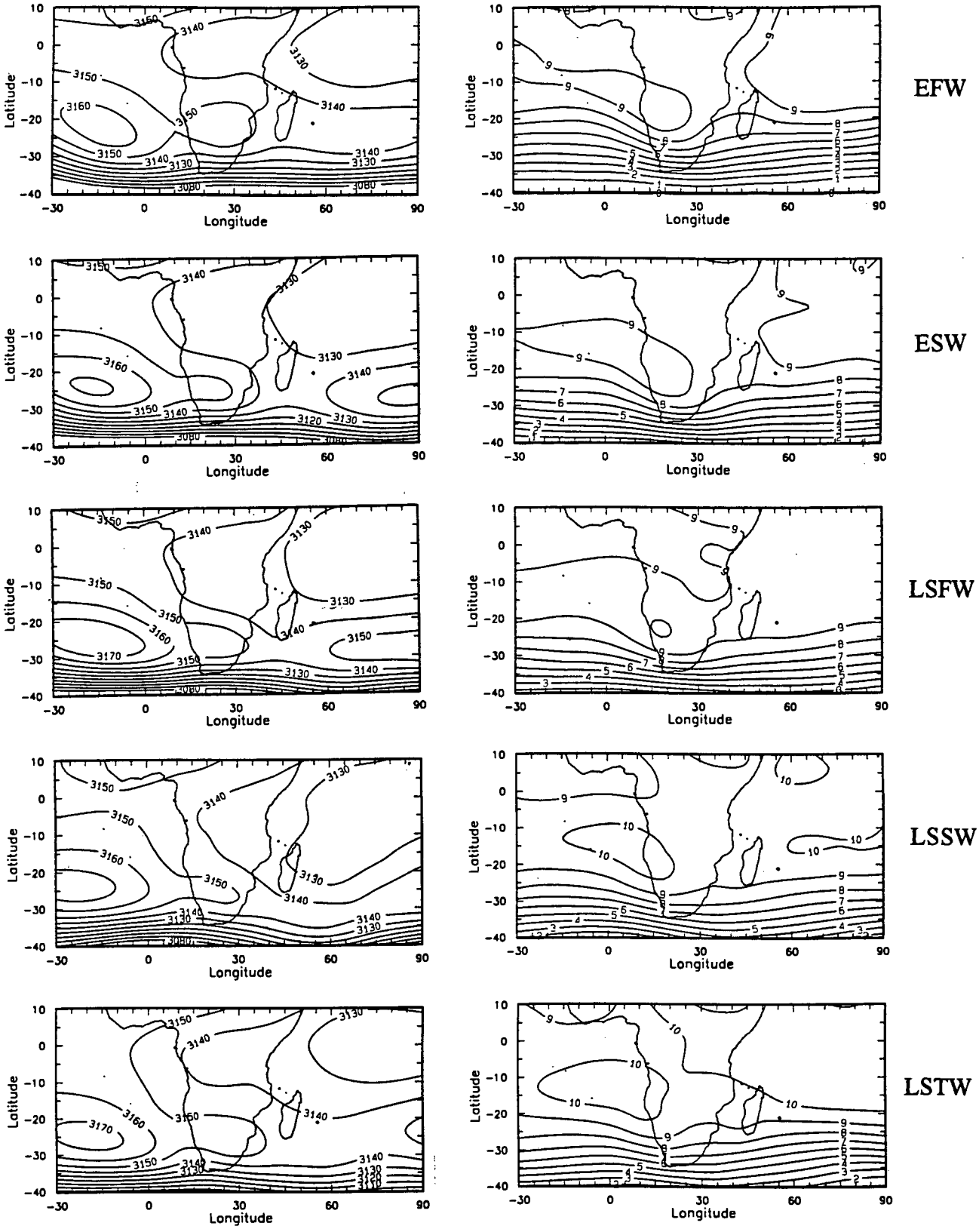

Figure 5.1 : Mean 700 hPa geopotential height (a) and temperature (b) for all five major wet spells. Contour intervals are 10 gpm and 1°C, respectively.

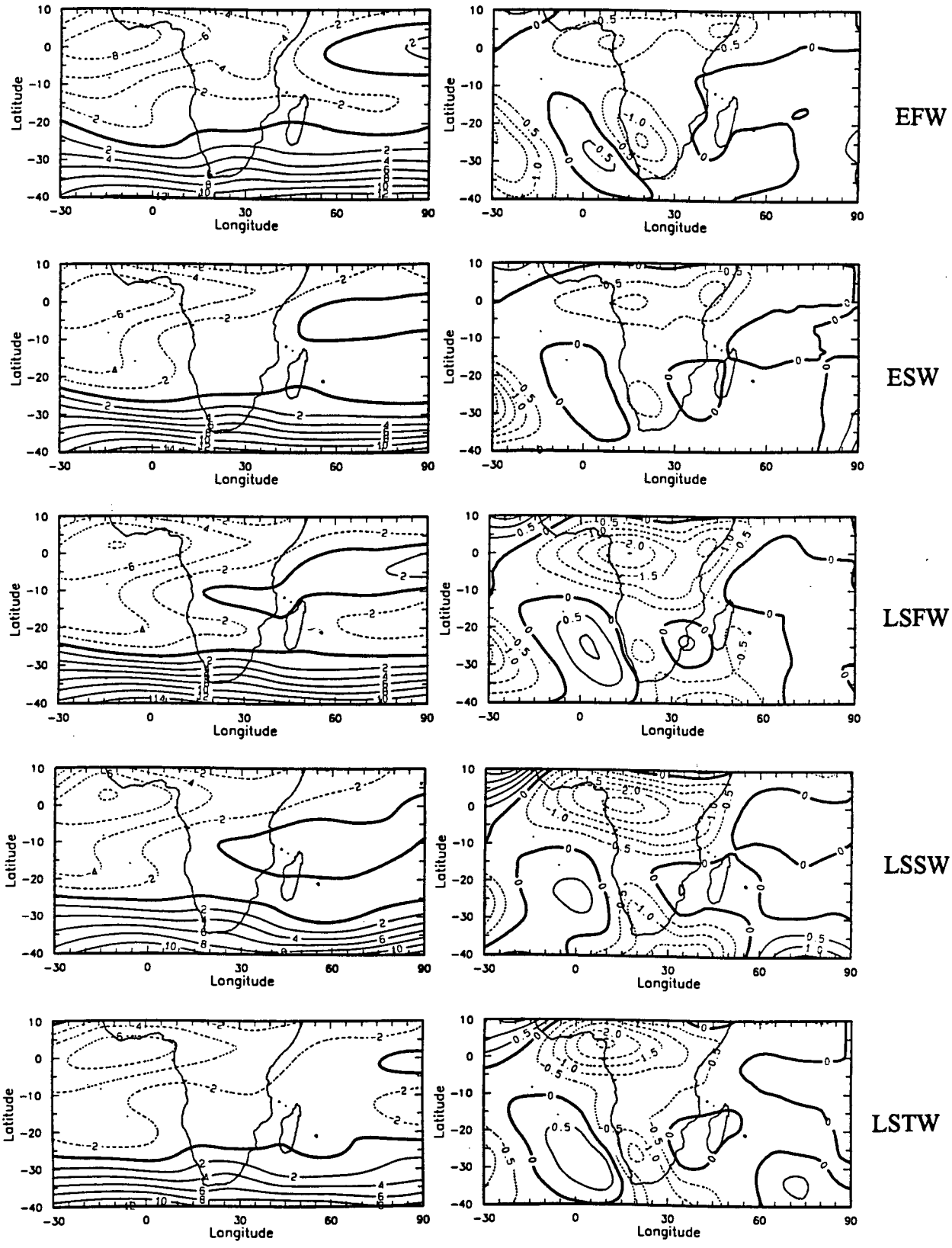

Figure 5.2 : Mean 700 hPa zonal wind (a) and meridional wind (b). Contour intervals are 2 and 0.5 m s^{-1}, respectively.

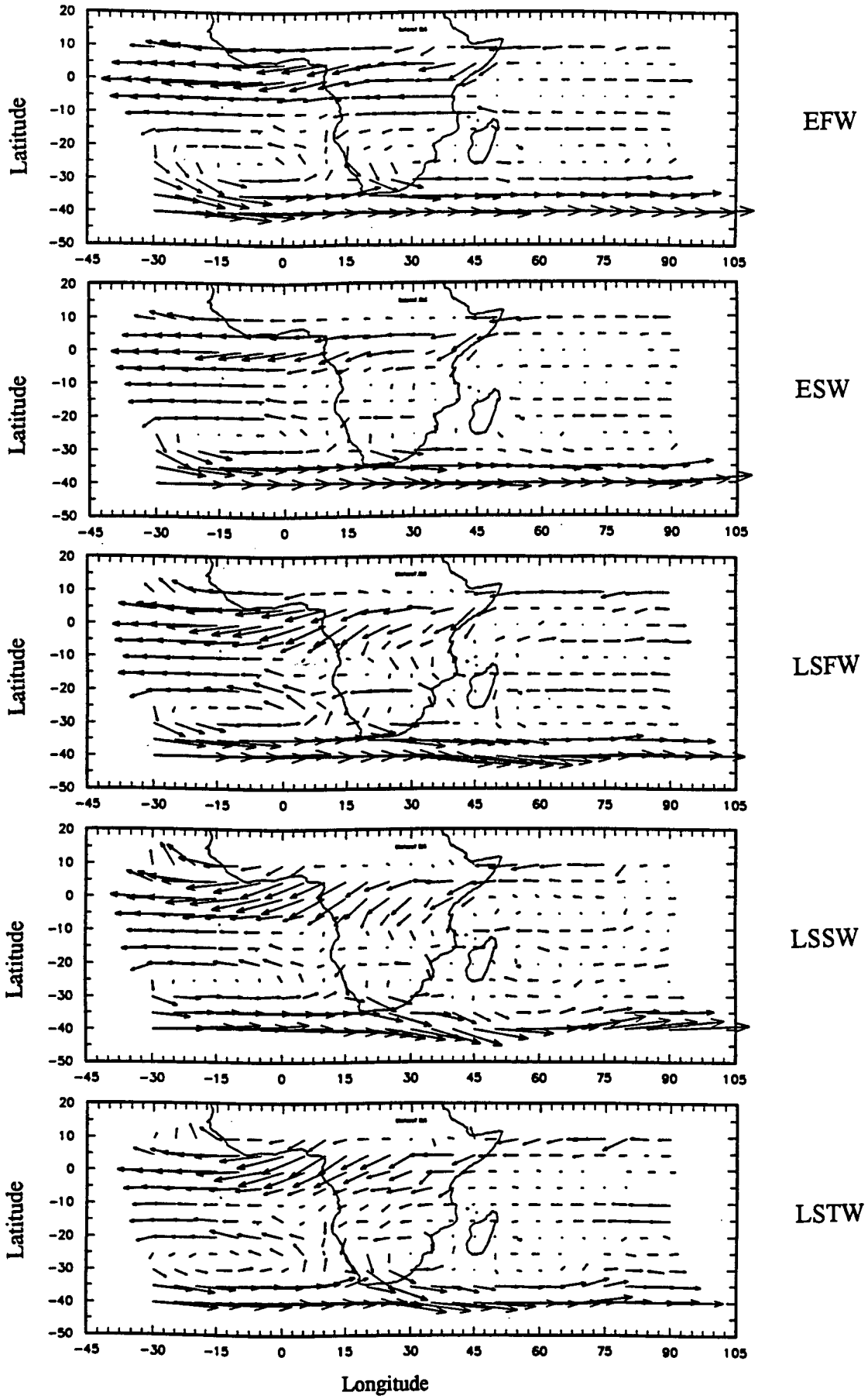

Figure 5.3 : Mean horizontal wind vectors at 700 hPa. The longest vector is equivalent to 13.5 m s^{-1}. Vectors are at 5° intervals.

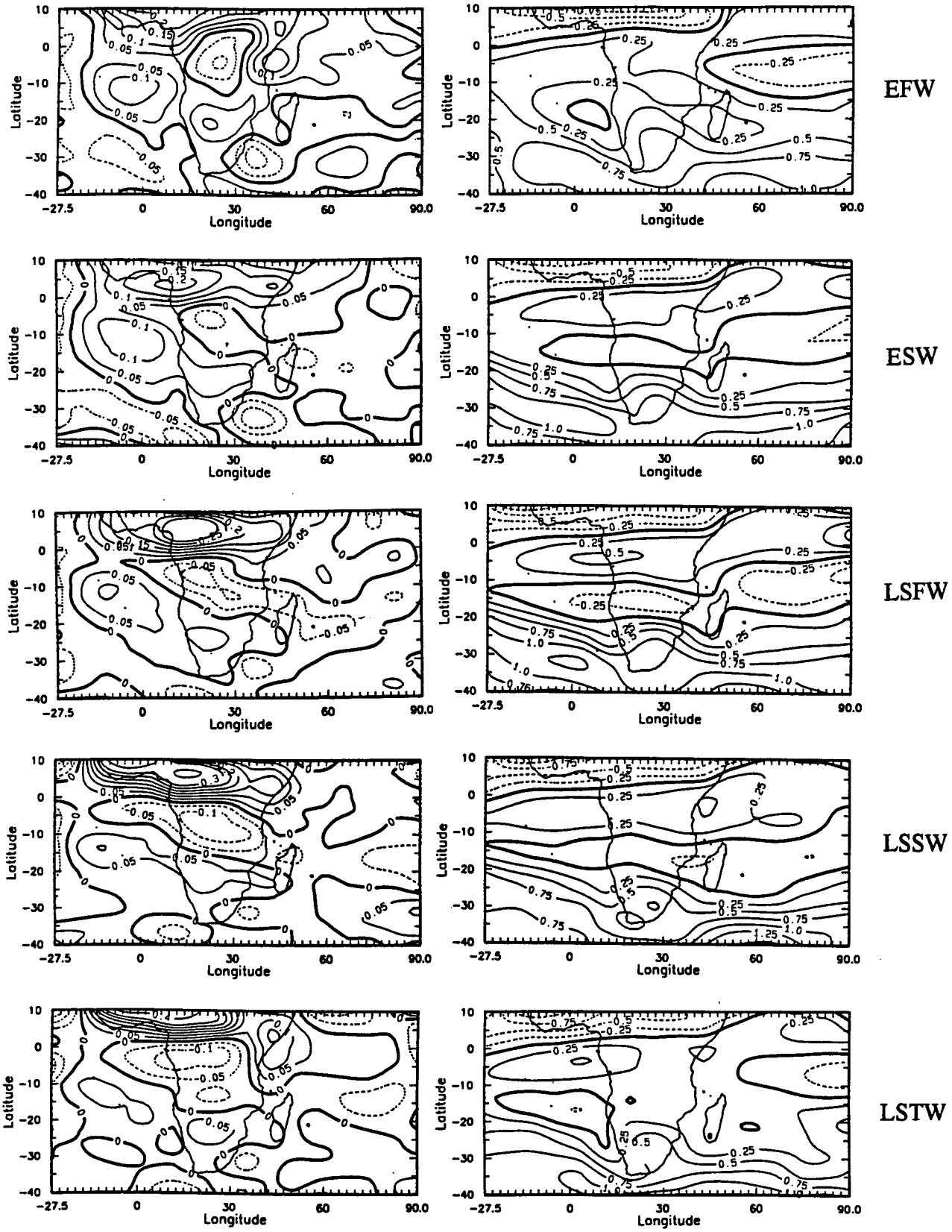

Figure 5.4 : Mean 700 hPa horizontal divergence (a) and vorticity (b). The contour intervals are 0.05 and 0.25 x 10^{-5} s^{-1}, respectively.

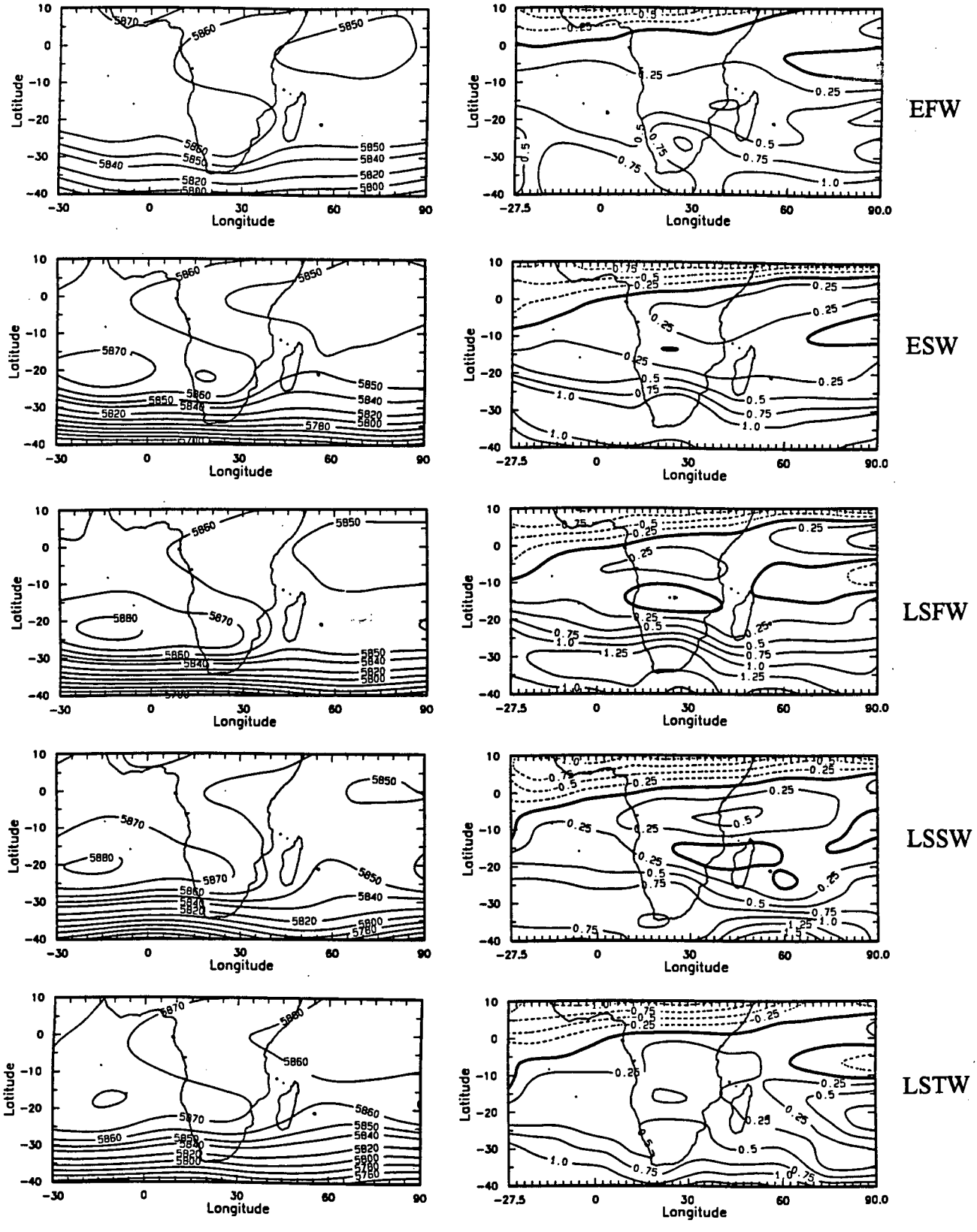

Figure 5.5 : Mean 500 hPa geopotential height (a) and vorticity (b). The contour intervals are 20 gpm until 5840 gpm and thereafter every 10 gpm for (a). The interval for the vorticity is 0.25 x 10^{-5} s^{-1}.

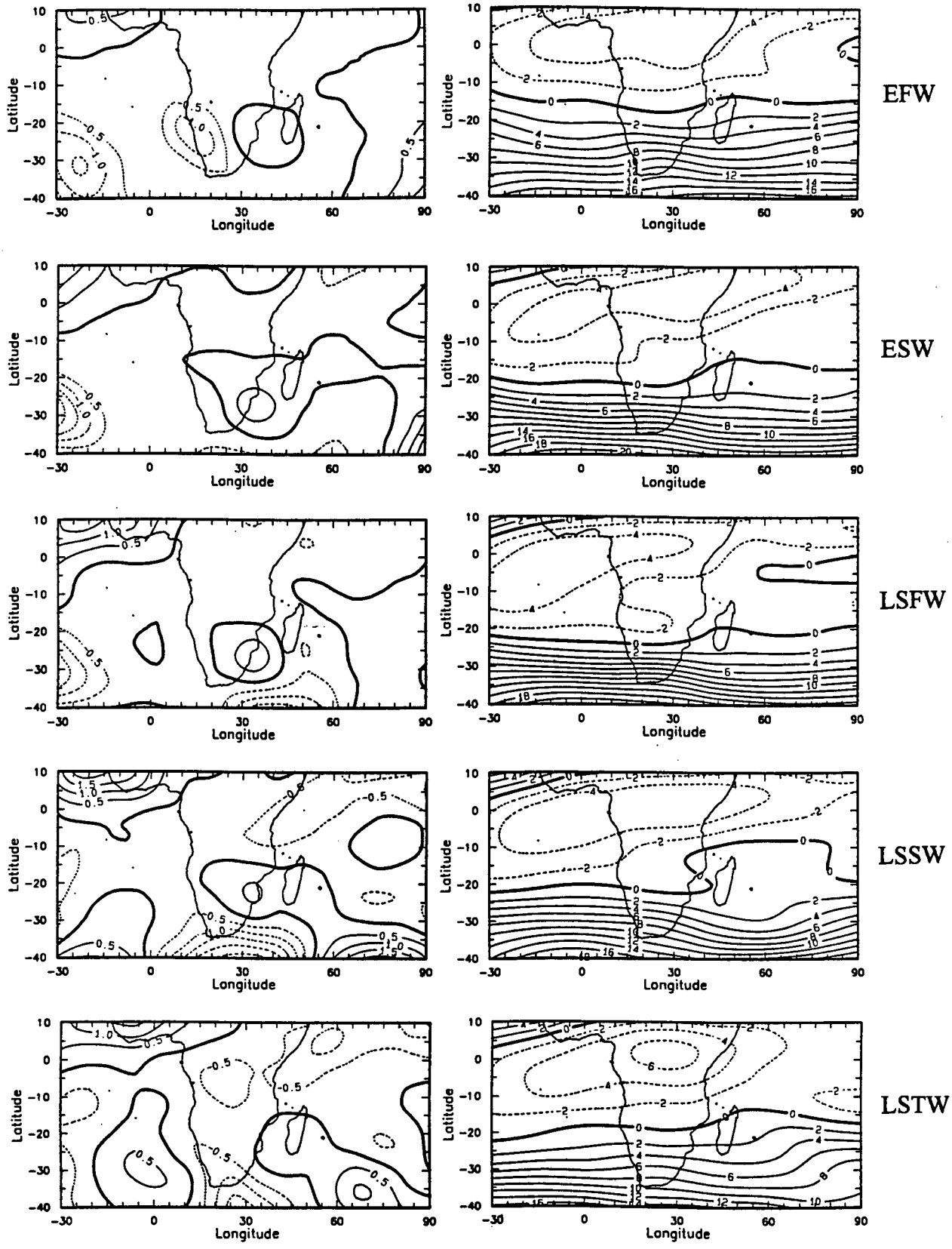

Figure 5.6 : Mean 500 hPa meridional wind (a) and zonal wind (b). Contour intervals are 0.5 and 2 ms^{-1}, respectively.

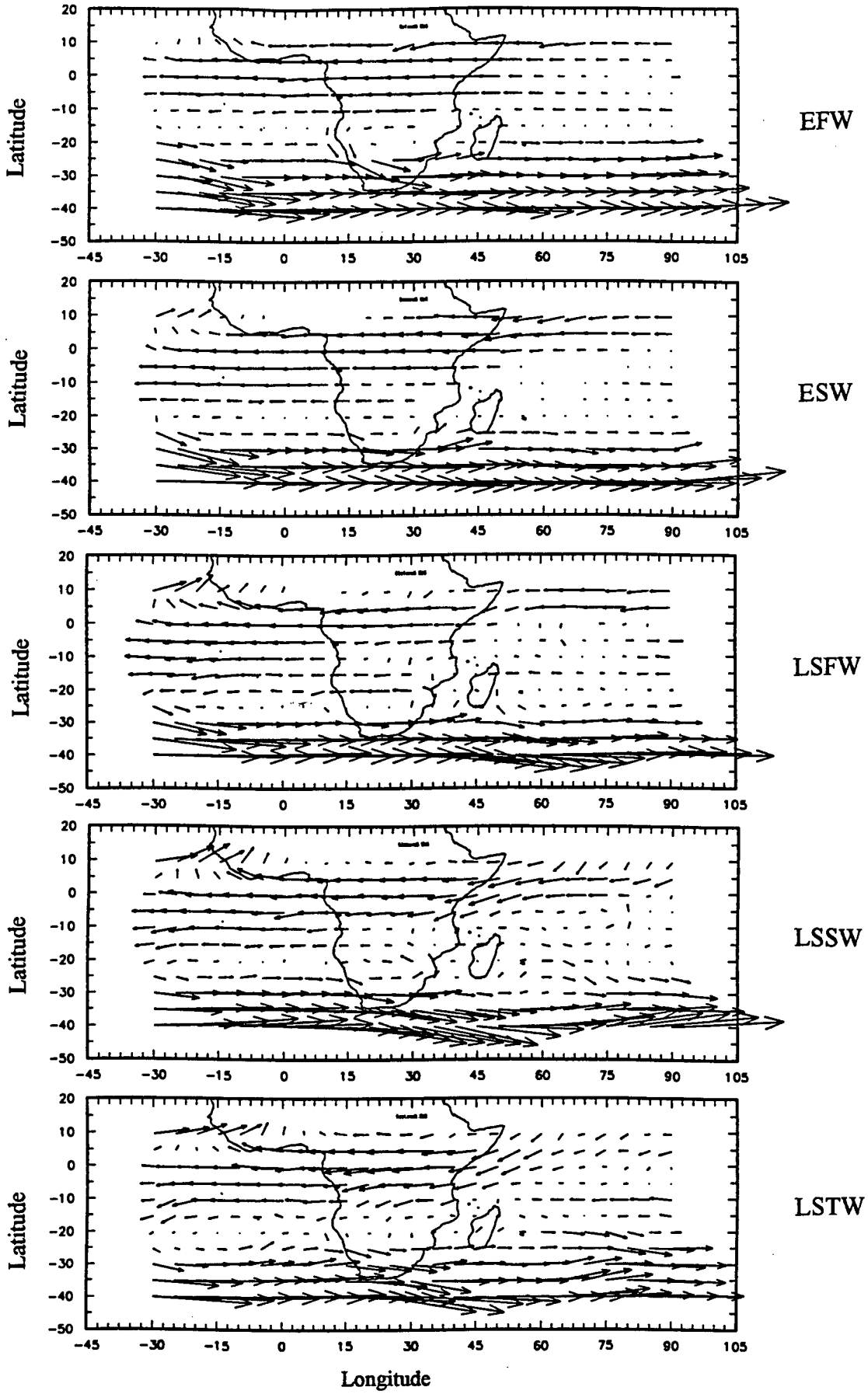

Figure 5.7 : Mean horizontal wind vectors at 500 hPa. The longest vector is equivalent to 22 ms^{-1}.

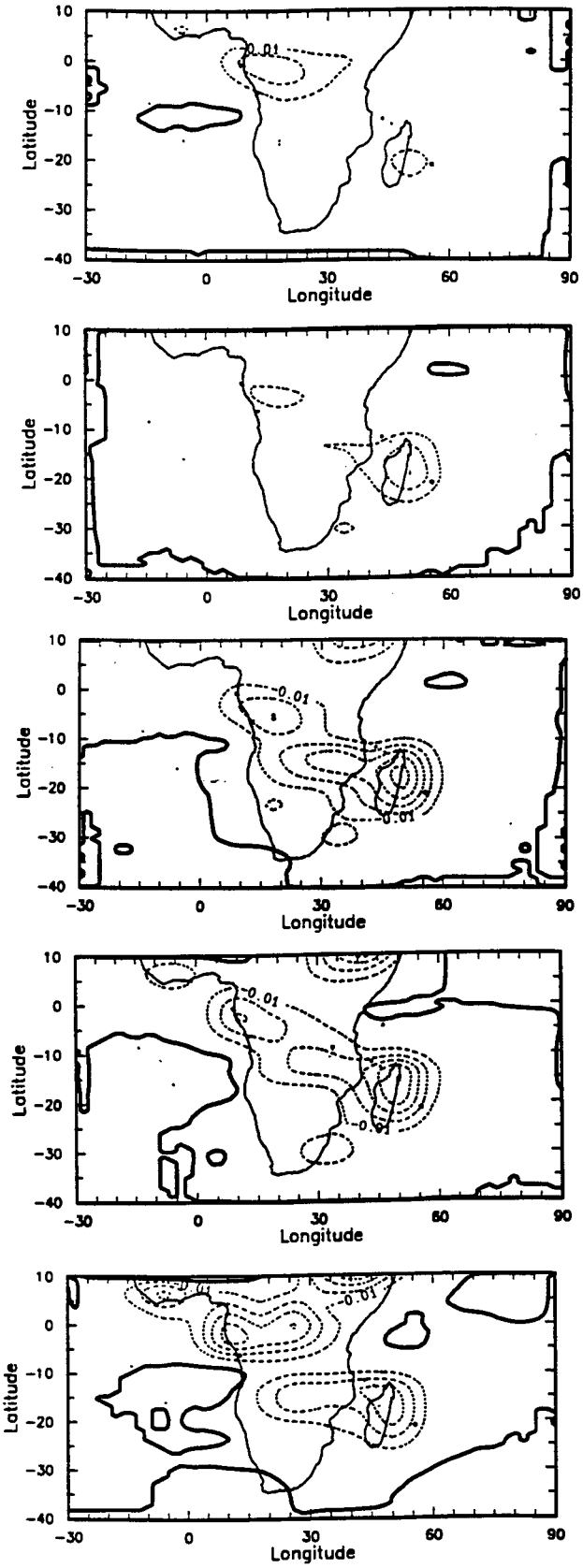

Figure 5.8 : Mean 500 hPa vertical velocity for all phases. The contour interval is 0.01×10^{-2} Pa s^{-1}.

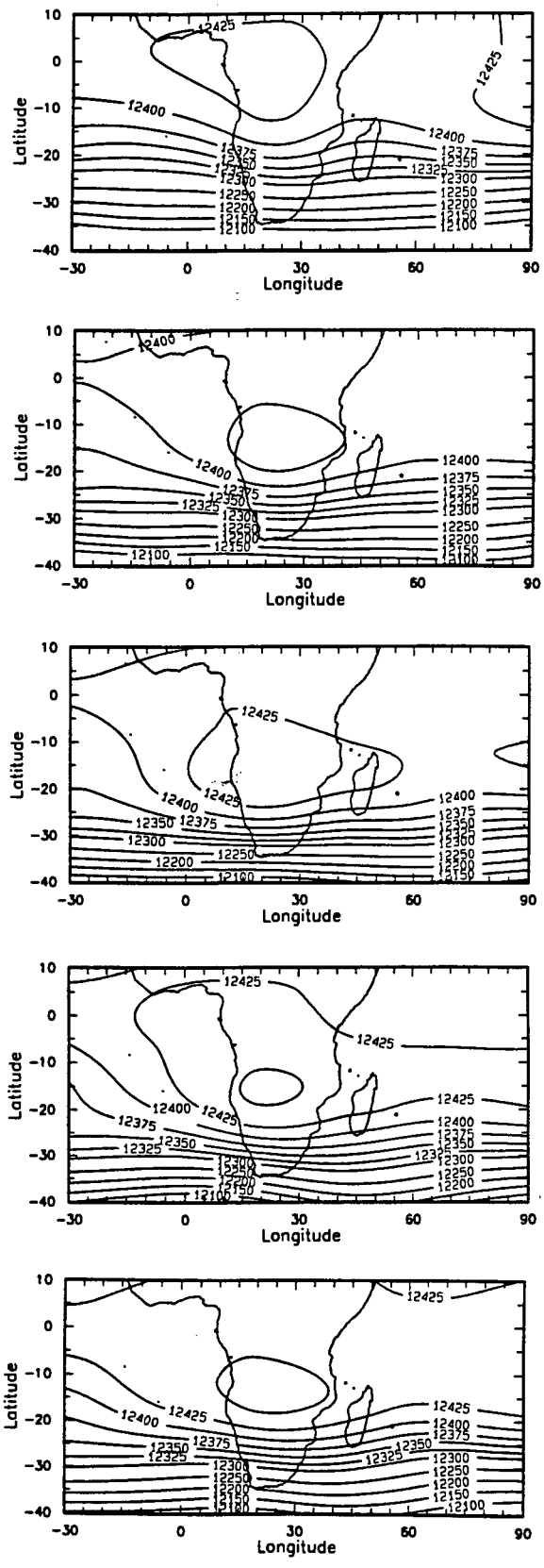

Figure 5.9 : Mean geopotential height for all phases at 200 hPa. Contours are at every 50 gpm to 12300 gpm and, thereafter, every 25gpm.

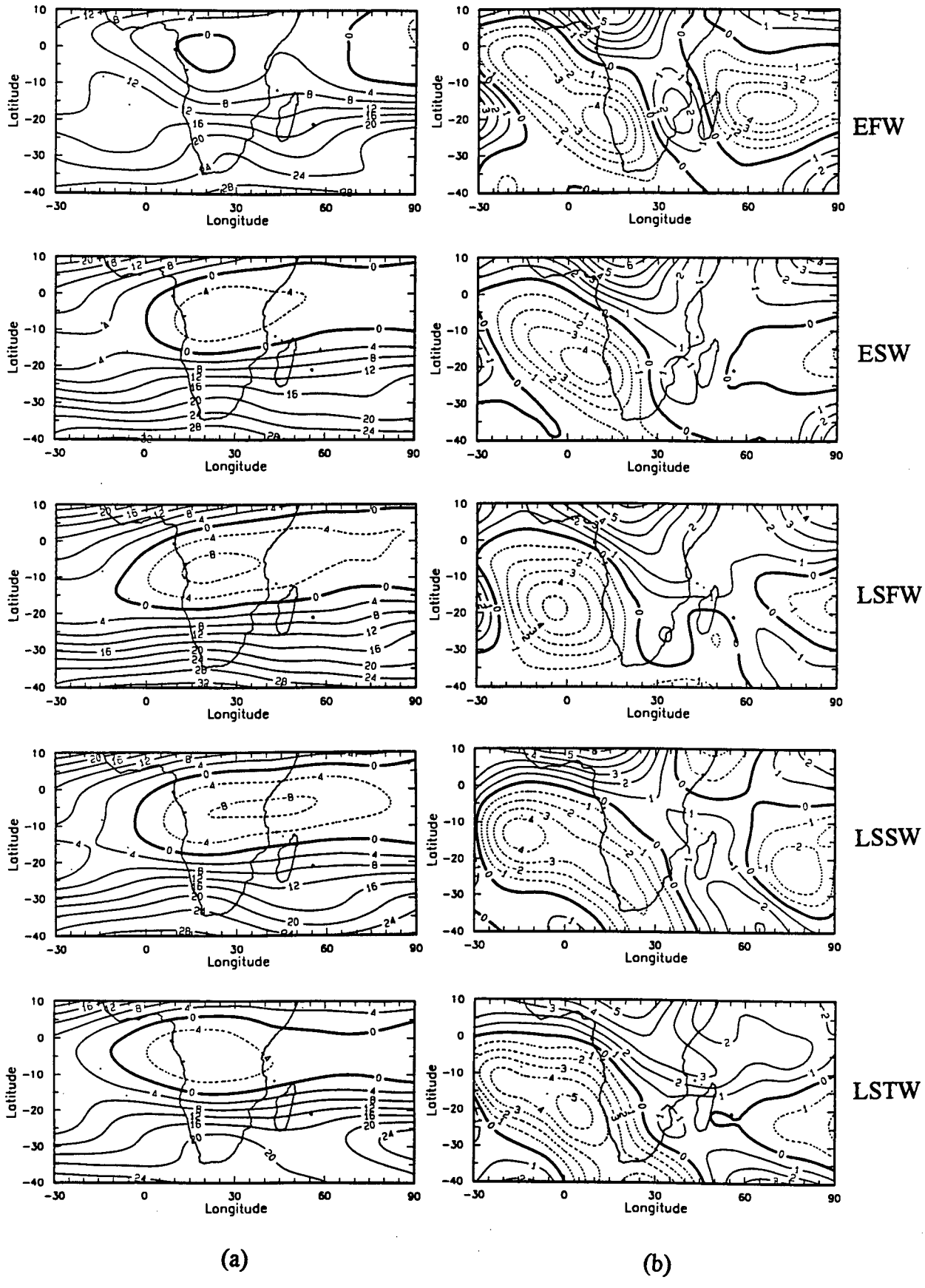

Figure 5.10 : Mean 200 hPa zonal (a) and meridional (b) wind patterns. Contour intervals are 4 and 1 m s^{-1}, respectively.

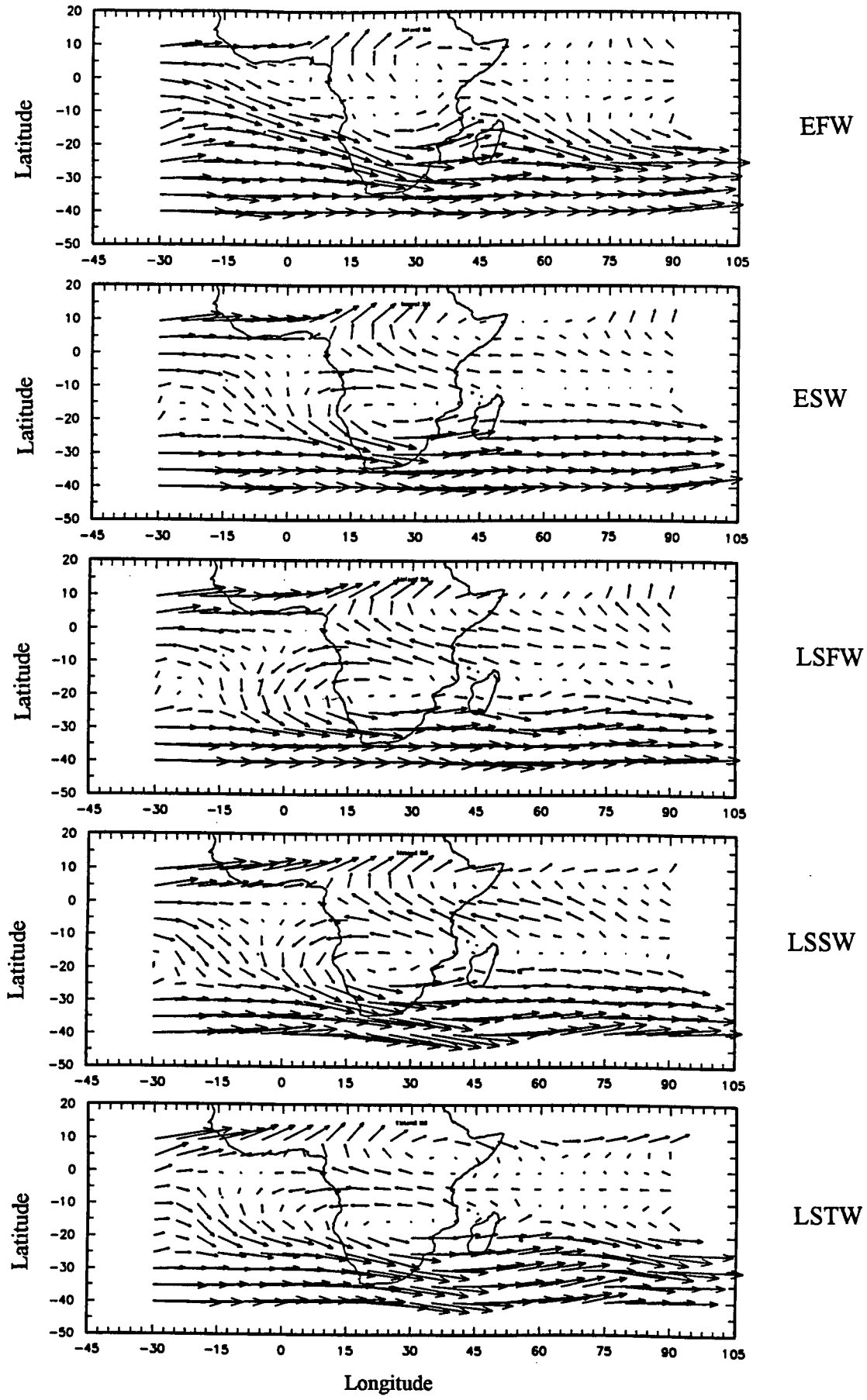

Figure 5.11 : Mean horizontal wind vectors at 200 hPa. The longest vector is equivalent to 40 ms^{-1}.

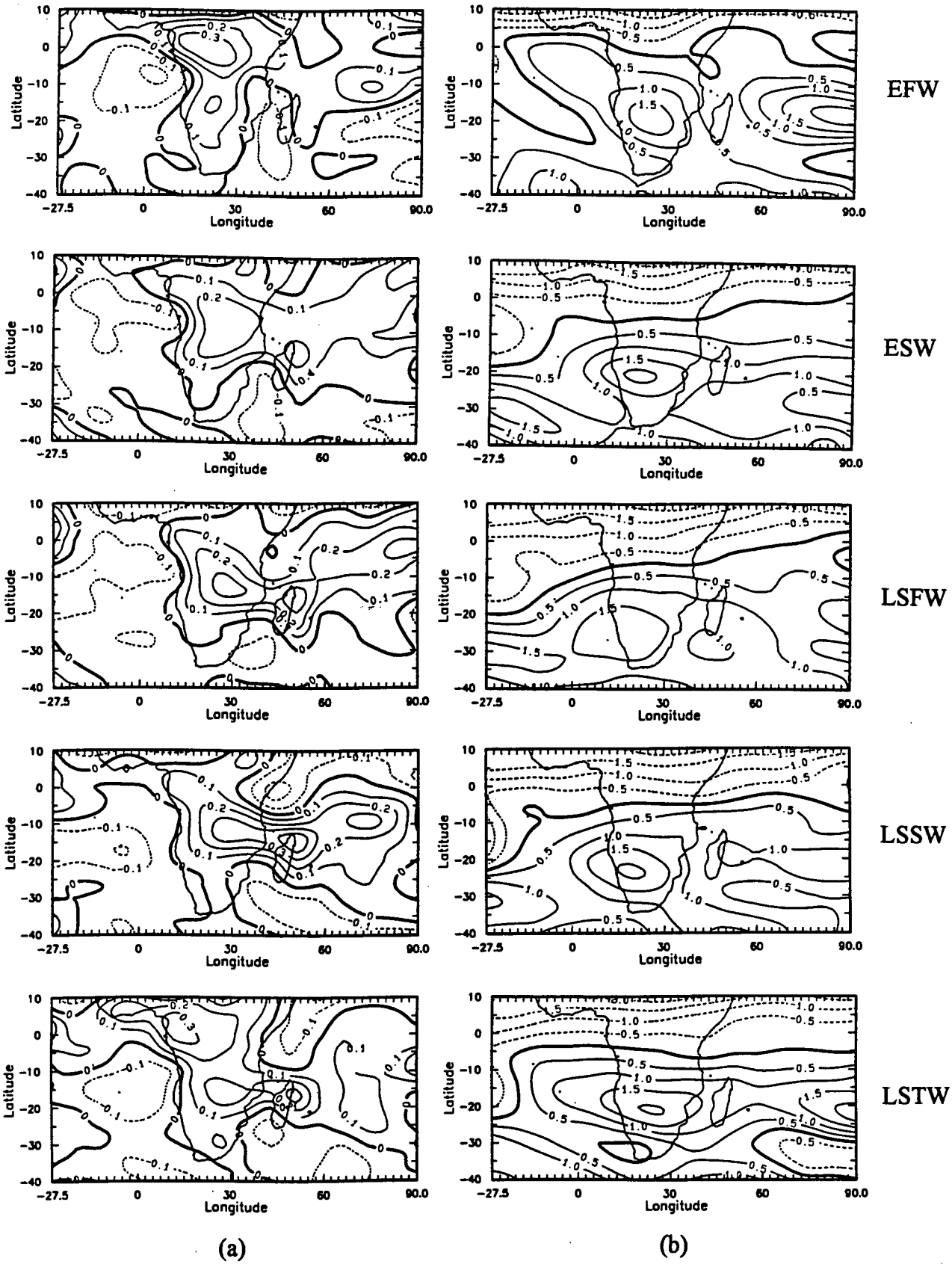

Figure 5.12 : Mean 200 hPa horizontal divergence (a) and vorticity (b). The contour intervals are 0.1 and 0.5 x 10^{-5} s^{-1}, respectively.

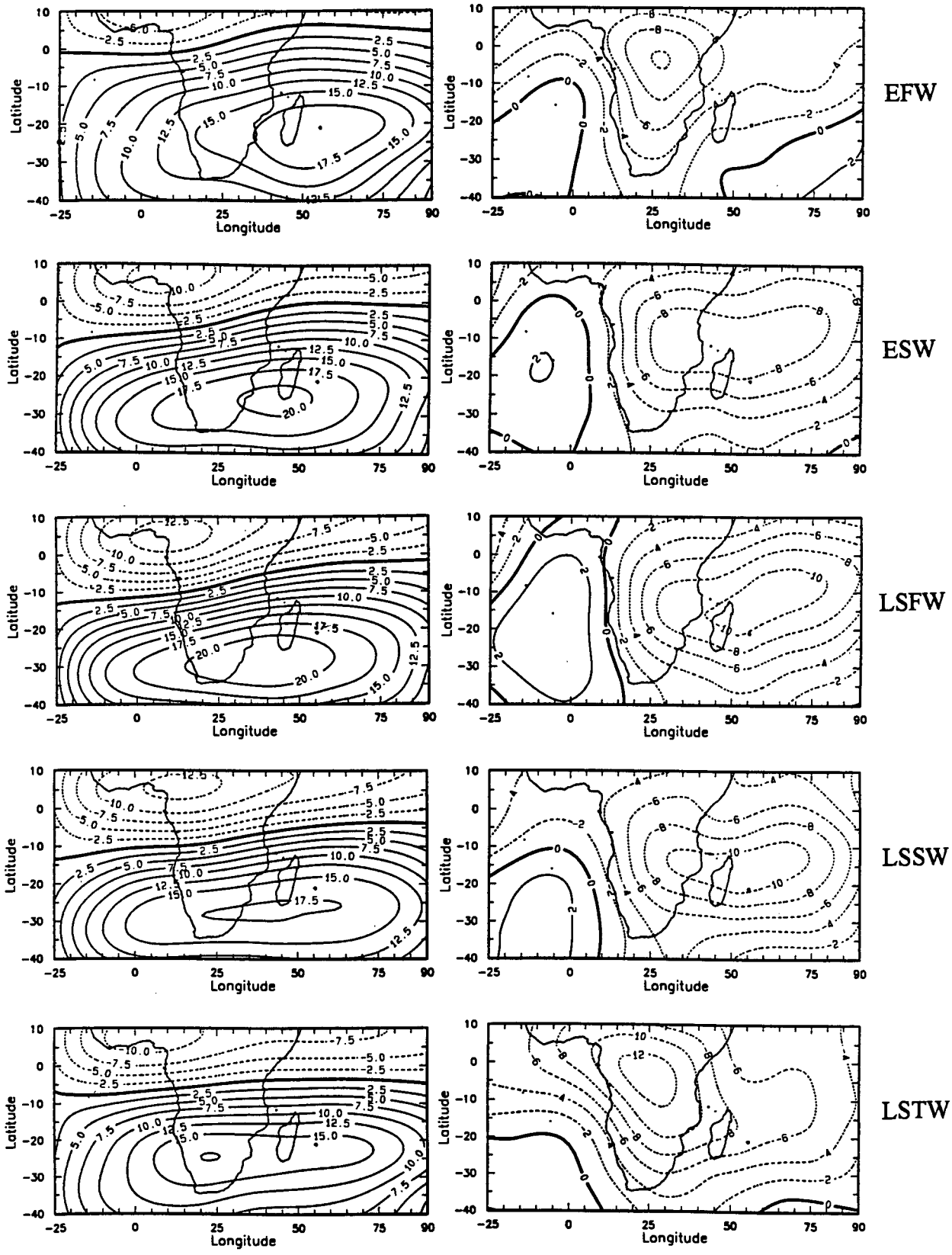

Figure 5.13 : Mean stream function (a) and velocity potential (b) at 200 hPa. The contour spacing is every 2.5 and 2 x 10^6 m^2s^{-1}, respectively.

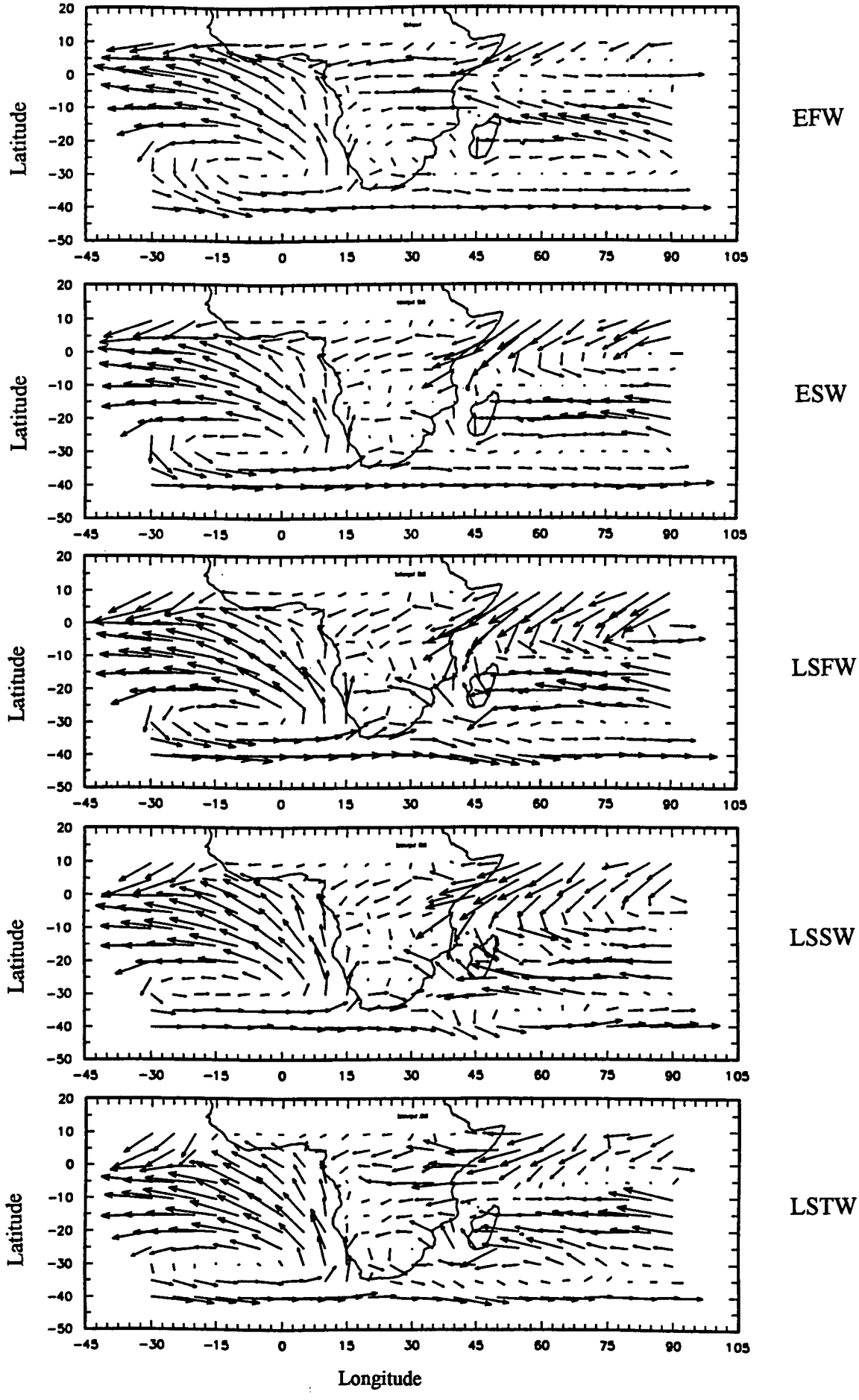

Figure 5.14 : Mean vertically integrated water vapour flux. The longest vector is equivalent to 225 g kg^{-1} m s^{-1}

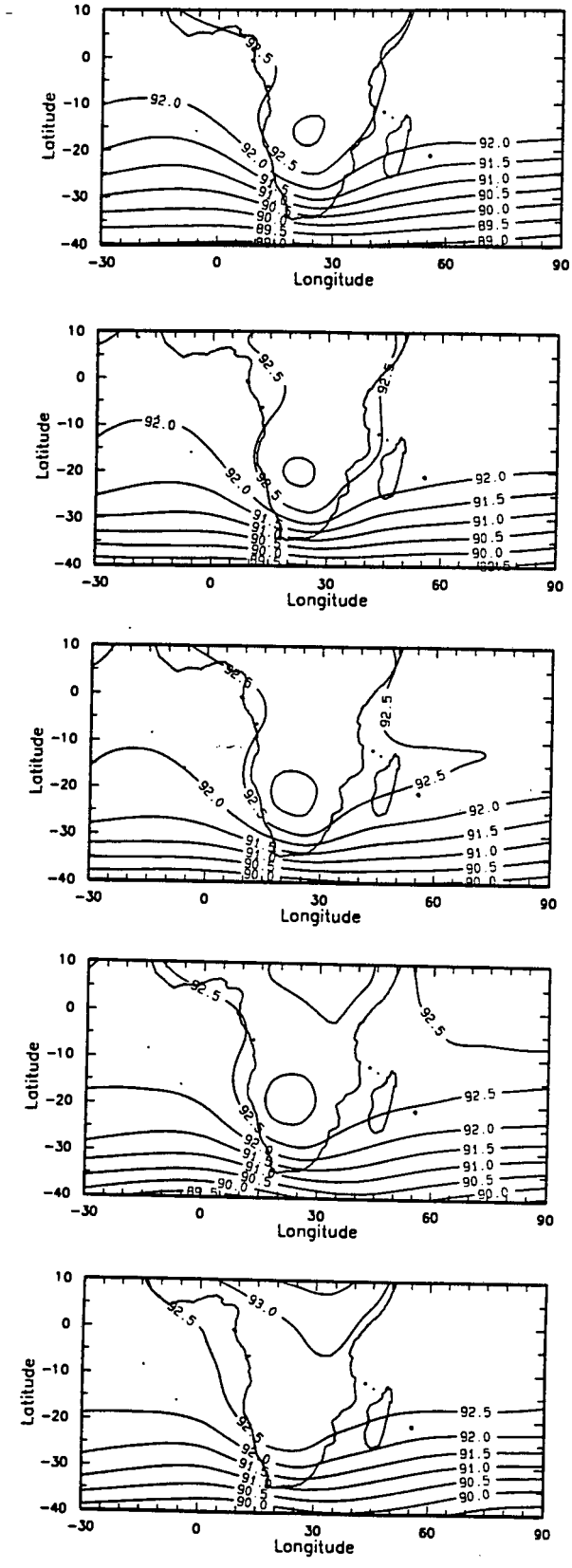

Figure 5.15 : Mean vertically integrated internal energy. The contours are at every 0.5 x 10^6 Jm^{-2}.

Chapter 6

Characteristics of Major Wet Spells During Peak Activity

6.1 Introduction

Chapter 6 is based upon the hypothesis that circulation mechanisms responsible for synoptically- triggered rainfall episodes over southern Africa are, to some extent, different from early to late summer. In other words, the amount and sources of moisture, energy and kinematic forces, vary as the summer season progresses. This chapter aims to, firstly, describe distinctive features and synoptic circulation patterns associated with pronounced wet spells as identified by Zimbabwe pentad rainfall data. The analysis illustrates wet spell structure in a seasonal progression rather than employing collective composites. Thus, the peculiarities of each wet spell are investigated and identified.

Reference to Chapter 4 shows that, in the long- term mean, effective southern African summer rainfall is composed of five wet spells (two for early summer and three for late summer). The early summer is composed of two wet spells (EFW and ESW) separated by a dry spell. The first wet spell (EFW), signifying the onset of the main rains over southern Africa, especially over the eastern regions, peaks in the pentad 27 November - 2 December, ± 1 pentad. Being the first major wet spell, EFW effectively determines on-farm operational decision making (eg. acreage for planting, crop type and requirements or inputs associated with early stages of crops). ESW has a peak during the period 17- 21 December, ± 1 pentad. This spell is not always evident or well defined every year. It is, however, important as it occurs just before the mid- summer dry spell which will be shown to single- handedly shape the outcome of late summer, hence crop yield (Chapter 8). Failure of ESW could herald the onset of prolonged drought instead of the expected brief dry spell. There are three major wet spells defining late summer, namely LSFW, LSSW and LSTW. LSFW is the most critical as it signifies the end of the mid- summer dry spell usually by mid- January. Any delay affects crop yield as permanent wilting of non-drought resistant crops, like maize, could ensue. Historically, these late summer wet spells peak during the periods 21-25 January, 10- 14 February and 22- 26 March, respectively. The first two are separated by between 15 and 20 days while about 30 days elapse between LSSW and LSTW.

Chapter 4 also illustrates that area- rainfall time series over southern Africa exhibit intra-seasonal oscillations whose interval varies between 15 and 30 days. Similarities and differences between and among the climate parameters that control precipitation during these spells are elucidated. The analysis here differs from Chapter 5 in that only the P0 pentad is used, whereas before, the surrounding passive phases are included (that is, from P-2 to P+1) to produce mean patterns. Shortcomings of composites and mean analyses have been discussed briefly in Chapter 5 and, thus, will not be repeated. Similarly, to avoid duplication, only wet spell patterns which show characteristics different from the overall period- mean are discussed. Quantitative departures from the mean circulation are the focus of Chapter 7.

The second section of the chapter proposes that early and late summer wet spell circulation patterns over southern Africa are different. Similar assertions have been inferred as early as the mid- sixties (Schulze, 1965) that there are significant differences in the synoptic circulation patterns between early and late summers over the interior of southern Africa. Van Heerden et al. (1988) contend that the rainfall in early summer is a result of temperate circulations while tropical controls are responsible for late summer rains. In this chapter, EFW0 and LSFW0 are used to identify the most conspicuous differences between early and late summers with the objective of investigating physical mechanisms associated with rainfall in the two periods. This is carried out through analyses of some kinematic and thermodynamic meteorological variables, including subtracting the LSFW0 field from the EFW0. For the rest of this chapter, these pentads of convective peak activity are referred to as EFW, ESW, etc.,

6.2 Methodology

Procedures regarding the determination of peak wet spells have been discussed in detail in Chapter 4. As a reminder, however, the peaks were identified from pentad rainfall time series representing each season in a six- year data set (1987- 1992 summers, inclusive). For each time series, rainfall anomalies above one standard deviation were regarded as wet. Peaks of these anomalies were identified and grouped (**Table 4.4**) using cut-off dates in conformity with stipulated criteria. Composites from all six seasons were formed, resulting in five wet spells comprising each summer (**Table 4.5**). Pentads corresponding to peak anomalies were labelled P0, upon which this chapter is focused. The periods of peak activity have been already been mentioned above. Peaks EFW and LSFW were

selected to represent early and late summer spells. Using ECMWF data and derived products, the spells were further analysed to obtain a measure of similarity and difference between early and late summer. The following sections describe results of the analyses. Except water vapour flux and related products, the results are based upon analyses at 700, 500 and 200 hPa. Analysis of water vapour is through a vertical column from the surface to 500 hPa.

6.3 Lower tropospheric circulation patterns : 700 hPa

6.3.1 Horizontal kinematic structure

The low level kinematic patterns are summarised in **Figure 6.1** in the form of wind vectors. During November (EFW), a trough exists over western southern Africa. The east is under a northerly airflow which has recurved from an easterly flow. This is attributed to anticyclonic ridging from the Indian Ocean where an axis is across northern Madagascar and Mauritius. The AOA is centred over 25°S, 25- 30°W and has no direct influence over Africa except along the west coast. About 15 days later (ESW), a dipole- like structure is evident over the interior of southern Africa with an anticyclonic configuration centred around 25°S, 25°E and a cyclonic flow northwest of it with a vortex near 15°S, 20°E. The resulting airflow consists of strong westerlies over Angola and Zambia which become northerlies across Zimbabwe, easterlies over Botswana and finally recurving over South Africa to join very strong westerlies to the south. The Indian Ocean, on the other hand, has undergone considerable transformation. Firstly, the IOA has receded well to the east of 80°E. A N- S trough appears over the Mozambique Channel. A clockwise (cyclonic) circulation with an axis along 15°S and centred near 75°E has become more dominant compared to the IOA, controlling westerly winds between the Equator and 10°S. The cyclonic region has effectively diverted the NE monsoons from the northern Hemisphere away from east Africa. This cyclonic flow has moved from along 5°S during EFW.

The dipole structure observed over southern Africa during ESW is replaced at LSFW by a trough (wind confluence) extending from the Mozambique Channel to Angola (MCAT). Easterly winds occur between 15 and 20°S across southern Africa (through central Namibia, Botswana and southern Zimbabwe). Equatorward of the trough, northerly to northwesterly winds flow across Zambia, Malawi and northern Mozambique, implying greater monsoonal influence over those regions. The patterns over southern Africa in the February wet spell (LSSW) are similar, with the MCAT still in evidence along 20°S, with

northwesterly airflow to its north and light easterlies south of it. The monsoon winds over equatorial Africa have strengthened due to anticyclonic ridging from the Indian Ocean. This ridge has moved southwestwards towards East Africa at the same time pushing the ITCZ cells and axis southwards to east of Madagascar. In the third spell (LSTW), southern Africa is now under anticyclonic flow from an anticyclone established near 25- 30°S, 25-30°E and cyclonic curvature over the central interior (15°S, 25°E) resulting in predominantly easterly to northeasterly flow over Zambia, Zimbabwe and Angola, easterly across Botswana and northwesterly flow along the west coast of South Africa.

In general, the 700 hPa total wind (vector) field at the peak of wet spells exhibits features that are also represented in the mean circulation, the most conspicuous of which are the west coast trough in November and the MCAT from December to February. The MCAT is more emphasised in the mean field due to the anti clockwise system across South Africa which is a permanent feature throughout summer. The anticyclone is relatively weak during wet spells, particularly in January and February.

6.3.2 Horizontal divergence and vorticity fields

Figure 6.2 exhibits the low- level horizontal divergence and vorticity for pentads when the five major wet spells are at their peaks. Divergence patterns are shown in **Figure 6.2a**. For the first episode (EFW), there is low-level convergence extending from eastern southern Africa to equatorial regions with local centres in the vicinities of 18°S, 30°E (central Mozambique) and 0°S, 20°E. This zone is interrupted by a ridge of divergent flow from northeast Africa where a peak exists near 8°S, 30°E. At ESW the ITCZ is well represented by a zone of convergence stretching continuously from the Atlantic Ocean (axis roughly along 5°S) into Africa (where it becomes meridionally oriented) and continuing to the Indian Ocean through Madagascar along 15-20°S. Maximum negative divergence is over 25-30°E (northern Zimbabwe). Immediately to the north of this band is a zone of positive divergence extending from the Atlantic to the north of Madagascar. Another divergent pattern starts in the eastern South Atlantic, spreads into western Southern Africa, crosses Africa south of 25°S, and extends through the south Mozambique Channel to the Indian Ocean. In relation to the previous wet spell (EFW), there are major changes in the circulation patterns, the most relevant to southern Africa of which is the intensification of the convergence along 15°S, due to the shift of the ITCZ.

In January (LSFW), a 15°- wide latitude band of convergence cuts across the middle of southern Africa, with an axis along 15°S from the Indian Ocean and Madagascar. The band is displaced equatorward towards the western flanks to continue along 8°S in the Atlantic. This can be assumed to be the position of the ITCZ at this time. Elsewhere, the flow is divergent, moreso over the African continent. For LSSW, the configuration is dominated by convergence (ITCZ) cutting across Africa like in the previous wet spell and divergent flow elsewhere. During this period, the ITCZ appears to have slightly weakened over eastern Southern Africa and Madagascar while the equatorial portion of it has intensified. This is supported by even stronger divergent motion north of the Equator, with the divergence continuing to spread into the Indian Ocean between 0 and 10°S.

During the third wet spell (LSTW), the convergent band (or the ITCZ) continues to maintain its general shape, but has now become broader over Africa and the Atlantic. It is weaker over southern Africa and Madagascar but strengthened over the Equator and the Atlantic. At the same time, the divergence off equatorial East African coast has spread further eastwards into the Indian Ocean. This could be responsible for the weakening of the southern arm of the ITCZ over southern Africa. South of latitude 20°S the flow is mostly weakly divergent and potentially ineffective.

The divergence patterns possess characteristic features similar to those of the mean patterns in **Chapter 5 (Figure 5.4a)**, particularly for late summer. However, there are features which stand out more clearly during peak activity. Details pertaining to the degree of similarity (or deviations from the long- term mean) are the subject of Chapter 7. As this is not the focus of this chapter, only a few examples are cited. The most conspicuous differences are for early summer over southern Africa. At EFW0, low- level convergence is over eastern regions which include Zimbabwe, Mozambique and Zambia. The feature is not apparent in the mean circulation, indicating the dominance of large- scale divergence over the sub- region during early summer. In addition, regions of low- level convergence associated with the ITCZ are more pronounced at peak activity; where it is more evident that the ITCZ is over southern Africa from the middle of December onwards. A meridional configuration over Africa is apparent. Further south, the convergence zone along the SE coast of South Africa discernible in mean patterns; is not reflected during peak activity, though inferred in February and March.

The vorticity pattern (**Figure 6.2b**) displays features which are similar to the mean patterns given in Chapter 5. Illustrated is the seasonal cycle (not evident in the divergence field), with anticyclonic motion prevailing at the onset of summer. The belt of cyclonic flow between 5 and 20°S is a permanent feature during wet spells from December (ESW) to February (LSSW). Thereafter, the patterns indicate a decline in cyclonicity over Africa, signalling a gradual progression towards the end of summer. The flow is still cyclonic in the Mozambique Channel- Angola Trough (MCAT) in the late March wet spell (LSTW). From the analyses, it can also be inferred that the MCAT is not developed at the onset of early summer, but rapidly develops by the time ESW peaks in December. The MCAT is the major role player regards rainfall in central southern Africa in December. During late summer, however, its part is masked due to the presence of ITCZ, particularly in February. Compared with the low- level divergence field, the 700 hPa vorticity patterns cannot delineate or describe a meridional arm of the ITCZ. Instead, between December and February, inclusive, the patterns are zonal across the domain, with alternating regions of cyclonic and anticyclonic motion.

6.4 Mid- tropospheric patterns : 500 hPa

6.4.1 Zonal and meridional wind components

Mid- level zonal and meridional wind components are presented in **Figure 6.3**. In general, the zonal wind field (**Figure 6.3a**) is similar to mean patterns. However, sub- tropical westerly winds show more equatorial penetration than the mean flow, especially over southern Africa. The equatorial monsoonal westerly belt in the Indian Ocean is notable at LSFW, and recurs in March. Considering that ESW and LSSW patterns resemble each other, it seems there is a 45- 60 day cycle in the tropical latitudes of Africa and the Indian Ocean.

Figure 6.3b displays the meridional wind flow. A standing wave pattern is evident poleward of 20°S with predominantly northerly winds west of Greenwich as well as in the western Indian Ocean and southerlies over and south of South Africa during EFW. Elsewhere, the winds are light. The standing wave- pattern apparent during EFW is also evident at the peak of ESW, but is now approximately 20° further east. Southerly winds stretch from south of the continent, through South Africa northeastwards over the Mozambique Channel and Madagascar to the equatorial western Indian Ocean. This was

the region covered by weak southerlies 15- 20 days earlier (EFW). Northerly winds still cover Africa north of South Africa and are slightly stronger than during EFW. Like in the zonal wind configuration, the meridional wind structure during this spell illustrates the shift of major activity from the Atlantic to the Indian Ocean. It is possible that this more meridional structure in the Indian Ocean, particularly during early summer, is due in part to the circulation patterns east of about 70°E (longitudes of the Indian Ocean Anticyclone) where southerly winds prevail from the extra- tropical regions in the Southern Hemisphere to the Northern Hemisphere. This is indicative of major blocking in the South Indian Ocean to the west of Australia.

At LSFW, the meridional flow over southern Africa consists of relatively strong southerlies south of about 20°S and weak northerlies north of it. A wave- train pattern exists in the extra- tropics where axes in the South Atlantic Ocean are oriented NW- SE. There also exists a zone of southerly winds over northern Madagascar and to the north into east Africa. There are well- defined southerly components over the equatorial Atlantic Ocean. At LSSW, the southerlies over southern Africa have declined in magnitude and extend into the Atlantic. A belt of relatively strong northerly winds oriented NE-SW extends into equatorial east Africa. This belt could be associated with the monsoonal circulation and is responsible for displacing the zone of southerly winds from the north of Madagascar eastwards to the central Indian Ocean (centred near 10°S 80°E). It links with the sub- tropics to the south of Africa along 40°E. Southerly flow over the SWIO has replaced the northerlies during LSFW. That in the equatorial Atlantic has remained southerly, but is now relatively weaker than before.

A pattern similar to that during LSFW is evident at LSTW, with southerlies and northerlies alternating south of 20°S. This time, however, the range of southerlies has widened, forming a "U" shaped pattern around southern Africa with highest isotachs in the vicinity of 40°S 35°E. The northerly flow over central Africa continues to dominate, pushing the equatorial Indian Ocean zone of southerlies further eastwards. The Mozambique Channel is under predominantly southerly winds which acts to suppress convection there.

6.4.2 Horizontal wind vectors

At the onset of early summer (EFW), an almost continuous belt of anticyclonic windflow runs between 15 and 20°S across the entire window region with local centres near 18°S, 20°W (in the Atlantic), 15°E (western Southern Africa) and 60- 70°E in the Indian Ocean (**Figure 6.4**). This belt, or anticyclonic ridge, separates easterlies from relatively strong westerlies on equatorward and poleward sides, respectively. Compared to EFW, the belt of anticyclonic wind flow is broader in the next wet spell (ESW) to cover up to 20 degrees of latitude over the Atlantic and Africa. The main axis over the Atlantic has shifted southwards by up to 10° of latitude. Over Africa, the col is replaced by a cyclonic circulation over the central interior. The Indian Ocean anticyclonic ridge is no longer evident. Instead, an anticyclone has developed to the northwest of Madagascar centred over the Tanzanian coast. These two adjacent circulation patterns collectively control a northerly wind component along 30°E (over Zimbabwe). The anticyclonic belt is even wider over the Indian Ocean where meridional patterns have emerged in the central basin between the Equator and 20°S. The airflow is still easterly north of the belt and stronger westerly to the south. The winds over east Africa and the western equatorial Indian Ocean have backed from easterly during EFW to northeasterly, signifying the influence of the northeast monsoon over equatorial southern Africa even at 500 hPa.

At the peak of the late summer first wet spell (LSFW), the anticyclonic belt is severed over Southern Africa by a trough oriented northwest- southeast. The South Indian Ocean anticyclone extends a ridge through Madagascar to Tanzania controlling a northerly airflow across Zambia and easterly flow over Zimbabwe. Compared to ESW, the airflow in the Atlantic has become more organised with a ridge along 25°S and centre near 10°W and easterly airflow to the north. Equatorial easterlies over Africa and the Atlantic have also strengthened at the expense of those in the Indian Ocean, suggesting a westward movement of circulation systems. Meanwhile, an area of cyclonic airflow has developed to the northeast of Madagascar with centre near 10°S, 60°E. This cyclonic region is not only evident during the late summer second wet spell (LSSW) but spreads outwards intensifying northeasterly airflow into East Africa (strengthening the monsoon). A trough lies over the south Mozambique Channel with a strong westerly airflow north between 10 and 20°S. Over southern Africa, the airflow is relatively light and variable up to 25°S, poleward of which the winds are westerly. The AOA ridge has moved slightly northwards and is also impacting slightly more on western southern Africa. About 30 days later (LSTW), the AOA ridge axis lies along 15- 20°S with a primary centre near 18°S, 25°W and a secondary one on the west coast of Southern Africa. There is also another ridge,

but weak and narrow, stretching from the Indian Ocean along the same latitude with one centre over the northern parts of Mozambique. The airflow in the Indian Ocean has become more zonal except over the west where it remains northeasterly. These northeasterlies, in turn, veer over Africa to become straight easterlies except over the central interior of southern Africa where they have a northerly component.

Comparison of active wet spells and the mean patterns of Chapter 5 highlights differences between them. Firstly, the flow is more meridional at peak activity. Of more relevance is the northerly flow over central southern Africa, attributable to a mid- level anti clockwise circulation between NW Madagascar and northern Mozambique/ southern Tanzania. The circulation is hardly represented in the mean patterns. Thus, the sub- tropical ridge detected from mean motion as a continuous belt between the Atlantic and Africa actually consists of cells of anti clockwise flow with either a col or trough over southern Africa. The ridge is virtually absent in January and February, when the effects of the ITCZ are greatest across the region.

6.4.3 Vertical velocity

Regions of rising and sinking motion, represented by vertical velocity can be seen in **Figure 6.5a**. During EFW, rising motion (negative values of omega) dominates the tropical Indian Ocean as well as most of Africa. The greatest ascent is over Africa where two centres exist; eastern parts of southern Africa (Zimbabwe and Mozambique) and along the Equator. These regions overlie areas of low- level convergence (**Figure 6.2a**). Ascent is greater and more organised at ESW. During this period, the centre of maximum ascent over southern Africa is displaced westwards to the central interior and attains peak intensity ($< -0.12 \times 10^{-2}$ Pa s^{-1}.

The beginning of late summer (LSFW) is characterised by vertical motion over most of southern Africa except the southwestern tip with the strongest uplift over the eastern half as well as Madagascar. The flow is basically subsident over the Atlantic and to the south of Africa and upward in the equatorial Indian Ocean. There is a weak link between vertical uplift zones over the two oceans. About 15 days later, (LSSW), the general pattern has not changed much. This time, however, the region of vertical motion over Africa has widened and the link between the oceans strengthened. In the process, a tongue of rather weak subsident air protrudes from the northwest Indian Ocean to just off east Africa. This tongue is also evident during the third wet spell (LSTW) when the whole of equatorial and

southern Africa experience relatively strong uplift with maxima along the Equator and 15° S, respectively. The link between the oceans is even more pronounced, indicating the approximate positions of lower- tropospheric convergence areas of the ITCZ.

In southern Africa, the region of upward motion overlies the position of the MCAT where the low- level circulation is mostly cyclonic and convergent. This is also the region of mean maximum low- level dew point and equivalent potential temperature (not shown) as well as the region of maximum mean vertically integrated internal energy (**Figure 5.14**). The area is in the vicinity of the zero zonal wind line (separating equatorial easterlies from sub- tropical westerlies), in the low- levels. Mid- level kinematic flow indicates light winds, pointing to a small vertical wind shear. The winds have a northerly bias, implying that the MCAT is a sink of equatorial moisture and energy. By the time late summer reaches its peak the atmosphere is nearly barotropic. Therefore, it can be inferred that thermodynamic factors dominate over kinematic controls at the peaks of late summer wet spells.

6.4.3 Vorticity

The mid- tropospheric vorticity pattern is shown in **Figure 6.5b**. Reference to the Figure indicates that almost the entire region surrounding and over southern Africa exhibit anticyclonic flow in the southern hemisphere in November (EFW). In the December wet spell (ESW), pockets of cyclonic flow are evident as manifestations of lower- level patterns between the Equator and the TSB. Otherwise the flow remains predominantly anticyclonic. The mid- tropospheric circulation in the southern hemisphere in January (LSFW) is mostly anticyclonic south of the Equator, like in early summer. The region under cyclonic motion in the tropical Indian Ocean as well as across central southern Africa is more organised than in December. It is short- lived over Africa and retreats to the Indian Ocean to extend from Mozambique to 70°E along the TSB during LSSW. By the end of the season the pattern reverts to that in November, when the cyclonic mid- level flow is only found in the central basin of the Indian Ocean. It should be noted that negative vorticity north of the Equator (and tropical easterlies) refers to anticyclonic flow. Hence, the entire domain analysed falls under positive anticyclonic vorticity owing to shear of the sub- tropical westerlies. This vorticity may limit the depth of convection over southern Africa.

6.5 Upper- level circulation patterns : 200 hPa

The upper- circulation can be inferred from the divergence field (**Figure 6.6a**). Upper divergence exists over the equatorial Indian Ocean, virtually over the whole of Africa south of 10°N and north of the Equator in the Atlantic Ocean at EFW. Local maxima over Africa occur near 15°S, 25°E and 5°S, 20°E. In the SWIO, the pattern is convergent through the Mozambique Channel to coastal Tanzania. The 200 hPa flow is also convergent over the eastern Atlantic. ESW indicates similar features. However, the divergence is greater, moreso in the tropical Indian Ocean, implying an increase in convective activity and rising motion in the region. The centres overlie convergence centres at 700 hPa (with little vertical displacement with height). Upper divergence over southern Africa is linked to major upper-level divergence in the equatorial Indian Ocean via northern Madagascar/ Comores Islands and has intensified and spread southwards since EFW. The divergence extends westwards to the Atlantic through West Africa. The configuration generally represents the upper- level outflow of the ITCZ. Like during EFW, convergence is still confined to the Atlantic Ocean and south of Africa. That over the South Indian Ocean and the Mozambique Channel has been squeezed out and weakened so that significant convergence is located only east of 75°E.

The pattern at the peak of LSFW is dominated by relatively strong divergence extending from the equatorial Indian Ocean with an axis along 10°S into central Southern Africa with primary maxima near 20°S, 25- 30°E (the position of Zimbabwe) and northern Madagascar. There is upper- level convergent flow over the Atlantic Ocean, extreme southern Africa and the South Indian Ocean. A small but significant tongue of convergence protrudes from the direction of Saudi Arabia. By the peak of the second wet spell (LSSW), this convergence area has intensified and spread southwards effectively weakening the broad divergent flow to its south and displacing it slightly southwards as well. The divergence over Africa spreads further westwards, resulting in a link being established with divergence over the equatorial Atlantic Ocean. In the meantime, the convergence over the Atlantic and South Indian Ocean are weakly linked. That in the Indian Ocean is stronger in February than in January and may maintain the relatively strong upper divergence over Madagascar.

In the March wet spell (LSTW), except for the extreme southwestern tip of South Africa, the whole continent experiences upper- level divergence, linked with that in the Atlantic at the Equator and the divergence over most of the Indian Ocean through Madagascar. While centres of maximum divergence remain quasi- stationary over Zimbabwe and Northern Madagascar, other centres are now evident over Equatorial and West Africa. Simultaneously, convergence over areas in the eastern South Atlantic and just to the south of Africa is stronger than in February, suggestive of low- tropospheric intensification of the AOA and recurrent ridging to the south of the Mozambique Channel.

In general, upper divergence and convergence are more intense at the peak of wet spells than in mean patterns. The convergence, which spreads from the northern hemisphere through northeast Africa to reach 10°S by the end of March is a notable feature associated with the monsoonal circulation at lower levels.

Vorticity patterns (**Figure 6.6b**) are generally similar to those of the long- term mean displayed in Chapter 5 (**Figure 5.11**). The circulations are more intense, though. Anticyclonic flow dominates the Southern Hemisphere with the strongest flow along 20°S over Africa and the Indian Ocean. Maximum values of positive vorticity exist near 30°E (Zimbabwe and Zambia) and 80°E. Another local maximum occurs in the South Atlantic Ocean, where it becomes quasi- stationary at 35°S, 10°W from December to February. At LSSW, the anticyclonic flow is interrupted by a band of cyclonic circulation from the Indian Ocean into South Africa along 30°S. In the same process, the core of active anticyclonicity over Southern Africa is displaced to the west (22°S, 15- 20°E). The 30°S cyclonic belt continues to strengthen and move westwards into the Atlantic Ocean by LSTW, further enhancing the anticyclonic circulation on either side of it. One of the consequences is a N-S dipole- like structure over southern Africa with centres of anticyclonic and cyclonic vorticity near 20°S, 30°E and 30°S, 20°E, respectively. A similar structure is also evident in the eastern South Indian Ocean (along the same latitudes towards 100°E).

The upper- tropospheric stream function patterns (**Figure 6.7a**) show positive values prevalent across southern Africa. The axis of highest values is along 20°S (the tropical- Sub- Tropical Boundary, or TSB) during EFW, with a primary maximum between Mauritius and Madagascar. The stream function intensifies and shows a slow poleward progression to lie along 25°S in February. Negative values spread southward into the southern hemisphere via the equatorial west Atlantic Ocean. From then on, the axis

retreats equatorward to be along the TSB by the season's end. The pattern conforms with the upper- level vorticity pattern, implying large- scale anticyclonicity dominating the Southern Hemisphere. Unlike mean vorticity patterns (which indicate a summer maximum in the South Mozambique Channel at LSFW), the stream function anticyclonicity peaks in December south of Mauritius and is weakest in February (LSSW).

The velocity potential field (**Figure 6.7b**) is also similar to the long- term mean. Negative values (implying large- scale divergence and rising motion beneath) of the velocity potential cover most of the region at the onset of early summer (EFW) indicating a centre along equatorial Africa, with positive values located in the southern regions of the Atlantic and Indian Oceans. The December (ESW) pattern is rotated clockwise, resulting in the axis of negative velocity potential being displaced southeastward to along 15°S and centred in the vicinity of 70°E. Simultaneously, positive values in the Atlantic Ocean have spread equatorward and dominate the western basin. The January (LSFW) pattern resembles that of the mean, with a centre NE of Mauritius (near 20°S, 65°E). By the peak of the mid- February wet episode (LSSW), the negative values have advanced westwards, weakening the region of positive values in the Atlantic and pushing them southward. The centre of highest negative values has also shifted to about 15- 20°S, 30- 40°E (Mozambique) compared to the Madagascar region in the mean. The first and last wet spells appear "connected" to the western Congo, while the middle three spells are connected (negative velocity potential) to the Indian Ocean ITCZ.

6.6 Moisture Distribution

Figure 6.8 summarises the vertically integrated water vapour flux between the surface and 500 hPa. In general, the circulation patterns of the water vapour flux resemble horizontal wind patterns at 700 hPa. At the onset of summer (EFW), moisture flux over Southern Africa is confined to the east, being advected from the Indian Ocean along similar latitudes by the IOA centred between 70 and 80°E at 30°S. There is slight flux confluence over Angola and the Caprivi Strip. There is very little influence from the Atlantic Ocean flux diffluence. During the mid- December wet spell (ESW), the flux confluence over Angola has deepened resulting in moisture advection over central Southern Africa (Zambia and Zimbabwe) from Angola rather than the Indian Ocean, as during EFW. There is also a zone of flux diffluence along 30°S over Africa which is directing low- level moisture into

the Mozambique Channel and increasing moisture confluence along 20- 25°S. This situation is conducive to low- level uplift and subsequent rainfall occurrence over these latitudes. Simultaneously, there is also trans-equatorial moisture advection in the west Indian Ocean towards East Africa, associated with the northeast monsoon. Some of this moisture is directed along the coast of Tanzania and northern Mozambique. Much of it is redirected into the Indian Ocean along 15°S to a cyclonic gyre near 15°S, 75°E. The moisture in the Atlantic remains confined mostly to the ocean.

At the start of late summer (LSFW), the moisture flux to central Southern Africa has increased, especially in the east (Zimbabwe and Mozambique). The moisture associated with the monsoonal activity has extended further as far as Madagascar. About 15 days later (LSSW), most of the moisture is concentrated in a cyclonic vortex east of Madagascar. Over Southern Africa, the low- level moisture is supplied from the SWIO to Zimbabwe and South Mozambique and from the equator to the central regions (mainly Zambia). When the third spell (LSTW) occurs, there is a large flux centred over eastern South Africa which illustrates moisture advection into Mozambique and Zimbabwe. There is little evidence of moisture advection into southern Africa due to monsoonal activity. In the middle three wet spells, a stream of moisture crosses southeastwards through central and southern Africa.

Precipitable water is another parameter that can be used as a proxy for moist convection. Its properties are illustrated in **Annexure 2**. At EFW (**Figure 6.9**), greatest amounts of precipitable water are located over the equatorial Atlantic Ocean with a tongue extending into the Zaire/ Congo region. The tropical Indian Ocean is also another potential region of precipitable water. The 50 mm isoline develops at the onset of austral summer and can be seen propagating southwestwards in the Indian Ocean as the season progresses to reach the Mozambique Channel in January (LSFW), after which the propagation ceases along 30°E. This reflects the high SSTs and convection associated with the ITCZ in the Indian Ocean. At the same time in the Atlantic Ocean, the precipitable water gradually increases systematically through the course of summer, peaking in March, when the 40 mm isoline reaches 15°S over Angola. Unlike in the Indian Ocean, the axis of highest values remains quasi- stationary in the vicinity of the Equator, consistent with the behaviour of the ITCZ in the Atlantic and the colder SSTs to the south. The eastern regions of southern Africa east of 30°E have more moisture content than elsewhere in late summer, the influence coming from the tropical Indian Ocean. The "demarcation" indirectly indicates the extent of moisture advection from the tropical Indian Ocean into the region, most of which is

deposited over Madagascar. An important feature is that the precipitable water is less than 30 mm over a large part of southern Africa in the first wet spell, suggestive of moisture being the limiting factor then. The LSSW spell illustrates the deepest layer of moisture over southern Africa.

6.7 Inter- comparisons: Early summer versus late summer

As indicated at the beginning of this chapter, early and late summer wet spells may be taken to be represented by EFW and LSFW, respectively. Meteorological conditions comprising these spells are most significant to agriculture in southern Africa. Intra-spell differences among early and late summer wet spells are relatively minor compared to the differences between early and late summer, hence the classification. Comparison is carried out by subtracting the LSFW field values from those of EFW. Emphasis is placed on the mid- tropospheric circulation, as lower levels can contain random noise and patterns are more influenced by local effects like topography which have a bearing upon the boundary layer.

Mid- tropospheric patterns of geopotential height are also representative of lower levels. At 500 hPa (**Figure 6.10**), the tropical and extra- tropical boundary over southern Africa is demarcated along 15- 20°S latitude (TSB). Positive heights are in the tropics while negative values are exhibited at higher latitudes where the greatest differences are along 30- 35°S. The implication is that the 500 hPa geopotential height surfaces are lower in poleward of the TSB in early summer. This could be partially attributed to the more baroclinic, extensive nature of the circumpolar vortex.

The zonal difference pattern at 500 hPa (**Figure 6.11**) illustrates a band of enhanced westerly relative flow in the early summer roughly between 10 and 32.5°S stretching from the Atlantic, across southern Africa and spreading southwards in the Indian Ocean with maximum flow along 22.5°S. Thus, there is increased equatorward penetration of westerly winds in early summer. Northward of 10°S and poleward of 32.5°S from the Atlantic to about 50°E, the relative flow is more easterly (or less westerly). A local maximum exists in the western Indian Ocean just off the east coast of Africa at the equator. Meridionally, the middle- level circulation over the South Atlantic Ocean and southern Africa (**Figure 6.12**) is dominated by a northerly wind difference. Polewards of 20°S patterns alternate in a standing wave- like pattern.

The 500 hPa vertical velocity pattern (**Figure 6.13**) shows increased vertical uplift in the late summer over most of the Indian Ocean and tropical southern Africa with a maximum along 15- 20°S over northern Madagascar. A tongue extends into northern Mozambique and Zimbabwe. This tongue is significant as its axis is in the vicinity of the TSB over southern Africa which is a "semi- permanent" feature of the regional circulation during late summer wet spells. Over Madagascar, the tongue is where the monsoon penetrates the TSB. As shown earlier in the same region, convergence and cyclonic circulations depicting the presence of the ITCZ are clear during late summer but absent at EFW. Enhanced uplift is found over the Congo and the South Atlantic Ocean in EFW, relative to LSFW.

The low- level vorticity difference field is illustrated in **Figure 6.14**, revealing a zonal structure of alternating positive and negative vorticity. A band of positive values stretches across the entire domain between 10 and 20°S, the signs indicating greater cyclonic vorticity during LSFW. Negative values across sub- tropical southern Africa indicate greater anticyclonic vorticity in late summer. A similar situation obtains in the mid- level relative vorticity field (**Figure 6.15**), where a systematic configuration of alternating bands about 15 latitude degrees width exists. Positive anticyclonic rotation between 10 and 25°S and negative values on either side. The axis of positive vorticity difference coincides with the position of the TSB adds to the notion that the TSB and the attendant Botswana Upper Anticyclone (Chapter 8) play a more prominent role in determining central southern Africa late summer rainfall intensity and spatial distribution than is currently acknowledged. Negative relative vorticity in the band from the Atlantic Ocean through South Africa can indicate enhanced baroclinic cut- off lows along 30°S in the early summer, complimenting geopotential height patterns of **Figure 6.10**. In the upper troposphere (200 hPa), anomalous negative cyclonic tendencies are found in the southern latitudes while positive ones cover tropical regions (**Figure 6.16**). The cyclonic patterns at higher latitudes are consistent at all levels of the troposphere and refer to a sub- tropical jet stream which is stronger in earlier summer. The dipole- like pattern between South Africa and Madagascar is not apparent.

Figures 6.17 and 6.18 indicate the divergence difference fields in the lower and upper troposphere, respectively. In the low levels, the difference pattern indicates only small anomalies between early and late summer, except over equatorial Africa. There, a bias towards more convergence during late summer compared to early summer in tropical

southern Africa. This pattern coincides with that of the mid- level relative vertical motion. At upper levels, the patterns are a reversal of and overlying those at 700 hPa. Late summer 200 hPa relative divergence and convergence areas are dominant across equatorial and sub- tropical southern Africa, respectively. The dipole- like structure between South Africa and the northern Mozambique Channel is more apparent than at lower levels.

The EFW-LSFW difference patterns are more apparent from the velocity potential divergent vectors at low and upper levels (**Figure 6.19**). Reference to the 700 hPa fields indicates that at EFW, there is divergence along 5°N as well as NE Africa. Another divergent flux is exhibited over Namibia. Weak convergence exists over the continent, stretching from South Mozambique to the Congo region. The late summer features (LSFW) indicate greater divergent potential over equatorial Africa and a secondary region across South Africa. Upper- level features at LSFW are dominated by divergence across the central interior of Africa with a centre near 5°S, 20°E, overlying the region of flux convergence at 700 hPa. Upper flux divergence also exists in the tropical SW Indian Ocean (associated with the ITCZ) and over southern Africa centred near 20°S, 25- 30°E, the region of Zimbabwe.

The total wind (vector) field (**Figure 6.20**) is dominated by a broad band of westerly airflow differences between 5°S and 30°S from the Atlantic to the Indian Oceans. The band swings equatorward in a trough off the east African coast possibly due to topographic effects of Madagascar, very high SST and response to the phase of the monsoon. This means that the upper- tropospheric sub- tropical westerly component is significantly stronger during early summer compared to late summer. Also evident are regions of maximum clockwise and anti- clockwise flow along 30°S from Greenwich to southwest South Africa and just off the west coast of Africa along the Equator, respectively. Further south, the pattern is easterly poleward of about 35°S from near 70°E to the Atlantic, suggesting that mid- latitude westerlies there are more intense in late summer but with a reduced impact on southern Africa.

Figure 6.21 is an algebraic difference between vertically integrated water vapour fluxes for early (EFW0) and late (LSFW0) summers. The most noticeable differences between early and late summers are in the equatorial Indian Ocean where, firstly, there is a relative southeasterly flux around 10°S most of which remains in the Ocean by recurving along the east African coast. Thus, there is reduced moisture transfer from northern to southern

Hemisphere in the western Indian Ocean during early summer, a feature consistent with the known onset of the NW monsoon over Madagascar after December. Of immediate importance to southern Africa is the TSB region featuring eastward fluxes.

6.8 Discussion and summary

This chapter has investigated characteristic features at wet spell peaks during austral summer over southern Africa. The chapter has illustrated changes that take place as summer progresses, including sources and sinks of moisture, seasonal cycle, tropical and extra- tropical interaction as well as differences between early and late summer. The rest of this section highlights outstanding observed features and, where possible, provides inferences and causative mechanisms.

Comparisons of divergence between 700 and 500 hPa shows that convergence associated with the ITCZ is deep only over eastern Southern Africa and Madagascar. The meridional shape of the ITCZ as it crosses Africa to the Atlantic Ocean at 700 hPa is largely absent at 500 hPa. Instead, the flow is divergent, suggesting shallow convection over these areas in February and March. Thus, it can be inferred that the ITCZ is most active over southern Africa and in the southwestern Indian Ocean in January between 10 and 20°S. This is in partial agreement with the findings of Nicholson and Chervin (1983), Janowiak (1988) and Jury and Pathack (1991), as already been mentioned in Chapter 2 of this thesis.

From the water vapour flux analyses, it can be inferred, firstly, that the Atlantic Ocean does not directly advect any moisture into southern Africa during the peak wet spells. Its influence remains largely an oceanic affair although it can influence early summer rainfall over western southern Africa. It could be playing an indirect role by reinforcing the anticyclonic system regularly observed over eastern South Africa which, in turn, directs low- level moisture into eastern southern Africa (Zimbabwe and Mozambique, mostly). In addition, it is apparent that the monsoonal influence over southern Africa grows from the middle of December. Its direct role is confined to the northeast. By the end of March, the monsoons have receded. Thus, the bulk of the low- level moisture into southern Africa between December and March comes from the Zaire region and the Mozambique Channel.

There is close great resemblance between the water vapour analyses and horizontal wind circulation patterns at 700 hPa. This suggests that it is either the steering level of moisture over southern Africa or is closest to this level.

Geopotential analyses suggest that changes over the Atlantic Ocean are a dominant factor in the mid-troposphere over southern Africa. In addition, the AOA relaxes and spreads north of 20°S and moves steadily northwards at approximately 5° latitude per 15-20 days. The equatorial Indian Ocean appears to be the source of low geopotential heights, but the changes in magnitude between wet spells do not significantly impact on southern Africa.

According to meridional wind circulation patterns, the mid-tropospheric flow over the Atlantic remains generally unchanged during late summer, suggesting that the AOA is quasi- stationary throughout, controlling southerly winds off the west coast of Southern Africa and largely northerlies further west. Elsewhere the patterns are highly variable, especially to the south of Africa and in the Indian Ocean where the winds are up to 180° out of phase between consecutive wet spells. Two reasons are plausible. The change over could be indicating the seasonal onset of the monsoon and the sub- tropical response. It is equally possible that mid- tropospheric waves are generated every 50- 60 days in the South Atlantic Ocean and are propagated eastwards at approximately 50° longitude every 15- 20 days or their multiples. This seems to confirm the existence of intra- seasonal oscillations noted in **Chapter 4**. However, the evidence is insufficient from this analysis to make concrete inferences and warrants further investigation using other levels in a temporal framework.

Another feasible explanation could be that this mid- tropospheric circulation pattern from meridional wind analysis is a manifestation of clearly defined patterns of either the lower or upper troposphere. Overturning at these levels should result in a Hadley cell type of pattern. Simultaneously, the flow over equatorial Southern Africa remains predominantly northerly, progressively strengthening during the course of late summer, suggesting the sustained and increasing influence of the monsoons. Thus, the western Indian Ocean appears to be the source of moisture over southern Africa in the later part of the season.

From the vertical motion analyses the mid- tropospheric position of the ITCZ during late summer can be discerned. The axis is ill-defined over the Indian Ocean where very little upward motion (hence little or shallow low- level convergence) is evident. Over Africa, the rising motion is meridionally oriented. In general, two major preferred axes are

illustrated; one along 15- 20°S latitudes, in the vicinity of the Mozambique Channel-Angola Trough, up to Madagascar and the other roughly along the Equator and continuing into the Atlantic Ocean. Over the South Atlantic the flow is persistently subsident, associated with the semi- permanent AOA.

The position of the ITCZ is also well illustrated from the analyses of the divergence field in the low-levels. The positions coincide with vertical motion analyses at 500 hPa, implying little or no vertical tilt with height. The zones of convergence are quasi-stationary throughout. However, the peak upward motion shifts from eastern southern Africa in January to the western equatorial Atlantic by the end of March also signifying the end of the seasonal cycle. The change seems to be accompanied by the intensification of an anticyclonic ridge from the Saudi Arabian region.

Upper- level analysis shows that equatorward of 20°S, the flow is predominantly divergent throughout late summer with the rest of southern Africa experiencing weak convergent motion in January and February. It appears the source of the upper divergence is the Indian Ocean in January. This divergence shifts westwards in the tropics such that by the end of March (LSTW), the link with Africa is severed somewhere near the East African coast. Outside the tropics, the flow is generally eastward. The progression of wave trains is slow and, to some extent, every 50- 60 days the cycle is repeated (LSFW and LSTW). The Atlantic Ocean Anticyclone is displaced gradually southwards but throughout remains further north compared to the Indian Ocean Anticyclone (IOA) which is weak except in February. The anticyclonicity off the east coast of South Africa is due to reinforcement by the AOA rather than the IOA.

Comparing the two early summer wet spells, two patterns stand out conspicuously. Firstly, there is very little evidence of monsoonal effect on southern Africa during the first wet spell at the end of November. In addition, there is no organised convective activity which can be attributed to the ITCZ. It is the Indian Ocean Anticyclone which provides the low- level moisture flux and convergence over most of southern Africa, including the western plateau areas. The winds from the northern hemisphere in the western Indian Ocean do not recurve enough over Africa, but are predominantly easterly and only become northeasterly in the Atlantic Ocean. During the second wet spell, the monsoonal influence is evident although the trajectory of the airmass is indirect. Secondly, the relative westerly 200 - 500 hPa flow in the Indian Ocean latitudes between 10 and 20°S during the

first wet spell, retreats in the late summer. This is primarily a change from baroclinic to barotropic conditions as the mid- latitudes gradually warm during the course of summer.

Finally, there is some "reluctance" in the part of early summer synoptic configurations to produce precipitation because the mid- troposphere is relatively dry. The process requires external forcing from baroclinic disturbances such as cold frontal systems and cut off-lows which break down the sub- tropical high pressure belt and slow down the zonal flow in the sub- tropics. Convection is encouraged by westerly wave surges into tropical southern Africa. It is the kinematic influence of these westerly waves that act as triggering mechanisms for early summer convection. The build- up of moisture and energy, hence convection, is relatively slow. By late summer, the atmosphere has "organised" itself. Over southern Africa, the synoptic patterns are controlled either by the two troughs (Mozambique Channel- Angola trough, or MCAT and the west coast trough) for wet spells or the Botswana Upper Anticyclone, in the case of dry spells. In wet situations, the semi- permanent wind and moisture confluence associated with the troughs coupled with solar heating in the central interior of the region act as catalysts and along which convection readily takes place. Thus, precipitation production requires less effort compared to early summer.

As mentioned at the beginning of this section, this chapter has determined characteristic features associated with each wet spell in the season. The diagnostic study has illustrated similarities and differences among the spells as well as showing that the convective mechanisms between early and late summer are rather different. As regards operational weather forecasting and real- time monitoring capabilities, however, the findings are inadequate since they display instantaneous "pictures" of the atmosphere at the peaks of wet spells. It is necessary to investigate the wet spells from initiation to decay. This life cycle study approach, as noted by Knutson and Weickmann (1987), provides a framework for identifying fluctuations in weather patterns which can be associated with these intra-seasonal oscillations. This is the basis of the following chapter (Chapter 7).

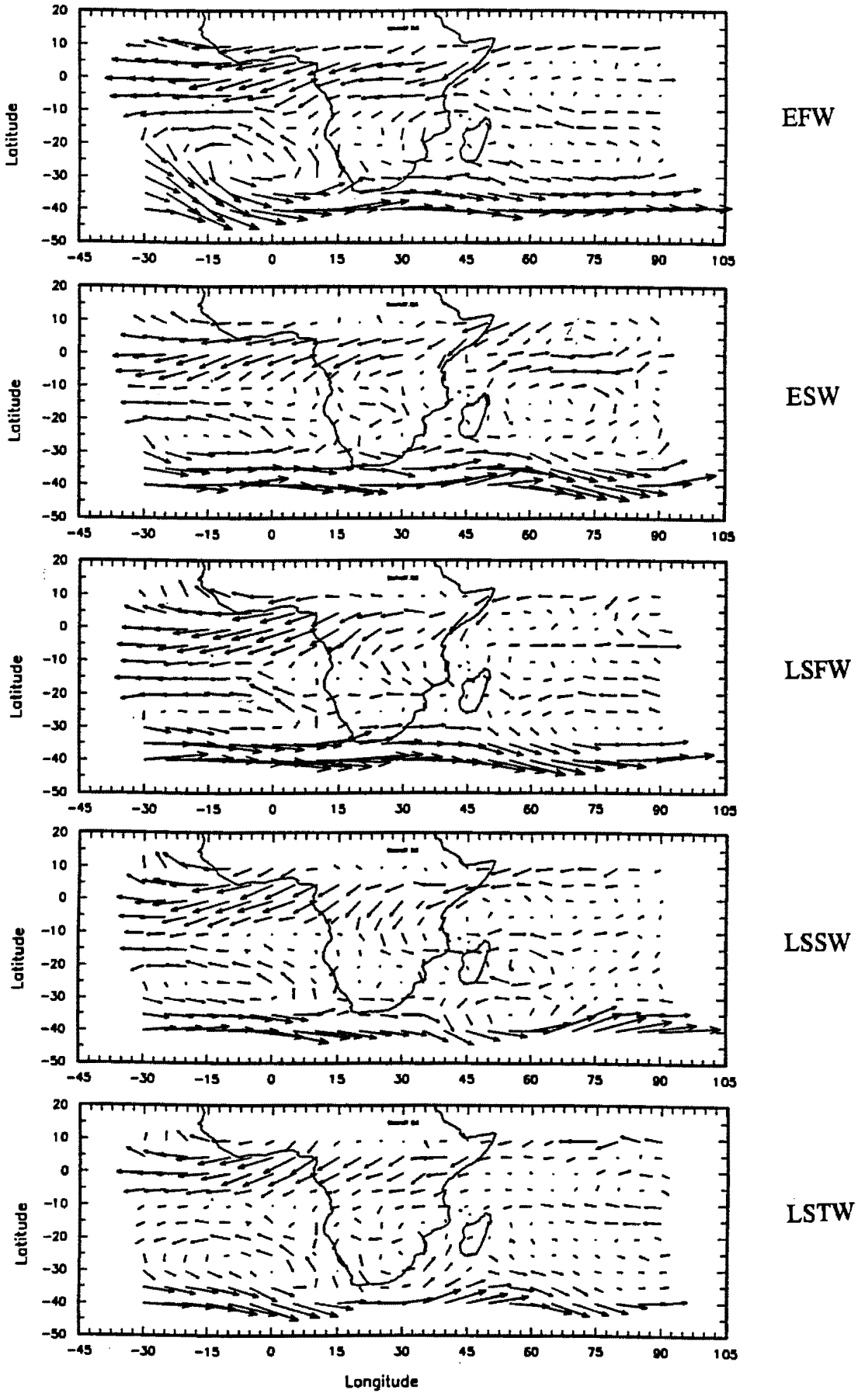

Figure 6.1 : Horizontal wind vectors at 700 hPa at the peak (Pentad P0) of each major wet spell. The longest vector is equivalent to 17 ms^{-1}. Troughs are indicated by bold lines.

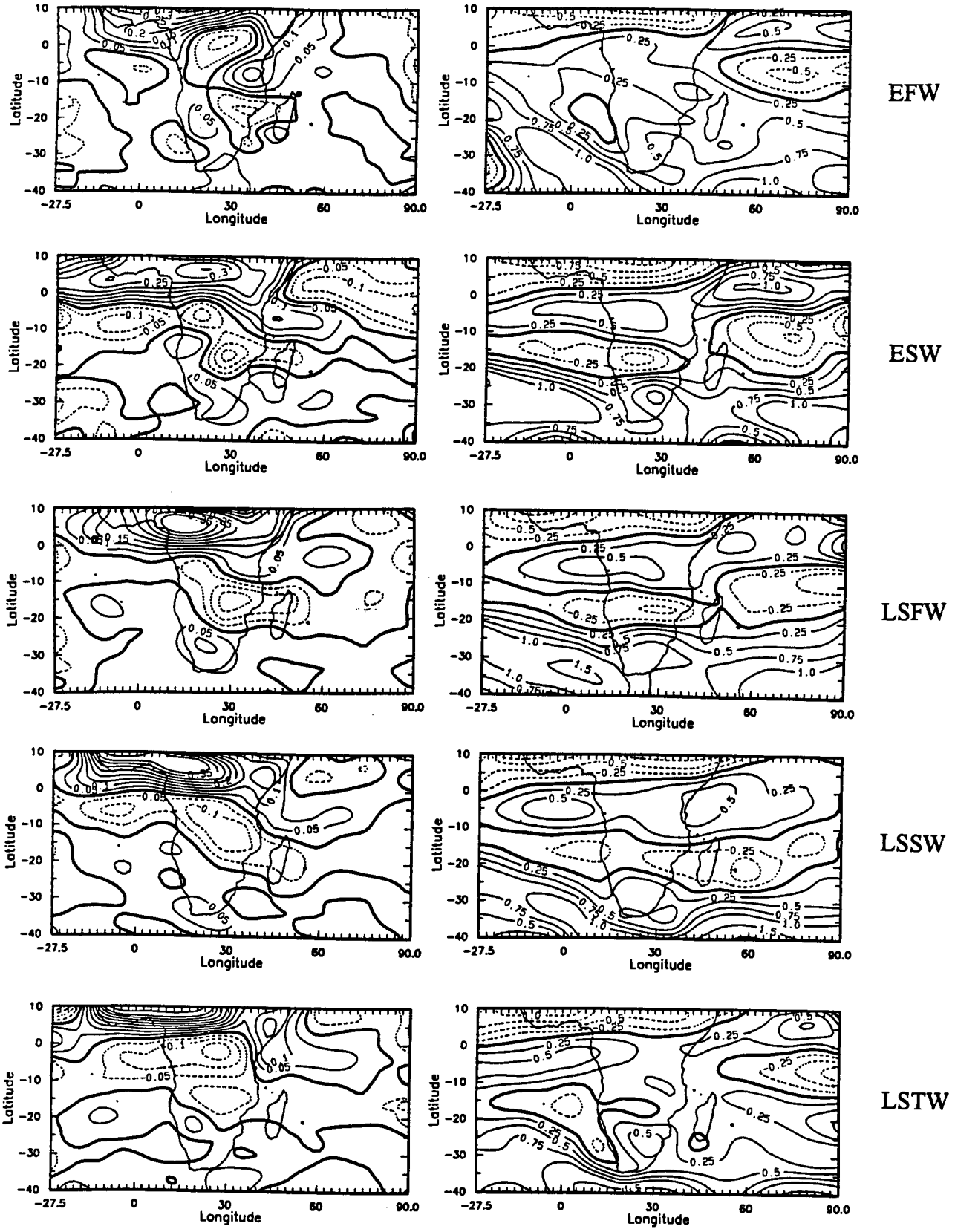

Figure 6.2 : 700 hPa divergence (a) and vorticity (b) for each wet spell at peak activity (Pentad P0). Contour intervals are 0.05 and 0.25 x 10^{-5} s^{-1}, respectively

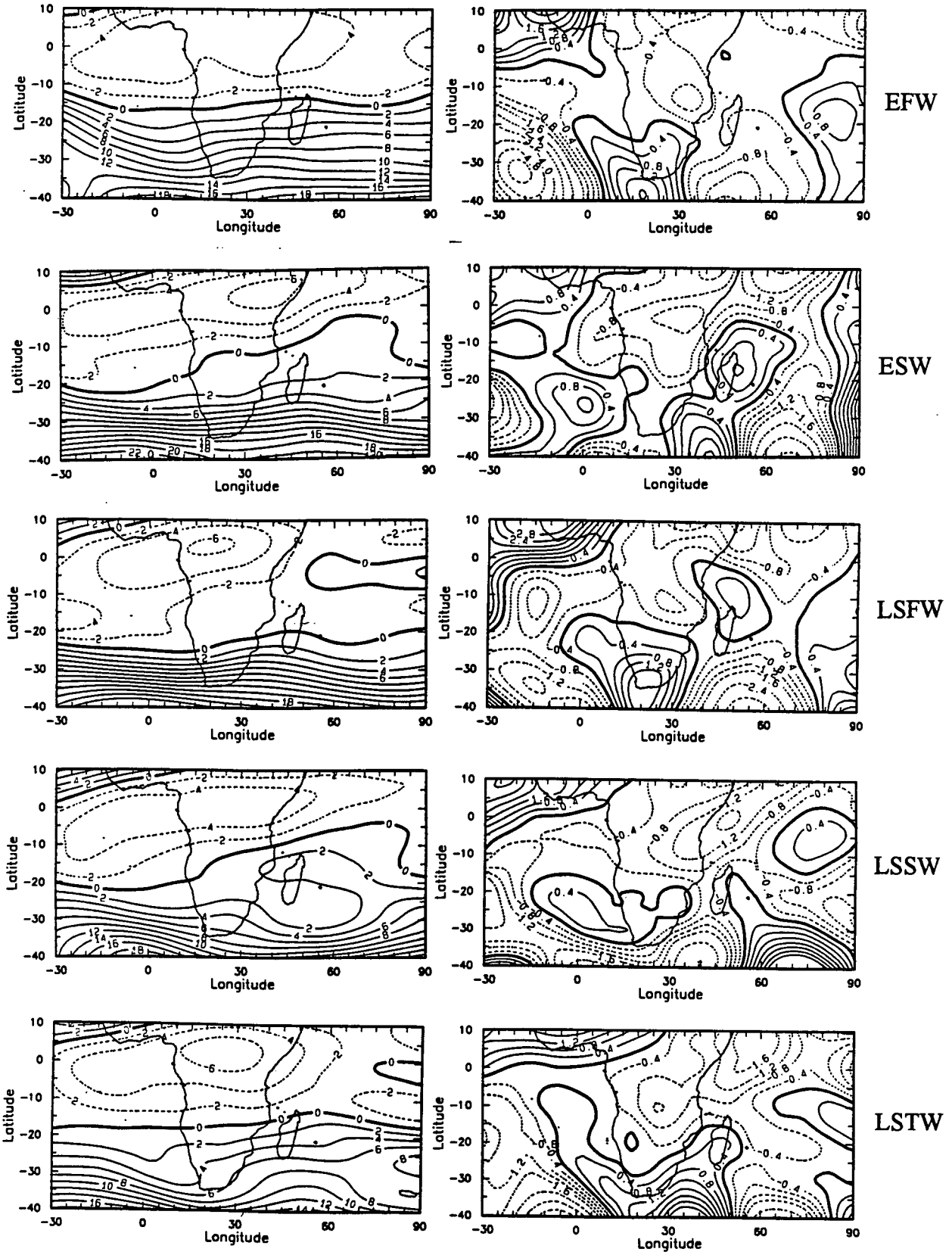

Figure 6.3 : 500 hPa zonal wind (a) and meridional wind (b) for each wet spell during peak activity. Contour intervals are 2 and 0.4 ms^{-1}, respectively.

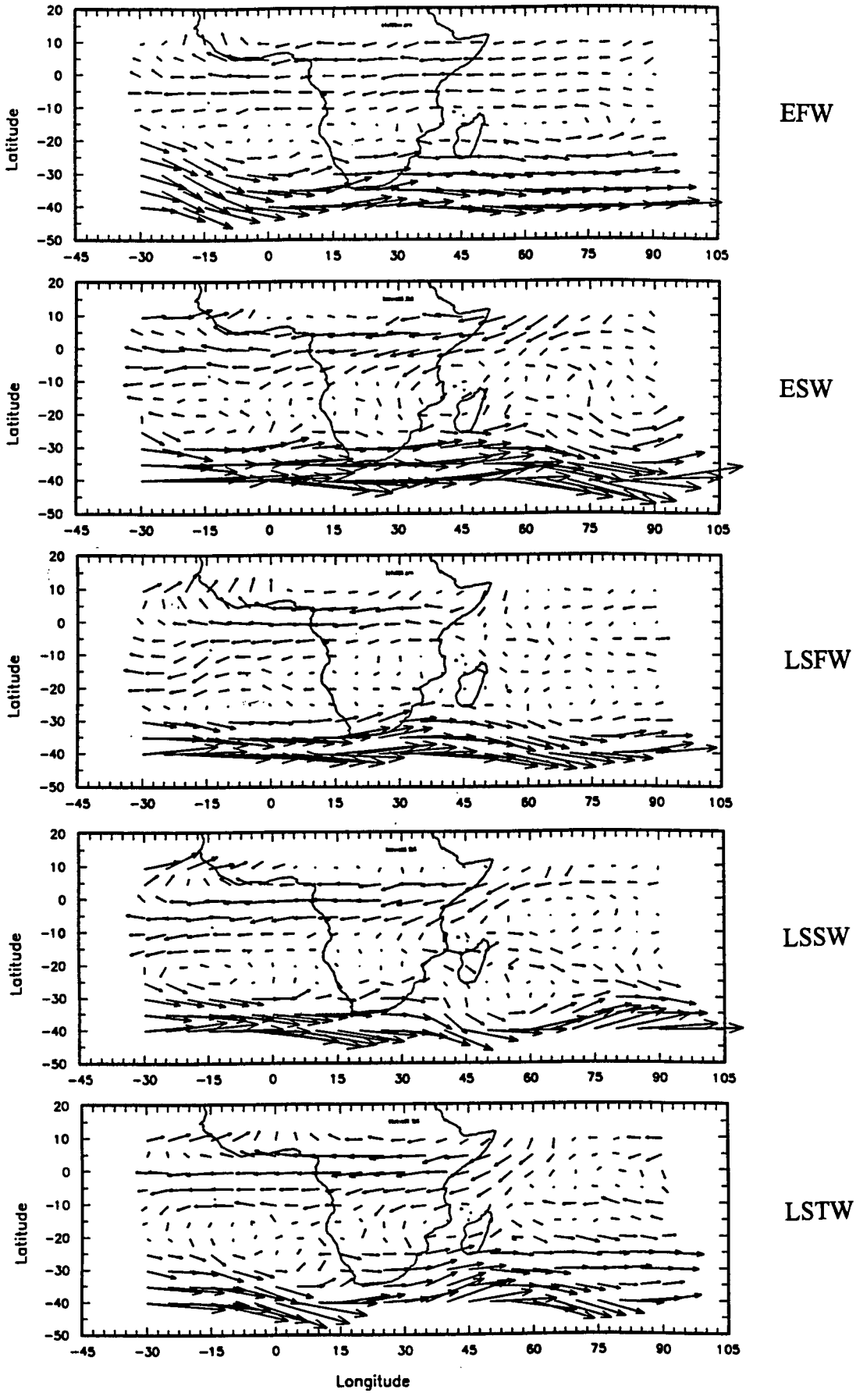

Figure 6.4 : Horizontal wind vectors at 500 hPa at the peak (Pentad P0) of each major wet spell. The longest vector is equivalent to 22 ms^{-1}.

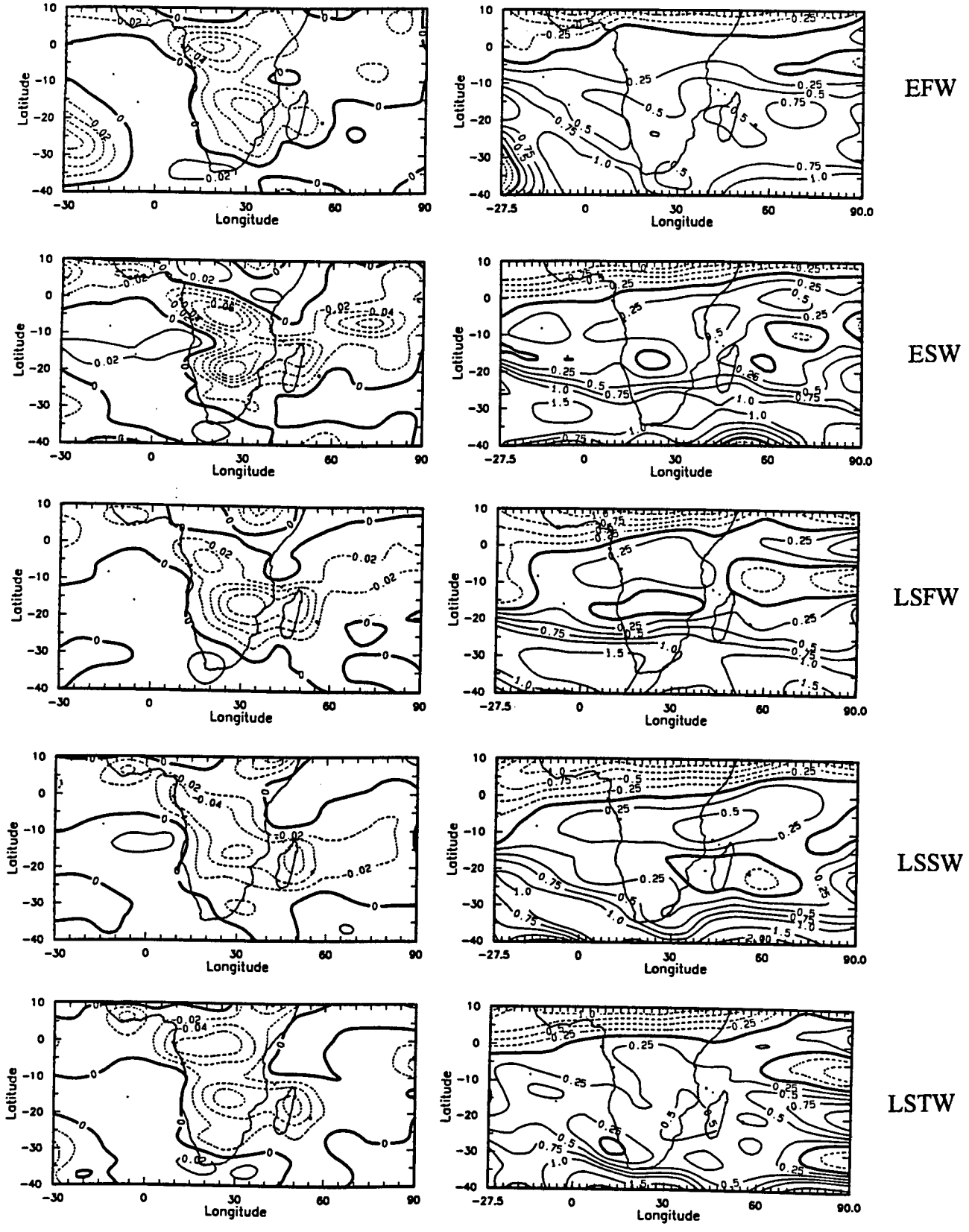

Figure 6.5 : 500 hPa vertical velocity (a) and vorticity (b) for each wet spell during peak activity. Contours are at every 0.02 x 10^{-2} Pa s^{-1} and 0.25 x 10^{-5} s^{-1}, respectively.

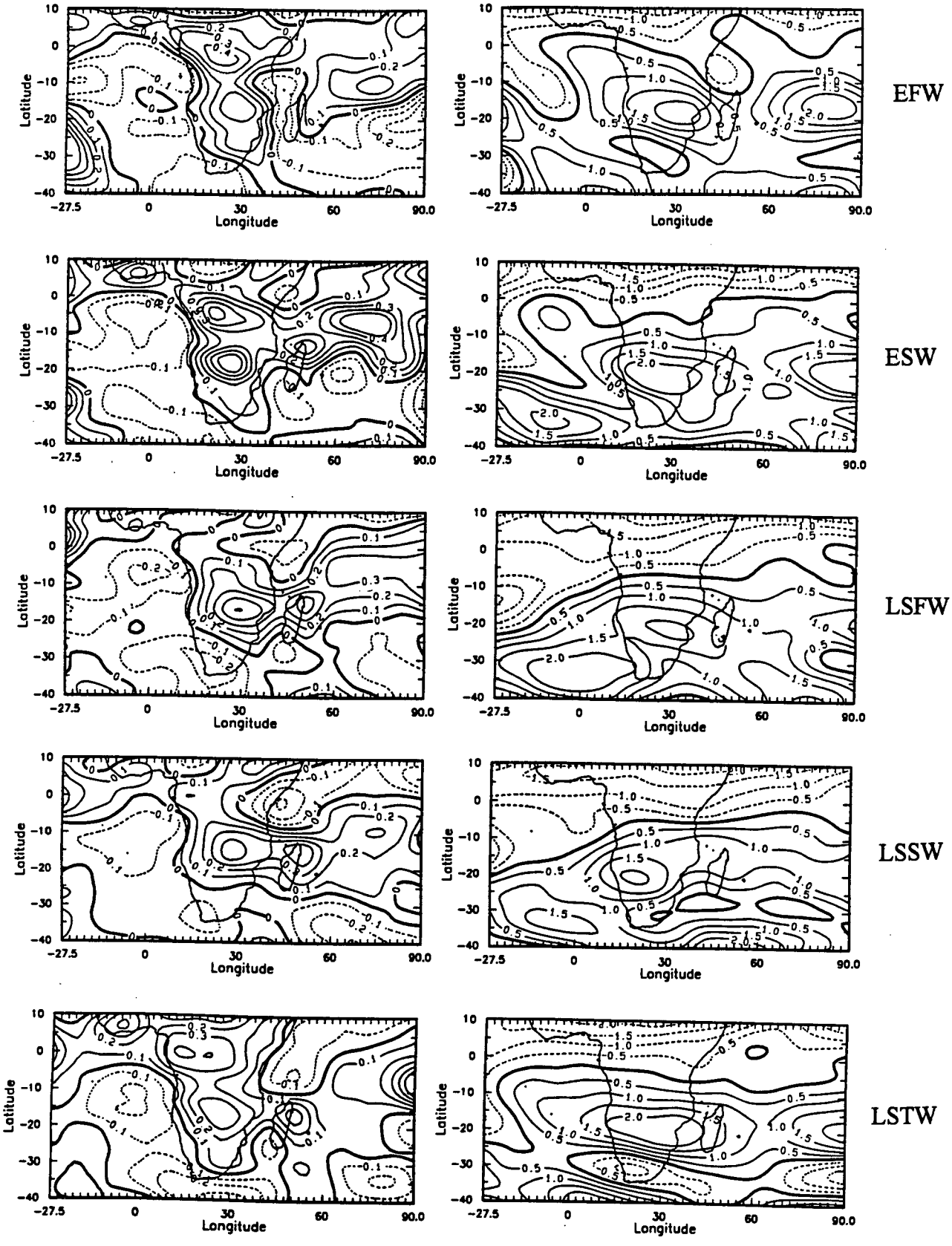

Figure 6.6 : 200 hPa divergence (a) and vorticity (b) for each wet spell at peak activity (Pentad P0). Contour intervals are 0.1 and 0.5 x 10^{-5} s^{-1}, respectively

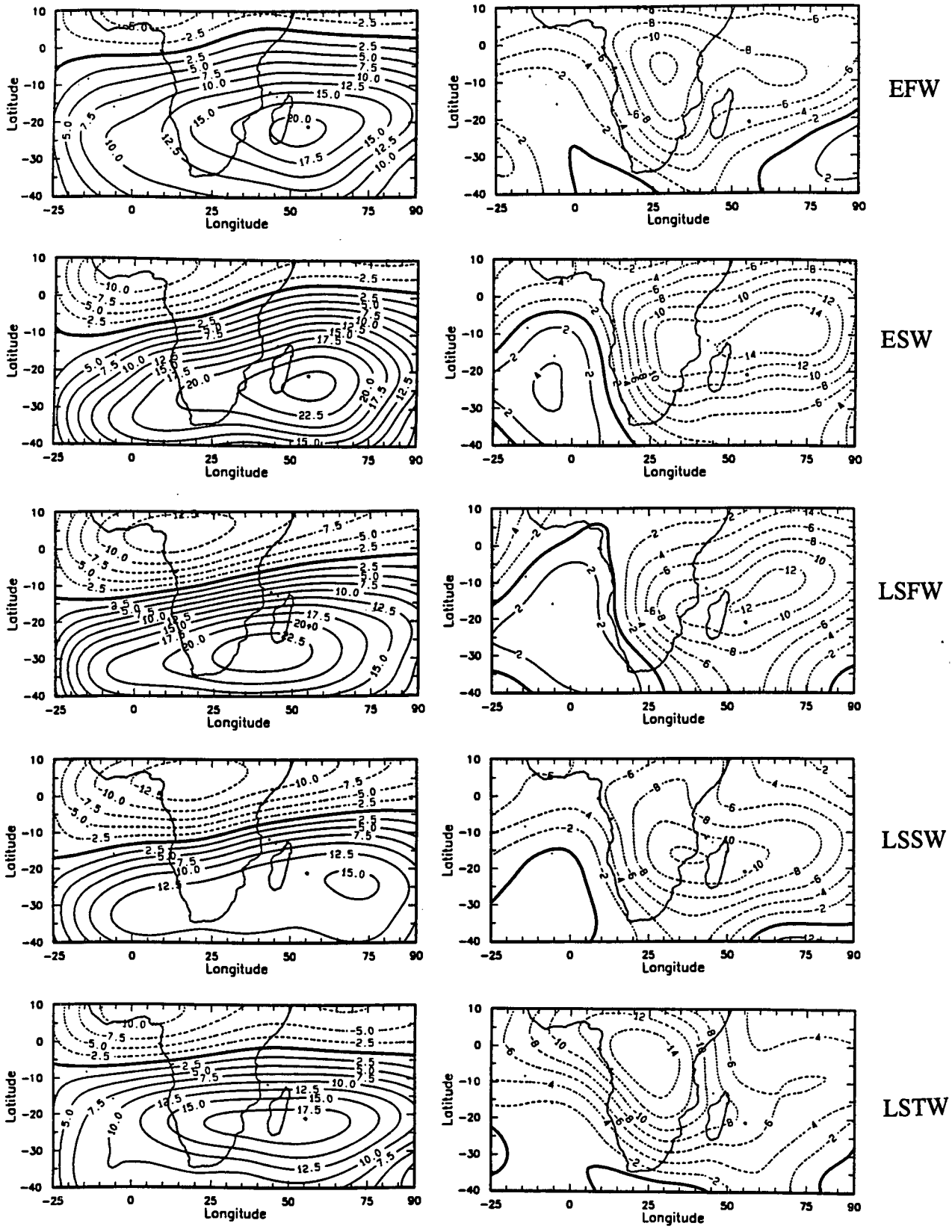

Figure 6.7 : Stream function (a) and velocity potential (b) at 200 hPa. The contour spacing is every 2.5 and 2 x 10^6 m^2s^{-1}, respectively.

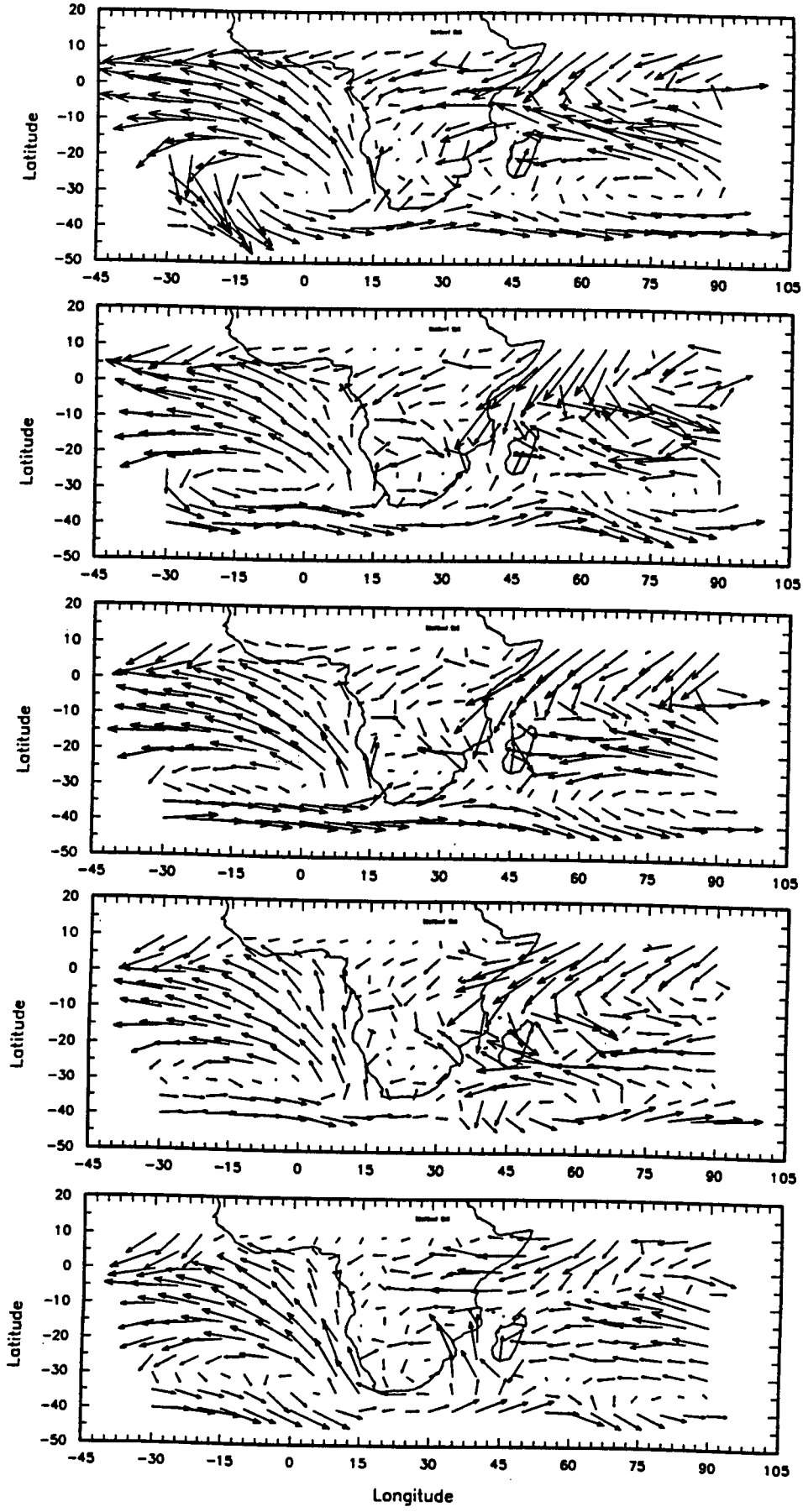

Figure 6.8 : Vertically integrated water vapour flux. The longest vector is equivalent to 225 g kg^{-1} m s^{-1}

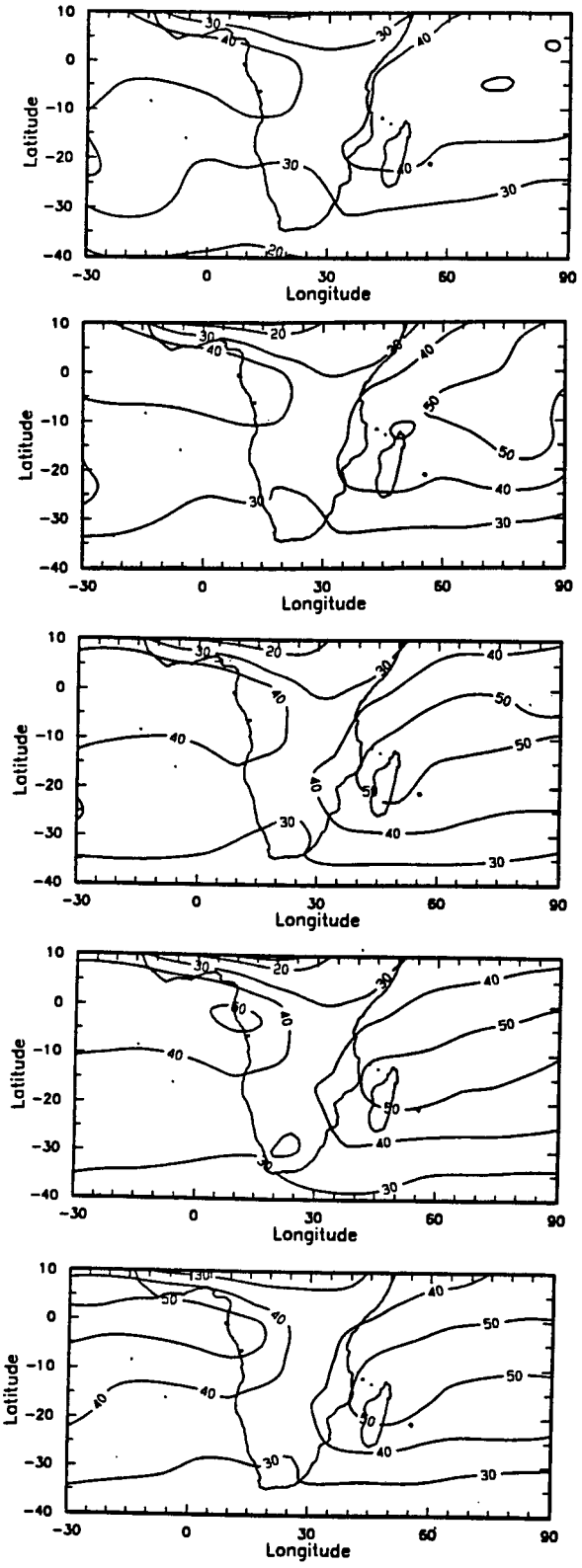

Figure 6.9 : Precipitable water for wet spells at Pentad P0. Isolines are at every 10 mm.

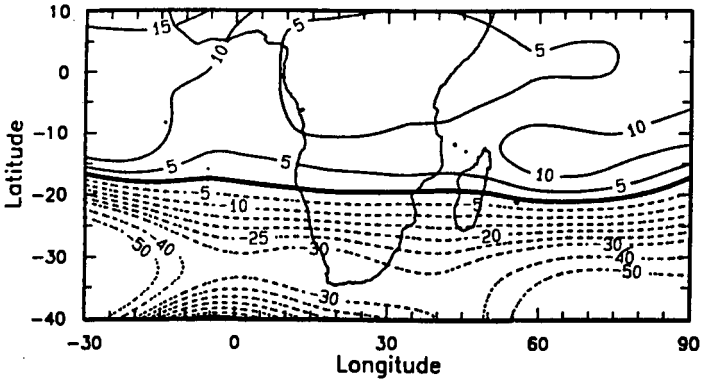

Figure 6.10 : Intercomparison : EFW0 - LSFW0 500 hPa geopotential height field. Contour spacing is every 5gpm.

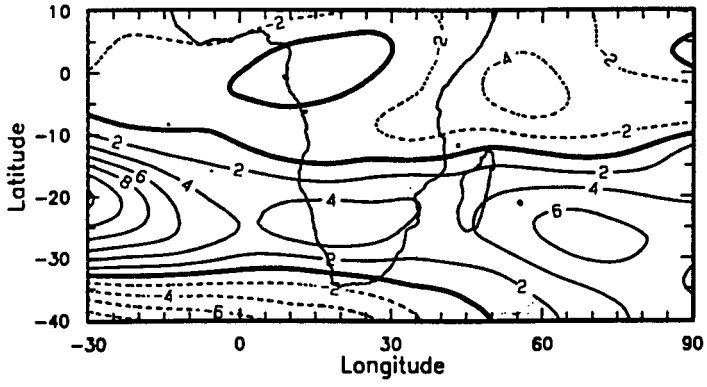

Figure 6.11 : Same as Figure 6.10, but for 500 hPa zonal wind difference. Contours are at every 2 m s^{-1}.

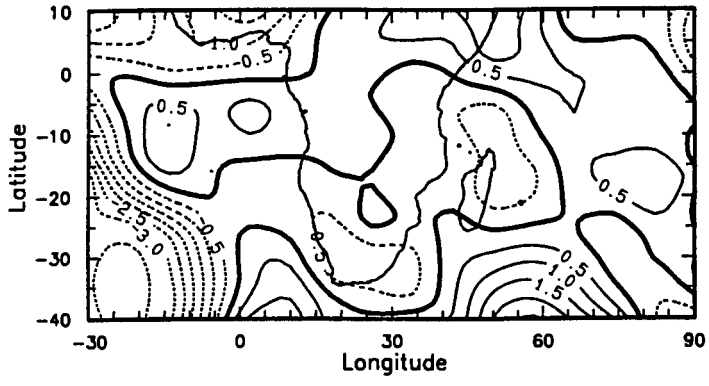

Figure 6.12 : Same as Figure 6.10, but for 500 hPa meridional wind difference. Contours are at every 0.5 m s^{-1}.

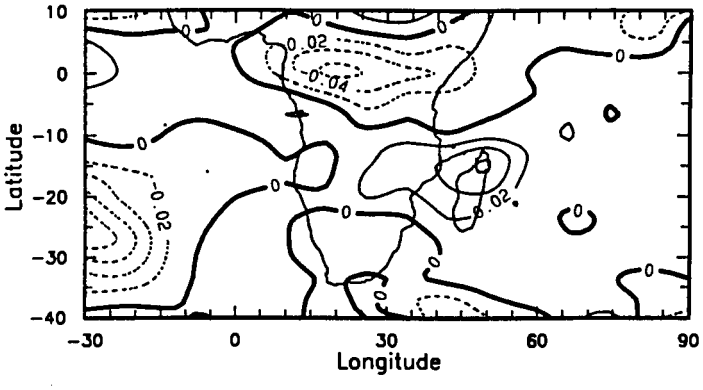

Figure 6.13 : Same as Figure 6.10, but for vertical velocity at 500 hPa. Contour interval is 0.02 x 10^{-2} Pa s^{-1}

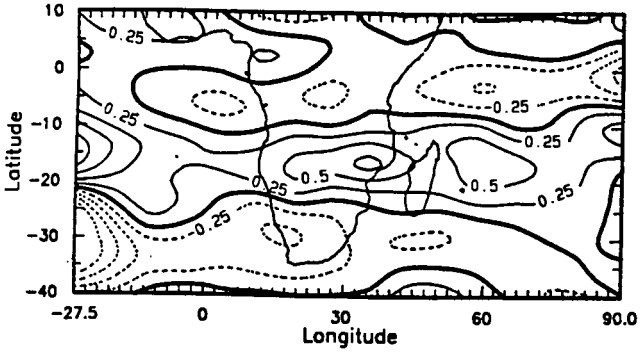

Figure 6.14 : Same as Figure 6.13, but for 700 hPa vorticity where contours are at every 0.25 x 10^{-5} s^{-1}

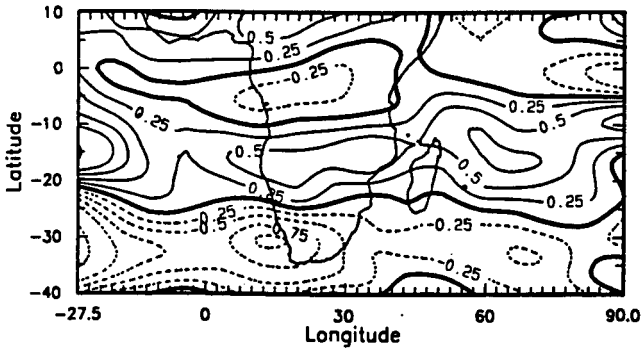

Figure 6.15 : Same as Figure 6.14, but for 500 hPa vorticity where contours are at every 0.25 x 10^{-5} s^{-1}

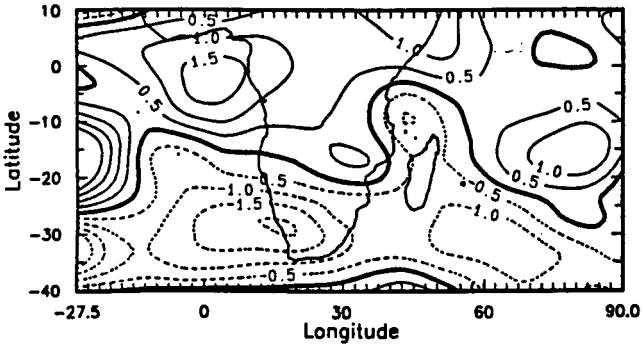

Figure 6.16 : Same as Figure 6.14, but for 200 hPa vorticity where contours are at every 0.5 x 10^{-5} s^{-1}

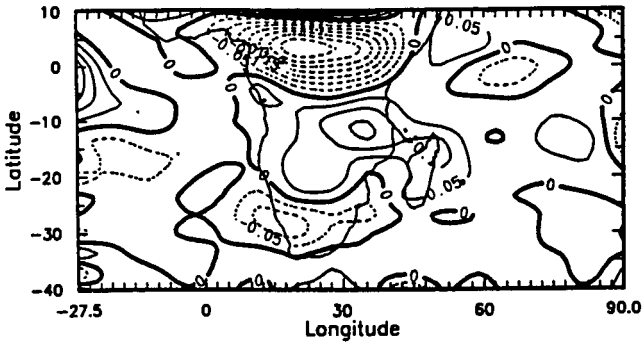

Figure 6.17 : EFW-LSFW 700 hPa divergence. Contour interval is 0.5 x 10^{-5} s^{-1}

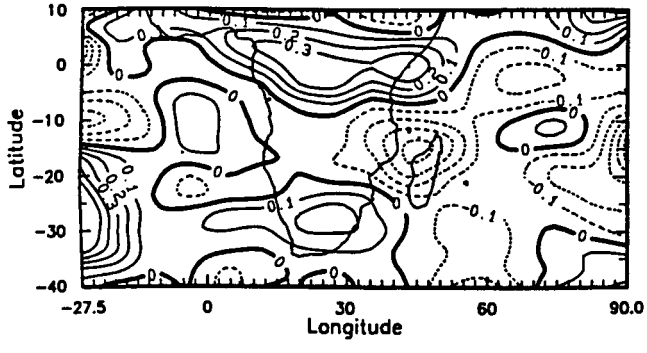

Figure 6.18 : Same as Figure 6.17, but for 200 hPa divergence where contours are at every 0.1 x 10^{-6} s^{-1}

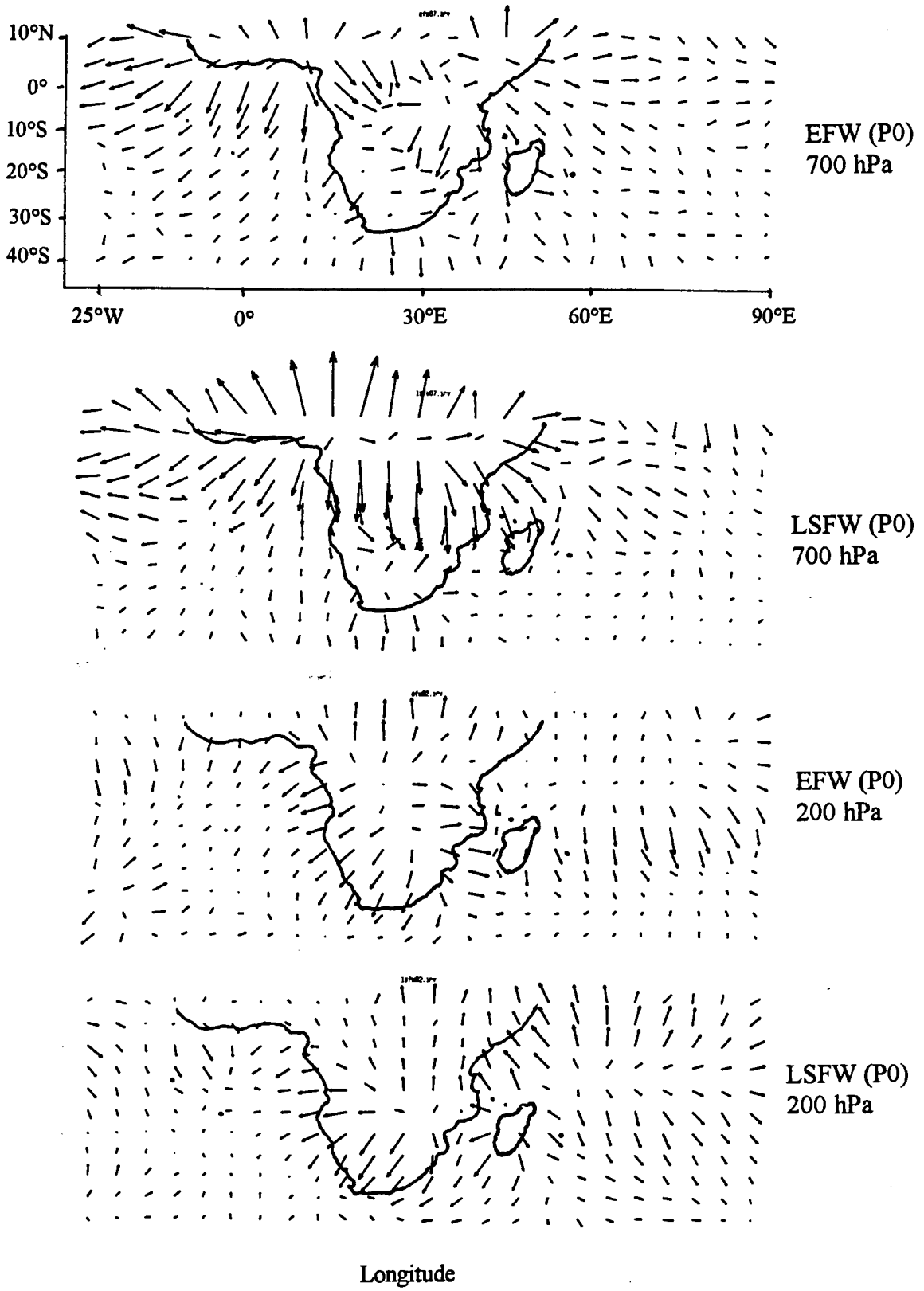

Figure 6.19 : Irrotational components of divergence for EFW0 and LSFW0 at 700 and 200 hPa. The longest vector is equivalent to 3.6 and 5.2 x 10^{-6} s^{-1}, respectively

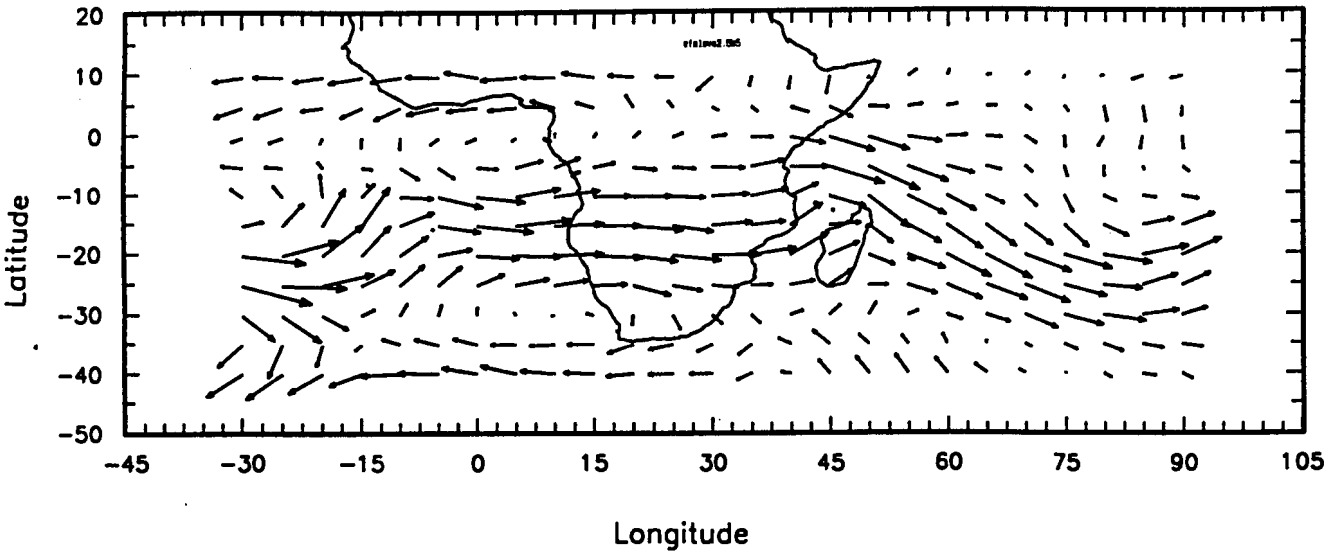

Figure 6.20 : Intercomparison : EFW-LSFW 200 hPa horizontal wind vectors.
The longest vector is equivalent to 22.5 m s^{-1}.

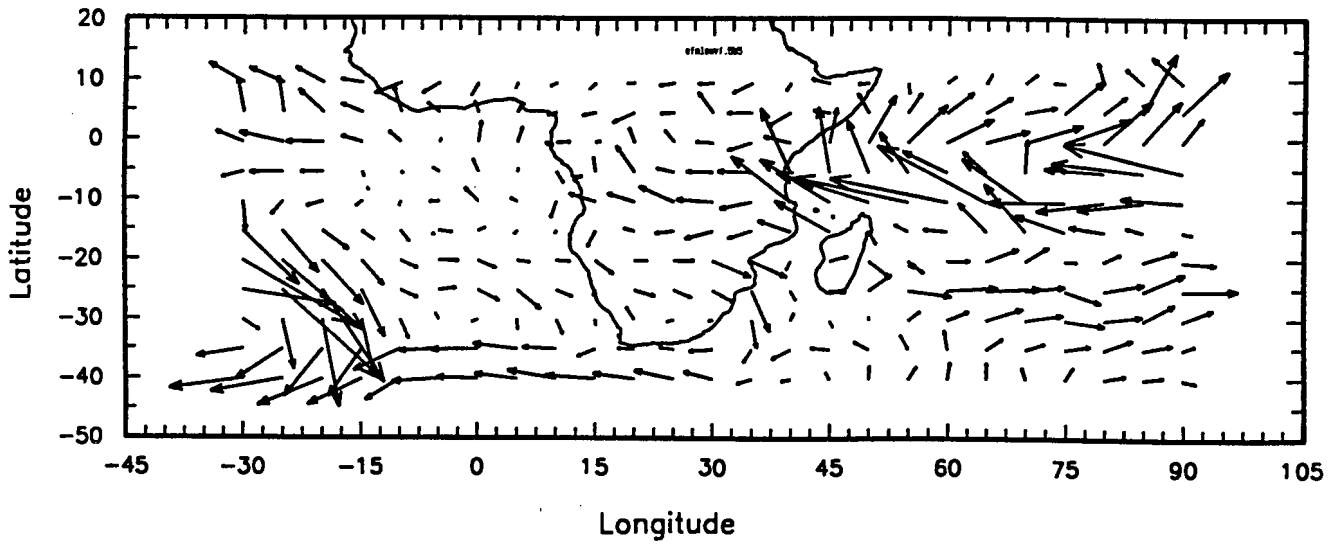

Figure 6.21 : Intercomparison : EFW- LSFW vertically integrated water vapour flux.
The longest vectors is equivalent to 245 g kg^{-1} m s^{-1}.

Chapter 7

Life Cycles of EFW and LSFW Anomalies

7.1 Introduction

From a weather prediction perspective, mean circulation patterns offer little guidence. Instead, detailed knowledge of synoptic events from precursor development through evolution to decay is more critical. It is fundamental to understand the threshold tolerances of regimes so as to allow operational forecasters to identify those situations when impending changes are more likely (Reinhold and Yang, 1993). Convective weather regimes have been observed to initiate, develop and even persist with or without any stimulus from changing planetary boundary conditions (like sea- surface temperature), since the energetics of transitions are mostly baroclinic and the transitions themselves only last a few days. Besides, it has already been noted (for example, Trenberth, 1984; Lau, 1985; Hunt and Gordon, 1988 and Trenberth and Branstator, 1992) that it is only on seasonal and longer time scales that large- scale boundary forcing of the atmosphere emerge as significant. There are some triggering mechanisms that are primarily responsible for establishing convective wet spells, and others causing them to collapse. In other words, the changes may commence from within the individual synoptic- scale events (Lau, 1981; Legras and Ghil, 1985; Blackmon et al., 1986 and Vautard and Legras, 1988, to name a few). One possible avenue to study the behaviour of these regimes is through life cycle analysis, hence this chapter.

Life cycle analysis involves a multi- stage approach to understanding peculiarities or characteristics of any system in transition. In this type of analysis, kinematic pictures of transitions describe amplitude, structure, etc., while radiative thermal relaxation from differential heating and low- level frictional effects (Ekman pumping) at different phenological phases play major roles from regime onset to collapse. The approach has been used elsewhere before. For example, Dole (1982, 1986, 1988) studied persistent anomalies while Reinhold and Pierrehumbert (1982) investigated weather regimes. Rui and Wang (1990) investigated the characteristics and structure of the 30- 60 day intra-seasonal oscillation using a four- stage life cycle: initiation, intensification, maturity and dissipation. The procedure has the added advantage of identifying preferred regions of

development and dissipation which statistical techniques like lagged correlations, cross-spectral analyses and empirical orthogonal function analyses cannot describe adequately.

It was illustrated in Chapters 5 and 6 that circulation controls associated with major wet spells over southern Africa are largely a function of time and vary as the season progresses. The end result is they bring about precipitation, however spatially varied and lagged, over the region. This chapter focuses only on EFW and LSFW, two wet spells that are deemed to exert the greatest impact on the southern African summer season from an agricultural viewpoint. The spells determine the onset of the relatively short and long rains over the region. The analysis is a significant extension of Chapter 6. In this case, however, each selected wet episode is analysed sequentially with the following objectives:

- firstly, to determine the meteorological evolution of each spell through analysis of a four- stage process from initiation or formation to dissipation (a total of 20 days) with the view to understanding the precursors, structure and factors dominant at every phenological phase,

- to understand the physics and dynamics of the atmosphere over southern Africa and its immediate environs with particular emphasis on sources and sinks of moisture and air mass trajectories, preferred regions of development and, finally,

- to investigate the anomalies of each wet spell from observed peculiarities for operational medium- range weather forecasting and realistic early warning. As mentioned in Chapter 2, research on southern African climate variability has so far focused mainly on diagnostic analyses or historical analogues and offer little in the form of predictive potential.

7.2 Methodology

For both EFW and LSFW, pentad departures from normals (hereafter anomalies) are determined for each of four phases; namely P-2 (or initiation/ formation), P-1 (development), P0 (maturity) and P+1 (dissipation/ decay) in the summers 1987- 1992 as per **Table 4.5**. The long- term mean is determined as described in the period mean analysis of Chapter 5 (**Section 5.2**) and deviations are computed with respect to the mean EFW and LSFW and not the whole season. Selected meteorological parameters are

analysed. For easier interpretation, water vapour fluxes and wind vectors are expressed as total values and not anomalies. The analyses are carried out for all standard levels. However, for consistency, only three of the standard atmospheric levels are utilised, namely 700, 500 and 200 hPa.

7.3 Early Summer First Wet Spell (EFW)

Reference to Chapter 4 (**Table 4.4**) shows that the EFW, from initiation to decay, occurs between November 17 to December 6 in the long- term. This spell effectively determines the on- farm decision making and subsequent operations with regard to crop sowing/ planting.

7.3.1 Low- tropospheric circulation : 700 hPa

Figure 7.1 reveals anomalous north- south ($v'T'$) and east- west ($u'T'$) transports of temperature at 700 hPa during the life cycle of EFW. Positive anomalies suggest a northward advection (southerly transports) of cooler temperature, and vice versa. Thus, at EFW onset (P-2), poleward transports exist over Africa and are stronger over SW southern Africa, attributed to relatively higher temperatures (Chapter 5, **Figure 5.1**). Positive anomalies predominate the Indian Ocean with greatest equatorward motion over the eastern basin. Negative anomalies occur over a wider domain a pentad later (P-1) and the core of highest values shifts to the equatorial eastern Atlantic. At maturity (P0), positive anomalies stretch from 10°S in the eastern Atlantic through SW Africa to the southern ocean. This rapid development in the SE Atlantic displaces poleward transports over southern Africa northeastwards, where highest negative values are located near 15°S, 30°E (Zambia and north Mozambique). The negative anomalies entend from the equatorial Atlantic to the SW Indian Ocean. The general pattern is maintained into the dissipative stage (P+1). However, the southerly transports or cooler air advection spread to dominate southern Africa, limiting northerly transports over Africa to tropical regions. Negative anomalies in the SWIO are stronger. The overall sequence consists of poleward and warmer air advection into and across southern Africa prior to the peak of EFW, after which the anomalies gradually reverse from the south of the sub- continent, becoming equatorward as the life cycle ends. Also worthy of note are positive anomalies in the East Indian Ocean with an arm towards east Africa between the Equator and 15°S which

persist throughout the life cycle of EFW. This is indicative of blocking in the eastern longitudes of the ocean. It, therefore, provides an important channel of interaction between higher latitudes and the Equator, through which, in this case, the extra- tropical to equatorial transfer of energy, temperature, etc., takes place.

The zonal component (east- west) advection of low- level temperature is illustrated in **Figure 7.1b**. In this Figure, negative anomalies are taken to imply a combination of warmer temperatures and westward wind anomalies. The converse is also the case. During the formative and development phases of EFW, negative anomalies of zonal eddy temperature covariances predominate tropical regions. Over southern Africa, the lowest values are located across Angola. A 10- 15° latitude band of positive values exists from the Atlantic through southern Africa to the Indian Ocean with its axis along 25°S. Highest values shift with time from the Indian Ocean westwards to be over southern Africa at P-1 and in the central Atlantic five days later (P0). However, at P0 the positive anomalies from the SWIO penetrate northwestward into all but the extreme west of southern Africa, indicating a predominant westerly airflow across the sub- region. Negative anomalies in the Atlantic Ocean then spread eastwards into southern Africa splitting the westerly flow, resulting in one band along the MCAT and the other linking the anomalies in the two oceans. Apparent from zonal patterns is the zonality of anomalies prior to maturity, with the zero line in the vicinity of the TSB. The anomalies over southern Africa then become more meridionally oriented from P0 and have reversed, generally. The result suggests relatively warm air advection from tropical Africa to the SWIO. There is also an eastward transport of warm air from the West Indian Ocean along the Equator at P-2 and 5- 10° latitude further south at the time EFW decays, a pattern noted in earlier chapters.

Geopotential height anomalies (**Figure 7.2**) indicate a standing short wave pattern in the extra- tropics (poleward of the TSB) when EFW is initiated (P-2) with negative anomalies to the south of Africa and in the extreme southeast of the window region. Elsewhere over the continent weak positive anomalies exist. The pattern shifts eastward during development and the short wave temporarily dissipates, leaving a broad band of negative anomalies poleward of 30°S from the Atlantic to about 40°E. Positive anomalies over southern Africa are still within 5 to 10 gpm of the mean. The standing wave re- develops at the peak of EFW (P0) with a shorter wavelength compared to that at P-2. The negative anomalies extend a tongue from the SWIO into SE southern Africa, indicative of a low level trough over the sub- region during this period.

In general, the patterns in the extra- tropics have become more meridional, penetrating the TSB to 10°S. They propagate eastwards, though slowly, such that at the dissipation stage (P+1), the negative anomalies are located over southern Madagascar and the south Indian Ocean. The "trough" over southern Africa is still in evidence but has been displaced northeast to overlie the preferred location of the Mozambique Channel- Angola Trough (MCAT). On either side of the region of negative anomalies are strong positive anomalies, indicating the re- establishment and re- intensification of the AOA and the IOA and a deepening of the trough.

Circulation patterns of the divergence anomaly (**Figure 7.3a**) indicate very little low- level changes taking place throughout the 20- day period when compared to the long term mean in terms of magnitude. The systems undergo a rather slow development from dry to wet during the earlier stages (P-2 and P-1) of the wet spell. During this period, all but the extreme southwest of southern Africa and the central Mozambique Channel are experiencing a relative divergent motion. At P0, apart from the extreme southeast, the airflow is more convergent across the sub- continent, moreso over Zambia and Mozambique. About five days later (P+1), relative divergence prevails over the region, except along the Angola- Mozambique trough. During the mature and dissipation stages of EFW, a standing wave is apparent over Africa. This is evidenced by alternating areas of divergence and convergence oriented from the southwest to the northeast. The pattern is clearer from analyses of actual values (not shown).

With reference to the vorticity anomaly patterns (**Figure 7.3b**), P-2 patterns for EFW at 700 hPa show NW- SE bands of alternating cyclonic and anticyclonic circulation anonalies across the entire domain. Of relevance to southern Africa is the cyclonic band stretching from the equatorial Atlantic Ocean through the region to the SW Indian Ocean. Five days later (P-1), the cyclonic tendencies over tropical Africa shift slightly southwards and extend in a tongue through northern Madagascar to the Mauritius region. Further south, the tendencies poleward of 30°S have also increased. The combined influence (plus the channeling effect) has strengthened the anticyclonic tendencies over southern Africa. Meanwhile, anticyclonicity from the Indian Ocean has spread into Tanzania. By the time the wet spell peaks (P0), the patterns have become more meridional again with the NW- SE bands. The short wave feature is better illustrated with a band of cyclonic flow affecting all but the extreme northeast of southern Africa. The anticyclonic flow from the Indian Ocean through East Africa at P-1 has continued to spread westwards to link with that in the Atlantic through equatorial Africa. The standing wave is maintained at P+1.

However, a blocking situation in the Indian Ocean has shortened its mean wavelength from about 35-40° at P0 to around 20°. This has enabled the anticyclonic tendencies to spread into the south of southern Africa where there is a maximum near 25°S, 20- 25°E, effectively limiting low- level cyclonicity to the tropics.

7.3.2 Middle- level circulation : 500 hPa

Alternating bands of anomalous 500 hPa northerly and southerly wind components are evident at P-2 from the meridional wind anomaly field (**Figure 7.4a**), with the northerlies stretching from the Atlantic through southwest Africa to the SWIO. The rest of southern Africa is under the influence of a southerly component from the South Indian Ocean through Madagascar and Mozambique. Five days later (P-1), eastern central Africa (Zimbabwe, Zambia and Mozambique) and Madagascar are still under a weak southerly wind regime while northerly flow prevails over the rest of the sub- region. Relatively strong southerly winds in central Indian Ocean apparent at P-2 are also indicated but have weakened somewhat. At the peak of the wet spell (P0), the patterns over southern Africa have reversed, due to the eastward progression of the systems. The southerly wind regime in the Atlantic Ocean has advanced into southern Africa to affect the southwest. At the same time, the rest of the Africa and most of the western Indian Ocean are under northerly flow. The pattern over southern Africa is such that the southerlies are on the leading edge of the intensifying AOA, comprising the upstream trough across southern Africa during this period. By P+1, the southerly winds over southern Africa have spread south-eastwards leaving only the tropical areas under northerly winds. The pattern in general begins to re-organise in preparation for the next cycle, thus showing some semblance with P-2 patterns.

The zonal wind anomaly patterns are shown in **Figure 7.4b**. The changes during the transition period prior to the peak wet spell (P-2 and P-1) are slow, with about 12°S separating relative easterly from westerly components in the north and south, respectively. However, at P0 there is a major change. This time the patterns become more meridional, severing links in the westerlies over the Atlantic and Indian Oceans. The wind over all but the extreme southwest of southern Africa has become more westerly (or less easterly) associated with the troughing from the SWIO (P0). Further north in the equatorial Indian Ocean, the relative easterly winds have increased and continue to do so in the decay phase. The westerly wind influence over southern Africa has decreased by P+1 due to incursions

from the Atlantic Ocean. The westerlies, however, continue to prevail in the region from Angola across most of Zimbabwe and Zambia through Mozambique (associated with the MCAT) to the southeast of Madagascar, where there is a maximum. In general, the zonal wind anomalies also portray an eastward progression, with westerly anomalies in the SE Indian Ocean at P-2 and over the SW Indian Ocean by the time of EFW dissipation (P+1).

The total wind field (**Figure 7.5**) closely follows that of the geopotential height anomaly (z', **Figure 7.6a**). The formative (P-2) and development (P-1) stages of EFW are characterised by an anticyclone centred near 20°S, 20-25°E which controls an anti clockwise circulation over southern Africa. At maturity (P0), the anticyclone collapses rapidly. However, the zone of anti- clockwise flow between 10 and 20°S since P-2 remains in evidence, producing a col over Africa. This zone depicts the middle level position of the sub- tropical high pressure belt. The flow across southern Africa is predominantly westerly poleward of this zone. The anticyclone over Botswana begins to re- establish itself again during P+1, as does the sub- tropical belt from the Atlantic to the Indian Ocean.

The most significant changes of the geopotential height anomaly, z' (**Figure 7.6a**) can be noted poleward of 10°S throughout the 20- day period. The anomalous pattern indicates a general eastward progression during this period as well, illustrated by the shift of lower geopotential heights from the south Atlantic Ocean in the initiation stages of EFW (P-2) to the SW Indian Ocean in the decaying phase (P+1). The reversal of the anomalies over eastern South Africa between P-2 and P0 indicate an eastward movement of about 25° of longitude within 10 days, after which the systems slow down. In the process, the Atlantic Ocean Anticyclone re- intensifies, the Indian Ocean Anticyclone is displaced to the east and replaced by a trough- like pattern extending into southern Africa.

The short- wave pattern evidenced from wind and geopotential height anomalies is even more pronounced in the vorticity anomaly field (**Figure 7.6b**) at 500 hPa during the initiation (P-2) and development (P-1) phases of EFW. The wave- train is oriented SW-NE and commences from the south Atlantic Ocean. During the 10- day period, the region of relative anticyclonic flow stretches from the equatorial Atlantic Ocean through southern Africa to the SWIO, where it strengthens. A cyclonic tendency extends across Africa to the Indian Ocean along 20°S. As noted from horizontal wind anomalies, the patterns "flip-flop" within about five days between P-1 and P0 such that, during the latter pentad, anomalous cyclonic flow dominates extra- tropical southern Africa (from 20°S

southwards). Anticyclonic vorticity over central southern Africa is sgnificantly reduced at the peak of EFW. At P+1, the pattern over the sub- region reverts back to that during dissipation with a band of relative cyclonic flow affecting the middle third of southern Africa. The belt is sandwiched between anticyclonic circulation over South Africa and as well another band equatorward of it which stretches from Zaire through Madagascar to the south Indian Ocean.

7.3.3 Upper tropospheric Flow : 200 hPa

The upper- level meridional wind pattern (v'), as at lower levels, also displays a short-wave pattern in the Atlantic Ocean and over Africa at P-2 (**Figure 7.7a**). A narrow band of anomalous southerly flow crosses southern Africa from Mozambique along 20°S. A band of northerly flow is initiated from the equatorial Atlantic Ocean and moves southeastwards passing through South Africa to the SWIO. A northerly component is also apparent in the Indian Ocean to the east of Madagascar. The wave becomes more evident five days later (P-1) with crest and trough centred approximately 15° longitude apart along 20°S (tropical sub- tropical boundary). A southerly wind anomaly is located over the central Mozambique Channel. At P0, the standing wave has weakened. The centres of action have been preserved, though, and have been displaced equatorward to lie along 12- 15°S. Another short- wave pattern has formed south of Africa and the Indian Ocean. By P+1, the wave is gone. The circulation is dominated by an anomalous northerly wind stretching from west Africa and traversing southern Africa diagonally to the SWIO.

The life cycle of the zonal wind (u') commences with an easterly anomaly south of Madagascar and a westerly anomaly to the SW of Africa (**Figure 7.7b**). Easterly anomalies are confined to equatorial regions of Africa (Zaire) and the central Indian Ocean during P-2 and P-1. There is a rapid change from P-1 to P0, when easterly wind anomalies spread outwards from Africa westwards to the Atlantic Ocean and eastwards to be over northern Madagascar by P0. The enhanced sub- tropical westerlies shift from the SE Atlantic to the SW Indian Ocean, also noted at 500 hPa. In the dissipation phase (P+1), anomalous westerly winds are experienced across the middle third of southern Africa (from Namibia to Mozambique) and in the SWIO, the only region whose airflow remains relatively westerly throughout the 20- day cycle.

The horizontal wind vectors at 200 hPa (**Figure 7.8**) indicate an anti clockwise circulation dominating tropical regions of Africa and the Indian Ocean. A short amplitude wave is in development with a trough over Africa and crests in the central Atlantic Ocean and in the Mozambique Channel at P-2. The wave becomes fully established by P-1, oscillating between 10 and 30°S. It has moved slightly eastwards maintaining a westerly to northwesterly flow across southern Africa. The crest has shifted 10° longitude from the Mozambique Channel to 50°E and its amplitude has grown in the process. During P0, the wave appears to collapse due to the re- development of an anticyclone over Africa centred near 10°S, 20°E. This has pushed the crest in the Atlantic westwards and intensified the system over Madagascar. The pattern is maintained during the decay of EFW (P+1) with the anticyclone directing an anticlockwise circulation in tropical Africa. The circulation from 15°S polewards has veered to predominantly westerly.

At P-2, positive geopotential height anomalies (z') are concentrated in the SWIO around 40°S, 60°E and over extra- tropical southern Africa (**Figure 7.9**). Below normal (negative anomalies) heights are located in the south Atlantic Ocean as well as over tropical Africa and the Indian Ocean. The systems show eastward movement by P-1. Negative anomalies in the Atlantic Ocean are just off the west coast of Africa. Positive anomalies in the Indian Ocean have been re-distributed with one portion moving about 20° further east to near 80°E, the other re- inforced over southern Africa by anomalies from the Equator. Over the Indian Ocean, the anomalies remain mostly negative with a local minimum just to the north of Mauritius. The eastward progression continues such that, by P0, negative anomalies influence South Africa from a centre in the SWIO. Positive anomalies dominate the South Atlantic Ocean. These advance to the Indian Ocean through Madagascar to cover all but the SWIO by P+1. However, the systems have stagnated since P0, due to blocking in the central south Indian Ocean where an anomalous ridge extends northwestwards to Madagascar.

Reference to the divergence (**Figure 7.10a**) and vorticity (**Figure 7.10b**) shows a convergence anomaly covers southern Africa at P-2 between 10 and 25°S, linked to that in the south Indian Ocean. At the same time, cyclonic circulation extends from the Indian Ocean across southern Africa over the region experiencing upper- level convergence. There is also anticyclonic flow through South Africa, where a link between the oceans is provided. During the developmental phase (P-1), all but the extreme northeast of southern Africa is under anticyclonic flow. The area under convergence is restricted to the northeast and upper level divergence begins to dominate the flow. One pentad later

(P0), strong upper divergence occurs over southeastern Africa. The vorticity patterns show an equatorward displacement, with cyclonic tendencies now occurring over southern Africa poleward of 20°S, restricting anticyclonic tendencies to the tropics where a local maximum occurs over Mozambique. Generally, the patterns over southern Africa at maturity are opposite to those during P-2. As noted in the meridional wind patterns, the patterns shift equatorward during dissipation (P+1), resulting in divergence anomalies in the tropics and anomalous convergence over extra- tropical southern Africa. The decay of EFW over the sub- continent is rather slow with patterns quasi- stationary and more stratified. The regions of anomalous cyclonicity and anticyclonicity are more emphasised.

7.4 Late Summer First Wet Spell (LSFW)

LSFW usually commences in mid- January, typically reaches a peak around January 23 and dissipates rather rapidly thereafter. Failure of this wet spell often spells disaster for maize production over southern Africa.

7.4.1 Lower tropospheric flow: 700 hPa

Horizontal temperature transports

Meridional transients (T'v') : Figure 7.11a

In the formative stages (P-2), negative anomalies (northerly or warm wind tendencies) cover most of Africa, except across eastern central Africa. The band of negative values initiates in the Northern Hemisphere through NE Africa, comes down the western flank of Africa (Angola and Namibia), spreads to include Botswana and South Africa and proceeds to the Indian Ocean SE of the continent. The overall pattern over southern Africa is an anti clockwise pattern across the central interior. About five days later (P-1), anomalies in the Atlantic Ocean have advanced northeastwards to over South Africa. Linkage occurs with Indian Ocean anomalies through the Mozambique Channel, temporarily severing the links between negative anomalies over Africa and the SWIO. The blocking situation in the Indian Ocean is again apparent during the mature stage of LSFW (P0), evidenced by the negative anomalies which have remained rather quasi- stationary in the SWIO to the SW of Madagascar since P-1. In this period, positive anomalies (hence cold southerly wind tendencies) from the Atlantic Ocean have spread further into southern Africa to include

southern Namibia and Botswana. Equatorward of this, northerly thermal transport anomalies prevail. Most of the western Indian Ocean is under a warm thermal wind advection. Only a narrow band over and immediately east of Madagascar remains affected by southerly flow. The ENE progression from the Atlantic Ocean continues during decay (P+1). Anomalous southward thermal fluxes now cover the SE Atlantic and western half of southern Africa with minimum values along the west coast at 25°S. This action has displaced positive anomalies across southern Africa northeast wards with axis of highest values from Angola to Madagascar. The dipole- like structure is indicative of anti clockwise circulation across southern Africa centred over the central interior in the vicinity of Botwana.

Zonal transients (T'u') : Figure 7.11b

An area of eastward warm eddies exists from the southeast Atlantic Ocean, through Africa south of the TSB into the SWIO at P-2. Another zone is evident in the western Indian Ocean stretching from the Tanzanian coast through northern Madagascar to east of Mauritius. The area under positive (eastward) anomalies expands during development of LSFW so as to cover most of southern Africa and the Indian Ocean with local maxima in the SWIO and between 5 and 10°S in the central Indian Ocean. The relative eastward movement of systems in the Atlantic continues such that at P0 negative anomalies cover Namibia and western Botswana in particular. Positive anomaly patterns extend into central southern Africa where a local maximum exists over Zambia. Another band of positive anomalies links the two oceans through eastern South Africa. By P+1, negative anomalies occur over the continent. Positive anomalies extend from the South Atlantic Ocean across southern Africa and dominate the Indian Ocean with highest values to the northeast of Mauritius and Madagascar along the TSB.

Geopotential height anomaly (z')

At P-2, geopotential height anomalies are positive over all but the extreme southwest of southern Africa (**Figure 7.12**). The patterns shift eastwards such that negative anomalies are transferred to eastern South Africa and the SWIO five days later (P-1). During maturity (P0), the negative anomalies have stagnated in the SWIO and have penetrated north into southern Africa as far north as the TSB. The heights over southern Africa recover during the dissipation phase, displacing the negative anomalies from the region to the Indian Ocean east of Madagascar.

Divergence and vorticity fields

At P-2, a pattern of alternating regions of divergence and convergence can be observed from the southwest Atlantic Ocean to north Africa such that convergence stretches from the equatorial Atlantic through southern Africa to Madagascar (**Figure 7.13a**). The low tropospheric vorticity (**Figure 7.13b**) is generally weak during the initiation (P-2) and development (P-1) stages. However, anticyclonic circulation is dominant everywhere over southern Africa, except the extreme south. At the peak of the wet spell (P0), convergence exists linking the Atlantic and the Indian Oceans via central southern Africa and Madagascar. Maximum convergence is along 20°S over Africa (northern Zimbabwe, Zambia and Mozambique) indicating the position of the ITCZ in the region. Divergence over South Africa has increased in area and magnitude. During this period, the flow over central southern Africa (from Namibia to northern Mozambique) has become weakly cyclonic, extending from the Atlantic Ocean. Five days later, both patterns have changed markedly. Over Africa, the circulation has reversed, with divergence dominating tropical southern Africa and continuing eastwards to the central Indian Ocean. The centre of divergence is at 15°S, 25°E. There is relatively strong anticyclonic motion over the sub-region and centred near 18°S, 20- 25°E. Most of the east Atlantic Ocean is under convergent motion. Convergence over Africa associated with the ITCZ has vanished, indicating the rapid dissipation of the convective regime.

7.4.2 Middle- tropospheric patterns: 500 hPa

In general, meridional wind anomalies (v') are small throughout LSFW at the 500 hPa level (**Figure 7.14a**). The cycle commences with positive anomalies (anomalous southerly wind) covering central and eastern southern Africa (from Angola spreading eastwards to the SWIO through Madagascar). The patterns become more meridionally oriented at P-1 with bands extending continuously from the northern hemisphere southwards beyond 40° S. Weak negative anomalies prevail across most of the continent leaving only the Mozambique coast still under a southerly wind regime. During P0, positive anomalies cover South Africa. These anomalies are displaced to eastern regions by P+1. Thus, the winds become predominantly southerly in the east and northerly in the west, illustrating the presence of a middle level anticyclone. This is a reversal of the circulation at P0. The main pattern is that of a standing wave in the mid- latitudes at P-1 and P0.

The corresponding zonal wind anomalies are displayed in **Figure 7.14b**. During evolution (P-2), the pattern shows a continuous belt of enhanced mid- level westerlies approximately between 20 and 30°S across the domain with a jet over Namibia. Elsewhere, tropical easterly anomalies can be noted traversing the Equator from the Indian to the Atlantic Ocean. At P-1 easterly wind anomalies cover tropical southern Africa and are linked to the equatorial Indian Ocean. The rest of southern Africa is under the influence of positive anomalies (westerly winds) with highest values in the SWIO along 35°S. The 500 hPa wind anomalies in the Indian Ocean are predominantly westerly. During P0, westerly winds cover a wider area of southern Africa with a maximum near 30°S, 40°E. By P+1, however, the patterns over the sub- continent revert to those 10 days before (P-1) with the tropical regions under easterly flow and the rest in a westerly regime. The final pattern is an anti clockwise circulation anomaly coincident with increased geopotential height anomalies), hence re- establishment of the anticyclone over Botswana.

The horizontal wind vectors (**Figures 7.15**) show three basic flows evident during the formation of LSFW (P-2). The first is a band of easterly wind vectors dominating the tropics but confined to the northern hemisphere over the Indian Ocean. The second and third are mainly due to the anti clockwise pattern originating along 22- 25°S in the Atlantic Ocean controlling easterlies (westerlies) from Africa to the north (south). The vectors in the central Indian Ocean are rather too weak to be of major influence regarding southern Africa. However, they are controlled by a clockwise circulation immediately to the north of Mauritius as well as an anti clockwise flow further east. At P-1, the patterns in the Indian Ocean remain rather chaotic due to several vortices, but a notbale break in the easterly wind regime occurs just north of the Equator. Deformation takes place immediately south of the Equator to the north of Madagascar, causing a split flow. A major component of the easterly wind regime re- establishes itself over tropical east Africa and traverses the continent as northeasterly winds as far down as 15°S. The anti clockwise belt in the Indian Ocean pushes eastwards across southern Africa and forms a weak link with that in the Indian Ocean. Of signficance over southern Africa is the resulting confluence between the south easterlies and north easterlies along 15°S, a configuration conducive for heavy precipitation. During maturity, the sub- tropical ridge temporarily collapses over southern Africa. The MCAT is apparent instead. By P+1, the belt re-develops, resulting in a well- defined anti clockwise circulation over the central interior of the sub- continent. This substantiates earlier inferences based upon observations from geopotential height and temperature transport anomalies at lower levels. The main factor is the "break- up" of the anticyclone over southern Africa at P0.

Geopotential height anomalies are relatively small in the tropics (**Figure 7.16a**). Positive values dominate the patterns throughout the life cycle of LSFW. However, at P-2, there are negative anomalies to the SW of South Africa as well as the SE of Mauritius, indicating a relatively weak sub- tropical high pressure belt. As LSFW develops (P-1), patterns poleward of 30°S propagate eastwards such that negative anomalies extend from 20°E to the eastern Indian Ocean. At maturity, as during early summer, the negative anomalies in the SWIO penetrate into southern Africa as far north as the TSB. A weak standing short- wave is apparent with a wavelength of approximately 70° of longitude. At P+1, the pattern resembles that at 700 hPa with positive values extending to higher latitudes through Africa. This pattern is different from that of EFW in that the eastward progression continues even after maturity.

In the middle levels, anticyclonic flow from the Atlantic Ocean extends into southern Africa between 10 and 25°S (**Figure 7.16b**). Another band of anticyclonic vorticity covers the tropical Indian Ocean and east Africa. The flow is cyclonic polewards of 25°S as well as over Madagascar. At P-1, the pattern shows southeastward progression. Anticyclonic flow still prevails over southern Africa and extends to the SW Indian Ocean through south Madagascar. The flow across the extreme southwest of the sub- continent is more cyclonic than before. The pattern continues to move eastwards such that by the peak of the wet spell (P0), southern Africa is under cyclonic circulation, linked to that in the equatorial Atlantic Ocean. There is strong anticyclonic flow ahead of and behind the system, stronger off the west coast of South Africa and from the south Mozambique Channel to the south Indian Ocean. Thus, during maturity, extra- tropical southern Africa and Madagascar experience opposing vorticity regimes in the middle levels. A pentad later (P+1), the systems over the region reorganise themselves, to indicate alternating bands of cyclonic and anti- cyclonic flow. There is strong anticyclonic motion over central southern Africa where a local maximum exists near 20°S, 20°E.

7.4.3 Upper- level circulation patterns : 200 hPa

At the start of LSFW (P-2), geopotential height anomalies (z') are higher than the period average over the equatorial regions of Africa and the Indian Ocean (**Figure 7.17**). Significant negative values occupy virtually the whole of eastern Atlantic Ocean as well poleward of the TSB (20°S) with lowest values to the SW and SE of South Africa and Madagascar, respectively. The positive values then spread south eastwards to dominate southern Africa and eventually link with those in the southeast Atlantic by P-1. The local centre of positive values shifts from the equator to the south Mozambique Channel. The trend is maintained towards mature stages of LSFW such that by P0, the negative values are confined to the central and western Atlantic as well as over South Africa and areas to its SE. At decay, the pattern changes over southern Africa, with negative values centred in the south Atlantic protruding into and across southern Africa, displacing positive anomalies east towards the centre of the Indian Ocean.

Upper horizontal meridional and zonal wind anomalies are displayed in **Figure 7.18**. The meridional pattern indicates alternating northerly and southerly winds over the Atlantic Ocean and Africa in the formative stages of LSFW. A 30°- wide longitude band of northerlies stretches from the Northern Hemisphere through West Africa down to higher latitudes of the Southern Hemisphere, grazing the west coast of southern Africa. Immediately east of this band is another of southerlies of similar dimension prevailing over the African continent. The flow in the Indian Ocean is less meridionally oriented. Southerly winds dominate the equatorial areas while the opposite is the case elsewhere. By P-1, the patterns have translated eastwards, are now oriented NW- SE and extend into the South Indian Ocean. The southerlies stretch from West Africa to the SWIO through Zambia and Madagascar, while northerlies originate from the central equatorial Atlantic Ocean through sub- tropical southern Africa to higher latitudes of the Indian Ocean. Five days later, at maturity (P0), northerly anomalies dominate the eastern Atlantic Ocean as well as Africa (except over southwest southern Africa). More relevant is a NW- SE band through Zimbabwe linking the Atlantic Ocean and the SWIO. The anomalies in the Indian Ocean are southerly. At dissipation, a N-S orientation is re-established, with southerly anomalies dominating the Atlantic Ocean and northerlies dominating southern Africa and the Madagascar/ Mauritius region.

The zonal circulation shows a rapid transformation from initiation to development. At P-2, the anomalies are westerly virtually over all but the higher latitudes with highest

values along 25°S. At P-1, the alternating pattern observed in meridional motion is also evident, whereby a band of westerly anomalies extends from the equatorial Atlantic Ocean through South Africa to the SWIO where a peak exists. At the same time, equatorial easterly anomalies are noted from the Indian Ocean to Africa, linked to another band from the South Indian Ocean through Madagascar. A broad belt of upper westerly anomalies originates off NE Madagascar and spreads to the SE Indian Ocean. At P0, the patterns are more zonal, and equatorial easterly anomalies from the Indian Ocean merge with those in the Atlantic Ocean. At the same time, westerly winds prevail over sub- tropical southern Africa as well as poleward of 30°S in the Atlantic Ocean. One pentad later (P+1), the westerles extend from the central Atlantic Ocean between 5 and 20°S to cover southern Africa and NW Madagascar. They reform in the SWIO and spread eastwards to the SE Indian Ocean. Elsewhere, the anomalies are easterly. The main feature is the enhancement of westerlies "downstream" of South Africa in the wet phase.

The corresponding vector field is presented in **Figure 7.19**. Reference to it shows that 10 days prior to peak activity (P-2), the upper level flow is dominated by a well defined anticyclonic ridge with axis roughly along 16°S from western Central Africa through northern Madagascar into the Indian Ocean. There is a local maximum centred in the vicinity of 18°S, 18°E. To the north and south of it are easterlies and westerlies, respectively. As the cycle progresses, the anticyclonic flow over Central Africa is maintained but the anticyclone shrinks meridionally and stretches into the Atlantic. The ridge axis also shifts slightly polewards to around 20°S during development and maturity, resulting in zonal flow north of 15°S and poleward of 22.5°S. During this period, the northerly winds in the Atlantic are shifted westwards, weakening in the process. In the last 5 days of the cycle (P+1), the patterns reverts to that at the beginning of the cycle (P-2), including the ridge axis and slight troughing in the Mozambique Channel. The winds, however, are generally weaker.

Comparing with EFW, the upper anticyclone over southern Africa is much more developed at all the four phases of LSFW; whereas during EFW, the anti cyclonicity increases during the course of the cycle. The airflow across southern Africa at EFW has a northwest- southeast trajectory (originating in the equatorial Atlantic Ocean). Thus, northwesterlies prevail over western southern Africa during early summer. With reference to LSFW, the upper anticyclone is the controlling factor, suggesting that the dynamics and physics associated with rainfall causation are internal rather than external. The anticylone "blocks" the equatorial Atlantic Ocean northwesterlies until after LSFW has matured.

Anomalies of divergence and vorticity are presented in **Figure 7.20**. Reference to the divergence pattern illustrates that during the formation of LSFW (P-2), the upper level pattern consists of convergence stretching from the south Atlantic Ocean to the SW Indian Ocean. Divergence extends across Africa to the tropical Indian Ocean, including Madagascar. The centre of anomalous convergence shifts slightly westwards with height from over Mozambique at low levels. In the next phase (P-1), convergence over central southern Africa has shifted equatorwards to 10°S, replaced by divergence starting from the Angolan coast southeastwards to the SW Indian Ocean. By the time the wet spell peaks, the configuration has progressed southeastwards. There is well- marked upper divergence over southeastern Africa covering Botswana, Zimbabwe and Mozambique. This divergence is split by convergence from the south Indian Ocean through south Madagascar resulting in some divergence extending to the tropical Indian sector. The centre of divergence overlies that of low level convergence also at the peak. The extreme west of southern Africa experiences upper- level convergence.

Regarding vorticity, the initiation process commences with a tongue of anticyclonic vorticity down the western flank of Africa from the northern hemisphere to South Africa (P-2). There is also another region of anticyclonicity in the central Indian Ocean towards east Africa. South of Madagascar a narrow zone of cyclonic vorticity is found. During the development process (P-1), the southern hemispheric pattern consists of alternating bands of cyclonic and anticyclonic vorticity in wave form all with axes oriented NW-SE and coinciding with regions of upper- level divergence and convergence (P-1, **Figure 7.20a**). One band of cyclonic vorticity extends from the northern hemisphere over Africa to the south Indian Ocean via northern Madagascar. Another band initiates in the central Atlantic Ocean and grazes the South African coast towards the Indian Ocean. Of immediate concern to southern Africa is the band of anticyclonic flow from the equatorial Atlantic through most of the region to the south Indian Ocean in the developing stage. The area of maximum anticyclonicity is SE of South Africa, replacing the cyclonic flow five days previous. The second anticyclonic band is in the Indian Ocean and affecting east Africa. The overall impression is an anticlockwise movement compared to the previous pentad such that the patterns in the tropical Indian Ocean have progressed westwards while those over the Atlantic Ocean and southern Africa have moved southeastwards.

At maturity, the general movement of vorticity maxima is southeastwards since the previous pentad. Anticyclonic flow dominates central southern Africa, from Angola/

northern Namibia to Mozambique and continuing to the south Indian Ocean while cyclonic motion prevails in a narrow band covering southern Namibia and most of South Africa. By the decaying phase (P+1), the wave pattern has disintegrated, leaving a more zonal configuration with anticyclonic flow mainly over the equatorial Atlantic Ocean and Africa as well as the southern hemispheric Indian Ocean down to about 30°S east of Madagascar. Over southern Africa, apart from a small tongue extending from the Atlantic Ocean through Namibia to eastern South Africa, the circulation is cyclonic. The configuration is almost a reversal of that during the peak of the wet spell five days before (P0), signifying a rapid transition from peak convection to dry.

7.5 Water vapour flux

Figure 7.21 shows water vapur fluxes during EFW from formation (P-2) to decay (P+1) integrated between the surface and 500 hPa. The south Indian Ocean plays a leading role during P-2, supplying most of the moisture to Africa, especially in the tropical regions. The monsoons are not yet fully established but are exerting some influence on and to the north of the Equator. While some confluence is apparent just off the east African coast, deformation also occurs in the region resulting in some moisture returning to the central Indian Ocean along the equator. Over southern Africa, the moisture is advected westwards from the Mozambique Channel which seems to be the primary source of moisture. The west coast trough is evident. Further west in the Atlantic Ocean, the bulk of the moisture is transported from the southeast towards the Equator. Only a small amount is carried overland into Africa.

Five days later (P-1), the anti clockwise system in the south Indian Ocean has moved 20° longitude eastwards to beyond 70°E. The shift has culminated in moisture advection as far as Madagascar with no further westward displacement to southern Africa. The anti clockwise circulation over South Africa is still there but considerably weaker, mostly due to the withdrawal of the IOA. In its place is the west coast trough over the central interior at P0, due to influence from the AOA. Moisture ahead of the trough has originated from the south Indian Ocean and the Mozambique Channel. This moisture is converging with that from the south Atlantic Ocean. The trough rapidly collapses during P+1, retreats westwards to its preferred location and is replaced by anti clockwise circulation centred over South Africa which transports moisture into northern Mozambique. The IOA

continues its eastward progression. Meanwhile, up north, the monsoon flow, which has been increasing steadily, has crossed the Equator and has an impact on east Africa.

Figure 7.22 shows the flux of water vapour associated with the four phases of LSFW. During the formative stage (P-2), there is cross-equatorial advection of moisture in the Indian Ocean, linked to the northeast monsoon. Part of this moisture is advected back to sea just south of the Equator (between 5 and 10°S). A significant amount, though, reaches the east Africa coast, most of which is deposited onto northern Mozambique while the remainder is transported into tropical Africa. The rest of southern Africa derives its moisture from the south Indian Ocean between 10 and 25°S. The moisture is reduced by the time the flow crosses the Mozambique Channel and moves over land in the vicinity of 20°S. Also in evidence are the Angola- Mozambique Channel and the west coast troughs. The fluxes in the Atlantic Ocean only influence the west coast of southern Africa.

At P-1, the patterns in the Indian Ocean have changed little, the NE monsoons still bringing moisture onto east Africa and Madagascar. In this period, there is more meridional moisture advection into southern Africa from the tropical band. There is less moisture from the SWIO as compared to five days before. An anti clockwise circulation (evident of a low level anticyclone there) contributes by increasing moisture convergence over the central interior, especially across Zimbabwe and Botswana. The clockwise circulation associated with the Angola low is causing the northerly flux over Zambia. The configuration during P0 was dealt with in detail in Chapter 6 (**Figure 6.10**) and so will not be repeated here. Of importance is the Angola- Mozambique Trough, separating northerly flux vectors equatorward of it from mainly easterly vectors to the south. During dissipation (P+1), the moisture transfer from equatorial regions to southern Africa is absent. The sub- region experiences a moisture regime similar to that during P-2, with the SWIO playing a primary role and the anticyclone over eastern South Africa contributing to the easterly vectors between 15 and 25°S. The source of moisture in the LSFW appears to be from both the Mozambique Channel and the Congo, whereas in EFW, the northern Mozambique Channel is more important. Again, the blocking effect of Madagascar is highlighted.

7.6 Vertically integrated internal energy

Figure 7.23a indicates internal energy anomalies throughout the life cycle of EFW integrated vertically between 850 and 300 hPa. At the formative stage of EFW (P-2), positive values prevail over the African continent, extending from the northern hemisphere to the SWIO. The highest values across Africa are in the central interior of southern Africa (18°S, 25°E). This is due to differential heating and a sub- tropical wave- train. The core of positive values at higher latitudes in the vicinity of 55°E are mostly due to radiative cooling. The oceans are relatively "cool", particularly outside the tropics and over the Atlantic Ocean. The Indian Ocean exhibits a tongue of negative values from the extreme southeast into the east coast of tropical Africa through Madagascar. During development (P-1), positive anomalies dominate the flow. Simultaneously, the patterns show southeastward movement. The resulting pattern indicates a new maximum of positive energy in the south Mozambique Channel.

At maturity (P0), only eastern South Africa and a small area over Zimbabwe show negative values, possibly a result of reduced temperature associated with prolonged cloudiness. The centre of positive values is displaced northeastwards to the northern Madagascar region. At dissipation (P+1), the eastward progression of systems is arrested. The trough (zone of least values) lies over Africa, a pattern which is a complete reversal of that at P-2. At the same time, the positive anomalies in the oceanic extra- tropical areas ridge towards Africa, deepening the 'trough' across southern Africa, especially over central regions (Mozambique, Zimbabwe and Zambia). Hence, positive internal energy is "consumed" and converted to negative departures during the life cycle of EFW.

Late summer (**Figure 7.23b**) exhibits similar patterns to early summer. However, differences are apparent. The tropical- extra- tropical interaction is less vigorous, possibly due to the more barotropic nature of the atmosphere. When the life cycle of LSFW commences (P-2), positive anomalies predominate the tropical regions of the Indian Ocean. The centre of highest values over southern Africa are located more to the northwest (Angola) than at the centre in early summer at the same stage. Strong negative anomalies are poleward of the TSB. At development (LSFW, P-1), a standing short- wave feature is exhibited poleward of 10°S with axes oriented NW- SE. As during early summer, the centre of maximum internal energy is to the south of the Mozambique Channel. The wave is short- lived and collapses by P0, leaving positive values everywhere but the oceanic region to the SE of South Africa similar to EFW. The axis of highest

values stretches from Madagascar to the northern hemispheric areas of Africa. As LSFW decays (P+1), the patterns become more zonal with negative anomalies restricted to poleward of the TSB, particularly over the southern Atlantic and Indian Oceans. This dissipation pattern is unlike EFW.

7.7 Discussion and summary

Chapter 7 has analysed two wet spells (EFW and LSFW) representing early and late phases of summer over southern Africa. The analysis has studied these spells from evolution through maturity to dissipation using departures from the long- term period mean. In general, preferred regions of development and decay have been identified, directions and extent of propagation of systems detected and, more importantly, differences and common denominators between early and late summer highlighted. It must be emphasised, again, that the anomalies are based upon mean data from a 6- year base, a period which may be rather short for firm conclusions to be made. However, the period is long enough for inferences and plausible scenarios to be constructed, the following of which are some.

The low- level horizontal temperature transports show more contrasts than similarities between early and late summer wet spells. While anomalies over southern Africa display similarities at P-2, with poleward transports prevailing, the Indian Ocean has greater impact on eastern regions of the sub- continent. A standing short wave is more pronounced for LSFW, even at P-1. Significant similarities are found at P0 when there is a NW- SE oriented band of warm northerly (poleward) air advection stretching from equatorial Africa through Mozambique to the SWIO during LSFW. EFW anomalies, on the other hand, merely spread into southern Africa from the south. Another major difference is the eastward propagation illustrated during the life cycle of LSFW when the axis of northerly poleward transports from the western flanks of southern Africa at initiation to the Mozambique Channel at maturity (**Figure 7.11a**). During the same period, positive meridional anomalies translocate from the SE Atlantic at P-2 to the Mozambique and Madagascar at P+1.

Corresponding eastward thermal transport patterns show zonal orientation for EFW and meridional motion for LSFW during the formative and developmental stages. There is also more evidence of downstream blocking in the Indian Ocean during EFW, hence quasi-

stationarity over southern Africa and the SWIO during and after maturity. The equatorial zone of eastward transports in the Indian Ocean at EFW is small and is weakest at P0. In contrast, the zone, located off equatorial east Africa when LSFW evolves, spreads and eventually dominates the Indian Ocean by the time LSFW dissipates. The evolution of westerlies in the equatorial Indian Ocean was also shown by Wang and Rui (1990), among others (Chapter 2). From this analysis, augmenting the results of Chapters 5 and 6, it appears that the tropical intra- seasonal convection anomalies (TICA) of Wang and Rui are more pronounced from January onwards.

Water vapour flux fields also show different patterns, particularly over Africa and the Indian Ocean. Most of these have already been discussed in the previous section. In early summer, the flow is predominantly zonal and from the east across tropical Africa. Madagascar acts a major barrier of moisture flux from the south Indian Ocean that is otherwise intended for southern Africa. The bulk of the moisture is directed to equatorial east Africa (Tanzania) in the formative and developmental phases of EFW. When the Indian Ocean Anticyclone displaces the westward fluxes northwards, part of the moisture is re-directed towards eastern southern Africa to influence northern Mozambique, Zambia and Malawi at the peak of the wet spell. During LSFW, a northerly flux occurs over tropical Africa. The flux propagates westwards in the early stages. By the time the spell peaks, the moisture is from the Congo/ Zaire region. At the same time and unlike for EFW, the other moisture flux into southern Africa is from the Indian Ocean to the south of Madagascar. Easterly vectors in the vicinity of the TSB are more organised and stronger than at EFW. Thus, there is a well marked moisture convergence across central southern Africa along the MCAT, a feature either weak or ill- defined at the onset of summer. The monsoon effect is well defined along east Africa and affecting NW Madagascar. As already been mentioned, there is little evidence of its direct influence on most of southern Africa.

From the low - level vorticity anomaly patterns, systems in the equatorial Indian Ocean seem to move southwestwards at about 5- 10° latitude per pentad. They do so slowly throughout the life cycle of EFW. This is clearly indicated by the region of cyclonic motion which straddles the Equator at P-2 to be between 10 and 20°S at P+1. Lower tropospheric zonal temperature transports (covariances $T'u'$) also illustrate a similar trend and are found immediately on the equatorward side of the cyclonic region. The propagation is not so pronounced for LSFW. The region of cyclonic motion in the tropical Indian Ocean is wider, though, than at EFW, due to the convective activity associated

with the ITCZ. So are the low- level eastward temperature eddy transports associated with the monsoon.

The anomalies have demonstrated the existence of short waves particularly over the Atlantic Ocean and Africa oriented NW- SE. The feature is rather deep as it manifests itself at both upper and middle levels at P-2 and propagates down to the lower troposphere, as shown by 700 hPa vorticity anomaly patterns, where it is apparent at P-1. The upper level meridional wind anomalies indicate the sub- tropical westerly wave reaches peak amplitude five days prior to maturity. The wave then progresses east-southeastwards to the Indian Ocean, stagnates and deepens during the dissipation stage. This can be due to apparent blocking in the vicinity of 70°E, where another dominant system is situated in early summer. The geopotential height, zonal and meridional wind fields exhibit this movement. The eastward displacement is more rapid during LSFW in the middle levels.

While the systems move eastwards, upper- level meridional wind anomaly analyses show a simultaneous equatorward shift in the tropical Indian Ocean as well. This suggests an anti-clockwise circulation at upper levels centred over Africa around which systems over the Atlantic Ocean propagate southeastwards through southern Africa during the initiation and development stages. The systems are later blocked in the eastern Indian Ocean and when EFW decays, they are forced to recurve equatorwards in a northwest direction. The equatorward displacement during late summer is attributed to the middle and upper tropical easterlies shown in the total wind field, whose major contribution is in the zonal wind component.

It is apparent from the above (and more from earlier sections) that while there are some similarities between early and late summer, detailed study involving life cycles of only two of the wet spells exhibits significant departures, particularly trajectories of the airmasses and controlling mechanisms. The major differences between the two should be associated with the physics and dynamics of the atmosphere over tropical southern Africa, where there is an organised low- and middle- level meridional exchange of energy, moisture and momentum between the Equator and the TSB in the build- up to the late summer wet spells. As evidenced by the vertical velocity fields of Chapter 6, the subsequent deep convection over the continent is illustrated from kinematic patterns by well- marked upper- level outflow. Such a process and interaction are limited during EFW as shown at

the upper levels where a NW jet stream from equatorial regions affects western southern Africa.

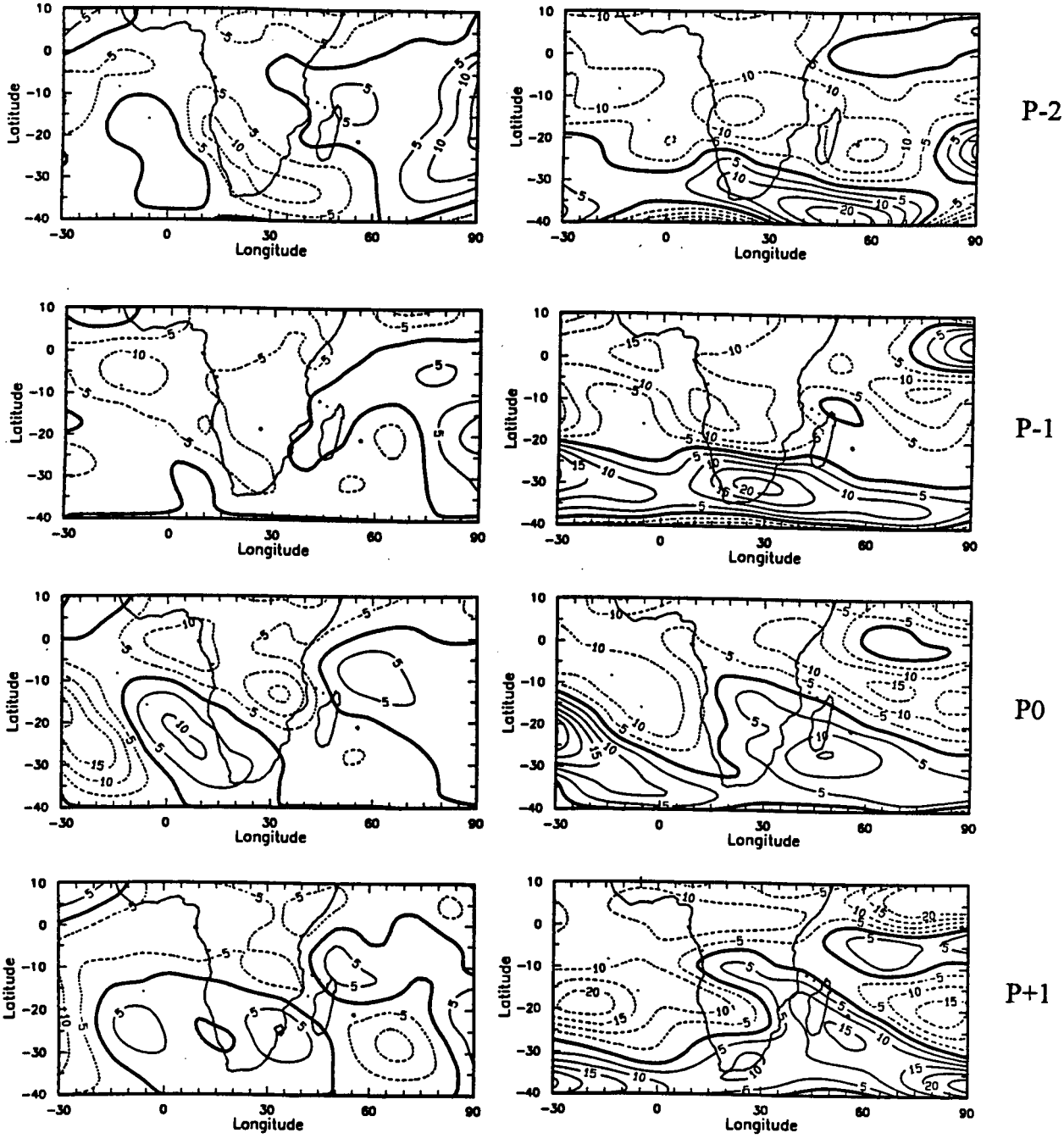

Figure 7.1 : 700 hPa meridional ($T'v'$) (a) and zonal ($T'u'$) (b) eddy temperature covariance anomalies for the life cycle of EFW.
Isolines are at every 5 °C m s^{-1}.

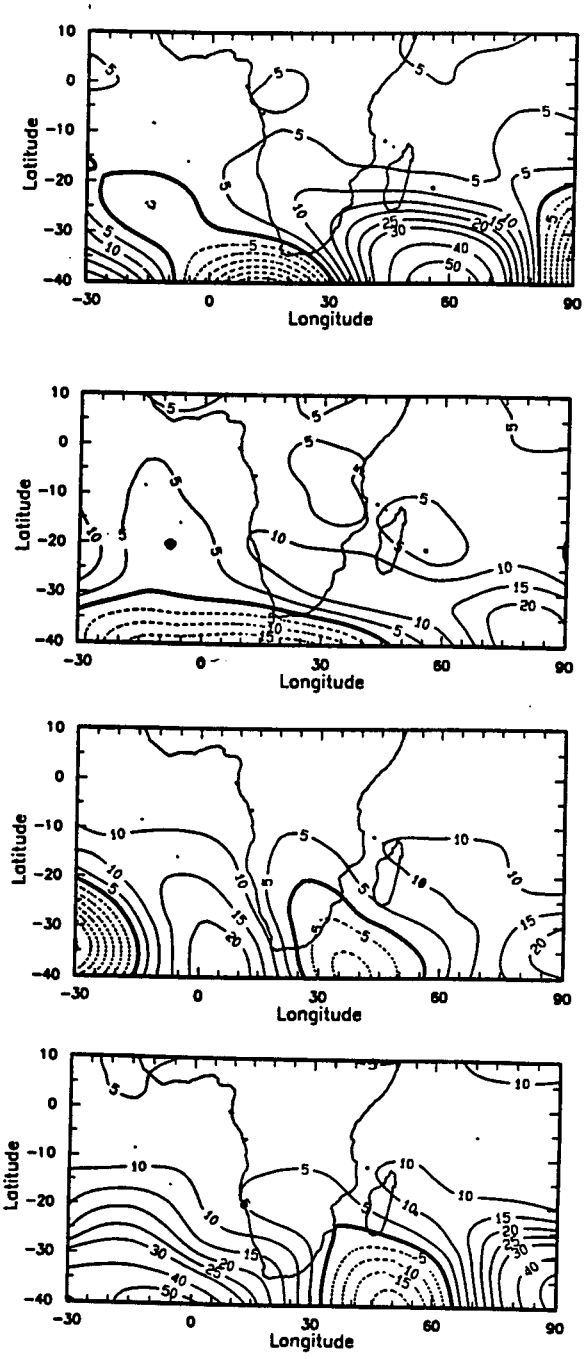

Figure 7.2 : 700 hPa geopotential height anomalies for EFW.
Contour interval is 5 gpm.

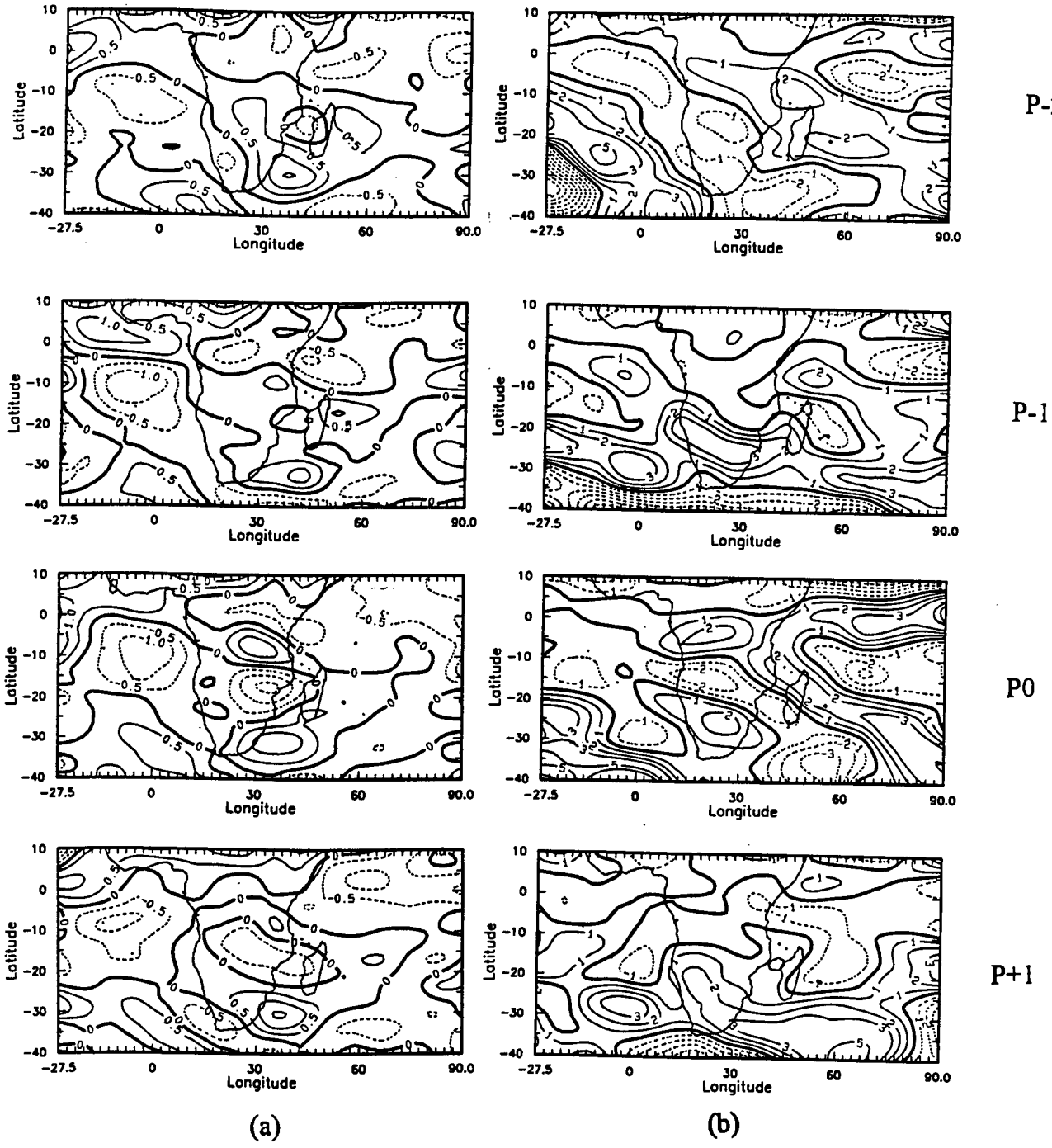

Figure 7.3 : Divergence (a) and vorticity field anomalies for EFW at 700 hPa. Contour intervals are 0.5 and 1 x 10^{-6} s^{-1}, respectively.

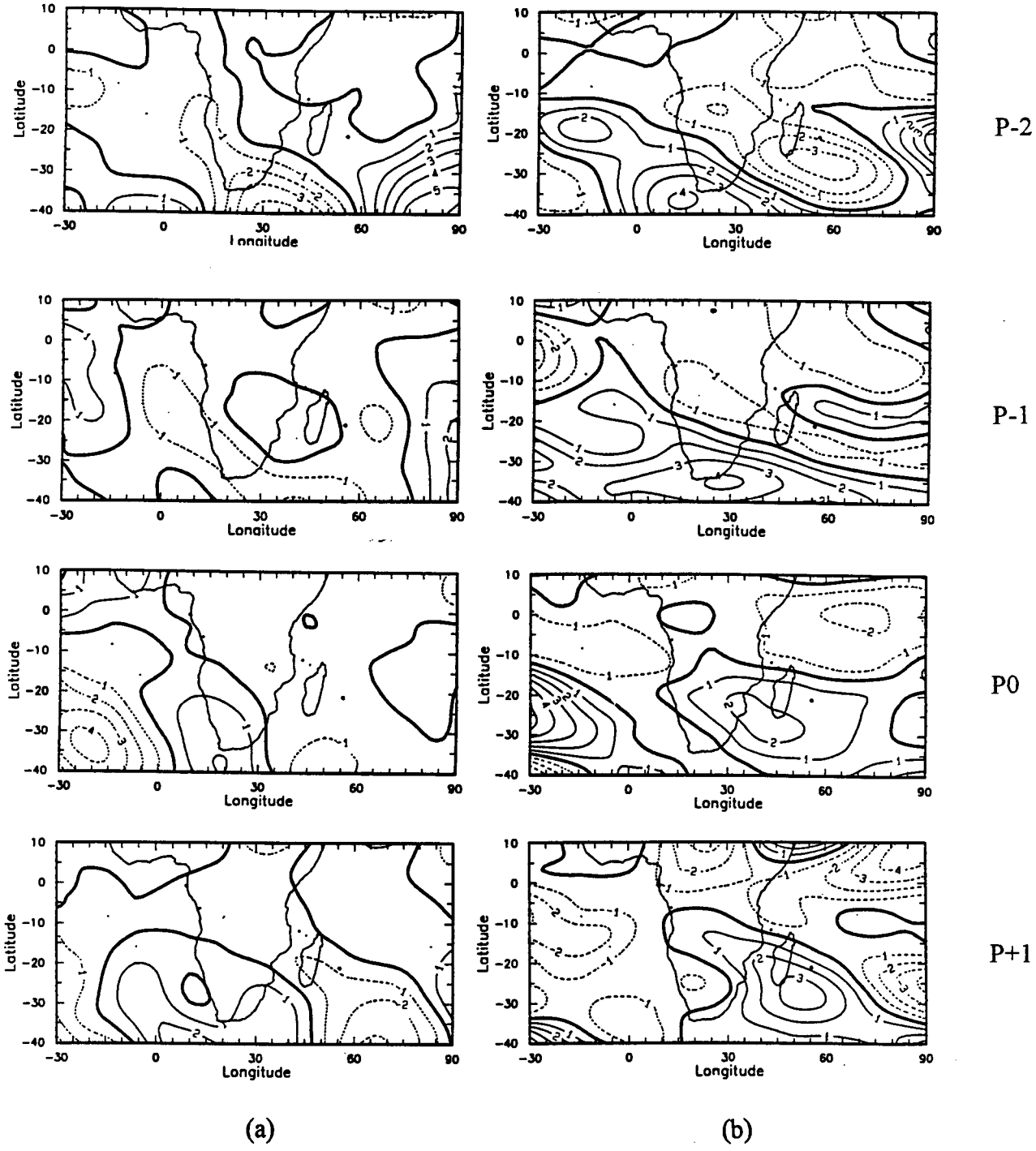

Figure 7.4 : 500 hPa meridional (a) and zonal (b) wind anomalies for EFW. Isolines are at every 1 m s^{-1}, respectively.

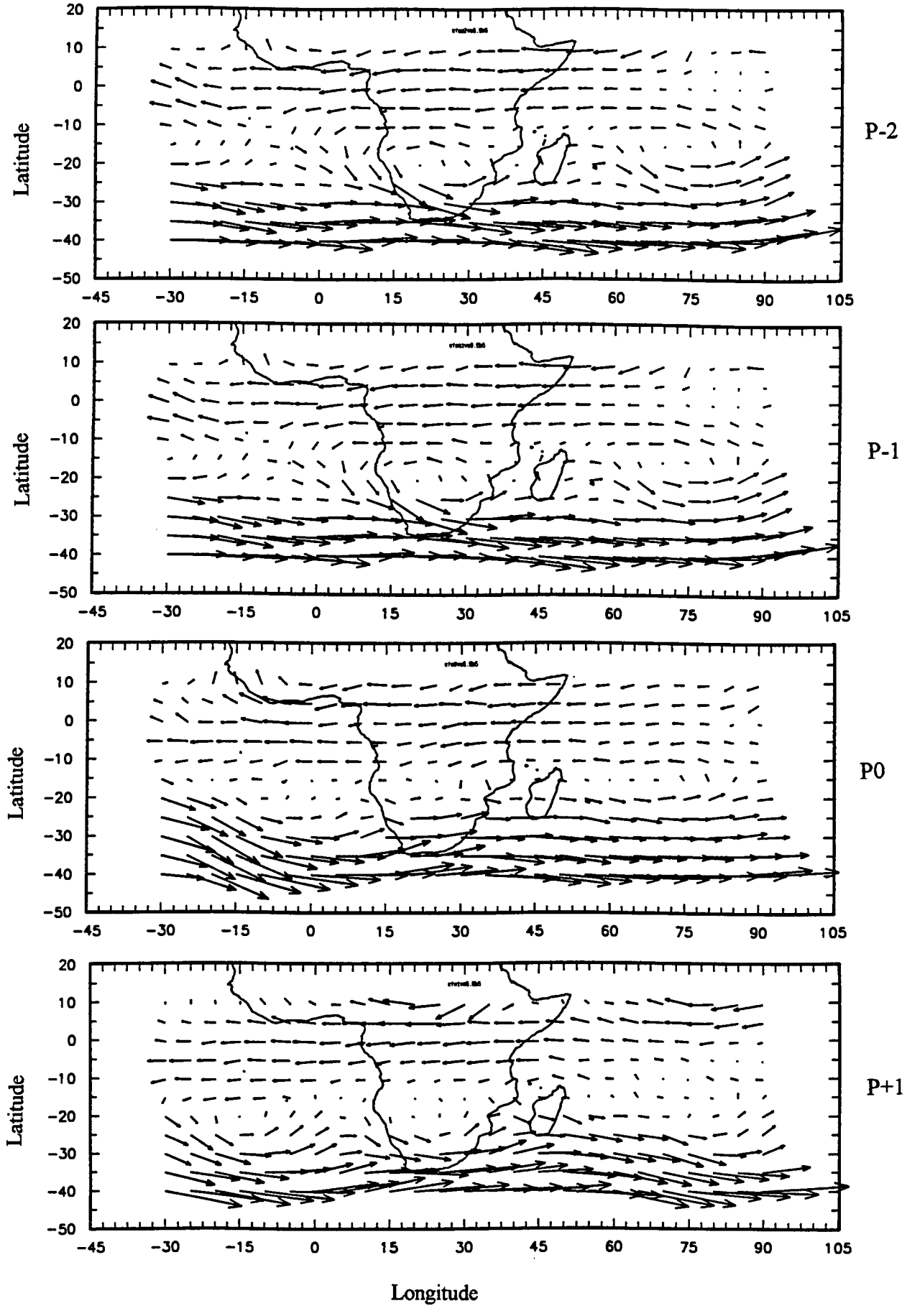

Figure 7.5 : 500 hPa total wind field for EFW. The longest vector is equivalent to 22.7 m s^{-1}. Vectors are at 5° intervals.

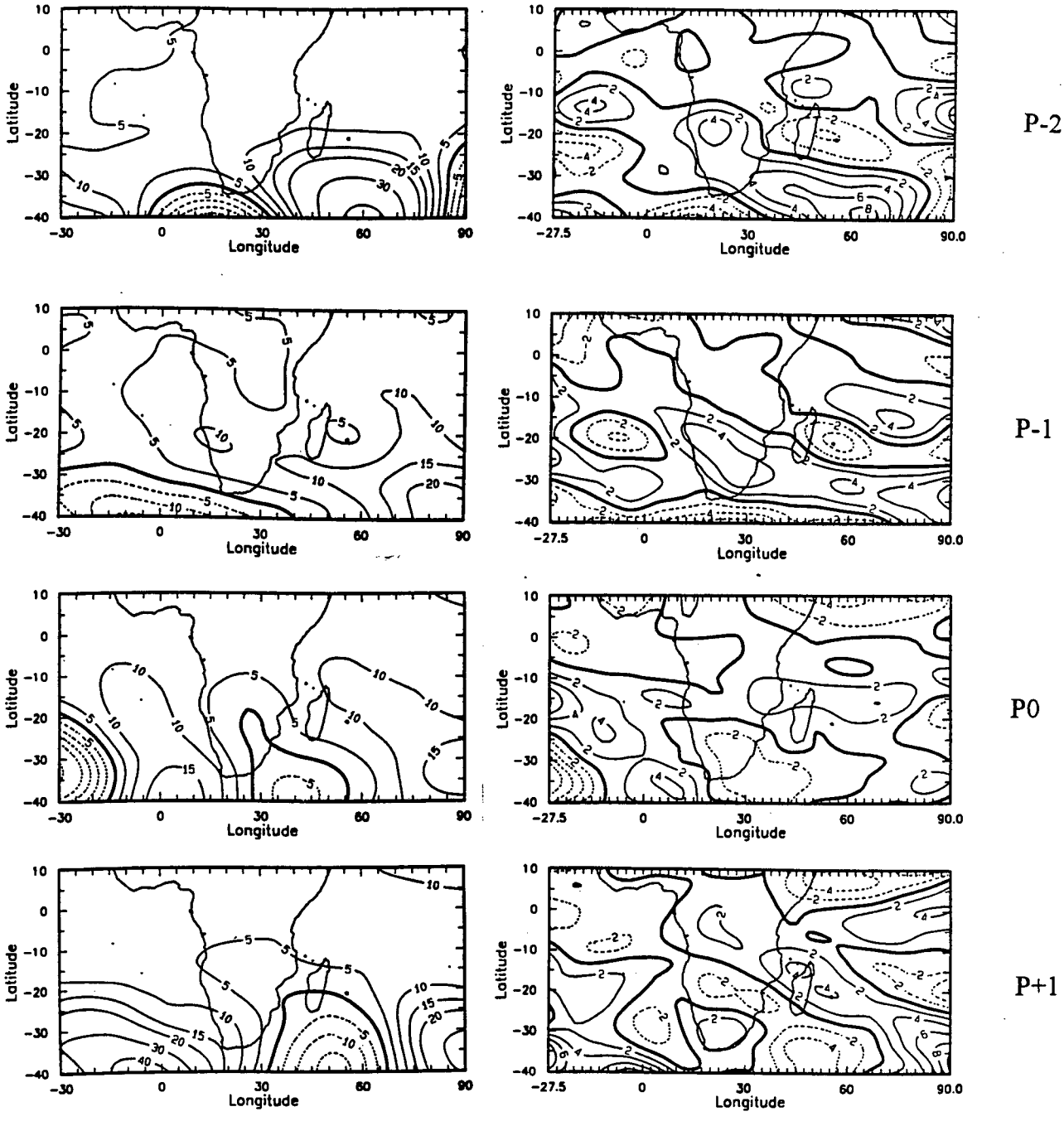

Figure 7.6 : 500 hPa geopotential height (a) and vorticity (b) anomalies for EFW. Contour intervals are 5 gpm and 2 x 10^{-6} s^{-1}, respectively.

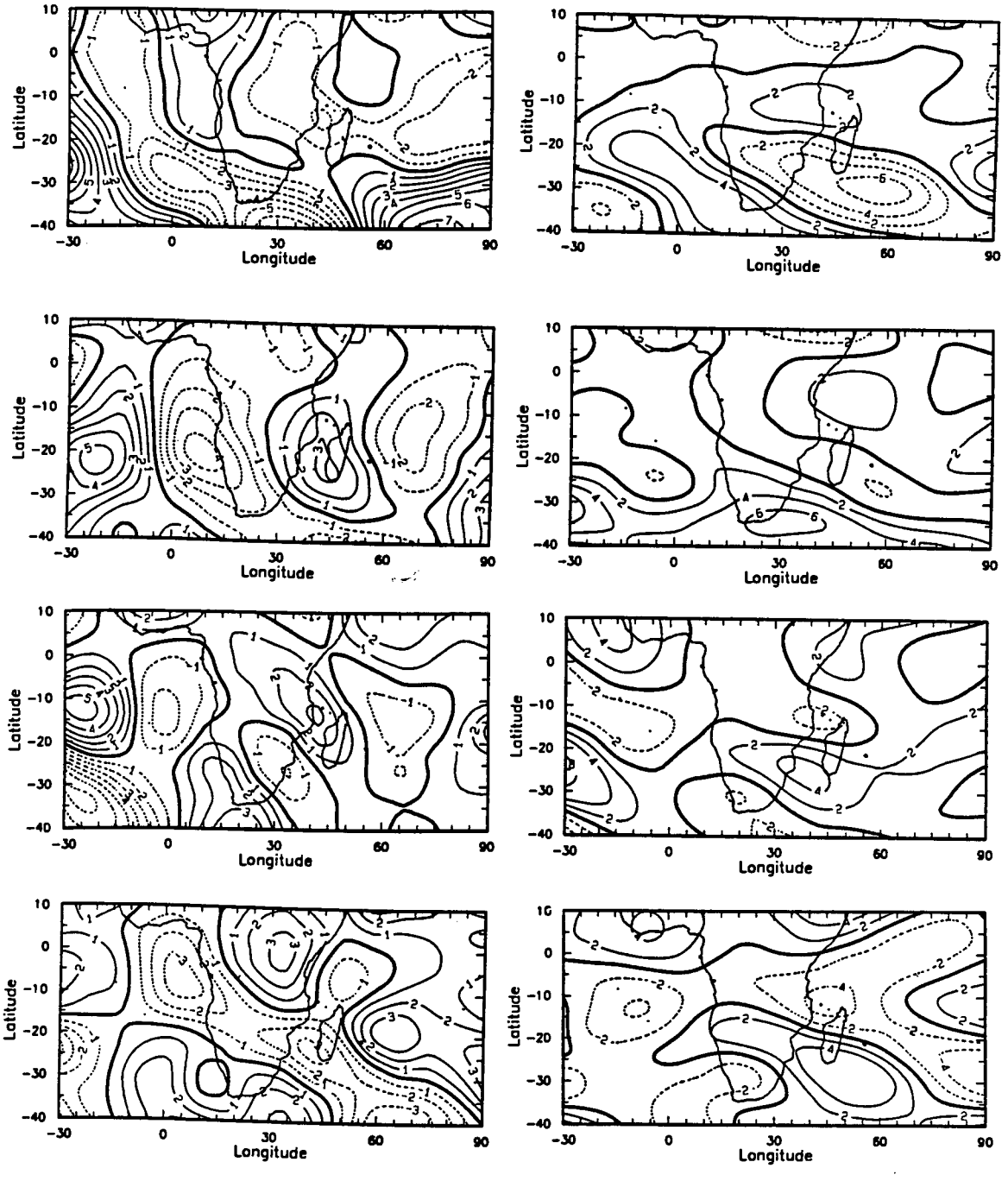

Figure 7.7 : 200 hPa meridional (a) and zonal (b) wind anomalies for EFW. Isolines are at every 1 and 2 m s^{-1}, respectively.

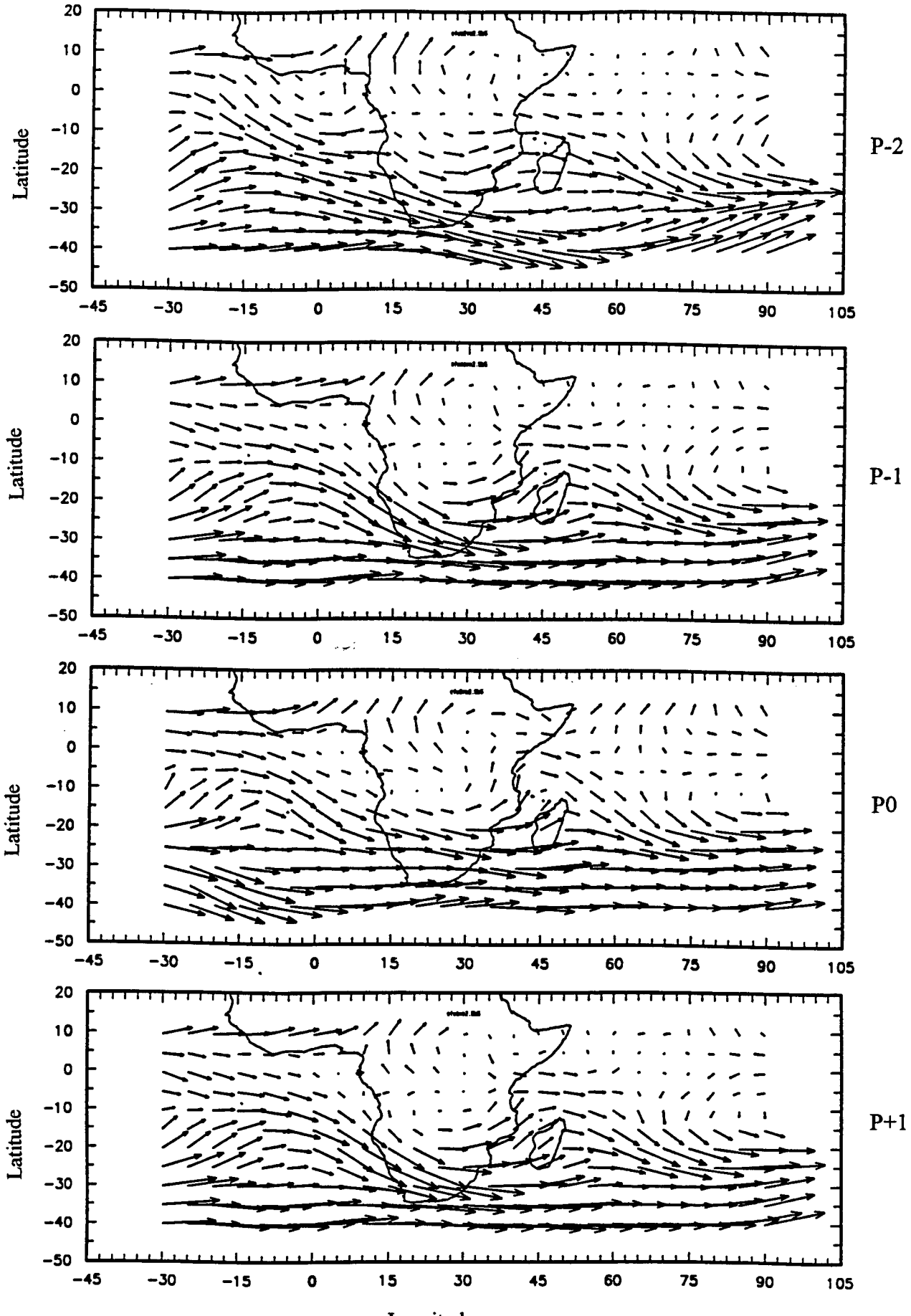

Figure 7.8 : 200 hPa total wind field for EFW. The longest vector is equivalent to 32.5 m s^{-1}.

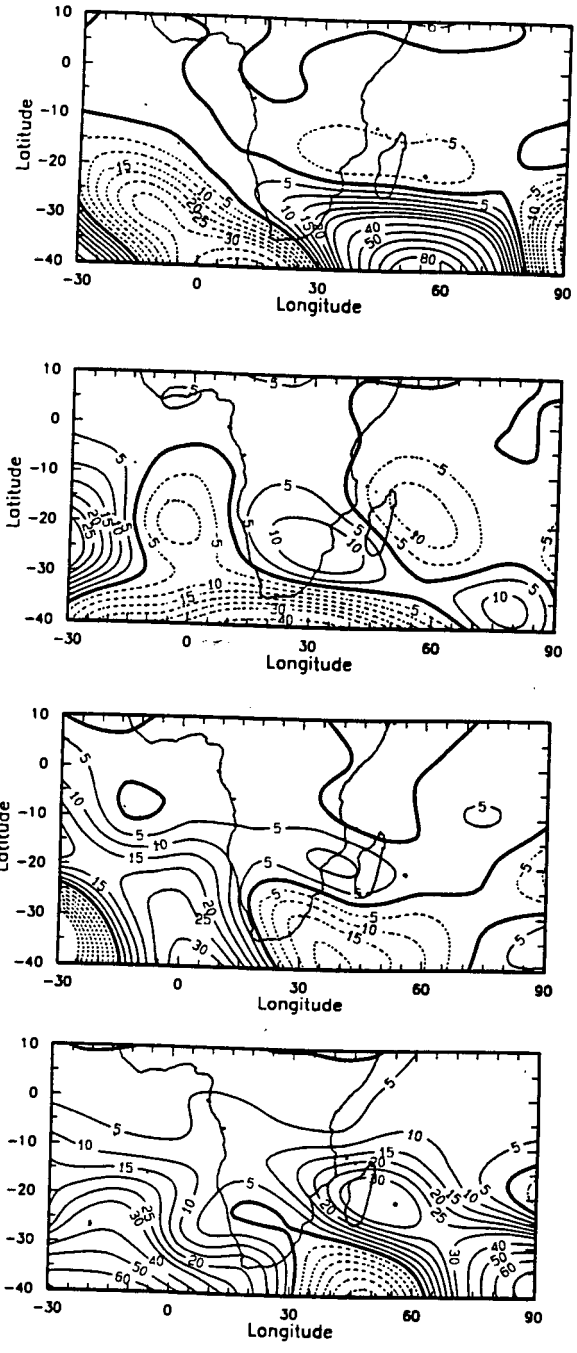

Figure 7.9 : 200 hPa geopotential height anomalies for EFW.
Contour intervals is 5 gpm.

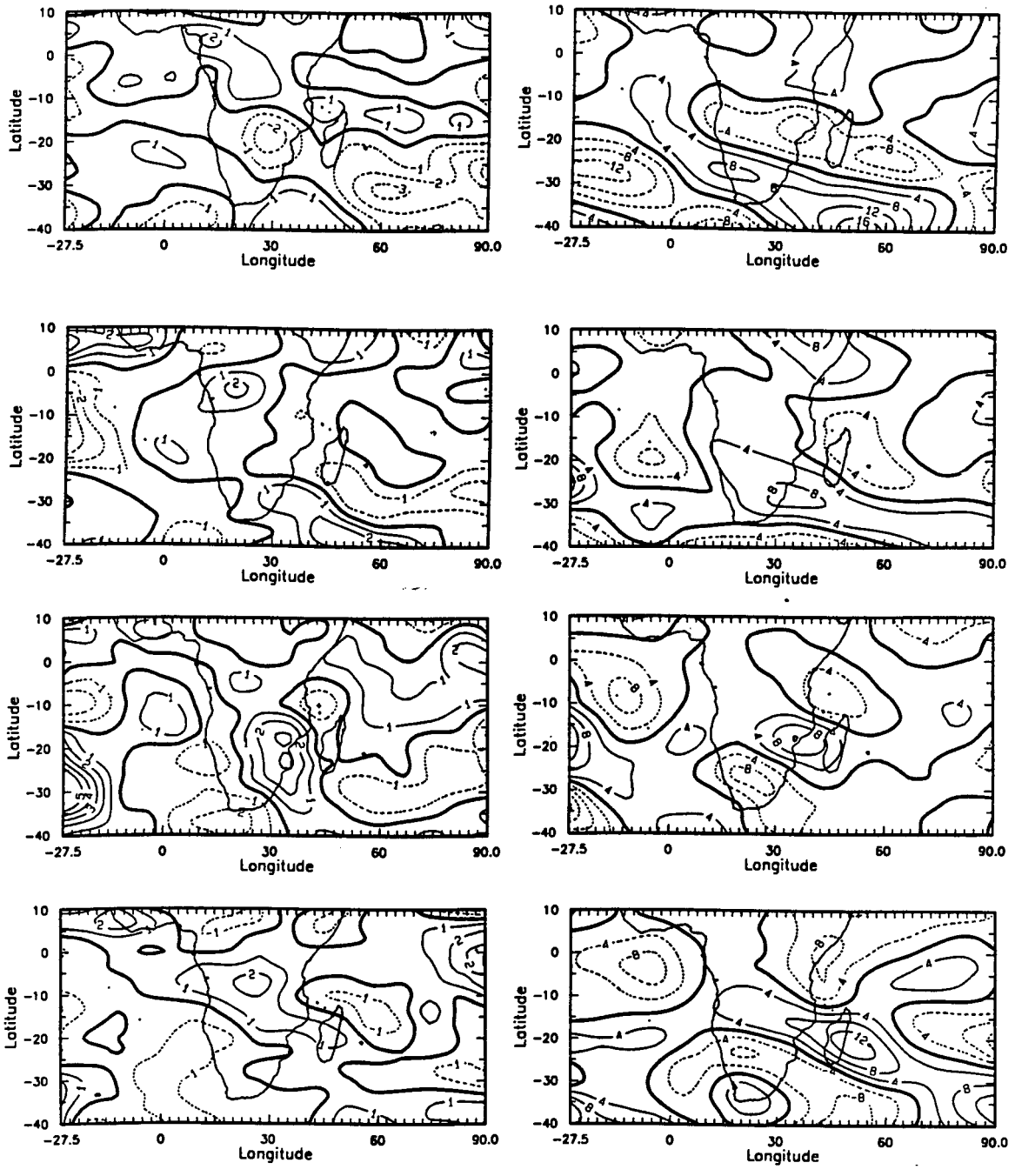

(a) (b)

Figure 7.10 : Divergence (a) and vorticity field anomalies for EFW at 200 hPa. Contour intervals are 1 and 4 x 10^{-6} s^{-1}, respectively.

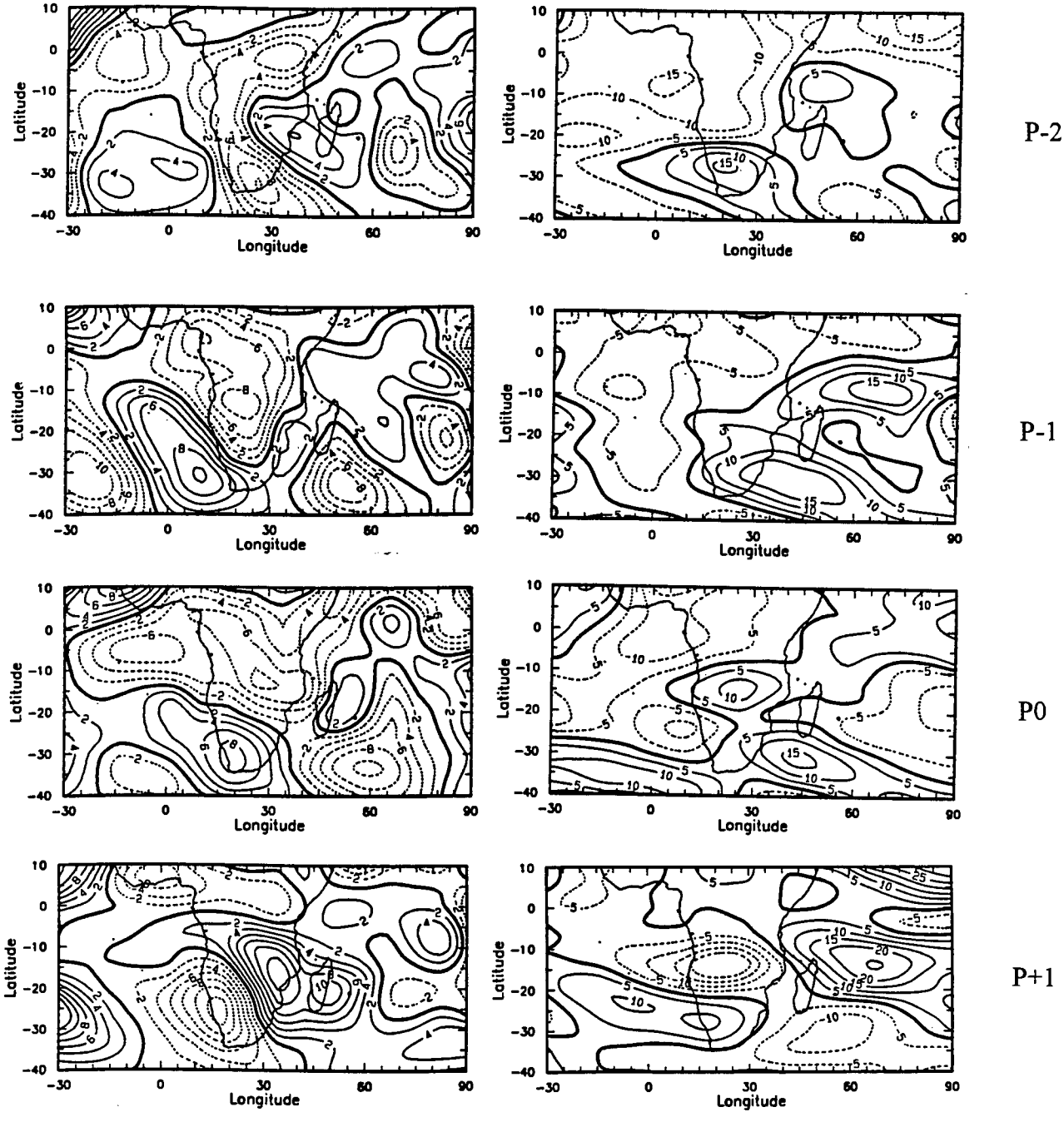

Figure 7.11 : 700 hPa meridional (a) and zonal (b) eddy temperature covariance anomalies for the life cycle of LSFW.
Contour intervals are 2 and 5 °C m s^{-1}, respectively.

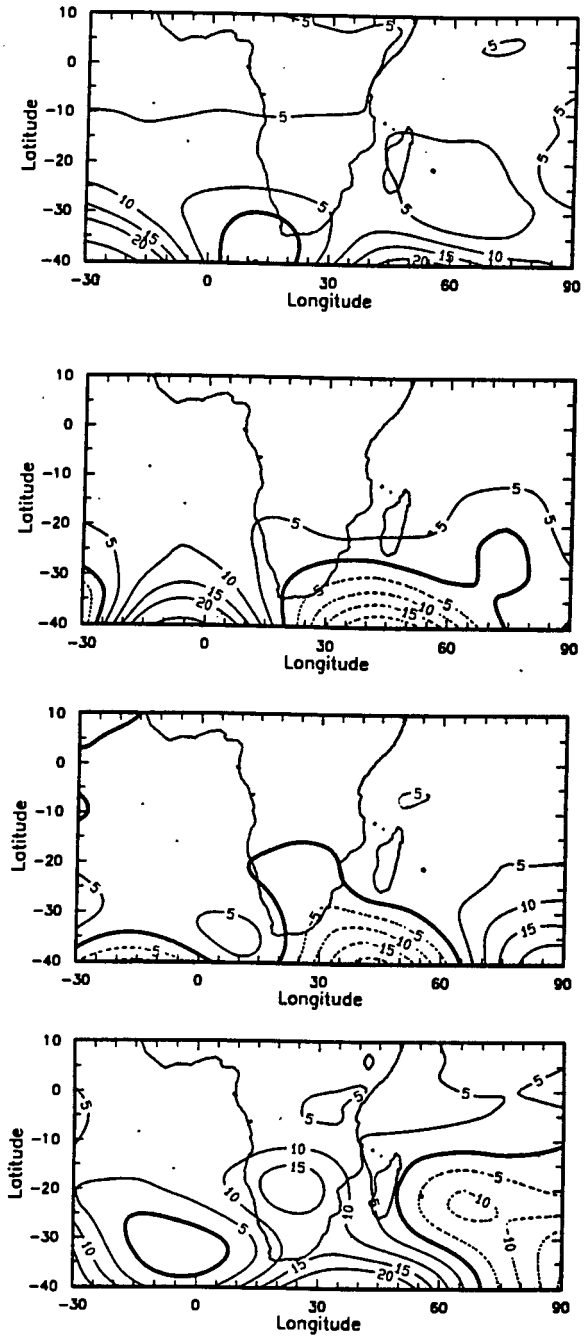

Figure 7.12 : 700 hPa geopotential height anomalies for LSFW.
Contour interval is 5 gpm.

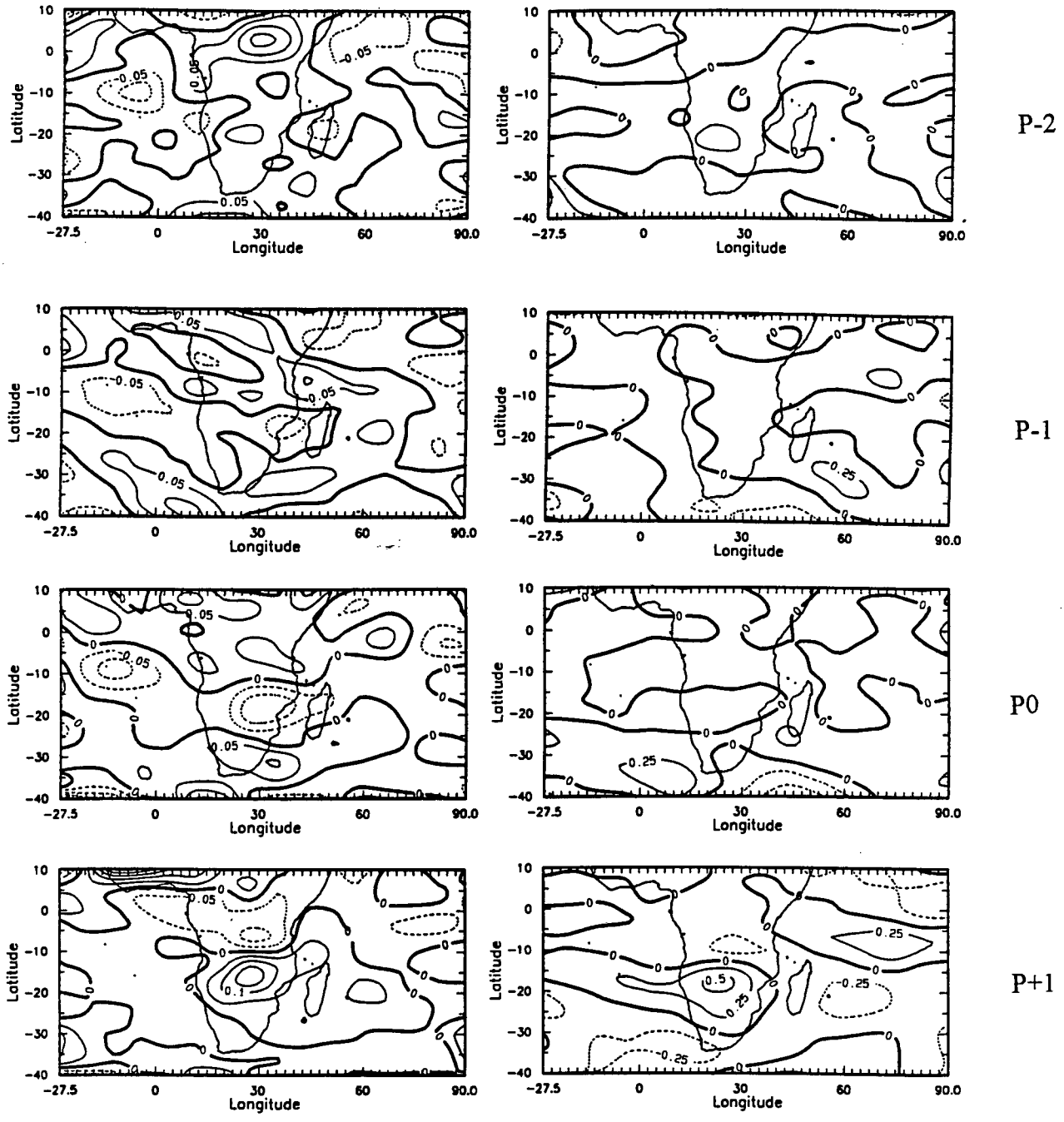

Figure 7.13 : Divergence (a) and vorticity field anomalies for LSFW at 700 hPa. Contour intervals are 0.05 and 0.25 x 10^{-5} s^{-1}.

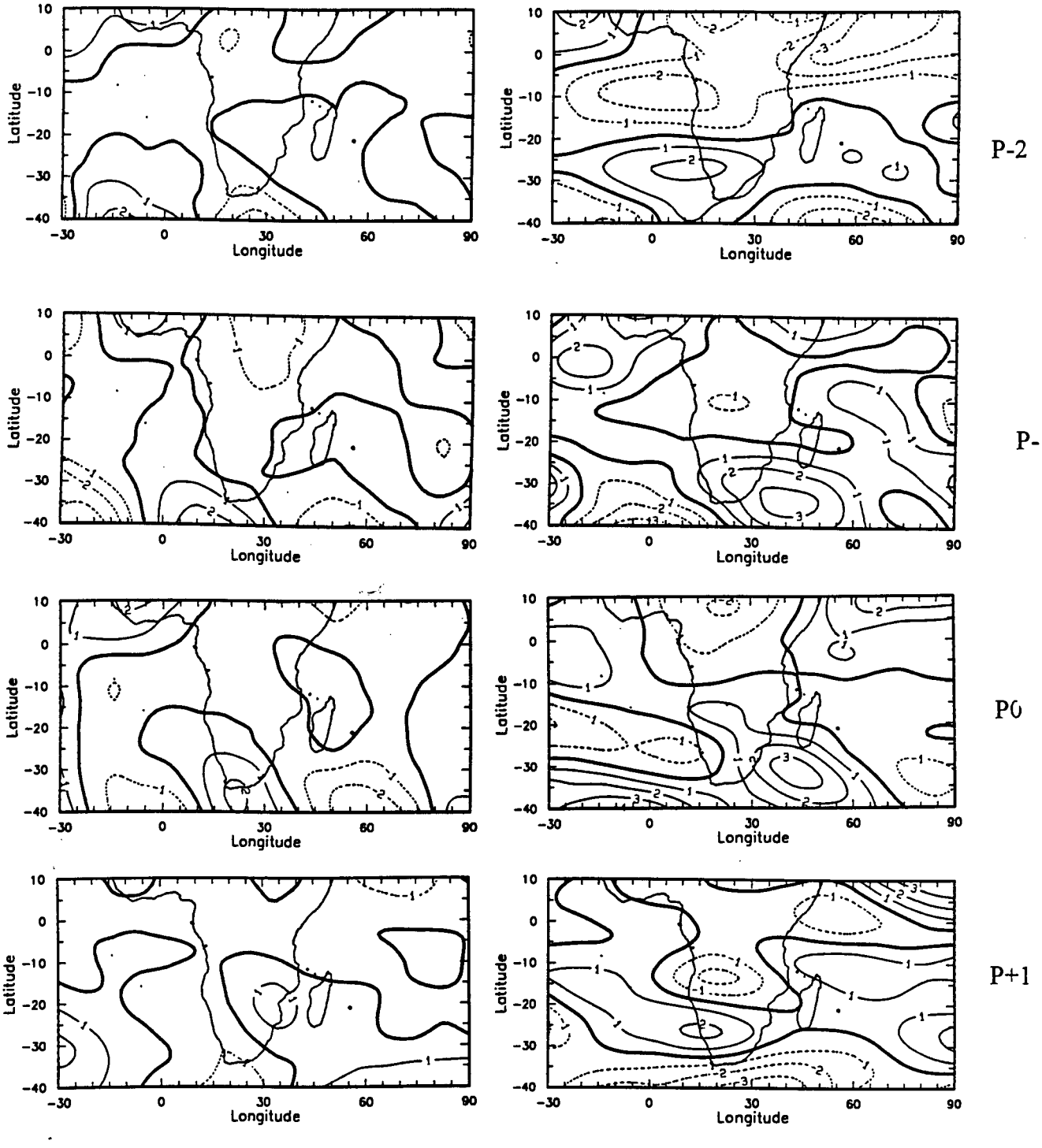

Figure 7.14 : 500 hPa meridional (a) and zonal (b) wind anomalies for LSFW.

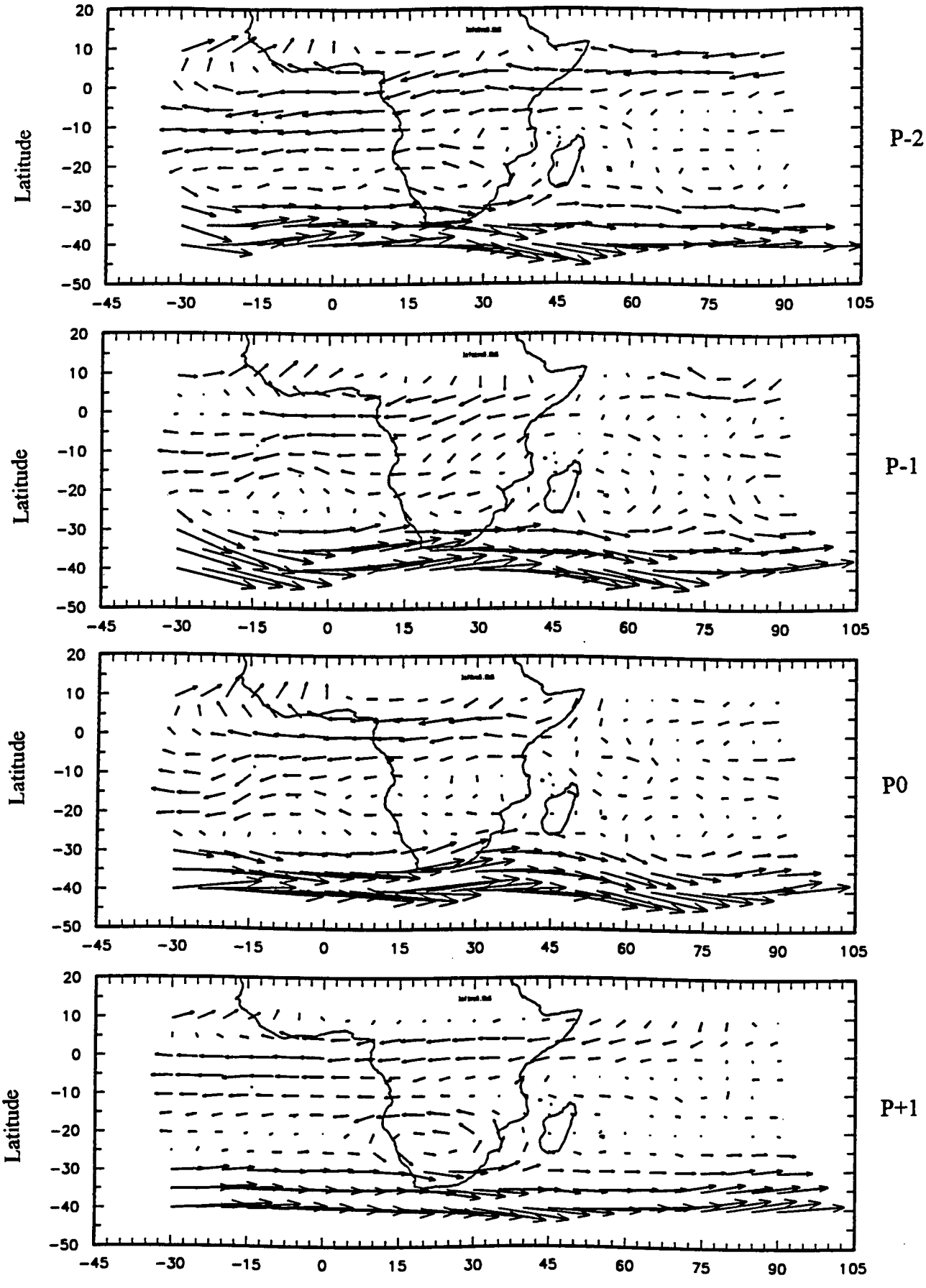

Figure 7.15 : 500 hPa total wind field for LSFW. The longest vector is equivalent to 26.7 m s^{-1}.

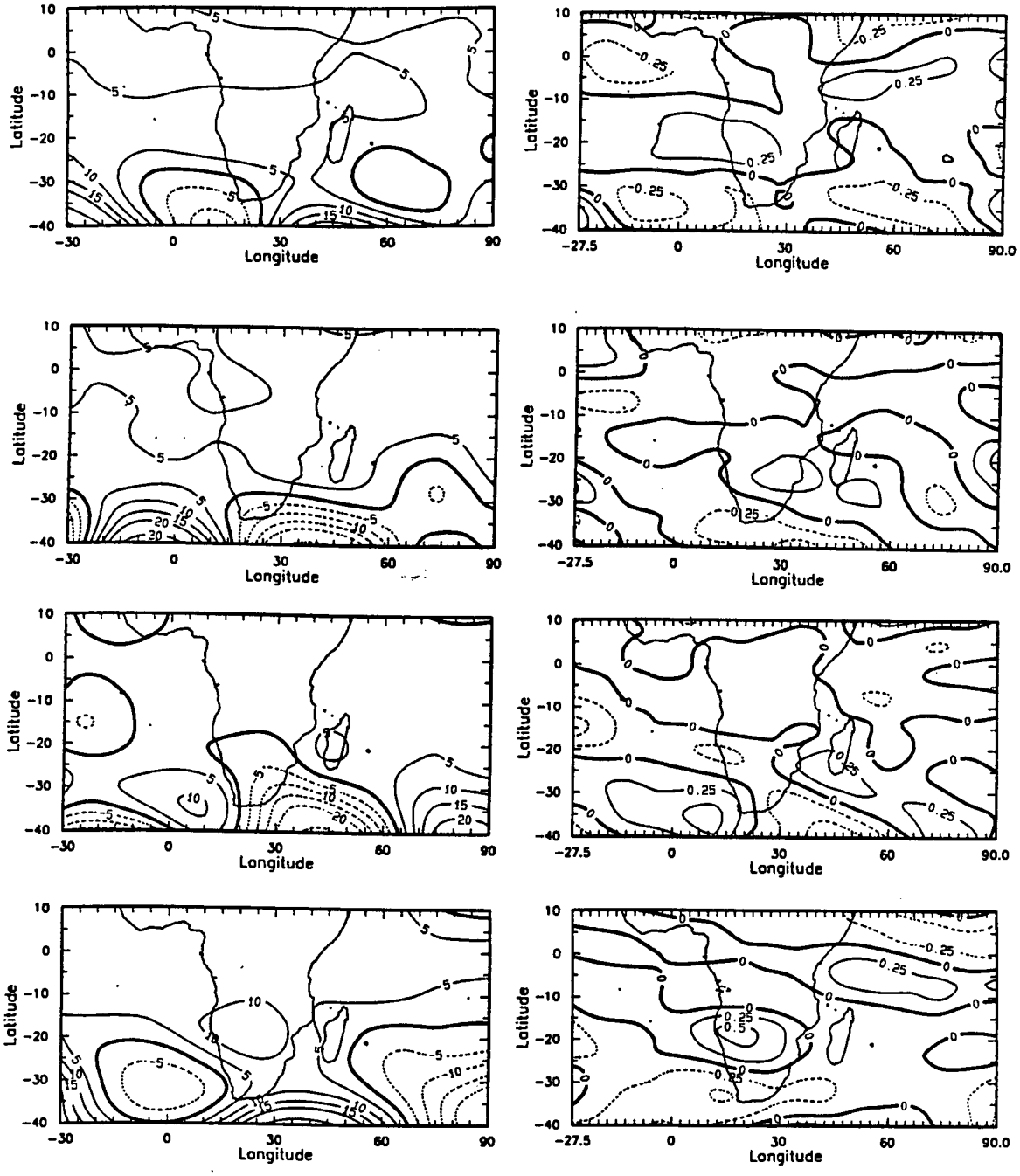

Figure 7.16 : 500 hPa geopotential height (a) and vorticity (b) anomalies for LSFW. Contour intervals are 5 gpm and 0.25 x 10^{-5} s^{-1}, respectively.

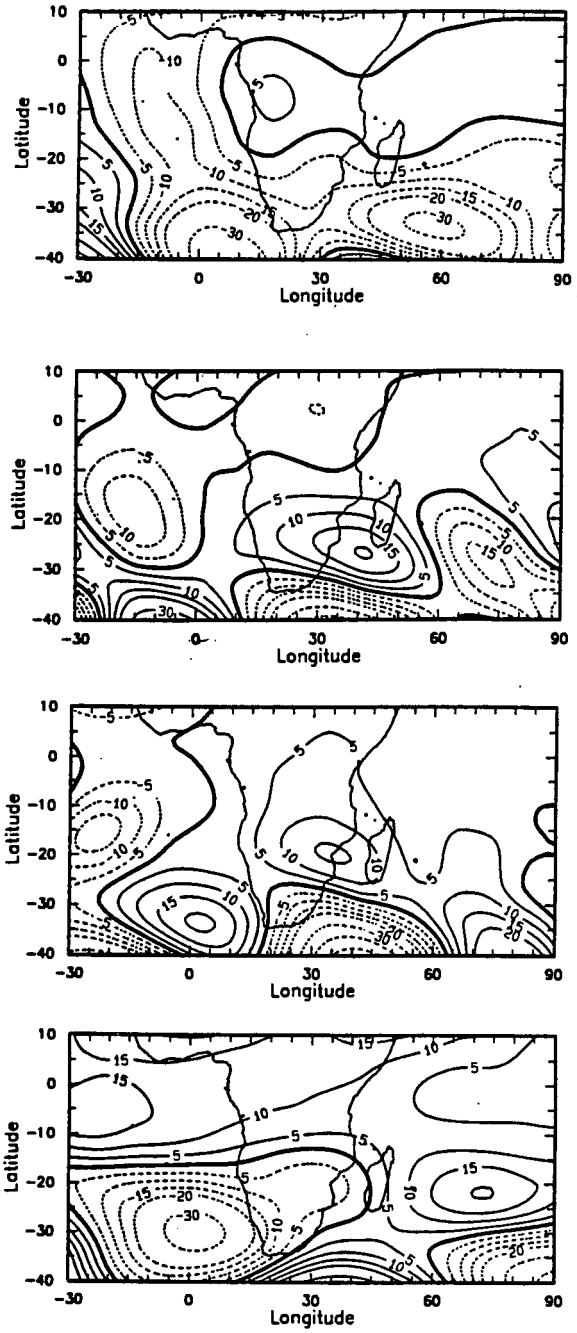

Figure 7.17 : 200 hPa geopotential height anomalies for LSFW.
Contour interval is 5 gpm

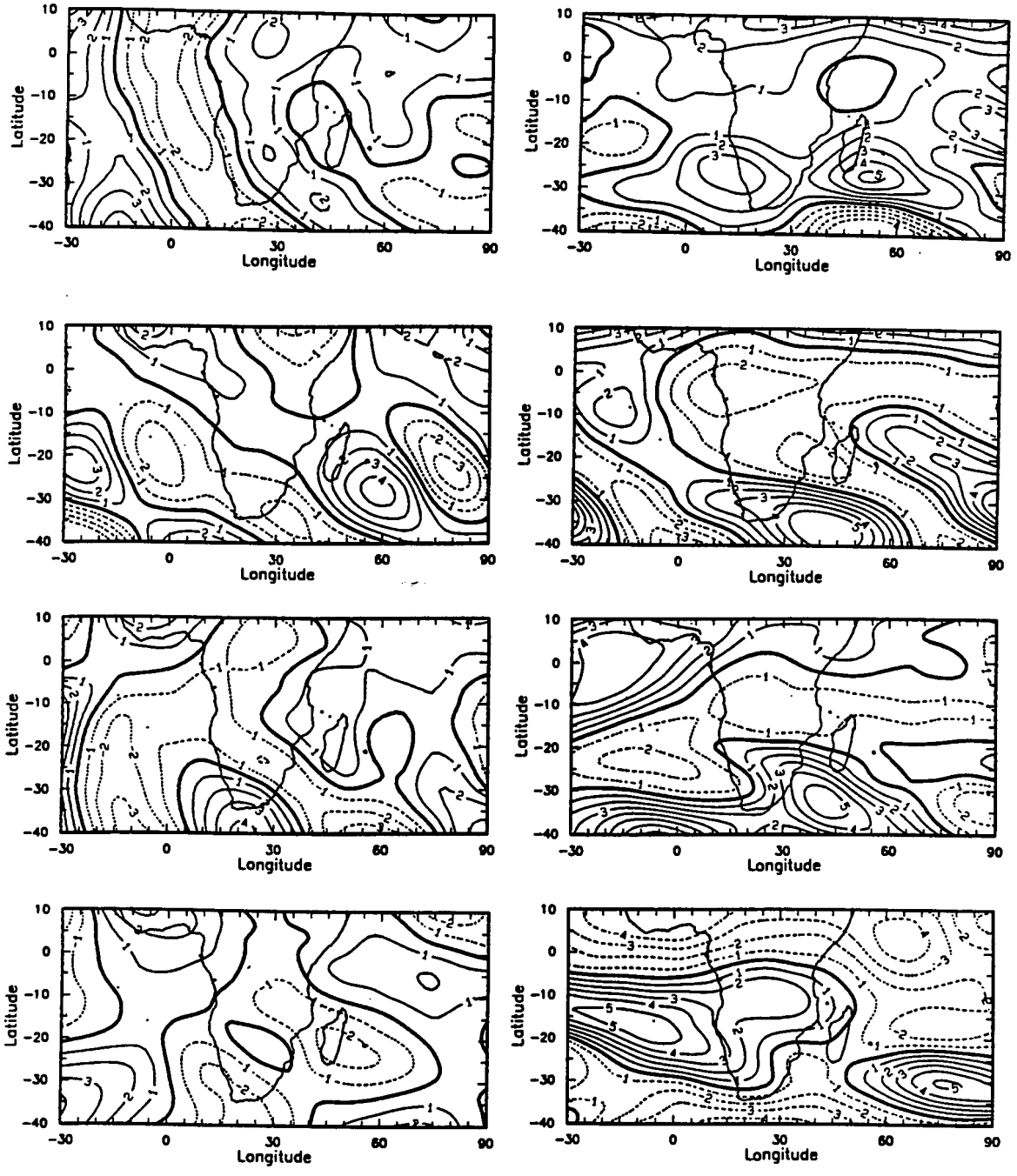

(a) (b)

Figure 7.18 : 200 hPa meridional (a) and zonal (b) wind anomalies for LSFW. Isolines are at every 1 m s^{-1}, respectively.

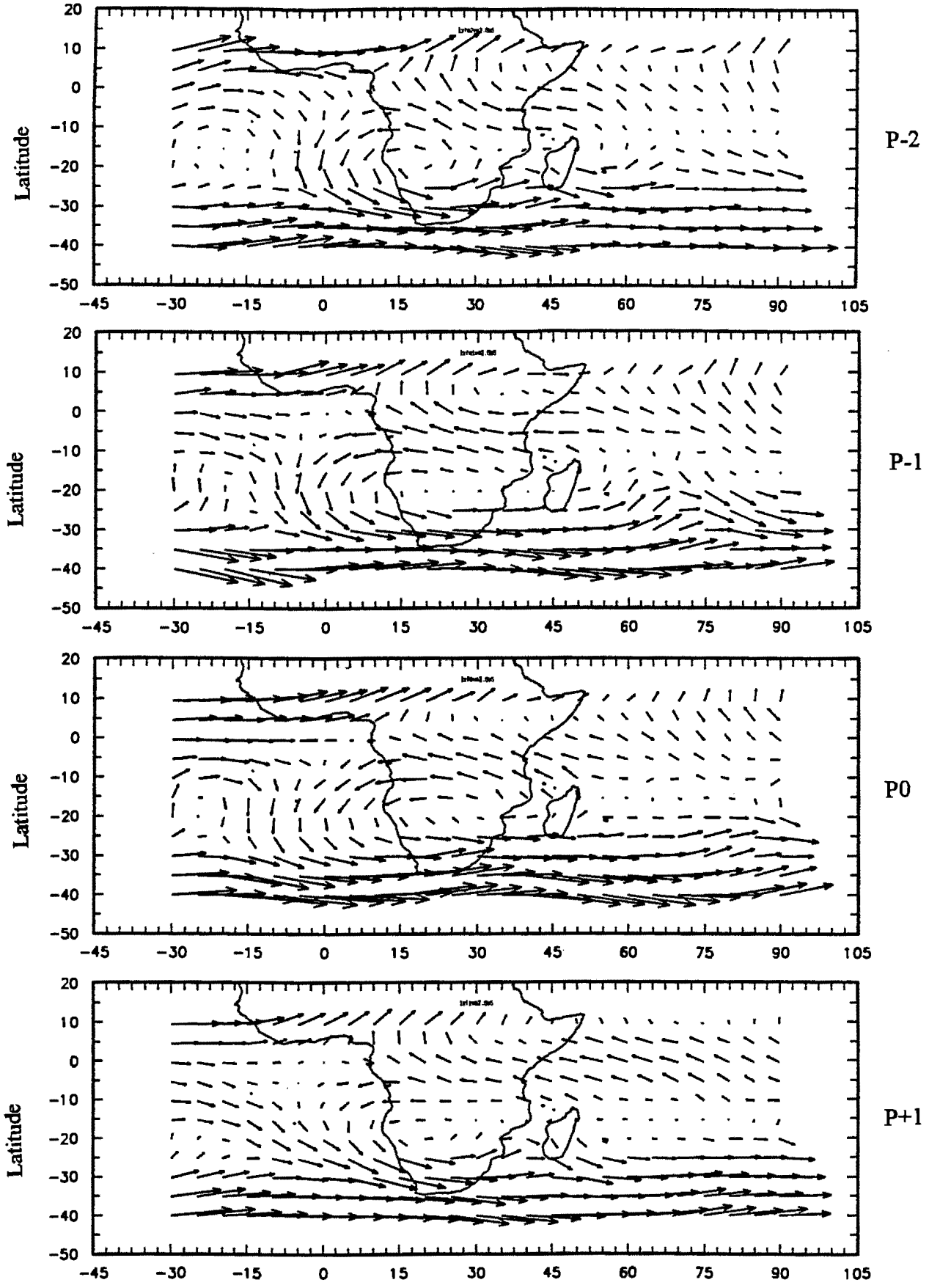

Figure 7.19 : 200 hPa total wind field for LSFW. The longest vector is equivalent to 35.4 m s^{-1}.

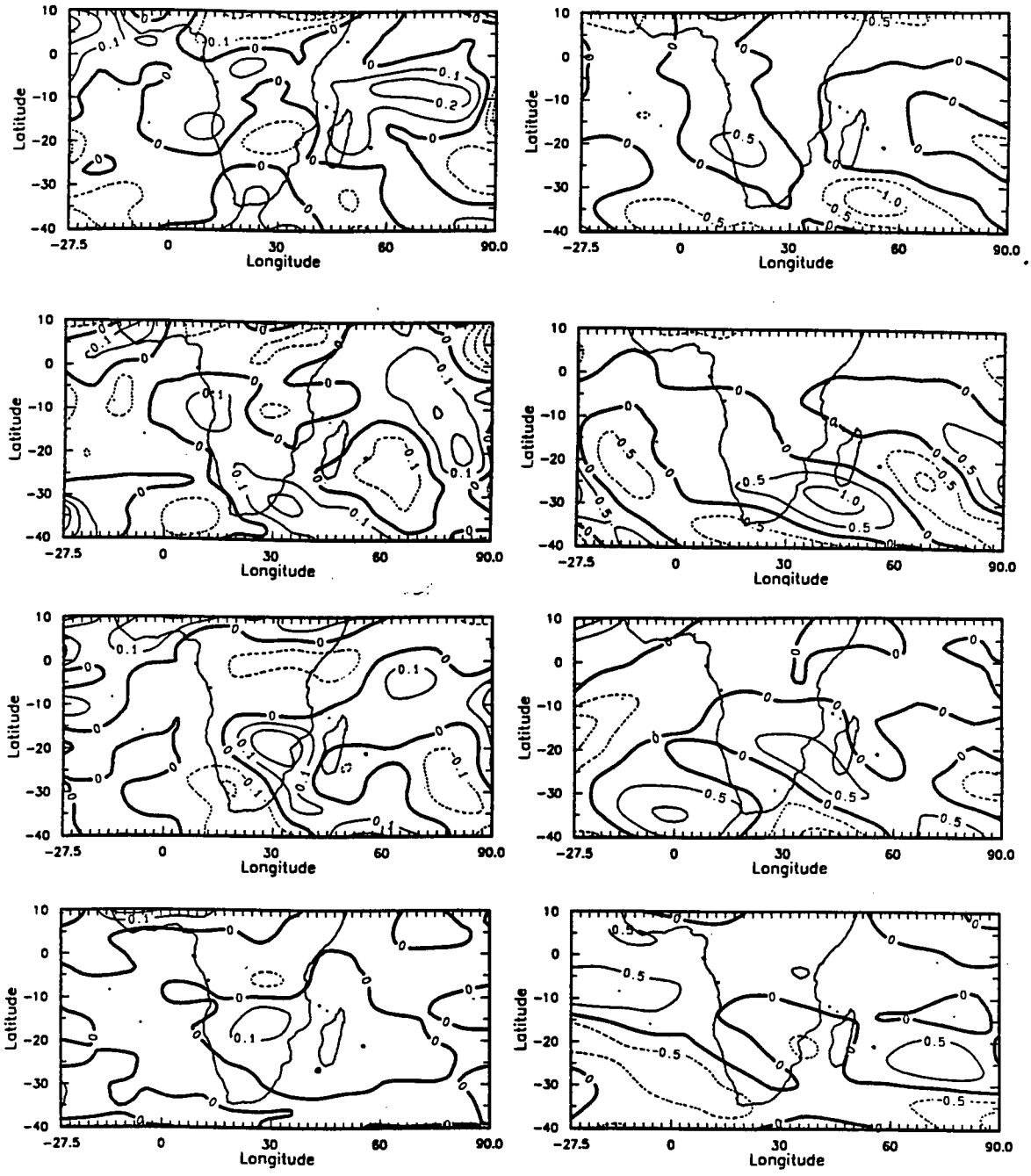

Figure 7.20 : Divergence (a) and vorticity field anomalies for LSFW at 200 hPa. Contour intervals are 1 and 0.5 x 10^{-5} s^{-1}, respectively.

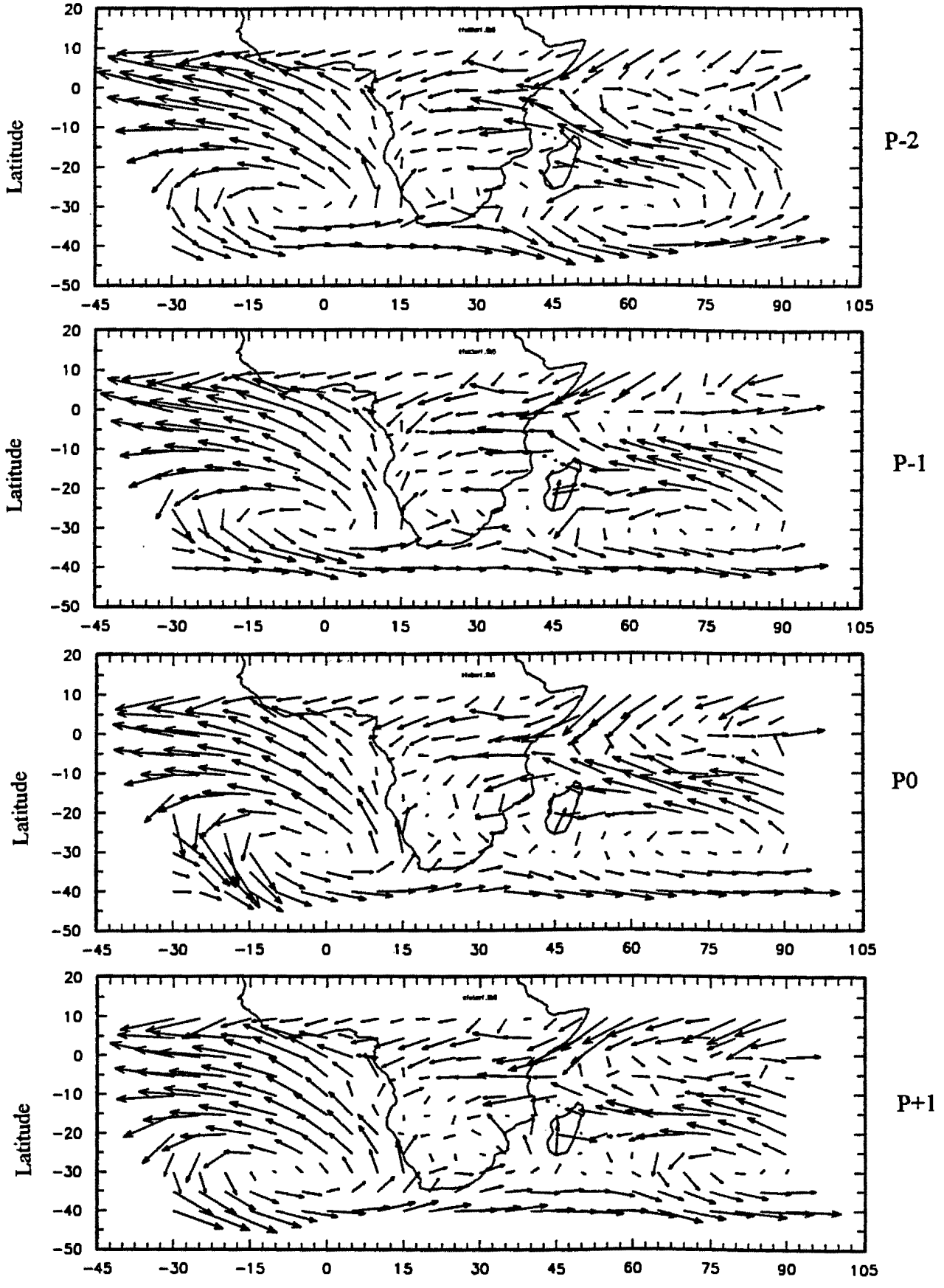

Figure 7.21 : Water vapour flux for EFW, integrated from the surface to 500 hPa. The longest vector corresponds to 260 g kg^{-1} m s^{-1}

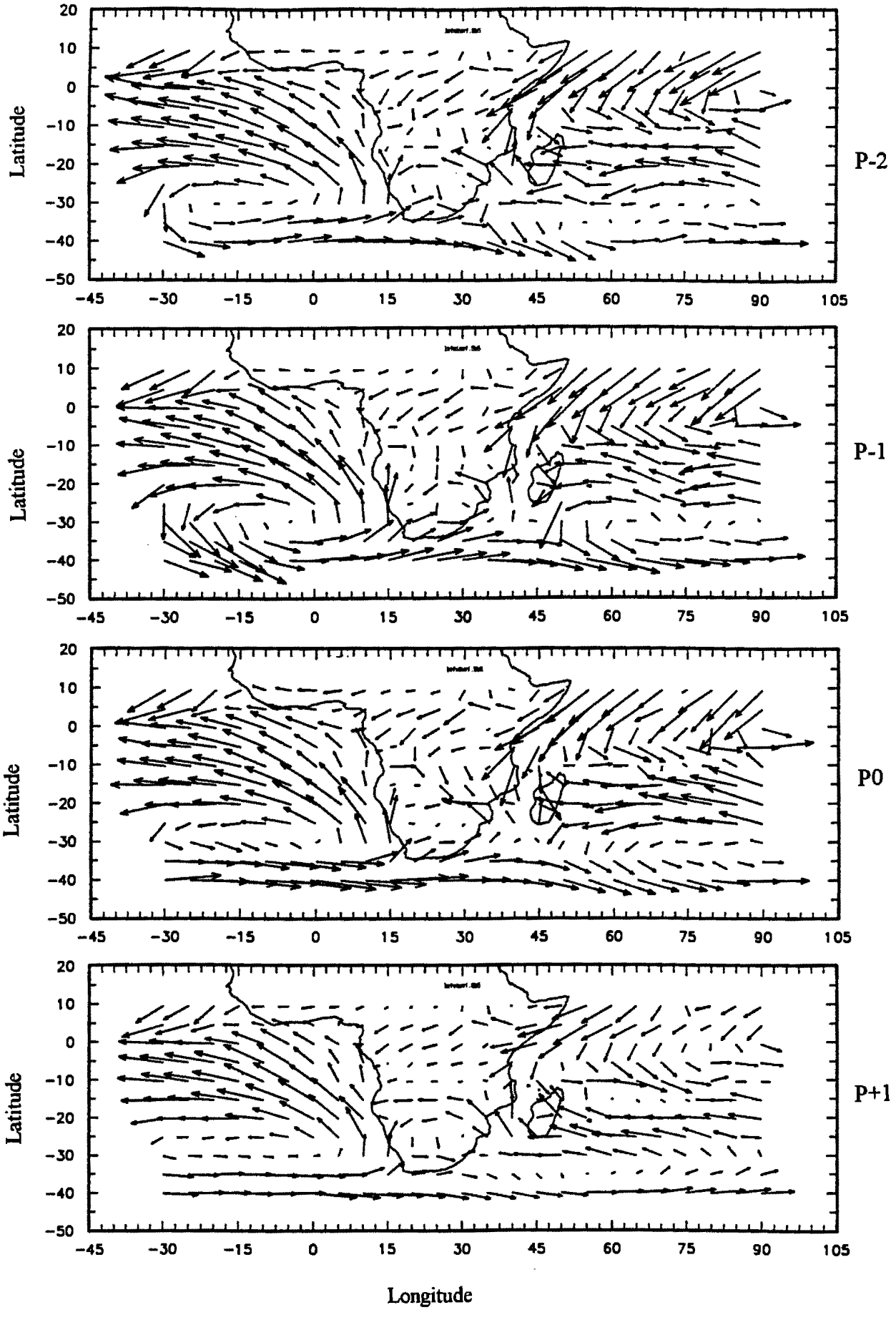

Figure 7.22 : Water vapour flux for LSFW, integrated from the surface to 500 hPa. The longest vector corresponds to 270 g kg^{-1} m s^{-1}

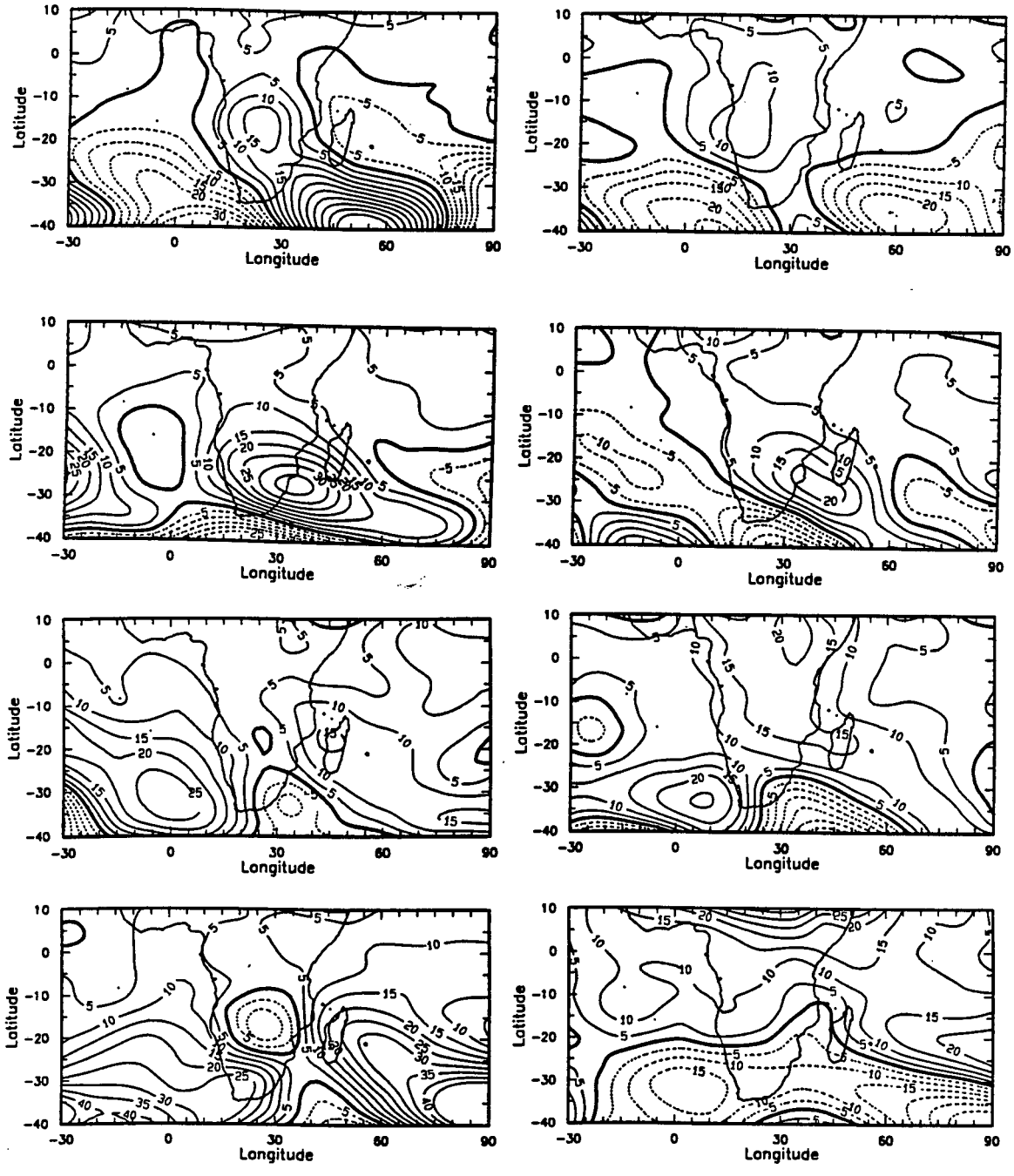

Figure 7.23 : Vertically integrated internal energy for EFW (a) and LSFW (b). The integration is between 700 and 300 hPa. Isolines are at every 0.5 x 10^{8} J kg^{-1}.

Chapter 8

Intra- Seasonal Dry spells and The Botswana Upper High

8.1 Introduction

It was illustrated in Chapter 4 that the austral summer rainfall over southern Africa is composed of wet and dry spells alternating in distinct quasi-oscillatory modes with frequencies of about 15- 45 days. There are two major dry spells and two minor ones. The first major dry spells (MSD) usually occur from the end of December to the middle of January while the other (LSD) is experienced from the end of February until about mid-March. Irregular minor droughts may also be evident. They are of relatively shorter duration, normally lasting a week (compared to the major ones which can remain dominant for 2- 3 weeks, or longer), the first occurring in the middle of December (ESMD) just after the first wet spell of the season and the second (LSMD) from the end of January through the first decade of February, after the late summer first wet spell. The spatial pattern is summarised in **Table 4.4 in Chapter 4**.

From a meteorological viewpoint, as well as thermodynamic considerations, dry spells and their extremes (droughts) are necessary for the earth- atmosphere system to maintain equilibrium. The constant re- organisation of convective and passive areas attempts to maintain a balance at various spatial levels ranging from meso- scale to planetary space scales, with source and sink regions and direct as well as indirect (teleconnections) links. This chapter focuses on regional dry spells over southern Africa only and attempts to investigate spatial patterns of meteorological parameters that best describe them. Reference to Chapter 4 shows that the transition from wet to dry regimes may be very short. This is in marked contrast to the period from initiation through development to maturity when there is a gradual build- up of moisture. Thus, it is problematic to predict dry spells well in advance since the forecast is largely dependent upon the correct identification of the peak of the wet spell prior to it. It is even more difficult to timely foretell when these dry spells are likely to prolong into droughts.

8.2 Methodology

Composites depicting the mid- summer dry spell (MSD) and the last summer dry spell (LSD) as determined from Chapter 4 were utilised. Briefly, dry spell pentads were defined as when standardised anomalies of pentad rainfall fell below 0.7σ (σ standard deviation) or persisted below . 0.5σ for three or more consecutive pentads. Compostites were constructed from these pentads, results of which are illustrated in **Annexures 4.1** and **4.2**. In the mean, MSD occurs between 27 December and 11 January. The LSD is a late summer phenomenon, usually between LSSW and LSTW (from 25 February to 16 March). In this chapter, ECMWF data for corresponding periods from 1986 to 1992, inclusive, are used to investigate the common denominators and peculiarities of dry spells.

To study the Botswana Upper High, a 2.5°x 2.5° box (3x3 grid points) is chosen from 500 hPa geopotential height analysis over southern Africa. The geopotential height parameter is preferred because, partly, it is relatively conservative on a day- to- day basis. In addition, inferences can be obtained regarding circulation patterns (e.g., presence or absence of anticyclonic tendencies, vorticity, divergence, uplift or subsident motion) without much loss of generality. The 500 hPa level is selected since any well- developed deep system (convective or subsiding) should manifest itself somehow in the middle levels. Being close to the level of non- divergence, the nature of circulations below and above it can be determined, as generally in the tropics, there is only one level of non- divergence, with either low tropospheric convergence (divergence) and upper- tropospheric divergence (convergence).

The box is bounded by 17.5°S, 20°E and 22.5°S, 25°E, centred over Botswana and contains 9 grid- points. A spatially- averaged geopotential height is determined for each day for all summers from 1987 to 1992. An overall period mean (1987- 1992) is then calculated and anomalies created, firstly, as algebraic differences, and also with respect to the standard deviation. Finally, a time series analysis of daily geopotential height anomalies was carried out for each season.

To comprehend further the characteristics of the atmosphere over the central interior of southern Africa, kinematic patterns at 700 and 200 hPa are investigated in a procedure similar to the geopotential height above (grid- point averages with centre at 20°S, 22.5° E). Subsequent series were cross- correlated with rainfall in the vicinity (the ZRI, Western

Transvaal Index and single station rainfall at Bulawayo (southwest Zimbabwe) and Maun (Botswana) shown in **Figure 8.7**.

8.3 Circulation characteristics

8.3.1 Lower tropospheric patterns : 700 hPa

Low- level patterns for MSD and LSD are shown in **Figures 8.1** and **8.2**. A slack temperature gradient exists equatorward of about 25°S. However, at MSD, there are two local centres of maximum temperatures, one over Namibia and Botswana and the other to the northeast of Madagascar (near 12- 15°S, 55- 65°E). By the time of LSD, however, the local area of maximum temperature over southern Africa has shifted northwestward to the eastern Atlantic. At the same time, the tropical Indian Ocean has warmed. This increase in temperature plays a significant role in increasing low level moisture potential and internal energy of convective cells, leading to an increase in cloudiness in the Indian Ocean. Dew point temperatures, on the other hand, are highest (and positive) in the interior of tropical Africa, negative elsewhere and generally decrease from the central interior of the continent (near 10°S, 25°E) polewards. During MSD, a ridge of relatively higher dew points extends from Africa into the Indian Ocean along the Equator to the warm pool between 70 and 85°E. In the latter dry spell, this ridge of moisture is located about 10° latitude further south in the Indian Ocean. The movement coincides with the changing location of the ITCZ, resulting from differential heating in sympathy with high SST. The lowest dew points are over the southeast Atlantic Ocean (mostly due to subsidence over the cold Benguela Current and consequent drying out) and at higher latitudes (attributed to relatively lower temperatures).

The north- south temperature transport field (*Tv*) at MSD shows alternating bands of northerly and southerly flow with respective centres between 20 and 30°S, approximately 20- 30° of longitude apart. Southerly transports are over the southeast Atlantic as well as the Mozambique Channel, Mozambique and eastern Zimbabwe. Sandwiched between these two regions are strong northerly components with a maximum over Namibia. The temperature transport in the Indian Ocean is very limited and a southerly component dominates the central waters. LSD posseses similar characteristics. Most of the airflow in the south Atlantic is light southerly. A dominant feature, however, is a dipole- like structure composed of northerly winds over southern Africa and southerly flow centred in

the south Mozambique Channel (near 20°S, 35°E). The southerly winds are stronger than during MSD and have spread further westward into southern Africa to include Zambia, Malawi and southern Tanzania, in addition to covering the whole of Madagascar. The dipole- like structure is still apparent and provides southerly and northerly temperature advection on the edges of the anticyclone that is centred over the central interior of southern Africa. The westward advancement is illustrated better by the zonal temperature transport (***Tu***) patterns. During the mid- summer dry spell, westerly flow prevails poleward of 25°S right across the domain with a maximum over south east South Africa. The axis of maximum eastward transport is on the poleward side of the sub-tropical ridge. There is also a tongue of westerly flow in the Equatorial Indian Ocean. In the February/ March dry spell, tropical "westerly monsoon" flow is initiated over the western Indian Ocean (about 15° longitude west of the corresponding MSD position) and these advect the unstable air from the continent to the oceans. The westward propagation in tropical regions is also manifested in the southwestward shift in the axis of the westerly band.

The corresponding geopotential height field (**Figure 8.2**) shows the position of the sub-tropical high pressure belt at 700 hPa which extends across the region almost uninterrupted with its axis along 25°S. The central regions of oceanic anticyclones are also evident just to the west of Greenwich and near 85°E. There is also a trough of relatively low heights stretching from the tropical Indian Ocean to equatorial Africa. The pattern in the February\ March dry spell (LSD) resembles that during MSD. There are differences, though, in the spatial distribution as well as magnitude over Africa and the Indian Ocean. This time the Atlantic Ocean Anticyclone (AOA) maintains a ridge across southern Africa with maximum heights over the central interior where there has been an increase of over 10 gpm. The Indian Ocean Anticyclone (IOA) is not evident. Instead, the heights over the tropical Indian Ocean have lowered in a manner similar to zonal temperature transports (**Figure 8.1**), possibly reflecting the relative increase in cloudiness over the Ocean to the northeast of Mauritius.

As expected, divergence dominates the low- level circulation over southern Africa between 15 and 30°S and centred over Botswana (20°S, 22.5°E). It links the two oceans with relatively weak convergence on either side of it. Also, worthy of note is the convergence over Madagascar, suggesting that dry conditions affecting southern Africa do not spread as far as Madagascar. In the later dry spell (LSD), the divergent flow still prevails over southern Africa, the pattern having spread southwards as well as eastwards to such an extent that only the extreme southwest corner of South Africa remains under

convergent circulation. The area of convergence over Madagascar has shrunk to only the northern regions. At the same time, the convergence just south of the Equator has strengthened with a centre near 5°S, 20- 25°E.

The similarities in the divergence fields suggest that, during major dry spells, a small Hadley cell- like structure is established on the African continent. The process is that air subsides over southern Africa at low- levels in the approximate latitudes of the Tropical- Sub- Tropical Boundary (TSB). The bulk of the attendent convergence is between the Equator and 10°S. There is a bias towards divergence across central southern Africa during the mid- summer dry spell and towards convergence just to the south of the Equator in the February/ March dry episode.

The circulation south of the Equator is mostly anticyclonic (Vorticity, **Figure 8.2**), more so over the southeast Atlantic Ocean and southern Africa. The southern African vorticity maximum exceeds $10^{-5}s^{-1}$ and extends in the SWIO. A region of cyclonic motion is apparent between 5 and 15°S in the Indian Ocean to just off the east African coast. Another smaller area of cyclonicity is illustrated in the central eastern Atlantic Ocean near Africa between 5 and 10°S. These cyclonic regions become linked during LSD in such a manner that a continuous band of cyclonic flow stretches from the Indian Ocean, through equatorial southern Africa to the Atlantic Ocean. The area of cyclonic motion in the Indian Ocean has moved southwards to engulf Madagascar.

It is apparent from both middle and late summer low- level vorticity patterns that the circulation during dry spells is more zonal than meridional, although anticyclonicity dominates in January. This suggests minimum interaction at low levels between the tropics and extra- tropics. Significant changes take place in tropical Africa, particularly between 10 and 20°S, where the westward propagation of cyclonic motion is evident Sub- tropical southern Africa remains largely unaffected during both dry spells, with the area of maximum anticyclonicity centred between 25 and 30°S, coinciding with the region of highest low- level geopotential height.

Horizontal wind vectors at low levels (**Figure 8.3, 700 hPa**) during MSD display anti clockwise systems associated with the sub- tropical high pressure belt with axis along 25- 30°S. Across Africa, the belt has a centre over eastern South Africa (25°S, 27.5°E). The belt separates easterlies in the tropics from westerly winds polewards of 30°S. The Indian Ocean Anticyclone is weak, but evident. While the flow in the Indian Ocean is relatively

light (less than 5 m s^{-1}), there is a belt of easterly winds around 15°S up to Madagascar most of whose winds recurve around the sub- tropical high pressure ridge to become part of the westerly regime further south. During LSD (**Figure 8.4, 700 hPa**), the anti clockwise system over northern South Africa is more established than at MSD, controlling easterly wind vectors between 10 and 20°S across the sub- continent. Also of significance are the weak easterly vectors in the Indian Ocean which remain over the ocean by recurving east of Madagascar to become westerlies along 10°S. In addition, unlike during MSD, there is no evidence of a link between equatorial and sub- tropical easterlies, indicating a shift of main activity equatorwards. It is also worth noting the absence of the Mozambique Channel- Angola Trough (MCAT), particularly for LSD, as well as the west coast trough from Angola to South Africa apparent during wet spells (Chapters 5 and 6, for example). The MCAT is replaced by easterly flow from the anticyclone centred over South Africa at 700 hPa. The anticyclone also suppresses the west coast trough, acting as a temperature advection mechanism from tropical Africa to higher latitudes.

8.3.2 Middle -level circulation patterns: 500 hPa

Mid- tropospheric geopotential height patterns reveal the Atlantic Ocean ridge extending into southern Africa, with maximum heights located over Botswana, hereafter referred to as the Botswana Upper High (BUH). There is no evidence of the Indian Ocean ridge. A broad weak trough exists over the tropical Indian Ocean. The Atlantic Ocean exerts its influence on the BUH in the February/ March dry spell (LSD). In general, the heights over Africa and the Atlantic Ocean have increased while those in the Indian Ocean have lowered. The wind vectors summarise the patterns better. They show the approximate middle level position of the sub- tropical ridge during the mid- summer dry spell (**Figure 8.3, 500 hPa**), although the ridge is almost absent in the Indian Ocean, as illustrated by geopotential height patterns. The dominant pattern is the BUH centred near 22.5°S, 25° E. There are also secondary centres in the central South Atlantic as well just to the north of Mauritius. During LSD (**Figure 8.4, 500 hPa**), however, only the BUH remains strong and dominant. A weak anti clockwise circulation is indicated in the equatorial Indian Ocean reaching as far west as the coast of east Africa. The winds are also relatively weak.

The vorticity pattern shows the whole region under anti- cyclonic flow with maxima in the south Atlantic and over central southern Africa (located on the eastward side of the BUH) (**Figure 8.5**). The middle- level position of the ITCZ cannot be inferred from the MSD

pattern. Instead, patterns typical of early summer patterns are depicted, indicating an influence from the Atlantic Ocean. However, the anticyclonic flow is greater over southern Africa during the MSD reaching a level of 1.5 x $10^{-5}s^{-1}$ in the composite. During LSD, the pattern is a reflection of the lower levels with the effect of the BUH being felt in addition to the tongue of cyclonic flow extending from the Indian Ocean across Africa between 10 and 20°S. The pattern is also generally indicative of mean tropical circulation in late summer, particularly in delineating the cyclonic region associated with the ITCZ in the Indian Ocean as well as Africa.

Another important parameter to describe middle level circulation is vertical velocity. Reference to **Figure 8.5** shows subsidence over the eastern and southern Atlantic as well as the southwestern half of southern Africa, in sympathy with the Anticyclonic ridge and the BUH. Elsewhere, there is uplift motion, the greatest of which occurs over equatorial Africa. However, during LSD, the area of generally sinking motion has intensified and shrunk over southern Africa, centred on Zimbabwe at 20°S, 30°E. Simultaneously, there is uplift over tropical Africa and Madagascar, again substantiating the inference that the dry spell in late February is confined to the continental plateau of southern Africa. The air over the whole sub- region is heterogeneous with dry air over sub- tropical regions and more moisture over Madagascar and equatorial Africa.

In summary, therefore, major dry spells are dominated by the BUH which is centred over Botswana in the middle levels and represented as an anticyclone over South Africa in the low levels. The anticyclone tilts northwestward with height. The BUH is characterised by subsident motion over most of southern Africa in late December- early January. There is no evidence of both the MCAT and west coast trough. Instead, a straight easterly regime exists in the latitudes of MCAT during dry spells. The zone of cyclonic circulation, exhibited in the mid- level vorticity field, is pushed equatorwards to lie along 10°S. North- south exchanges over tropical southern Africa are virtually absent during dry spells. The BUH has no direct impact on activities in the Indian Ocean. Reinforcement comes from the Atlantic Ocean. Thus, the dipole between southern Africa and Madagascar/ Mauritius referred to in previous research (for example, Mason, 1992; Jury, 1992 and Pathack, 1993) may not explain adequately the dynamics of dry spells. The westerly vectors in the tropical west Indian Ocean to some extent limit the influx of moisture from the monsoons otherwise intended for Africa. Somewhere between Africa and the Indian Ocean (probably along the east coast of Africa) lies an approximately east-west demarcation zone separating seemingly independent weather regimes on either side.

This scenario is most probable during dry episodes. The "demarcation" is absent for wet episodes of late summer when threshold tolerances on the boundary are exceeded, resulting in westward surges into Africa from the Indian Ocean. Hovmoller analyses of longitude versus time should shed more light on this and are considered in the next chapter.

8.3.3 Upper- level circulation: 200 hPa

Upper circulation features can be summarised from the total wind field (horizontal wind vectors). The BUH is the dominant feature over Africa during the mid- summer dry spell **(Figure 8.3, 200 hPa)** and, together with another anti- clockwise circulating system to the northeast of Madagascar, contributes to an easterly to southeasterly airflow over tropical Africa. The system also alters the course of the sub- tropical westerly air stream from the Atlantic Ocean towards South Africa. The AOA is not evident, implying that, despite being quasi- stationary throughout summer, the AOA is a relatively shallow feature. The pattern is more organised during LSD (**Figure 8.4, 200 hPa**). Apart from the BUH, a weak anti clockwise zone exists in the Indian Ocean along the same latitude as the BUH (around 20°S). The combination results in a predominantly southeasterly 200 hPa flow in the tropical regions of Africa and the Indian Ocean. Like during MSD, the upper level westerlies in the Atlantic split south of the Equator near Greenwich with one air stream going to the northern hemisphere while the other represents an important northwesterly flow around the southwest perimeter of the BUH, acting to spin- up and sustain it.

The corresponding geopotential height, divergence and vorticity fields are shown in **Figure 8.6**. An anticyclone exists over tropical Africa during the mid- summer dry spell (MSD) with a centre near 10°S, 20°E. This is the upper tropospheric position of the BUH, having been displaced northwestwards (equatorward) with height. The pattern is zonal polewards of 20°S where there are tight gradients. The BUH is no longer evident during LSD. Instead, the tropical heights have increased. The barotropic nature of the flow is well illustrated over the Atlantic Ocean as well as at higher latitudes.

The divergence pattern shows that, during the mid- summer dry spell, upper- level convergent motion stretches from the south Indian Ocean, through the south Mozambique Channel into southeast Africa as far as Botswana. There is also convergence over most of the Atlantic Ocean associated with subsidence within the low- level AOA air. Divergent

airflow is evident over the tropical Indian Ocean and the whole of Madagascar, tropical Africa and down the west coast of southern Africa. The strongest divergent circulation is over Madagascar as well as along the Equator over the Congo and Zaire. The areas under upper divergence shrink during LSD. The divergence in the tropical Indian Ocean and tropical Africa is more organised than during MSD. The divergent outflow from convective regions associated with the ITCZ is prominent. For both MSD and LSD, cyclonic circulation (**Figure 8.6b**) dominates southern Africa (with a centre near 20°S, 15-20°E), the south Atlantic and the southern Indian Ocean (where a local maximum occurs over Mauritius).

The broad- scale circulation is summarised by velocity potential and stream function (not shown). The general patterns are similar to those of wet spells where negative velocity potential values dominate Africa and the Indian Ocean. Minimum values along 10°S in the west Indian Ocean to the northeast of Madagascar during MSD occur in sympathy with anticyclonic outflow from embedded convective systems of the ITCZ. Positive values are located in the Atlantic Ocean centred between 20 and 35°S just to the west of Greenwich, associated with upper level cyclonic circulation of the Atlantic Ocean Anticyclone. During LSD, there is also a centre over Africa (8°S, 25°E), the region of highest vertically integrated internal energy (**Figure 5.14**). The axis of the lowest negative velocity potential coincides with the region of maximum positive upper- level divergence. The 200 hPa streamfunction pattern is positive (negative) south (north) of 5°S. The positive values are centred along 25°S in the south Mozambique Channel during MSD and along 30°S to the south of Madagascar for LSD. The pattern compliments the upper- tropospheric cyclonic flow dominating southern Africa and the adjacent oceans.

8.4 Vertically integrated water vapour flux

The water vapour flux fields (**WVF**) are represented by **Figure 8.3** and **Figure 8.4** for MSD and LSD, respectively. At MSD, the moisture fluxes are maximum over oceanic regions. There is some moisture from the northern hemispheric areas of the Indian Ocean that reaches east Africa. The moisture between 10 and 25°S is advected as far as Madagascar with little spilling over into the Mozambique Channel. Some moisture is available to southern Africa from the Indian Ocean in the band 5-15°S. A similar situation arises during LSD, although the westward band is 10° latitude further south. A significant quantity of moisture is returned to the central Indian Ocean through a zone between 5 and

15°S. The flow is greater than at MSD. Another noticeable difference between the two spells is the flux of moisture in the south Indian Ocean which has advanced further westwards towards southern Africa via the south Mozambique. Like during MSD, moisture advection over the sub- continent is limited.

8.5 Discussion

This chapter has indicated features characteristic of major dry spells. Similarities and differences have also been highlighted. The low- level zonal wind during major dry spells is dominated by tropical easterlies and anticyclonic sub- tropical westerlies while the tropical Indian Ocean between 0 and 10°S sees equatorial westerlies increase in late February and early March. The westerlies there originate around 50°E during the mid-summer dry spell and off the coast of Tanzania during LSD. Thus, the winds transport relatively warm moist air away from Africa towards the central waters of the Indian Ocean. These winds have recurved from the original easterlies on either side, especially those poleward of it (between 10 and 20°S). It is apparent from the low- level wind vectors during LSD that when dry spells prevail over southern Africa, the combined influence of an anti- clockwise gyre off equatorial east Africa and a clockwise circulation east of Mauritius limits easterly flow across Africa.

From the vorticity patterns, at the peak of the mid- summer dry spell, the whole of southern Africa experiences anticyclonic flow with a centre over the central interior, the greatest impact being felt in northern South Africa and the southern areas of Botswana and Zimbabwe. However, during the last major dry spell only the southern parts of the region remain under the influence of strong anticyclonic circulation. The tropical areas experience cyclonic flow, including the whole of Madagascar. Therefore, the region's circulation is spatially more variable during the latter dry spell over southern Africa.

The middle and upper levels over southern Africa are dominated by the Botswana Upper High (BUH). It is located over northern South Africa in the low levels, over Botswana in the middle levels and over Zaire/ Congo higher up, a northwest displacement with height of approximately 5° latitude between 700 and 500 hPa and from 500 to 200 hPa. The anticyclone has been observed to determine the success or failure of the crop growing season in southern Africa. It is therefore necessary to investigate its properties further so as to ascertain the frequency of dry spells in the region. To do this, a 9- grid point domain

representing the mid- level location of the BUH is analysed. **Figure 8.7** displays the box in question plus selected rainfall indices in the vicinity. The 500 hPa surface is analysed as it best exhibits the level of the BUH, from both the total wind and geopotential height. For easier interpretation and to avoid duplication, only the geopotential height is considered. Other parameters and levels are viewed at later. As indicated in the methodology section earlier in this chapter, the 9- grid point box is centred at 20°S, 22.5°E.

Spectral analyses of the 500 hPa geopotential height in the box are summarised in **Table 8.1.** The table shows the most dominant cycles apparent from the area- averaged daily geopotential heights from November to March, inclusive for the period 1986 to 1992.

Season	Dominant cycles (in days)			
1986 - 87	26.0	60.7	15.2	
1987 - 88	60.7	20.2	10.7	
1988 - 89	45.5	16.5	14.0	
1989 - 90	45.5	16.5	30.3	12.1
1990 - 91	60.0	36.0	9.5	
1991 - 92	30.3	22.7	14.0	

Table 8.1: Dominant cycles in daily 500 hPa geopotential height over Botswana (20°S, 22.5°E). The cycles are listed in decreasing order of importance.

Reference to the Table shows dominant cycles of 26- 30 days during the drought seasons of 1986/87 and 1991/92, 45 days during the relatively wet seasons from 1988 to 1990 and 60- day cycles for "average" seasons. This implies that dry spells recur more frequently during drought (or possibly, El Nino) years with major events occurring just about every month. Thus, on average there are about 5 major dry spells during dry summers compared to approximately 3 experienced in wet years.

Other higher frequency cycles are also in evidence. These include those of between 14- 16 days, 9-12 days as well as 20- 22 days. There is more low amplitude noise during wet seasons most of which simply indicate decay phases of wet spells rather the dominance of the BUH. These intra-seasonal oscillations occur throughout summer. Their amplitude and frequency depend upon the synoptic triggering mechanisms at the synoptic scale time frame. Thus, the ISOs occur irrespective of whether the cycle is wet or dry.

Figure 8.8 is a time series analysis of ***mean*** pentad geopotential height at 500 hPa normalised with respect to the standard deviation for 20°S, 22.5°E. A quasi- orderly alternating sequence of positive and negative anomalies is illustrated. Negative anomalies during the six- year period persist throughout October and coincided with above normal rainfall over central Africa, including Zimbabwe. The anomalies change to positive in, and remain generally so until the end of, November, after which they reverse, coinciding with EFW (the early summer first wet spell). If it can be assumed that positive geopotential height anomalies are more indicative of subsidence than advection, wet and dry spells can be inferred. The MSD is not well reflected because its occurrence is non- stationary with respect to the season, as indicated in Chapter 4. Late summer major wet (LSFW, LSSW and LSTW) and dry (LSMD and LSD) spells are also represented, again with large negative (positive) anomalies coinciding with wet (dry) spells or mid- level convection (subsidence).

Figure 8.9 illustrates time series of pentad geopotential height departures from the 1986-92 mean for each year. The figure is similar to **Figure 8.8**, except that the data is not normalised with respect to the standard deviation (the anomalies are mere departures from the mean). While acknowledging the variability in the daily data, trends are easily discernible, especially persistent anomalies. Significantly, there is no seasonal trend. In 1986/87 (referred to hereafter as 1987) positive anomalies were dominant virtually all summer from November, with few and far between negative anomalies. The positive anomalies also prevailed the following year with significant negative anomalies occurring only in February. The pattern completely reversed in 1989, a season with above normal rainfall. Positive anomalies occurred only at the end of December, associated with MSD, which started earlier than usual. During the next two years, the patterns reflected equally distributed frequencies of both anomalies, although biased towards negative anomalies in January and February during 1990 and from November to mid- February in 1991. In 1992, the patterns were similar to those of 1987, another El Nino year. The season commenced with negative anomalies in domination until the end of December. Thereafter,

they were persistently positive despite being briefly negative in January (due to LSFW) and the last half of March (LSTW).

Divergence and vorticity patterns further illustrate the circulation structure. **Figure 8.10** is a time series analysis of daily area- averaged divergence and vorticity at 700 and 200 hPa centred at 20°S, 22.5°E. The analysis is along similar lines as geopotential height, but is a 1986- 92 unfiltered pentad mean. At the low- level, vorticity is strongly negative at the onset of summer. As the season advances, the circulation progressively becomes less cyclonic until January when an alternate pattern of cyclonic and anticyclonic flow occurs, showing greatest anticyclonicity in mid- January (MSD). The alternating pattern continues into February from relatively strong anticyclonicity at the end of January. Cyclonicity then prevails again from mid- February till the end of the month. The flow in March reverts back to that of early summer. The corresponding low- level divergence series has characteristics opposite to vorticity, with divergence dominating early summer (November and December) and from mid- February to the end of March. Overall, low- level divergence and anticyclonic circulation are predominant for most of early summer and the last half of late summer. During mid- summer, the patterns alternate, in sympathy with wet and dry spells. The MSD, well represented at middle and upper levels, is inferred from the vorticity pattern.

At upper levels, negative vorticity (cyclonic flow) occurs throughout summer. Cyclonicity increases from the beginning of November and reaches a maximum around the first of December, after which it becomes strongly anticyclonic. Visual inspection of the series indicates some sort of periodicity of approximately 30 days. The circulation is biased towards positive divergence. As at lower levels, convergent spells are shortlived and, from daily analysis (not shown), appear to possess some form of periodicity of between 10 and 15 days. The duration is longer, though, from mid- February onwards. The circulation leading to the formation of the MSD is respresented near the end of December, suggesting a few days lead, in the mean. Therefore, a "trickle- down" effect is apparent, with anticyclonicity and divergence occurring earlier in the upper troposphere.

A periodogram analysis of the above series (**Figure 8.11**) confirms the existence of intra-seasonal oscillations in the divergence and vorticity in addition to the geopotential height. With reference to 700 hPa divergence, a 16.6 day mode is most frequent, followed by periodicities of 9.1 and 4.6 days, respectively. According to the 700 hPa vorticity field, the 38.5 day mode is dominant, then a 15.2- day oscillation. The 200 hPa divergence

periodogram resembles that at the low- level, with a 17- day mode dominating, followed by another at 11 days. The main difference lies in the oscillations whose periodicities lie under 10 days which are more apparent in the low- levels than at upper levels where the flow is more geostrophic. Perturbations at such high frequencies are unlikely to have a significant effect on low- level circulation and will most likely not trickle down. With regard to 200 hPa vorticity, the periodogram exhibits the 15.4- day oscillation and a secondary mode of slightly longer time wavelength (21.8 days). It is thus apparent that the mean atmosphere over Botswana exhibits a 15- 17- day oscillation, which is the most common characteristic found at both low and upper levels. This oscillation has also been detected in the pentad rainfall patterns of central southern Africa (Chapter 4), suggesting some form of link. The oscillation has also been observed and noted before (Chapter 2), particularly by Blackmon et al (1984) and Shapiro and Goldernberg (1993). Earlier, Madden (1979) found 16- day waves that were global in nature. The dominant modes of 20- 30 days as well as 40- 60 days observed by, among many others, Ghil and Mo (1991) and Levey (1993), can be best detected in the vorticity fluctuations at 200 and 700 hPa levels, respectively.

Daily fluctuations from season to season between 1986 and 1992 summers, inclusive, are summarised in **Table 8.2**. As expected, individual seasons exhibit more oscillations than the mean series. Apart from the oscillations depicted in the mean series, a 4- 8- day oscillation is common to nearly every season. This is compatible with observed weather patterns, including frontal systems, over southern Africa (Preston- Whyte and Tyson, 1988). Also evident is a 10-17 mode, with that near 15- 16 most recurring in the divergence field. There is no evidence to suggest that any harmonics exist, suggesting several wave trains in action. The 16- day wave train is apparent at both low and upper levels, leading one to infer that when the wave occurs, it is deep and can be traced from top to the bottom of the troposphere. The problem with this type of analysis is that it cannot indicate whether the occurrence is simultaneous or lagged, an important factor which is investigated next.

Summer	Div 700 hPa	Vor 700 hPa	Div 200 hPa	Vor 200 hPa
1986- 87	21.7, 10.2, 5-7	11.6, 38.5, 4.4, 6.0	50, 10.9, 18.9, 6.9, 2.7	50, 25.3, 15.2, 11.6
1987- 88	30.3, 4.4, 8.9	12.5, 38.5, 6.3, 5.6	19.2, 10.9, 2.8, 4.2	50, 21.7, 9.5
1988- 89	17, 11.6, 4.2- 4.8, 2.3	50.1, 21.3, 8.3, 4.3	12.7, 30.3, 7.6	12.7, 9
1989- 90	30.3, 2.4, 15.2, 3.8	nil	15.4, 6.6, 2.4	30.4, 50, 21.7, 15.2
1990- 91	17, 12- 14, 7.7	35.7, 14.3	16.7, 4.7	38.5, 10.9, 13.9, 8
1991- 92	13.9	15.2, 25, 9- 11, 6.1	50.7, 8.0, 6.1, 15.2	25.6, 13.9, 6.1

Table 8.2 : Periodicities in daily grid point (20°S, 22.5°E) divergence and vorticity at 700 and 200 hPa from 1986-87 to 1991-92 summers. Modes are in decreasing order.

8.5.1 Cross- correlation analysis

The following section is aimed at invetigating relationships between divergence, vorticity and geopotential height fluctuations over Botswana and rainfall in the vicinity. The objective is to detect any unique relationships among the parameters as a function of time and seek plausible controlling mechanisms.

Table 8.3 illustrates cross- correlation analysis between grid- point divergence, vorticity and geopotential height and rainfall at Maun (Botswana), Western Transvaal (South Africa), Bulawayo and the ZRI (Zimbabwe). The analysis uses pentad data from 2 November to 31 March (giving a sample size of 30 pentads) and carried out with the Statgraphics Package version 6. Only the best correlations, accompanied by corresponding lags, are illustrated.

Leading variable	Dependent Variable	Highest correlation	Corresponding Lag (pentad)
Divergence 700 hPa	Div 200 hPa	- 0.62	0
	Vor 700 hPa	- 0.44	+ 1
	Vor 200 hPa	+ 0.4	+ 1
	Geopotential height	+ 0.44	+ 1
	ZRI	- 0.42	0
	Bulawayo	- 0.37	+ 3
	Western Transvaal	- 0.57	0
	Maun	- 0.39	+ 4
Divergence 200 hPa	Vor 700 hPa	- 0.42	- 4
	Vor 200 hPa	+ 0.43	- 1
	Geopotential height	+ 0.38	+ 1
	ZRI	+ 0.56	+ 3
	Bulawayo	+ 0.64	+ 3
	Western Transvaal	- 0.28	- 4
	Maun	- 0.54	- 4
Vorticity 700 hPa	Vor 200 hPa	- 0.37	0
	Geopotential height	- 0.46	0
	ZRI	+ 0.6	0
	Bulawayo	+ 0.32	- 4
	Western Transvaal	+ 0.52	0
	Maun	+ 0.49	0
Vorticity 200 hPa	Geopotential height	+ 0.29	0
	ZRI	- 0.29	- 3
	Bulawayo	+ 0.21	+ 4
	Western Transvaal	- 0.29	+ 4
	Maun	- 0.38	- 3

Gpm 500 hPa	ZRI	- 0.33	+ 2
	Bulawayo	- 0.33	+ 3
	Western Transvaal	- 0.15	+ 2
	Maun	+ 0.27	- 5

Table 8.3 : Lagged correlations involving pentad mean divergence, vorticity, geopotential height at 20°S, 22.5°E and rainfall in the vicinity. Correlations are listed if significant above the 90% confidence limit.

The following, among others, can be inferred from **Table 8.3:**

- The highest correlations exist between 700 hPa divergence and 200 hPa divergence. The two levels are negatively correlated and the best correlations are at zero lag. The implication of this is that when there is low- level convergence, for example, more often than not, there is an attendant upper divergence with the level of non-divergence somewhere between. The converse is also the case. This configuration agrees with classical barotropic dynamics. The correlations between 700 hPa divergence and vorticity as well as mid- level geopotential height at lag +1 pentad indicates that low- level divergence leads low- level negative vorticity, upper positive vorticity and is followed by an increase in the geopotential height in the middle levels. The magnitudes of the correlations mean the correspondence is not always direct. The low- level divergence is inversely related to rainfall, a situation conducive for rising motion, hence precipitation, provided there is moisture present. The lagged correlations imply 15- 20 days (lags -3 to -4 pentads) lapse between convergence and subsequent precipitation over Maun and Bulawayo. The correlation coefficients are too low to be operationally useful as predictors. On the other hand, those with ZRI and Western Transvaal at lag 0 point towards convergent motion over the central interior of southern Africa during wet spells, evidenced by the Mozambique Channel-Angola Trough (MCAT) noted in previous chapters of this thesis.

- Without downplaying the correlations with other parameters, there is good agreement between upper divergence and precipitation over Zimbabwe (ZRI and Bulawayo) and Maun. Unlike for Zimbabwe, the rainfall at Maun leads upper divergence by up to 20 days. Thus, the situation at Maun can be used as an indicator

of upper divergence which, in turn, leads rainfall over Zimbabwe by 3 pentads. The lead time is operationally useful. It should be remembered the BUH at 200 hPa is equatorward of 20°S, 22.5°E. This can partially explain the low correlation coefficient between upper divergence and rainfall over Western Transvaal. Reference to the total wind field at 200 hPa shows a westerly- northwesterly airflow across South Africa emanating from the equatorial Atlantic Ocean.

- The low tropospheric vorticity is also well correlated with precipitation, more so with the ZRI, Western Transvaal and Maun, all at 0 lag. This has no predictive relevance, however. The relationship with Bulawayo rainfall is rather low to be reliably utilised, considering the - 4 lag value. Thus, during wet spells, the low- level circulation over central southern Africa is predominantly cyclonic, a characteristic that fits well with low- level convergence, mentioned above. The process is accompanied by a general lowering of the 500 hPa pressure surface, possibly due to increased cloudiness over the region. Similarly, dry episodes are characterised by low- level anticyclonic circulation and higher geopotential heights over the region, as expected.

- Despite being statistically significant, upper tropospheric vorticity fluctuations are relatively weakly correlated with precipitation. The parameter and level are thus poor indicators of imminent rainfall over southern Africa. Rainfall (and the converse) is better related to upper divergence such that positive divergence is associated with positive vorticity, although not always. The same applies to the geopotential height at middle levels. It has already been demonstrated in Chapters 5 through 7, and earlier in this chapter, that geopotential height changes across southern Africa are minimal throughout summer, though the values tend to increase as the season progresses. This is irrespective of whether the episodes are wet or dry. However, the fact that the correlations with rainfall are negative (except with Maun) is consistent with the finding that lowering of heights is usually indicative of increased cloudiness, hence increased potential for rain.

In summary, as far as rainfall prediction over southern Africa is concerned, the most useful predictor is upper divergence with regard to Zimbabwe. The signs can be detected up to three pentads prior to wet episodes. Indirectly, rainfall events at Maun in northern Botswana are equally useful, since they lead upper divergence. A possible scenario is rising motion associated with rainfall at Maun (cloud band initiation) gives rise to upper

divergence as compensation. The build- up is rather gradual (which may be attributed to a family of frontal systems passing to the south resulting in low pressure over the sub-continent). There is also significant low- level convergence. These prerequisites lead to rainfall over eastern southern Africa about 2 pentads later. Western Transvaal precipitation prediction (and conversely dry spells) is not conclusive from low and upper-level divergence and vorticity as well as mid- level geopotential height. This is because the best correlations are simultaneous, particularly with 700 hPa divergence and vorticity. Being outside the tropics, Western Transvaal could be affected more by extra- tropical influences.

The correlations of Table 8.3 can also be viewed in terms of dry weather regimes, including the BUH. Features associated with the BUH have already been mentioned. For example, low- level divergence is negatively associated with rainfall over the region. When positive, it is accompanied by mid- level downward motion over the area (**Figure 8.5**) and upper convergence (negative divergence) at lag 0. The link with subsidence is not always direct and simultaneous; lags are also apparent at different locations of southern Africa.

8.6 Summary

Investigations of Chapter 8 and comparisons between dry and wet spell situations of Chapters 6 and 7 reveal the following over southern Africa :

- a low- level (700 hPa) anticlockwise system exists over western South Africa for dry spells compared to the west coast trough in November and the Mozambique Channel-Angola Trough (MCAT) from December till the end of the season during wet spells.

- Divergence and convergence at low levels and particularly over southern Africa exhibit contrasting features.

- Cyclonic flow at 700 hPa is further north (between 10 and 15°S) during dry spells than when convection is at its peak over the region (**Figure 6.2b**). This is due to the intensification of anticyclonicity over the central interior associated with the BUH.

- There is sinking motion in the middle levels (**Figure 8.5**) during dry spells as opposed to general uplift during wet events (**Figure 6.5a**).

- Upper convergence is located over eastern regions (particularly Zimbabwe and Mozambique) extending from the SWIO during dry spells. This could be the related to the Tropical upper tropospheric trough (TUTT) outlined by Lyons (1991).

- Differences in moisture sources and sinks are evident from low- tropospheric water vapour flux patterns. During dry spells, there is no meridional transfer of moisture from the equatorial regions to southern Africa, a characteristic feature of wet (convective) situations. The MCAT is the determining factor.

As mentioned in Chapter 4, minor dry spells exist during summer. However, these occur more as opposing phases of wet spells rather than overturning of the regional atmosphere associated with the BUH. The time series analysis of 500 hPa grid- point averaged geopotential height over Botswana as well as rainfall in Chapter 4 indicate that, at times, the minor spells do prolong their duration, resulting in intra- seasonal droughts. The transition is subtle and operationally unpredicable as yet. Correlation analyses of divergence, vorticity and geopotential height with rainfall in the region show there is some predictive potential, but the relationships are too complex to single out (coefficients are either low or are best at lag 0) at present.

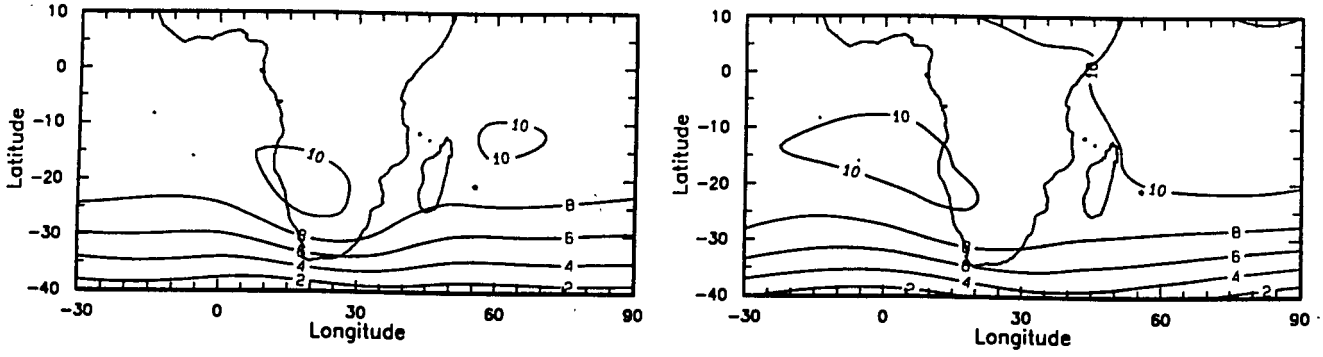

(a) Temperature (b)

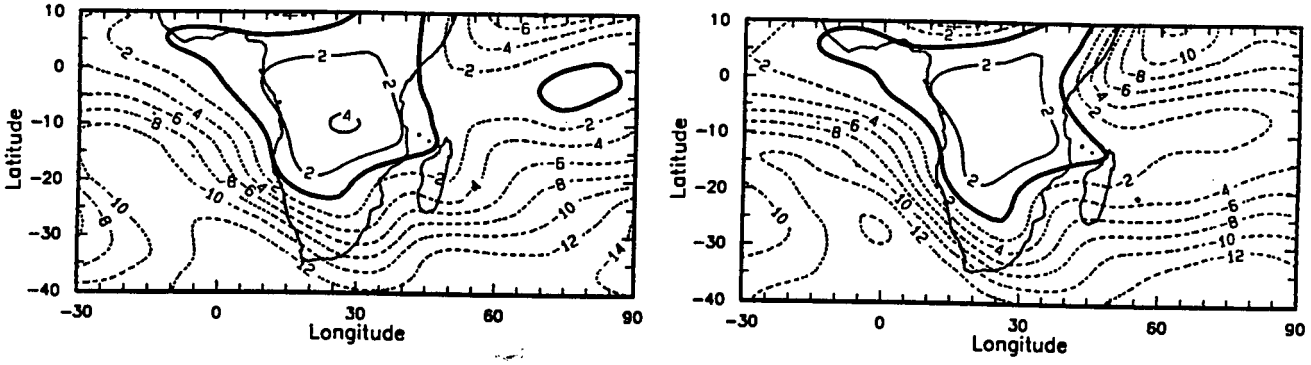

(a) Dew point (b)

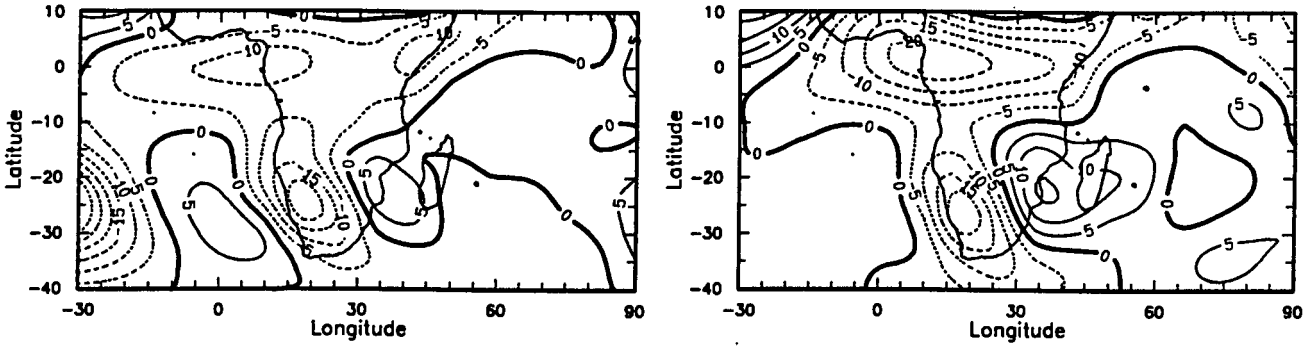

(a) Meridional temperature transport (*Tv*) (b)

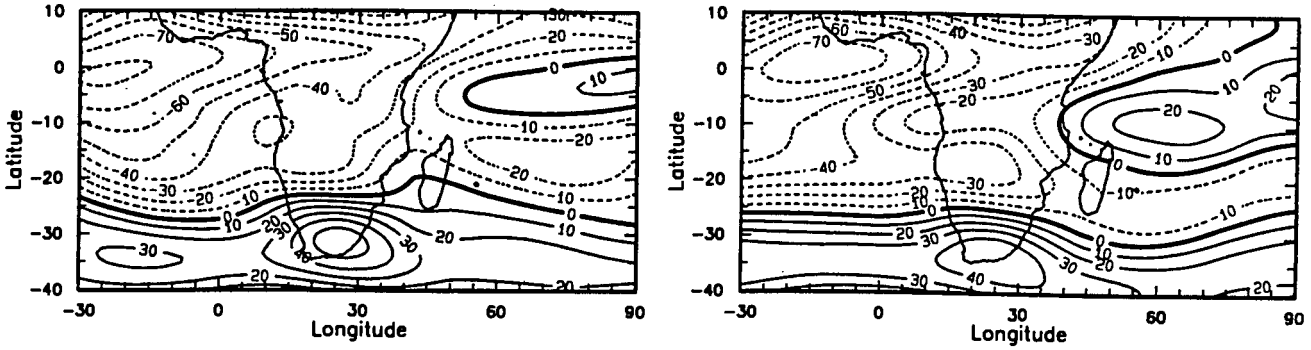

(a) Zonal temperature transport (*Tu*) (b)

Figure 8.1 : 700 hPa temperature (°C), dew point (°C), meridional and zonal temperature transports (°C m s^{-1}) for MSD (a) and LSD (b).

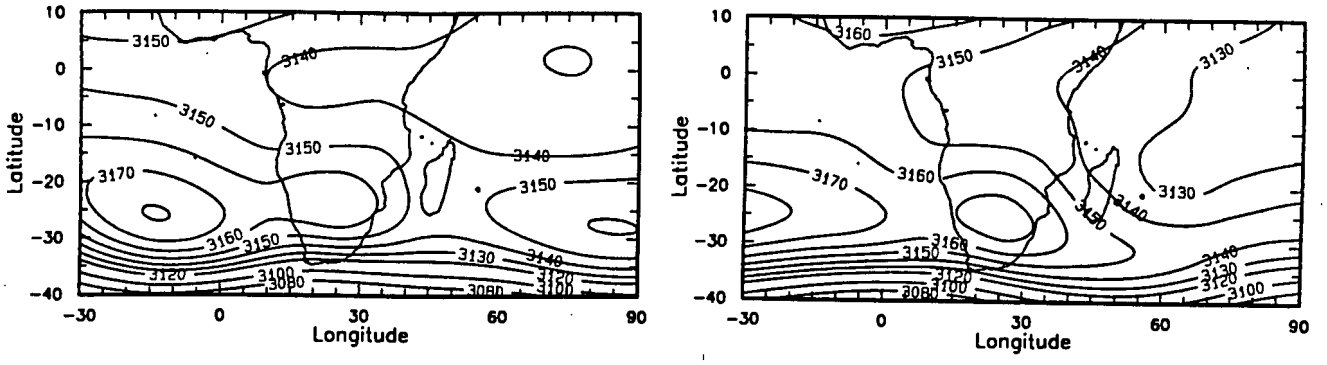

(a) Geopotential height (b)

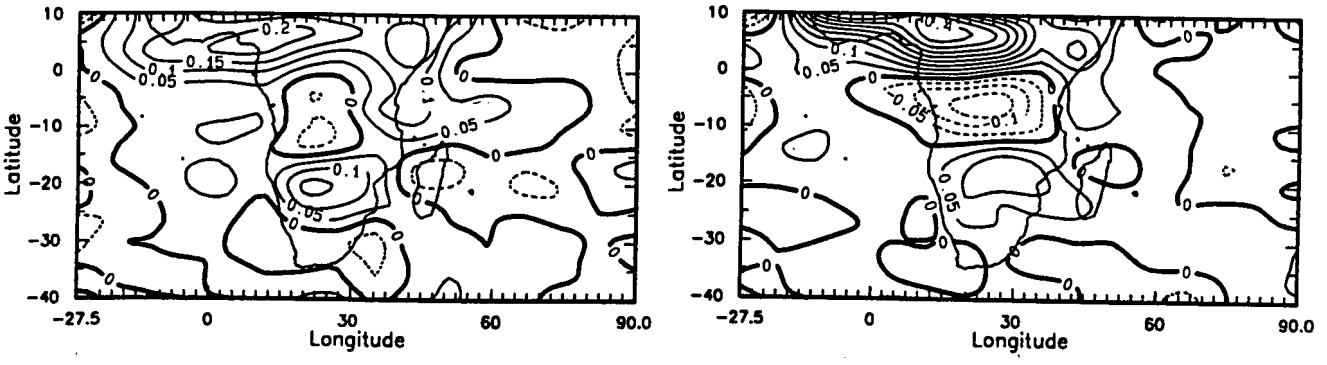

(a) Divergence (b)

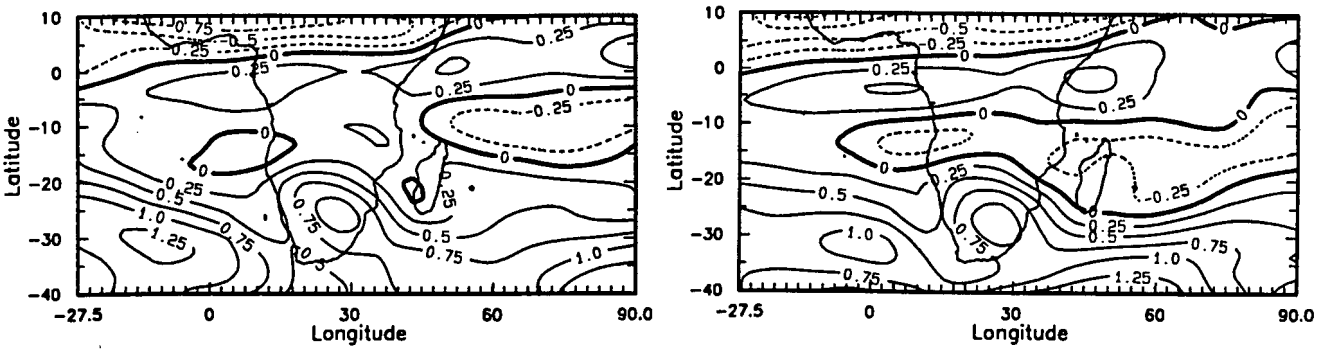

(a) Vorticity (b)

Figure 8.2 : 700 hPa geopotential height (gpm), divergence (x $10^{-5}s^{-1}$), vorticity (x $10^{-5}s^{-1}$) for MSD (a) and LSD (b).

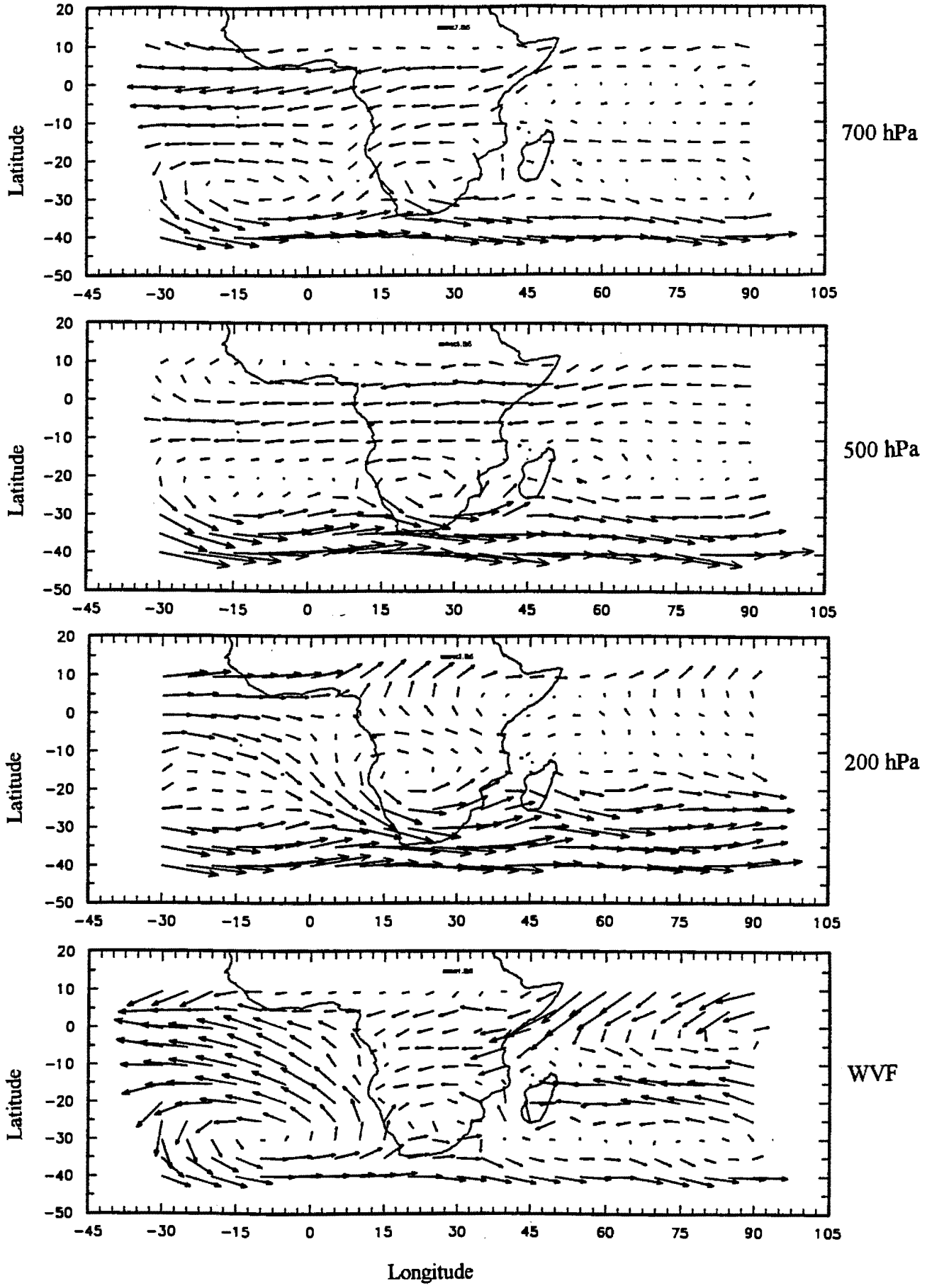

Figure 8.3 : MSD horizontal wind vectors at 700 hPa (a), 500 hPa (b) and 200 hPa (c) as well as vertically integrated water vapour flux (d).

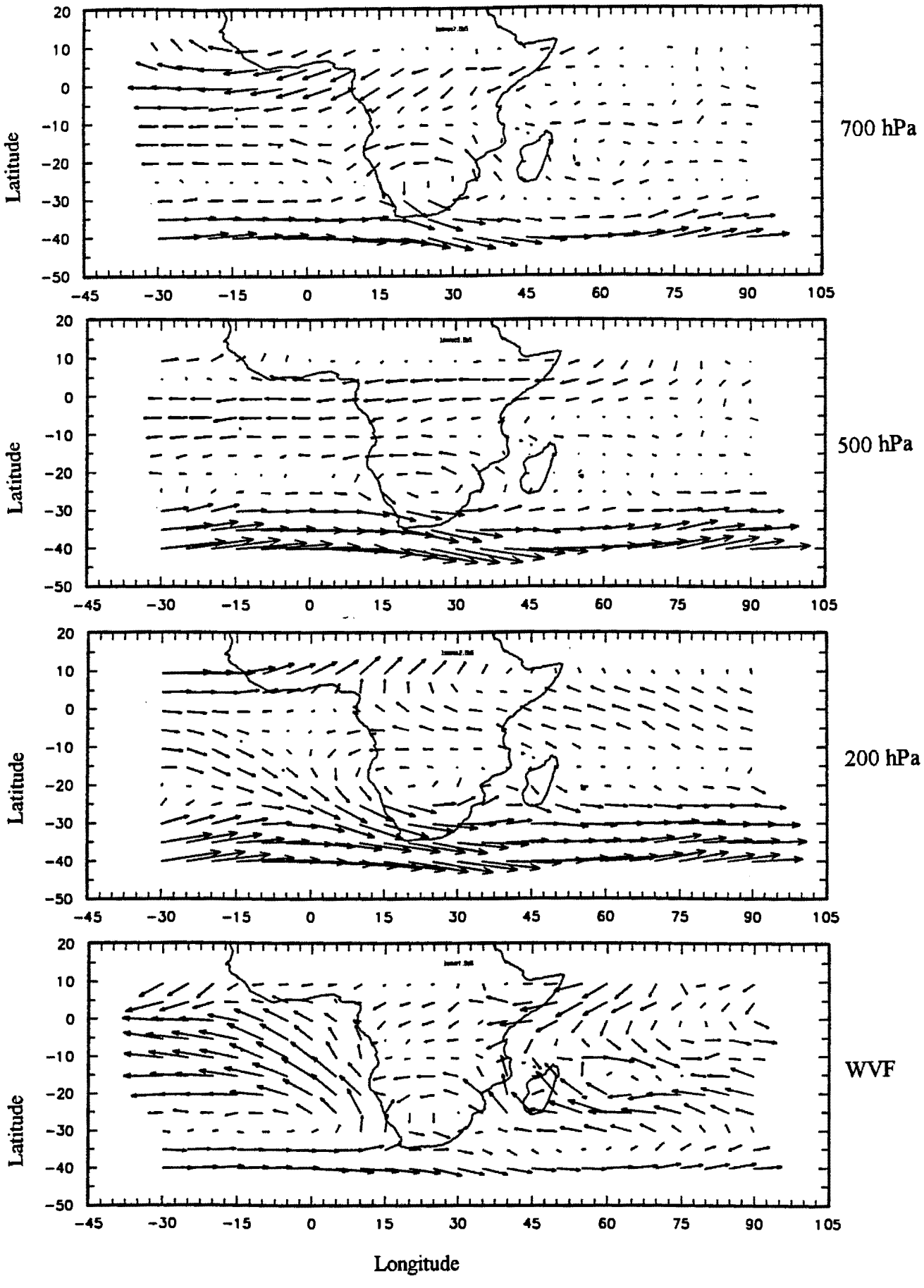

Figure 8.4 : LSD horizontal wind vectors at 700 hPa (a), 500 hPa (b) and 200 hPa (c) as well as vertically integrated water vapour flux (d).

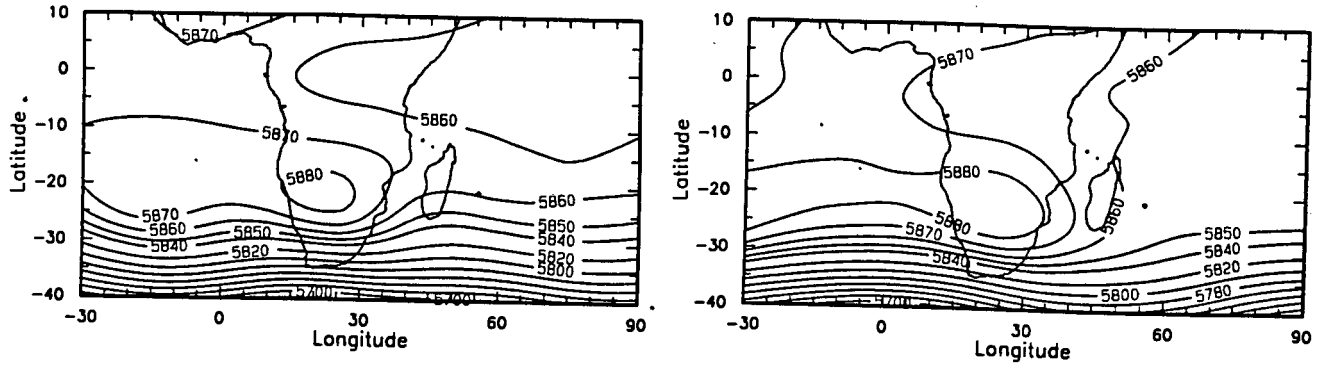

(a) Geopotential height (b)

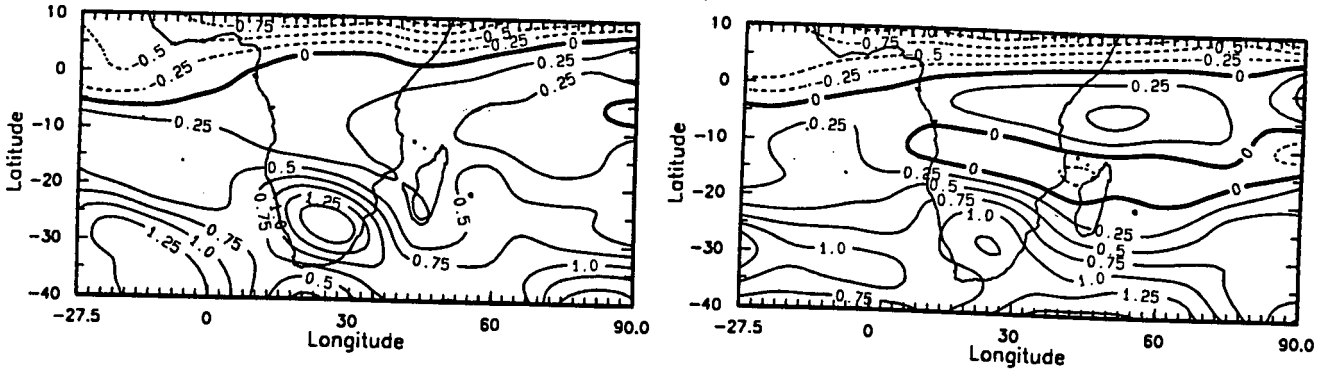

(a) Vorticity (b)

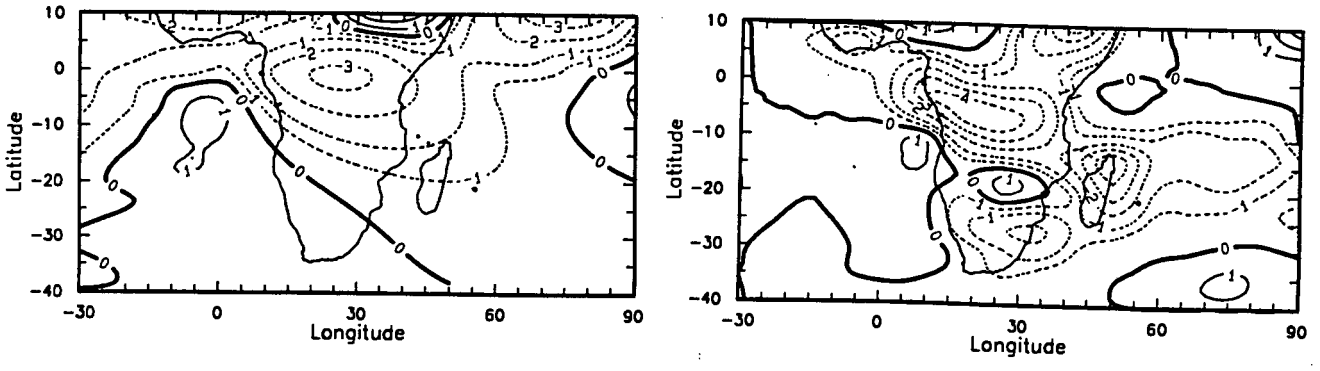

(a) Vertical velocity (b)

Figure 8.5 : 500 hPa geopotential height (gpm), vorticity (x $10^{-5} s^{-1}$) and vertical velocity (x 10^{-4} Pa s^{-1}) for MSD (a) and LSD (b).

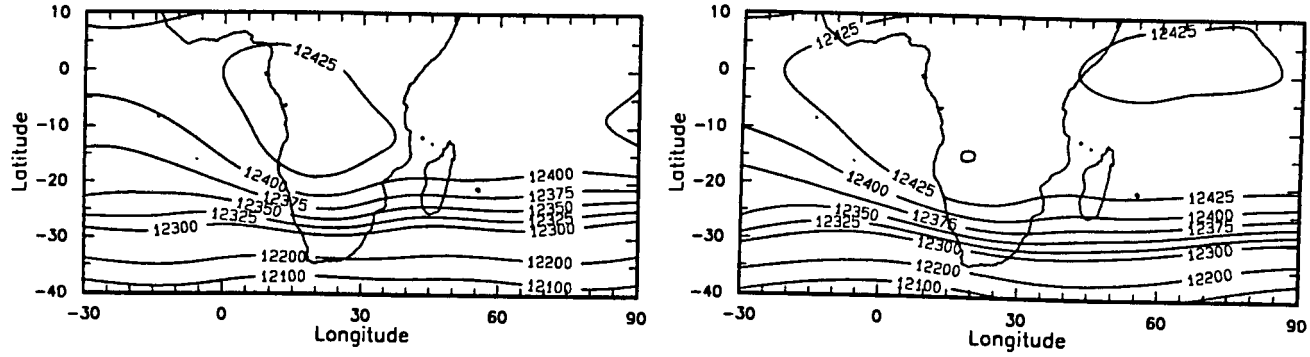

(a) Geopotential height (b)

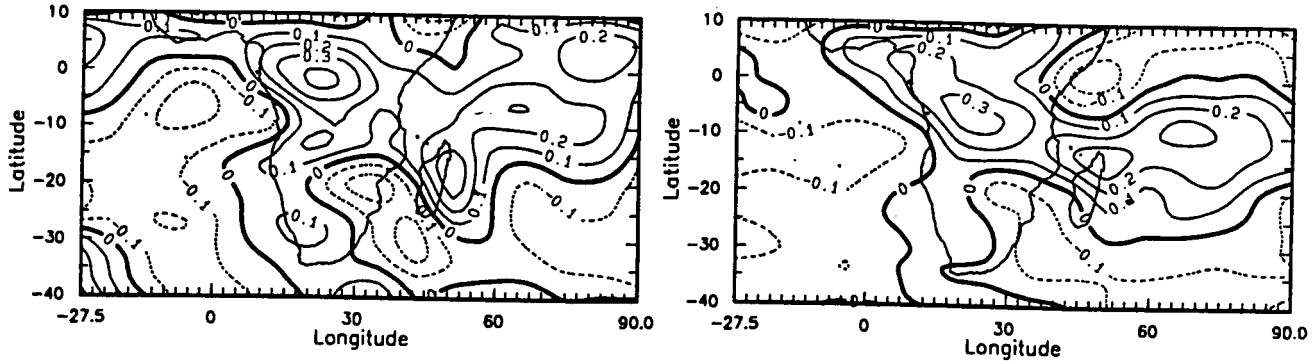

(a) Divergence (b)

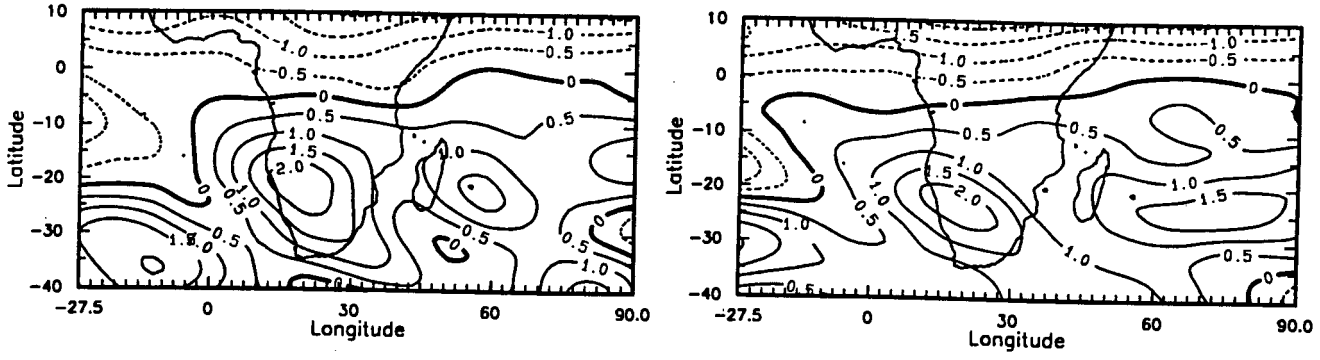

(a) Vorticity (b)

Figure 8.6 : 200 hPa geopotential height (gpm), divergence (x $10^{-5}s^{-1}$), vorticity (x $10^{-5}s^{-1}$) for MSD (a) and LSD (b).

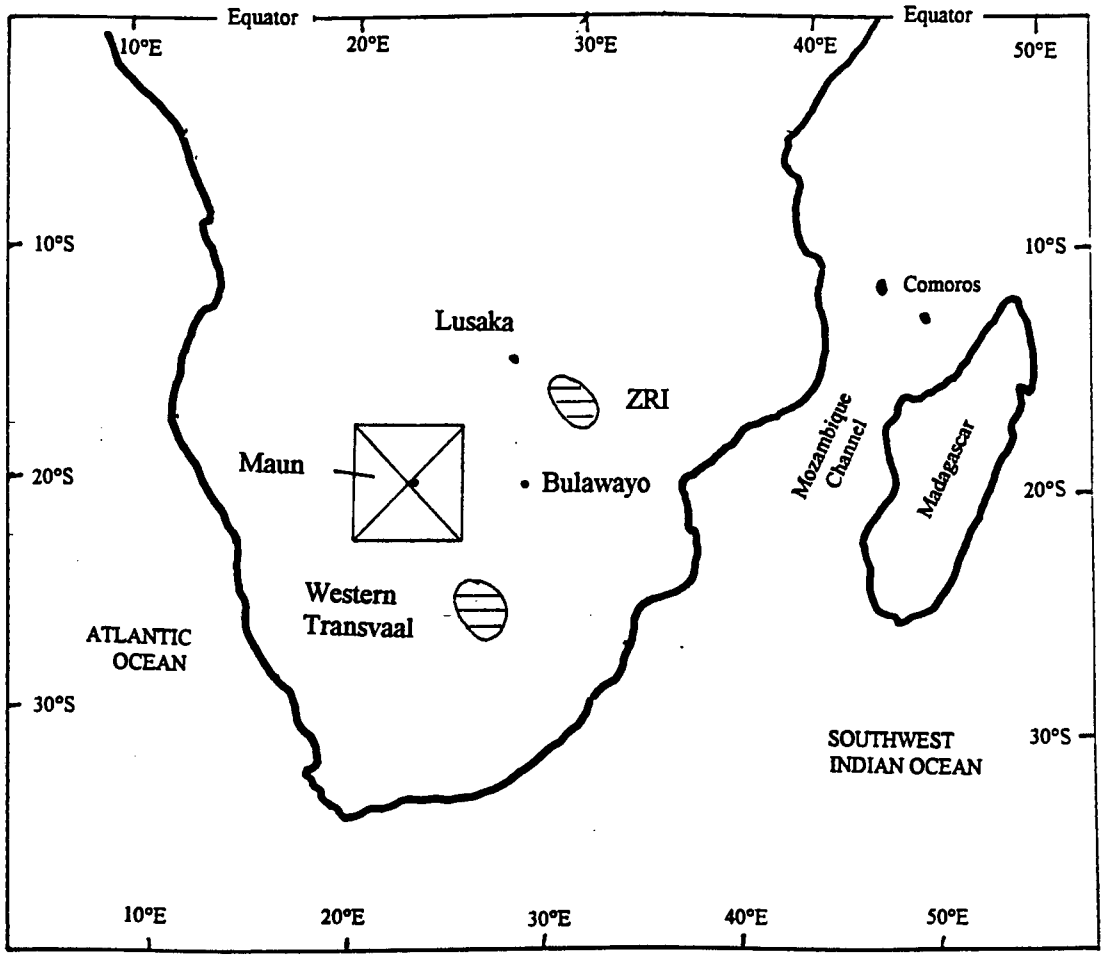

Figure 8.7 : Location of the 9 grid- point box and rainfall indices in the vicinity. The box is bounded by 17.5°S, 20°E and 22.5°S, 25°E (marked with a cross).

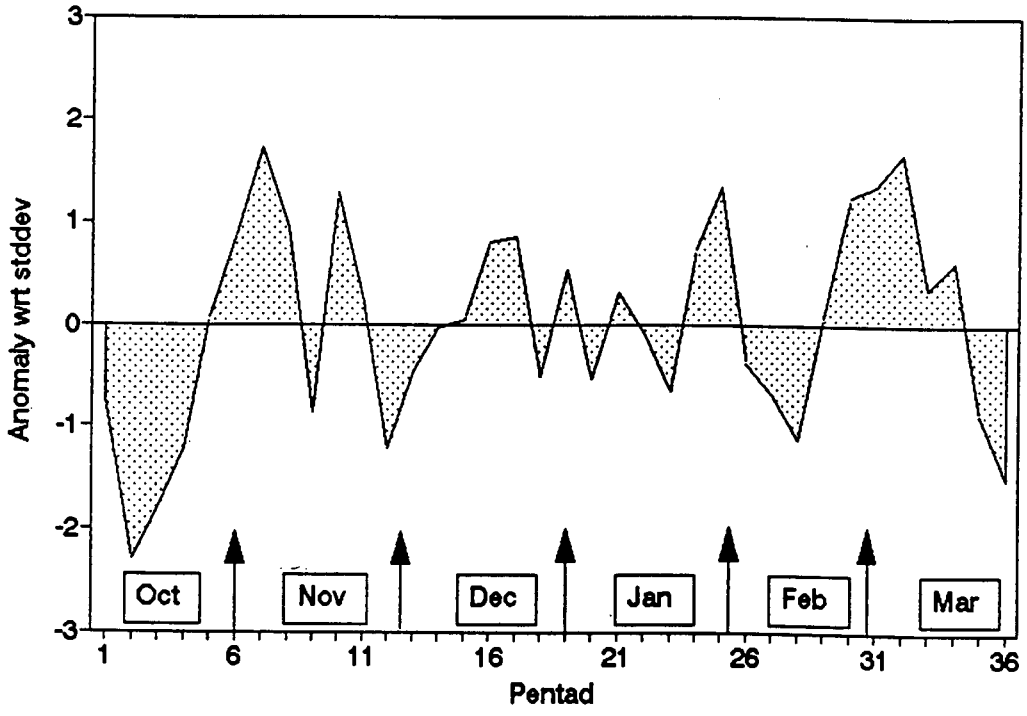

Figure 8.8 : Time series of 500 hPa mean pentad geopotential height (normalised with respect to the standard deviation) for box centred at 20°S, 22.5°E. Pentad 1 corresponds to 3-8 October and vertical arrow denotes month breaks.

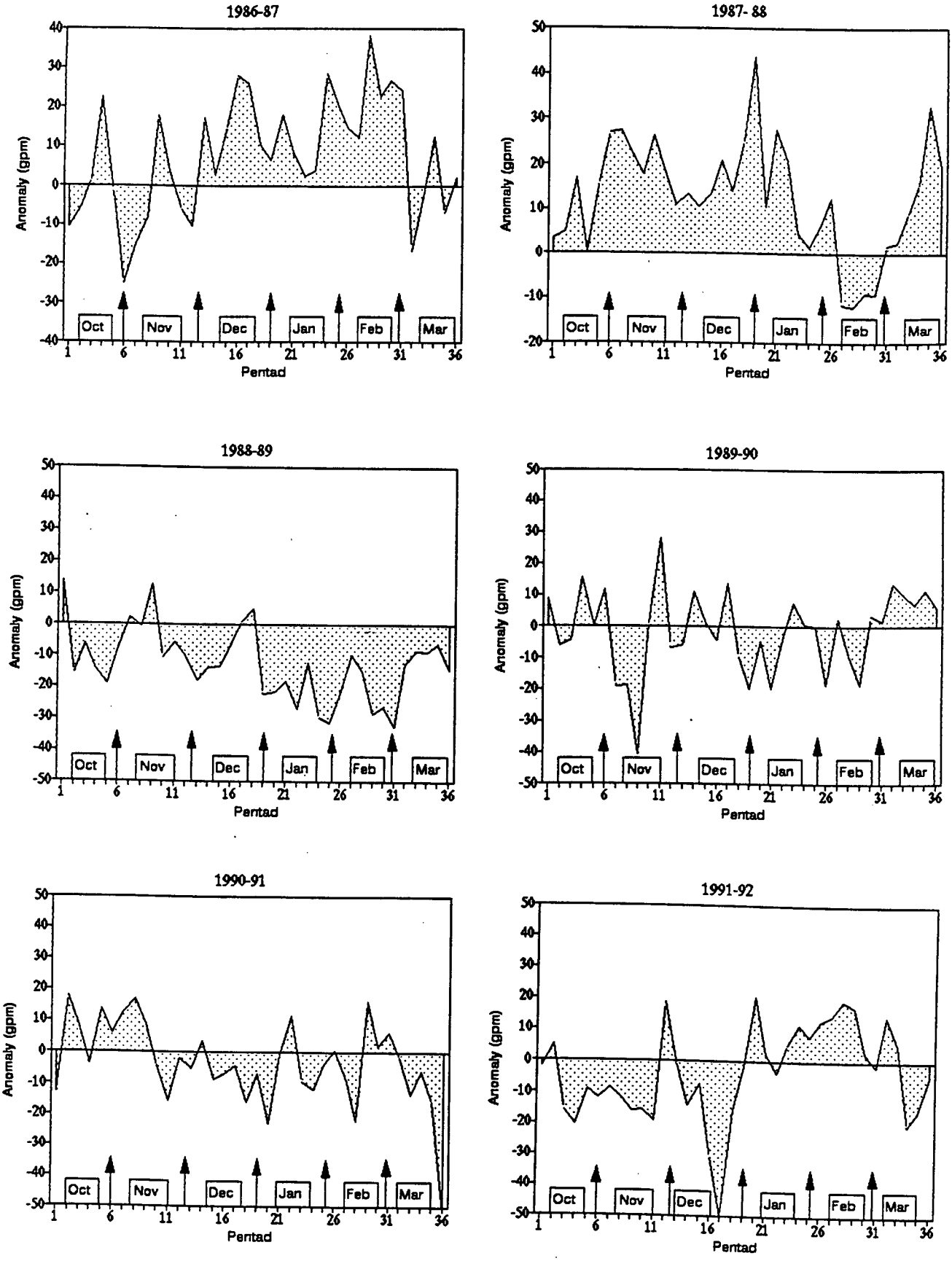

Figure 8.9 : Time series of 500 hPa pentad geopotential height seasonal departures from the 1986- 92 mean for box centred at 20°S, 22.5°E.
Pentad 1 corresponds to 3-8 October.

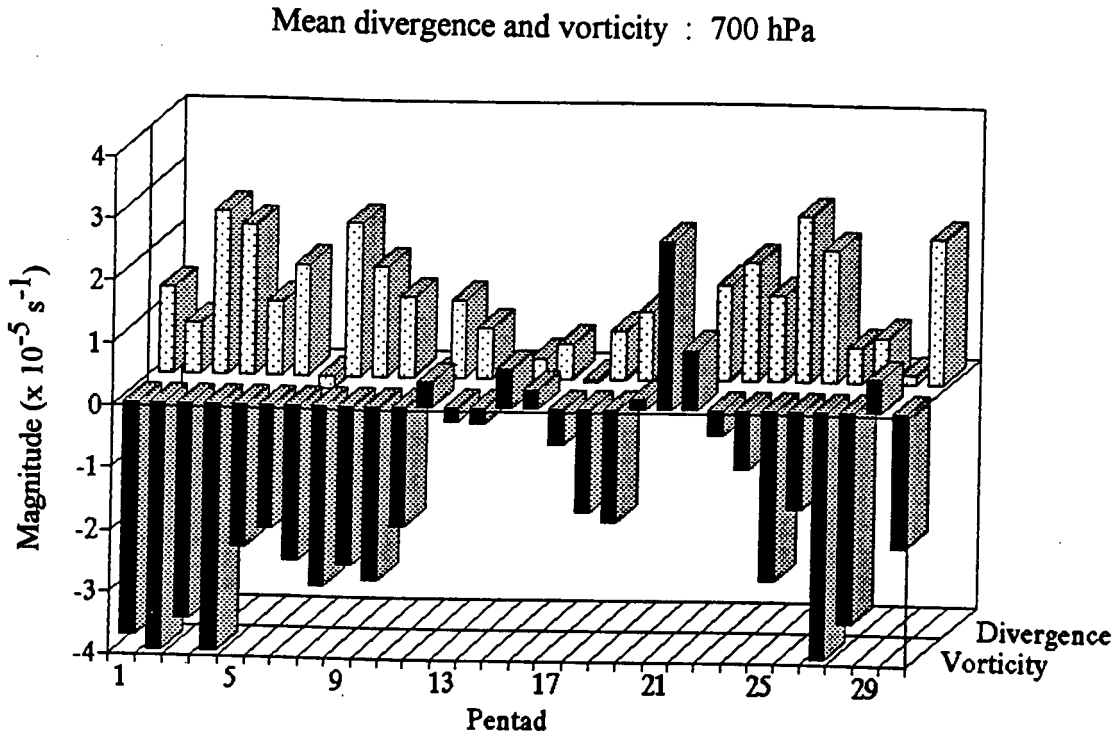

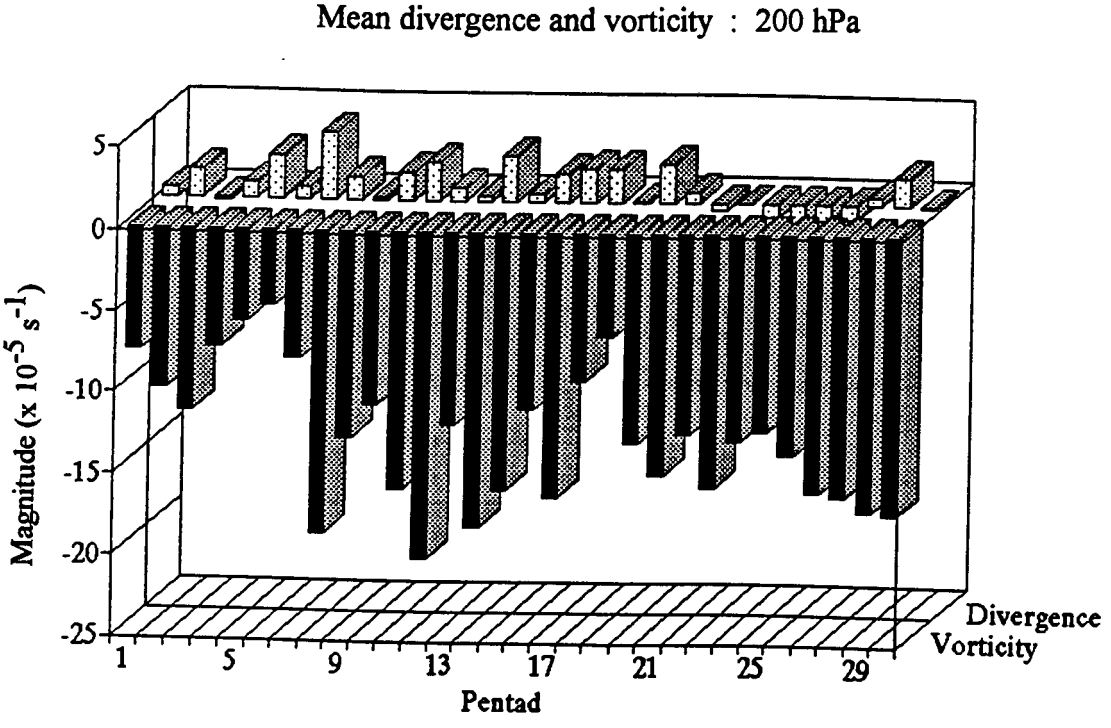

Figure 8.10 : Pentad 1986- 92 mean divergence and vorticity at 700 and 200 hPa for box centred at 20°S, 22.5°E. Pentad 1 in this case refers to 2-6 November period.

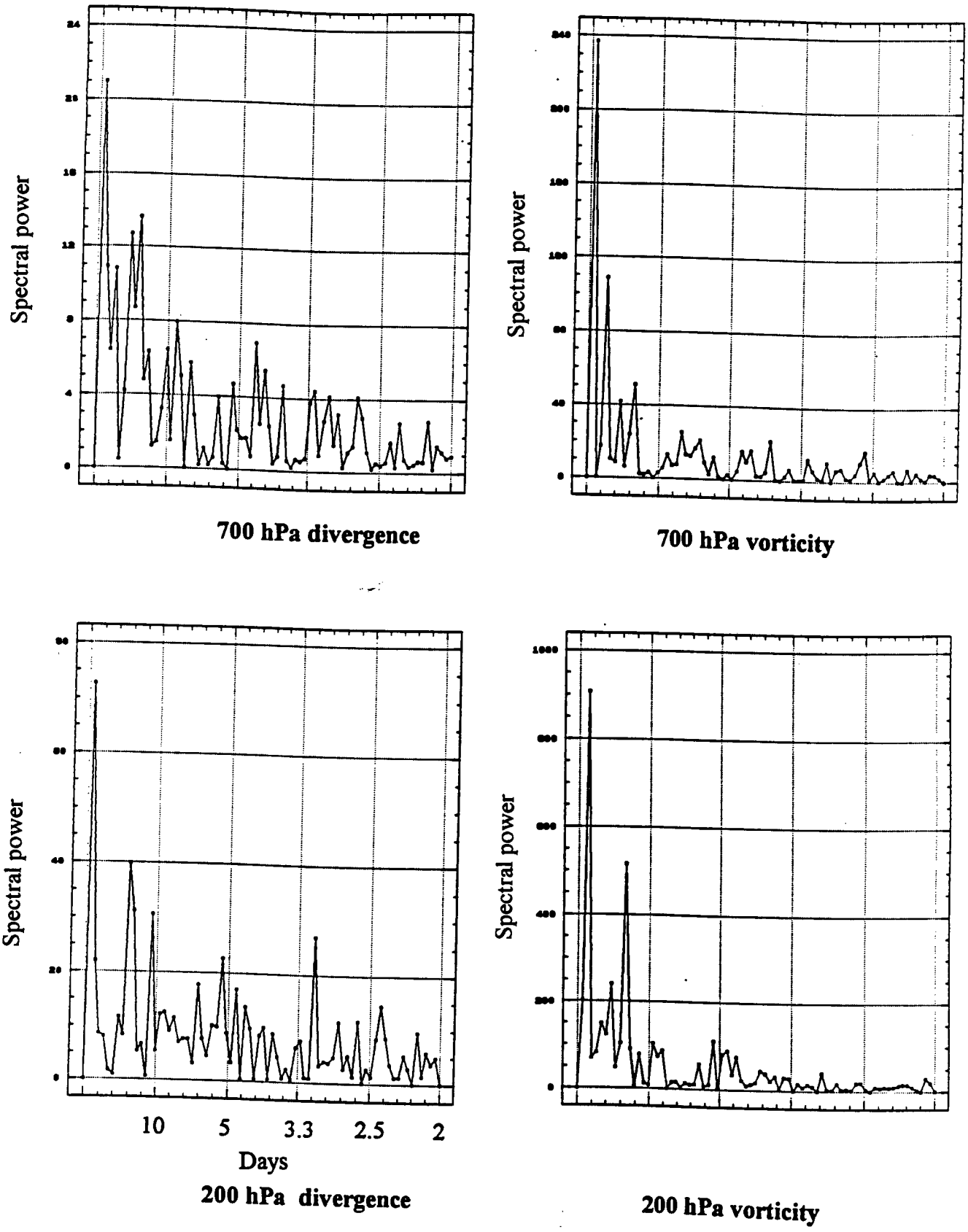

Figure 8.11 : A periodogram analysis of 700 and 200 hPa divergence and vorticity for box centred at 20°S, 22.5°E.

Chapter 9

Meteorological Characteristics along 20°S

9.1 Introduction

This chapter examines summer circulation patterns along 20°S. Chapters 5 through 7 have shown that the 20°S latitude is the demarcation zone between tropical and extra- tropical regions over southern Africa at 700 hPa. Referred to as the Tropical- Subtropical Boundary (or TSB), this zone is important in identifying transports of energy, temperature and moisture from the Equator to higher latitudes and vice versa. Harrison (1986) referred the 20°S latitude as the latitude where convection (hence heat and momentum) develops over southern Africa. More recently, Gutzler and Madden (1993) defined tropical regions as belts between 20.4°S and 20.4°N. The analysis is two pronged; to look at middle- and upper- level intra- seasonal propagation patterns in the horizontal from 1987 to 1992 summers. This is in the form of hovmoller plots (time versus longitude). The second stage involves analysing vertical sections during EFW and LSFW (first wet spells of early and late summer, respectively) as well as MSD (the mid- summer dry spell). The objective is to investigate the vertical structure as a function of time (20 day life cycles) for wet spells with respect to their phase in the summer season, features not readily identifiable from horizontal patterns.

9.2 Data and Methodology

The basic data are ECMWF 2.5° gridded data from October 1986 to March 1992 (temperature, wind - zonal and meridional, relative humidity and geopotential height) and derived products (divergence, vorticity, water vapour flux, precipitable water, specific humidity, stream function, velocity potential, etc.), and their anomalies. Each season is represented by pentad data from November to March, inclusive.

To examine characteristics along the TSB, a narrow band from 17.5 to 22.5°S is analysed from 30°W to 90°E at 500 hPa. A band is preferred, in this case, to a single latitude because eddy effects in the vicinity of 20°S may be identified better. Secondly, the TSB fluctuates about its mean position depending upon synoptic configuration. Here, only the geopotential height and horizontal winds (u- and v- components) are considered. The three can adequately describe characteristics or patterns at different phases of summer as they are central to transports and exchange of momentum, moisture and energy in the atmosphere. The final analyses are carried out in the form of anomalies (arithmetic differences from the 1987- 1992 mean).

For the vertical sections, life cycle stages of EFW and LSFW and composites of the MSD are selected. For wet phases, mean patterns of meteorological parameters and their derivative products (for, example equivalent potential temperature and divergence) are determined to establish background data for comparison. The means are determined from 1986- 92 base period using ECMWF data. Anomalies are then obtained, as in Chapter 7 of this thesis, as algebraic departures from the mean. As regards the MSD, actual parameters (not anomalies) are used. The analyses for all three phases are carried out for the entire domain. Interpretations are focussed upon the 20°S latitude band (the TSB). The vertical sections are analysed from the surface to 100 hPa between 30°W (27.5°W for divergence) and 90°E. Unlike for hovmollers, horizontal gradients through the troposphere along the TSB are too small for weighting functions to be instituted. Therefore, the 20°S latitude is considered to adequately represent the TSB.

9.3 Hovmoller analyses

9.3.1 Longitude versus time along 20°S

1986- 87

Figure 9.1 shows 500 hPa geopotential heights along the TSB from 1986- 87 to 1991- 92 summer seasons, inclusive. In the 1986- 87 summer, the most notable feature is a well-defined demarcation in the vicinity of 30°E longitude throughout summer. Over Africa, the heights were relatively low for most of November. They rapidly increased by up to 20 gpm in early December and remained steady for the remainder of the season, though the maximum heights were attained during the last third of February due to ridges surging in from the Atlantic Ocean. The patterns in the Indian Ocean were dominated by lower

heights throughout summer, the lowest being experienced from mid- November to early December. This period coincided with the EFW, the first wet spell of summer. Thereafter, they occasionally lowered over the Madagascar region every 10- 15 days until the middle of February. Further east near 80°E, a small but persistent ridge appeared from the end of January until the season ended. Thus, in general, apart from persistence, the systems were quasi- stationary with little horizontal displacement with time.

500 hPa zonal winds (**Figure 9.2a**) of the same season were predominantly westerly along the entire latitude at the beginning of summer and stronger in the eastern Indian Ocean. Easterly winds were in circulation across Africa, with a maximum in the central interior, for the whole of December. The easterlies dominated the Atlantic Ocean and Africa for most of late summer and were more intense on the African continent, and reaching a peak in the latter days of February. Elsewhere, the wind flow remained westerly except in the eastern Indian Ocean in January and February.

The meridional (*v*-) wind pattern in 1987 (**Figure 9.3**), like geopotential height, exhibited a standing wave- like structure virtually all summer. The season commenced with northerly flow over western southern Africa and southerly winds over the east. Southerly airflow dominated the circulation across the sub- continent, peaking in mid- December. In February, the pattern reverted to that during early summer with the Atlantic Ocean northerly winds affecting the west coast for the rest of the season. In the Indian Ocean, a narrow band of northerlies prevailed throughout summer, being between 40 and 60°E during early summer and east of 60°E in January before returning to earlier longitudes in the latter half of late summer. The overall pattern of meridional winds was a standing short wave (with a wavelength of about 45° longitude) throughout summer though with varying wavelengths and slight distortions.

1987- 88 summer

Geopotential heights at 500 hPa displayed the "demarcating" role of Africa, separating systems from the Atlantic and Indian Oceans. Compared to the previous year, there was more east- west movement. From November until the end of January, ridging from the Atlantic Ocean occurred with relatively high geopotential heights (ridges) over Africa during the second half of December. The ridges propagated westwards to the Atlantic Ocean thereafter. The declining trend continued, due to systems in the Indian Ocean which

were advancing steadily westwards, reaching a low in mid- February, when the systems travelled as far west as 10°W. From then on, the heights began to recover, reaching another peak in the middle of March.

Hovmollers of corresponding zonal winds show that the western half of southern Africa was under a westerly flow during early summer (November and December). The eastern half experienced a weak easterly wind. In January, the easterly circulation dominated the whole region from the Atlantic to the eastern Indian Ocean. Westerly winds developed in the eastern Indian Ocean at the beginning of February and began spreading westwards to just off the east coast of southern Africa in early March before receding. Meanwhile another area of westerly winds initiated in the eastern Atlantic and spread into western southern Africa until early March before retreating westwards. Thus, eastern southern Africa was under the influence of mid- level easterly winds throughout 1987/88.

Meridionally, northerly wind flow prevailed over the Atlantic and west coast of southern Africa in November. The flow rapidly spread eastwards in December across the continent to the Mozambique Channel (40°E). Thereafter, a band of southerly airflow began to propagate westwards to link with southerly winds which had formed in the Atlantic in early January. The subsequent pattern was a predominant southerly wind flow across southern Africa for most of late summer. Another band of northerly flow developed in the east Indian Ocean in December and propagated steadily westwards until it reached eastern regions of southern Africa in mid- February, remaining in effect until mid- March. The season as a whole was characterised by a short wave feature, similar to that in 1986/87, but only more defined in late summer. The pattern also indicates westward propagating systems with origins in the Indian Ocean, as seen in Jury et al. (1991).

1988- 89

During the 1988 summer, 500 hPa geopotential heights were in general lower than in the previous years. The patterns were similar, though with relatively higher values confined to the Atlantic Ocean. However, for just under a month from around 20 November the values were quite low over the Atlantic Ocean and central Africa, after which they recovered with one local maximum occurring over the sub- continent. From the end of December until the end of the season the heights changed little. Like during 1986- 87, values were lowest near 50°E, with minimum values recurring approximately every 45

days. The latter half of the season was under the Indian Ocean influence, substantiating earlier claims and observations regarding the role of the two oceans on the seasonality of southern African weather.

A standing short wave pattern of alternating southerly and northerly winds existed in the early summer with the former over the western half of southern Africa (Namibia and Botswana) and the latter covering the other half. The northerly component strengthened and then dominated in early December due to a merger with northerlies in the Indian Ocean centred near 50°E. In the meantime, southerly winds developed just off the west coast in early December and remained confined to the ocean up to the end of December after which they linked over southern Africa with another band that had initiated in the Indian Ocean in the Mozambique Channel. During this period, a westerly wind regime prevailed over the whole region and persisted until the middle of January in the Indian Ocean. The 500 hPa southerly flow remained over southern Africa until the end of January when northerly winds prevailed. There was a surge of southerlies from the Atlantic Ocean during most of February. At the same time, the circulation was predominantly easterly everywhere, except between 40 and 50°E from the beginning of February until mid-March. Also in March, the whole region from Namibia to Madagascar was under the influence of northerly (poleward) air flow.

1989-90

In the 1989 summer, the Atlantic Ocean played a more dominating role over southern Africa than the Indian Ocean, with ridges surging across southern Africa nearly every 45 days; in the middle of December, end of January and mid- March (**Figure 9.1**). Geopotential height patterns in the Indian Ocean were relatively passive, rarely penetrating beyond the east coast of Africa. The impact was most effective in February, reaching a peak between the 20th and 25th, when a trough system was building up in the proximity of Madagascar. In general, the lowest geopotential heights were in the vicinity of 50°E and displayed a cycle of approximately 45 days.

Zonal flow was westerly along the entire domain in early summer. Taking cognisance of the mid- level circulation over southern Africa, the westerly component suggests sub-tropical influence beyond the TSB until mid- December across the Atlantic and Africa, and until mid- January in the eastern Indian Ocean. Easterly winds prevailed over southern

Africa from mid- December to the end of January (reaching a relative peak in early January) before retreating to the Atlantic. The configuration typifies anticyclonic ridging from the Atlantic Ocean in such a manner that the easterlies are on the equatorward side of the axis of maximum anticylonicity. The flow in the Indian Ocean was predominantly westerly during late summer, peaking in February and spreading westwards to reach the Atlantic Ocean by the end of the month. The seasonal pattern fits well with observations that subtropical westerly wave action dominates early summer climate variability over southern Africa, a mid- summer drying follows and simultaneously represents a transition to late summer when the Indian Ocean exerts greater impact.

The *v*- wind component shows northerly flow over the Atlantic Ocean and southerly winds over southern Africa in November and December. The southerly circulation originated in the Indian Ocean and propagated towards southern Africa. In January, light winds prevailed over the subcontinent with opposing flow on either side of an anticyclone (northerly in the east and southerly in the west). From February till the end of the season a standing wave structure was established across the domain, with northerly airflow persisting over Namibia and Botswana and a band of southerlies occurring from eastern southern Africa to 60-65°E longitudes.

1990- 91

The beginning of summer until about mid- December closely resembled that during 1988- 89 when lowest geopotential heights prevailed simultaneously over the Atlantic as well as the Indian Ocean. There was a westward propagation of low heights in the Indian Ocean, however, reaching the longitudes of Madagascar at the end of December. In early January an anticyclone developed in the Atlantic Ocean and gradually spread to cover most of southern Africa by early March, before receding.

The zonal wind pattern also closely resembled that of 1988- 89 except towards the end of the season. Thus, the season commenced with westerly winds along the whole latitude. The easterly winds over southern Africa began a few days earlier compared to 1988- 89 and spread outwards to dominate the region from the Atlantic to the eastern Indian Ocean by early January. The circulation pattern remained thus until early March when the

westerly winds which had initiated in the east Indian Ocean in late February rapidly spread westwards to the Atlantic by mid- March.

The v- wind hovmollers show the existence of a short wave in November, with wavelength of about 40° longitude. The meridional winds were relatively strong. The systems in the Atlantic Ocean propagated slowly eastwards resulting in northerly winds dominating southern Africa in early December. Soon after, the winds over the continent shifted to southerly beginning on the east coast. Southerlies traversed the continent steadily westwards to the Atlantic Ocean and were replaced over Africa by another band of northerly flow from early January to mid- February. The southerlies in the Atlantic then spread back across southern Africa. Thus, northerly winds temporarily prevailed over all but the extreme east of southern Africa in the first half of March, before giving in to southerly winds. The overall pattern of 1990- 91 was a standing wave at the onset of summer, followed by westward- propagation from early December until mid- February after which the pattern reverted to standing mode with an irregular wavelength. The standing wave was virtually uninterrupted throughout summer in the Indian Ocean, such that the circulation changed little. Only the wavelength varied significantly. At the same time over southern Africa, the winds alternated at irregular intervals (northerly winds generally persisting relatively longer). This was mainly a result of alternating oceanic influences as well as long waves in the subtropical westerlies.

1991- 92

In the 1991 summer, the season commenced with the Atlantic Ocean Anticyclone (AOA) maintaining a ridge into southern Africa until the end of November. Low heights rapidly spread from the eastern Indian Ocean into Africa in December, the lowest located east of Madagascar. The AOA re-developed and established itself over most of the sub-continent till about 20 March. Meanwhile in the Indian Ocean, intra-seasonal oscillations of approximately 45 days were apparent. The overall pattern was similar to that in 1986/87, another El Niño year, as identified by persistent ridging from the Atlantic Ocean in late summer. Distinct intra- seasonal oscillations were only evident in the Indian Ocean in both years, although they were of a higher frequency in 1986- 87.

As illustrated from geopotential height, the 500 hPa zonal wind hovmoller patterns were similar to those in 1987 summer. The flow was mainly strong westerly across the region

in November and December. The winds then changed to easterly over Africa and the Atlantic and persisted over the continent up to mid- March, having attained a maximum in early and late February and early March. Intra- seasonal oscillations of about 15- 20 days were detected. In the Indian ocean, westerly airflow remained in circulation throughout 1991- 92. In mid- March, the flow merged with the other westerly regime that had developed in the eastern Atlantic in early February.

The corresponding 500 hPa meridional flow over southern Africa consisted of northerlies in the west and southerlies over the east for most of summer. Southerly winds, briefly dominated the sub- continent from the end of December until mid- January. This was a period when the Atlantic and Indian Oceans were linked. From January until the end of the season, strong southerly airflow dominated most of southern Africa (reaching a maximum in early February). Thus, an anti- clockwise circulation was sustained over southern Africa, reinforcement coming from the Atlantic Ocean and return flow (with a southerly component) occurring mainly across Zimbabwe and Mozambique.

9.3.2 Summary of hovmollers

In the period under study, the following can be inferred from hovmoller analyses:

- The Atlantic Ocean is responsible for higher geopotential heights over southern Africa, particularly across sub- tropical areas. The Indian Ocean, on the other hand, is a source of relatively lower values and affects mainly tropical regions of the sub-continent. At 500 hPa, the Indian Ocean Anticyclone is ineffective as far north as 20° S. The tropical Indian Ocean exerts greater control in late summer.

- Intra- seasonal oscillations can be inferred. A periodicity of approximately 45 days (1987, 1990 and 1992) signifies the Madden Julian Oscillation (Madden Julian, 1972), which is identified from 500 hPa geopotential heights. In addition, 15-20 day oscillations were detected in the mid- level zonal winds. These findings are consistent with ISOs detected in rainfall patterns (frequencies of wet and dry spells) in Chapter 4.

- Meridional wind plots reveal a standing short- wave at the beginning (November) and end (March) of summer. The wave is also apparent in the zonal wind and geopotential height patterns but less intense. The meridional wind plots also show very little east-west propagation, except in the 1987- 88 summer. Worthy of note are predominant southerly winds over southern Africa, with maxima occurring usually at the end of December and February. These are also accompanied by easterly winds. The combination is strongly indicative of the Botwana Upper High. In all but 1987- 88 and 1990- 91, and particularly 1986-87 and 1991-92 years, the meridional flow over southern Africa is generally southerly, a relatively stable situation in the mid- levels.

- There is little interaction between the Atlantic and Indian Ocean during summer, evidenced by the 500 hPa geopotential height which exhibits this for almost all seasons. The African continent acts to dampen propagation from either oceanic region. The Atlantic Ocean rarely extends a ridge beyond the east coast of Africa (beyond 30° E). When the Indian Ocean systems penetrate southern Africa, the extent is usually as far as eastern areas (Mozambique and Zimbabwe). Thus, the "cut- off" in the region of 30°E determines the intensity and spatial influence of synoptic weather regimes during different phases of summer. Futher investigations in the vicinity of this zone are necessary as the study may help in explaining why eastern and western parts of southern Africa are sometimes under different weather systems.

- The similarities in the 1987 and 1992 summers could be more than a coincidence. Both were El Niño years, associated with prolonged dry spells over southern Africa during which easterly winds were predominant in late summer. The overall zonal wind patterns resembled those of geopotential heights, with regions of relative high geopotential height being regions of strong easterlies. Thus, dry weather conditions over southern Africa in the middle levels are associated with relatively high geopotential heights and attendant subsident east-southeasterly winds (see also Figure 8.3). The easterly flow Cross- correlations between geopotential height and rainfall in the region (Chapter 8) confirm this relationship. Another important finding is that the easterlies did not extend eastwards into the Indian Ocean. Instead, westerlies prevailed in the Indian Ocean throughout the season, implying advection of moisture eastward across the Indian Ocean, at least in the latitude of the TSB at 500 hPa.

9.4 E-W vertical sections along 20°S

Vertical sections describe tropospheric structure and, together with horizontal circulations, provide a 3-D perspective. Previous chapters of this thesis, beginning with Chapter 5, have concentrated on mainly three standard levels of the troposphere (700, 500 and 200 hPa). While they adequately described horizontal circulations and structures, they could not determine the vertical extent of some of the systems, hence this section. Vertical sections over southern Africa have been studied in detail by Harangozo (1989) using monthly data. The meteorological means in this thesis are based upon daily data, decomposed to pentad analyses. This analysis considers life cycles of wet spells over southern Africa. In this section, only life cycles of EFW, LSFW and MSD composites are investigated, to compliment horizontal patterns described in Chapters 7 and 8.

9.4.1 Mean patterns

Figure 9.4 exhibits vertical sections between 1000- 100 hPa along 20°S of mean meridional wind, zonal wind, equivalent potential temperature and horizontal divergence for EFW and LSFW. The cross- section extends from 30°W to 90°E and from 27.5°W to 90°E in the case of divergence. EFW and LSFW time composites are formulated as outlined in **Table 4.5** for life cycles and **Table 5.1** for period- mean analysis. The analyses are an extension of Chapters 5 and 7.

Mean v- wind

In the mean, the *v*- (meridional) wind shows a zone of southerly wind exists between 1000 and 500 hPa over the eastern Atlantic Ocean and Africa during EFW. The southerlies decrease eastwards with height to dissipate over eastern southern Africa. Higher up, northerlies prevail and the overall configuration is indicative of a Hadley type of circulation. The pattern reverses between 30 and 50°E (Mozambique- Madagascar longitudes) with middle and upper southerlies overlying lower tropospheric northerlies. Northerly flow covers all but the surface until 70°E where southerly winds extend vertically from the surface, reaching the eastern Indian Ocean at 200 hPa. Worthy of note, also, are upper patterns alternating at near- regular intervals at 200 hPa. The wavelength is approximately 25° longitude. In late summer (LSFW), southerly winds dominate the lower half of the troposphere from 20°W to 20°E (except between 800 and 600 hPa over

Namibia). They are weak from 20 to 40°E. Relatively weak northerlies dominate the Indian Ocean. The "Hadley cell" structure also exists at LSFW but also over the Indian Ocean. Unlike at EFW, the mean meridional wind at LSFW indicates a clear- cut demarcation at about 40°E throughout the troposphere, separating southerly winds over Africa from northerlies over the Indian Ocean. Another observation is that the Atlantic Ocean Anticyclone is strong and quasi- stationary whereas the Indian Ocean Anticyclone is detected east of 70°E (rather too far east to have an impact over Africa) and is weaker during late summer.

Mean u- wind

Zonally, both EFW and LSFW patterns indicate easterly flow in the low levels and westerlies aloft. The easterlies at EFW are shallower than those during LSFW by between 150 and 300 hPa. The upper tropospheric jet stream is also evident with a core in the vicinity of 200 hPa. The jet is much stronger in early summer and strongest over the eastern Indian Ocean. This is to be expected since the atmosphere is more barotropic during late summer. The low level easterlies along the TSB are consistent with mean horizontal circulation patterns of Chapter 5 (**Figure 5.2b**) and are an integral part of tropical features (Harrison, 1986). The westerly component along the boundary increases with height and in an eastward direction (manifested by the LSFW pattern). Upper westerlies are about half as strong in LSFW compared to EFW.

Horizontal divergence

Divergence, in addition to identifying regions of mass convergence and divergence, indicate areas of rising and subsiding motion (hence stability) and, depending upon moisture availability, can be used to infer potential convective situations. The mean divergence pattern during both EFW and LSFW show divergence in the low- levels over the Atlantic Ocean (associated with the Atlantic Ocean Anticyclone) and middle and upper convergence. Divergence spreads with height towards Africa and reaches 100 hPa near 15°E. There are differences between the two wet spells over Africa where the air remains divergent as far east as 45°E during EFW. For LSFW, however, the motion is convergent over Africa below 700 hPa. The mean flows in the Indian Ocean are similar, with low-tropospheric convergence and upper divergence. In both phases, the greatest convergence in the low- levels is over eastern Madagascar. Thus, as far as southern Africa is concerned, the atmosphere is less favourable for convective events, and is "reluctant" to precipitate in

EFW. In late summer, however, the mean pattern indicates a potentially unstable configuration conducive for convection.

Equivalent potential temperature (EPT)

Being a quasi- conservative parameter, EPT is used to monitor atmospheric moisture content, mixing depth and atmospheric stability. **Annexure 2** contains more details pertaining to the manner θ_e is calculated. Holton (1973) and Bolton (1980) are also useful references. Mean EPT patterns during EFW and LSFW phases are similar in that, firstly, temperatures decrease from the surface to around 700 hPa after which they increase with height. This is more apparent over oceanic regions. Below 700 hPa, temperatures are markedly higher over Africa, especially over western southern Africa, largely due elevated sensible heat fluxes. Although the 800- 600 hPa layer typically contains high water vapour content, the EPT analysis identifies this as a minimum. The layer acts to "erode" convection, particularly over the Atlantic at this latitude. Below 500 hPa, LSFW temperatures are warmer than at EFW everywhere along the TSB, due to increased surface heating, evaporative fluxes and mixing. The Indian Ocean is also warmer than the Atlantic in both phases. Higher up, the rapid increase in EPT is due to relatively more stable conditions and temperature inversions at the tropopause.

9.4.2 Anomaly patterns for EFW and LSFW

This section discusses life cycles of EFW and LSFW in the form of anomalies (departures from long- term period mean) using the pentad time frame P-2 to P+1 as before.

meridional wind anomalies (v')

Figure 9.5 indicates the vertical profile of v- wind. Negative (positive) wind anomalies suggest northerly (southerly) wind tendencies. Anomalies during the evolution of EFW show a northerly anomaly in the upper troposphere over the Atlantic Ocean. The anomalies slant eastwards with decreasing height to reach 850 hPa in the longitudes of Mozambique (near 35°E). Another band of negative anomalies exists over the Indian Ocean above 300 hPa. Elsewhere, southerly winds prevail. Throughout the domain, the strongest anomalies are near 200 hPa. Five days later (P-1), anomalies alternate quasi-

regularly as evidenced by local maxima at 200 hPa every 30- 40 longitude degrees which are vertically oriented. At maturity (P0), the meridional wind anomalies are almost a reversal of those at P-1. The structure is still vertically aligned. Negative anomalies cover the Atlantic Ocean while positive anomalies extend from 10°W to 20°E except in the lowest layers. The negative (poleward) anomalies again dominate the Indian Ocean except between 60 and 80°E. By the time EFW dissipates (P+1), the alternate pattern of positive and negative anomalies is confined to the upper troposphere, with the anomaly signs a reversal of those at P-1. Northward wind anomalies in the eastern Atlantic Ocean (from about 15°W to 5°E) tilt slightly westwards towards the surface. Upper- level poleward anomalies over Africa and the West Indian Ocean tilt eastwards to reach the surface in the Mozambique Channel. Of significance is the meridonal components of the upper- level jet which remains in evidence throughout the 20- day period. This jet is weakest at the maturity of EFW. A prominent feature is the eastward migration of upper poleward flow from the Atlantic to the Indian Ocean during the sequence.

LSFW meridional patterns are displayed in **Figure 9.5b**. There are more differences than similarities between meridional wind vertical profiles of EFW and LSFW. P-2 patterns of LSFW show southerly wind anomalies dominating the Atlantic and Africa while weak northerlies prevail over the Indian Ocean. The patterns are more organised at P-1 (as during early summer at the same stage) indicating alternating bands of positive and negative anomalies all extending from the upper tropospheric levels to the surface. There is also evidence of slight westward tilt with height. Negative anomalies lie between 20 and 55°E from the surface until 650 hPa before narrowing and shifting westwards by about 20° longitude. The core of maximum negative anomalies is at 200 hPa, along with other centres along the entire latitude from 30°W to 90°E. The alternating pattern is maintained at P0 over the Atlantic and Africa. However, negative anomalies in the Atlantic have advanced eastwards. At the same time in the Indian Ocean, the patterns have also shifted westwards. The overall process results in larger gradients between 15 and 60°E, hence upper anticyclonic flow over eastern southern Africa and Madagascar. This atmospheric structure reverses during decay with the systems having progressed eastwards by about 30° longitude. The flow over southern Africa is divided, with the western regions under a southerly anomaly and the eastern areas under northerly wind anomalies. Thus, when the cycle comes to an end, a clockwise circulation develops over the sub- region and covers the lower troposphere.

Zonal wind anomalies (u')

EFW patterns at P-2 (**Figure 9.6a**) show easterly anomalies dominating the patterns, leaving only upper levels over the Atlantic and the whole of the eastern Indian Ocean experiencing westerly wind anomalies. The core of maximum easterlies tilts SE from 200 hPa over Africa towards the Indian Ocean. During development (P-1), an alternating pattern is again evident. Maximum negative anomalies are at 500 hPa at 30°E (Zimbabwe). During maturity (P0), the pattern is dominated by positive (westerly) wind anomalies which extend from 5°E eastwards. In the Atlantic Ocean, a narrow band of negative anomalies exists near the Greenwich at all levels. At dissipation, the anomalies are a near- complete reversal of those at P-2, with easterly anomalies dominating the Atlantic Ocean and middle and upper levels over the Indian Ocean. At during P-2, there is evidence of westward tilt with height over Africa and the Indian Ocean.

LSFW zonal wind anomalies differ from those of EFW. In the formative dry stages of LSFW, anomalous upper westerly winds are dominant. Easterly anomalies are shallow and relatively weak, confined to the lower troposphere over the Atlantic and Africa. Another region of negative anomalies exists from the middle levels upwards east of 70°E. At P-1, the region of westerly anomalies remains in effect over Africa to a depth of 400 hPa, above which are negative anomalies. Negative anomalies increasingly prevail over the westerlies such that, by P0, only the region between 10 and 30°E, from the surface to 200 hPa remains under westerly anomalies. Unlike during EFW at the same stage of maturity, the core of maximum westerlies over Africa is not at 200 hPa but in the middle troposphere. By P+1, the negative anomalies stretch from Africa to the central Indian Ocean. There are positive anomalies in the Atlantic and the eastern Indian Ocean. The progression from westerly to easterly circulation through the sequence is a key feature of late summer wet spells.

Temperature anomalies (T')

For EFW, positive (warmer temperatures) anomalies predominate the surface layer over southern Africa in the formative phase (P-2) and slant westwards over the Atlantic Ocean (**Figure 9.7a**). A plausible explanation is that warmer temperatures over Africa are advected westwards to the Atlantic Ocean by easterly winds which are increasing with height over the region. Elsewhere, negative anomalies persist. Five days later, positive anomalies exist across Africa and the lower atmosphere over the Atlantic Ocean (from northerly wind anomalies coupled with subsidence). Negative anomalies dominate the

middle and upper levels (the coolest regions just below the upper- level jet stream), but slant to the surface between 50 and 60°E before giving way to weak low- level positive anomalies in the eastern Indian Ocean. The pattern over Africa reverses at maturity (P0), with negative anomalies covering the lower half of the troposphere before spreading outwards (eastwards at 600 hPa and westwards at 400 hPa) such as to dominate the rest of the troposphere. The relatively lower temperatures over Africa can be attributed to terrestial radiative cooling accompanying rainfall and prolonged cloudiness. During decay, everywhere in the region there are negative anomalies with positive anomalies on top. The negative anomalies are deeper over the Atlantic and Africa (up to 500 hPa at 5°E) than in the Indian Ocean, and suggest a residual effect of the wet spell. Strong positive anomalies arise in the upper- levels.

Temperature anomaly patterns during LSFW are similar to those of EFW only at P-2 over Africa and the Atlantic Ocean when negative anomalies dominate most of the middle and upper portions of the atmosphere, with the highest values between 300 and 200 hPa. Below 500 hPa there are relatively weak anomalies alternating across the entire latitude. At P-1, the patterns become more vertically oriented although negative anomalies control much of the atmosphere. Positive tendencies occur from 10- 40°E to a depth of 400 hPa. They are also located in the eastern Indian Ocean. During maturity, negative tendencies are limited to the lower troposphere (up to 700 hPa) across western Africa. Highest positive anomalies are located in the vicinity of 300 hPa at 30°E. The relatively warmer than normal temperatures over Africa and the Indian Ocean are due to latent heat release in increased convection associated with the wet spells and ITCZ. Near the tropopause, radiative cooling of penetrative cloud tops is evident and yields the 3- layer vertical structure inherent in tropical convective systems. At decay (P+1), negative anomalies occupy the region from 20 to 40°E between the surface and 300 hPa. A narrow arm stretches across the Indian Ocean around 700- 600 hPa. In general, the LSFW anomalies are weaker than those of EFW. This could be largely due to the barotropic nature of the atmosphere in late summer unlike the baroclinicity during EFW.

EPT anomalies (θ_e')

EPT anomalies for EFW and LSFW are displayed in **Figure 9.8**. EPT anomalies are different from temperature anomalies because of water vapour considerations in EPT calculations. At P-2, negative anomalies dominate the domain, with greatest departures over Africa and the west Indian Ocean from the surface to just below 200 hPa and values

decrease with height from -4°K at the surface at 30°E. Higher than normal θ_e' values are located in the Indian Ocean east of 65°E and extend from 900 to 100 hPa with a core near 750 hPa in the vicinity of 75- 80°E. One pentad later (P-1), positive anomalies prevail in the Atlantic Ocean and over Africa west of 30°E, displacing negative anomalies eastwards to the Indian Ocean. The vertical column of maximum negative values is located over the west Indian Ocean and weaker than at P-2. By P0, the eastward propagation results in a configuration opposite to that at P-2, with higher than normal EPT dominant over the Atlantic and southern Africa (+4°K at the surface) and negative values in the east Indian Ocean. At decay (P+1), negative anomalies cover Africa from the surface up to 400 hPa. Everywhere else, positive EPT anomalies predominate. The column of maximum values has shifted 20° longitude eastwards to be found at 50°E. The most conspicuous pattern from EFW EPT vertical profiles is the eastward propagation at approximately 15-20° longitude per pentad. The systems originate from the east Atlantic Ocean in the middle levels.

The EPT behaviour during LSFW is somewhat different from EFW's. A standing short wave of 60° longitude exists between the surface and 500 hPa at P-2, with negative anomalies covering Africa and the East Indian Ocean. Compared to EFW patterns at this stage, the Atlantic Ocean EPT are significantly warmer than its period- mean. During P-1, the wave has translated eastwards and positive anomalies cover the domain from 0 to 55° E and have spread upwards to 300 hPa over Africa. Significant negative EPT anomalies are located between 55 and 80°E throughout the troposphere. At maturity of LSFW (P0), the patterns over Africa have stagnated and positive anomalies have spread eastwards to cover all but the middle and upper East Indian Ocean. The surface area of maximum values (+5°K) has moved from its P-1 western southern Africa position to the eastern flank. Simultaneously, they have spread westwards to the Atlantic Ocean from 600 hPa upwards. The resulting pattern is a mature cumulonimbus form of configuration (mushroom) with EPT indicating convective outflows in the cirrus anvil in the upper troposphere. Negative θ_e' anomalies at P+1 cover the low- levels in the Atlantic Ocean and most of the troposphere over Africa and as far east as 60°E. Higher than normal EPT values have been displaced further east. Thus, LSFW pattern also indicate an eastward displacement during the life cycle. Like during EFW, there is little evidence of vertical (east- west) tilt with height. Another feature is the rapid change from P-1 to P0 where positive anomalies are advected into Africa from the Atlantic Ocean for EFW, compared to the slower pace for LSFW where there is a gradual build up. The LSFW sees a rapid

change from P0 to P+1 (decay) where positive anomalies over Africa are replaced by negative θ_e' of the same intensity and structure.

Horizontal divergence anomalies

Anomalies of the vertical distribution of horizontal divergence are presented in **Figure 9.9**. EFW patterns are in (a) where, at P-2, a NW- SE alternating pattern of weak divergence and convergence exist along the entire latitude. Divergence slants downwards towards the east and reaches the surface over eastern Africa and the western Indian Ocean (from 30 to 60°E). Significant convergence is found at 30°E in the upper levels and spreads downwards to cover the middle and upper atmosphere over the Indian Ocean. Thus, the atmosphere over southern Africa is kinematically stable at P-2. A pentad later, the patterns are disorganised over southern Africa and indicate low- level divergence dominating the eastern half and convergence the other. Relatively stronger divergence is between 30 and 50°E (from Mozambique to Madagascar) from the surface to 400 hPa. At maturity (P0), convergence extends from Africa to 60°E below 500 hPa, with divergence above. The atmosphere is most "unstable" in the vicinity of 30°E and overturning is likely there. P+1 is characterised by displacement of low- level convergence eastwards to Madagascar by divegence from the Atlantic Ocean. A notable feature from EFW divergence is the eastward translation of patterns throughout the 20- day period. Convergence is transferred from the Atlantic Ocean in the formative stage (P-2) to the Indian Ocean by the time EFW dissipates. This propagation has been detected in EPT anomaly patterns above.

The P-2 pattern for LSFW is similar to EFW's, but the atmosphere over Africa is more stable and vertically oriented. The opposite is the case over the western Indian Ocean where there is convergence below 500 hPa and divergence above. During development (P-1), the patterns of the two regions reverse. Weak low- tropospheric convergence is over Africa with attendant upper divergence. The configuration strengthens considerably in the maturity stage (P0), when the activity is over Africa and Madagascar (between 15 and 50°E) and strongest at 30°E virtually at all levels. Convergence occurs through a deep layer from the surface to 500 hPa. At dissipation, anomalies reverse over Africa, with low- level divergence beneath convergence from 600 hPa upwards. This rapid change from an "unstable" pattern to a "stable" situation is greater than at the same stage during EFW.

9.4.3 Mid- Summer Dry Spell (MSD) composite patterns

By definition, composites which make up the MSD include some days representing dissipation pentads of ESW (second wet spell of early summer) and initiation pentads for LSFW. This is despite cut-off pentads used as criteria in Chapter 4. Some of the meteorological parameters with properties which are quasi- conservative, like specific humidity (not shown) and equivalent potential temperature (**Figure 9.12**) show semblance with mean EFW and LSFW patterns, for reasons stated in Chapter 4 and Chapter 5. Only a few "representative" variables are considered and these are meridional and zonal wind components, EPT and horizontal divergence. ***Total values*** are used instead of anomalies.

The vertical variation of the ***u***- wind is presented in **Figure 9.10**. The pattern is a blend of EFW and LSFW mean zonal winds, expected as MSD occurs between these wet phases. Resembling more of LSFW (LSFW follows immediately after MSD), the pattern is dominated by easterly flow from the surface to about 600 hPa over the Indian Ocean and up to 300 hPa over the Atlantic Ocean. Like during wet phases, strongest easterlies are over oceanic regions, depicting the SE trade winds equatorward of the sub- tropical high pressure belt. The upper westerlies are strongest over the East Indian Ocean and significantly stronger than during the LSFW phase.

The meridional component of MSD (**Figure 9.11**) shows vertically oriented southerly winds between 20 and 45°E (from Zimbabwe to the Mozambique Channel), with a maximum at 550 hPa. The flow is linked to the Atlantic Ocean southerlies at low levels. In the middle and higher levels, a standing wave- like configuration is evident with northerly flow on either side of the vertical column of southerly wind over east Africa. This pattern is also similar the mean pattern of LSFW, with jet stream waves detected at 200 hPa. The overall pattern is indicative of a well- defined anticyclone centred near 20°S (the position of the Botswana Upper High, Chapter 8), characterised by strong northerly flow over the Atlantic Ocean with its core at upper levels. This feature is consistent with total wind (vectors) in Chapters 5 through 8.

The vertical profile of divergence is illustrated by **Figure 9.13**. The Atlantic Ocean is dominated by low- level divergence, and convergence aloft. The divergence identifies the extent of the AOA. Divergence spreads upwards over Africa with a core of maximum positive values at 700 hPa near 15-20°E. The values slant to the surface over Mozambique longitudes. There is an attendant upper convergence centred at 30°E. The

patterns reverse in the western Indian Ocean (Madagascar region) where upper divergence overlies convergence, the zero line along 600 hPa. The greatest contrast vertically is in the proximity of 50°E where low (upper) - tropospheric convergence (divergence) is at its maximum. A double dipole is present with contrasting regimes over southern Africa and the SWIO.

9.4.4 Discussion and summary of vertical sections

The vertical structure of the troposphere has been analysed along the Tropical Subtropical Boundary (20°S) during life cycles of EFW and LSFW, deemed representative of wet spells of early and late summer, respectively. A number of features stand out, the following of which are most conspicuous:

- Mean zonal and meridional wind patterns during both EFW and LSFW indicate the existence of an upper tropospheric jet stream in the vicinity of 200 hPa. The jet is more pronounced in early summer, when standing short waves of 40- 45° longitude wavelength stretch across the entire domain. In late summer, the jet is weakest over the longitudes of Africa and Madagascar, interrupted by the barotropic nature of the atmosphere and more deep convective activity associated with the ITCZ which is located slightly equatorward of the TSB at this time. Easterlies are up to 3 km deeper at LSFW than during EFW. Lower down, the Atlantic Ocean Anticyclone (AOA) is represented in the mean flow and is associated with southerly winds. Low-level easterlies suggest it is located to the south of the TSB. The equatorward flow from the AOA is linked to that over Africa in late summer.

- It is apparent from the meridional wind anomaly that early and late summer patterns at the formative and developmental phases of their cycles are rather different. During formation, for EFW, negative anomalies slant from the Atlantic Ocean at upper levels to the Mozambique Channel at 850 hPa. Most of the Indian Ocean is under the influence of anomalous southerly airflow except above 300 hPa. For LSFW, the reverse seems to be the case, with southerly winds in domination. Another contrast is the existence of northerly anomalies in the central Indian Ocean in late summer,

which are absent during EFW. The low tropospheric northerlies are attributed to the surge of monsoons.

- At development, EFW and LSFW patterns are similar to some extent, with quasi-vertically- aligned bands of poleward and equatorward anomalies alternating throughout the troposphere. There is slight evidence of tilt with height, particularly in the lower half of the troposphere. However, the tilt in early summer is biased westward with height while in late summer it is eastward. In general, the anomalies at LSFW are displaced east of positions at the same stage during EFW. For example, the core of upper northerly anomalies is near 0°E at EFW, P-1 and near 10° E during LSFW, P-1. While southerly anomalies cover southern Africa at EFW, the flow is in the opposite direction for LSFW.

- During maturity, low- level southerly and northerly anomalies over the Atlantic/ western southern Africa and eastern southern Africa, respectively, illustrate the clockwise circulation previously observed in the total wind vectors (Chapter 7) over the sub- continent, possibly due to troughing. At the same time, the anomalous southerly winds between 20 and 60°E during development in early summer are replaced by northerly airflow, showing a rapid transformation in the advection processes within a short period of five days. At dissipation, the patterns are also show marked contrast.

- Zonal wind anomalies depict easterly flow dominating the atmosphere over Africa and its immediate environs prior to the peak of EFW. These, as evidenced by vertically integrated water vapour flux (**Figure 7.21**), precondition the central southern Africa region by advecting moisture from the Indian Ocean. The anomalous westerlies then take over during the peak of the spell, covering all but the extreme west of southern Africa and virtually the whole of the Indian Ocean. In the case of LSFW, the cycle commences with positive anomalies dominating. This is also in agreement with moisture fluxes in **Figure 7.22** where moisture is indicated being transported from equatorial areas by corresponding northerly anomalies **Figure 9.13b**. Dissipation sees westward wind anomalies dominating Africa and the immediate oceanic regions, a reversal of anomalies with respect to EFW.

- Temperature anomalies during the formative stages of both EFW and LSFW are similar. Maximum temperature anomalies occur over Africa (thermal low according to Garanganga, 1989) prior to the peak wet spell. The anomalies are advected by low- and middle- level easterlies to the middle levels of the Atlantic Ocean. The pattern is most pronounced during early summer, especially during development (P-1). A rapid transformation takes place between development and maturity such that the temperatures in the low troposphere across southern Africa become relatively cooler owing to evaporative processes accompanying rainfall. During this period, the middle and upper levels are under negative anomalies for EFW but positive for LSFW, suggesting latent heating is more important in late summer. At decay, the atmosphere during EFW is more stable with cooler temperatures underneath relatively warmer air. The atmosphere remains potentially unstable for LSFW where negative temperature anomalies extend from the surface to 300 hPa from the longitudes of eastern southern Africa (Zimbabwe and Mozambique).

- Equivalent potential temperatures (EPT) show an eastward translation of anomalies for both EFW and LSFW. The propagation is more rapid and systematic during EFW where the displacement is between 15 and 20° longitude per pentad. In addition, the build- up of EFW is from the middle levels over the Atlantic Ocean whereas for LSFW, the transition from developmental stage (P-1) to P0 is more internal and gradual. Across Africa, LSFW EPT anomaly values are much greater than EFW's at maturity, including spatial coverage.

- Horizontal divergence anomaly patterns, like EPT anomalies, display the eastward progression along the TSB, from the Atlantic to the western Indian Ocean. This is more evident from EFW patterns where the displacement is more rapid. Convergence can be detected emanating from the Atlantic Ocean prior to the peak of EFW, a feature not quite clear for LSFW. Another important observation is the difference in the mean patterns over southern Africa, particularly in the low levels. In early summer, the lower troposphere displays a stable character (implying the atmosphere is mostly dry and convective spells are brief), attributed to the Atlantic Ocean influence. As regards LSFW, the opposite is the case, with a bias towards mean convergence, with influences coming from the Indian Ocean.

The vertical section analysis was also extended to dry phases of summer. The MSD was selected, separating early from late summer and, agriculturally, the most significant of all dry spells. Divergence profiles over Africa and the Indian Ocean longitudes immediately adjacent are generally opposite, with divergence (convergence) beneath upper convergence (divergence) across Africa (western Indian Ocean). This behaviour supports findings from horizontal analyses of Chapter 8 suggesting that dry conditions over Africa do not extend to the Indian Ocean. The Western Indian Ocean remains convectionally active and conditionally unstable while the atmosphere over Africa is quite stable.

Mindful of the fact that mean patterns of non- conservative phases of EFW and LSFW are similar to MSD patterns, it is safe to make comparison without loss of generality. Clear differences exist between MSD patterns and wet phases at maturity (P0). The patterns exhibit contrasting features. In other words, meridional flow reverses direction from that at the peak of wet spells to during dry spells. The westerlies dominating southern Africa at the peak of wet spells are replaced by easterly flow during MSD. The divergence anomalies at P0 indicate an opposite effect for MSD, particularly over southern Africa, where lower divergence (convergence) is predominant during MSD (EFW and LSFW). More differences between wet and dry spells are discussed in Chapter 10.

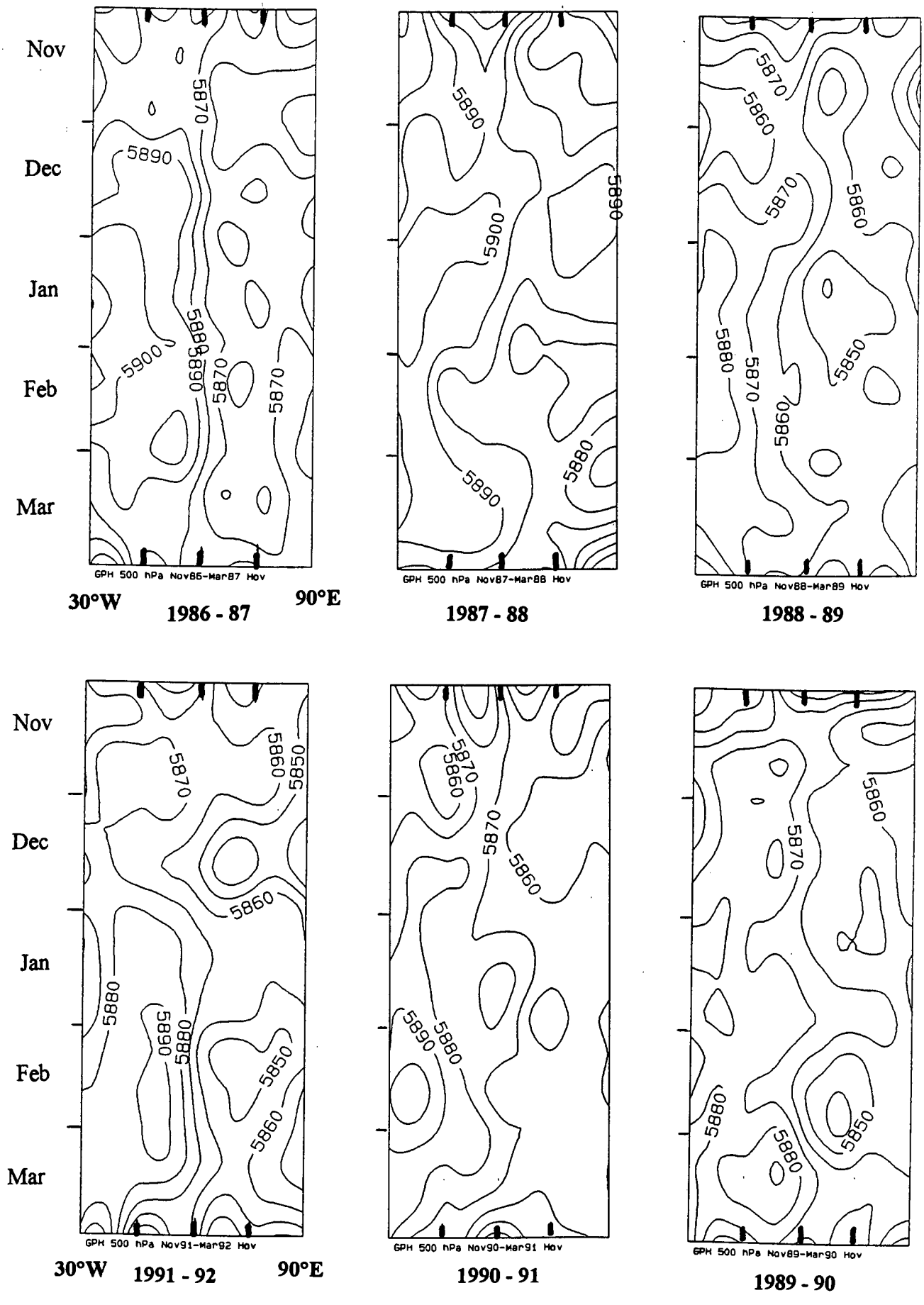

Figure 9.1 : 500 hPa geopotential heights along 20°S between 30°W and 90°E in the period 1986- 1992, November- March. Contour interval is 10 gpm. Configuration is clockwise. Ticks are 30° longitude apart.

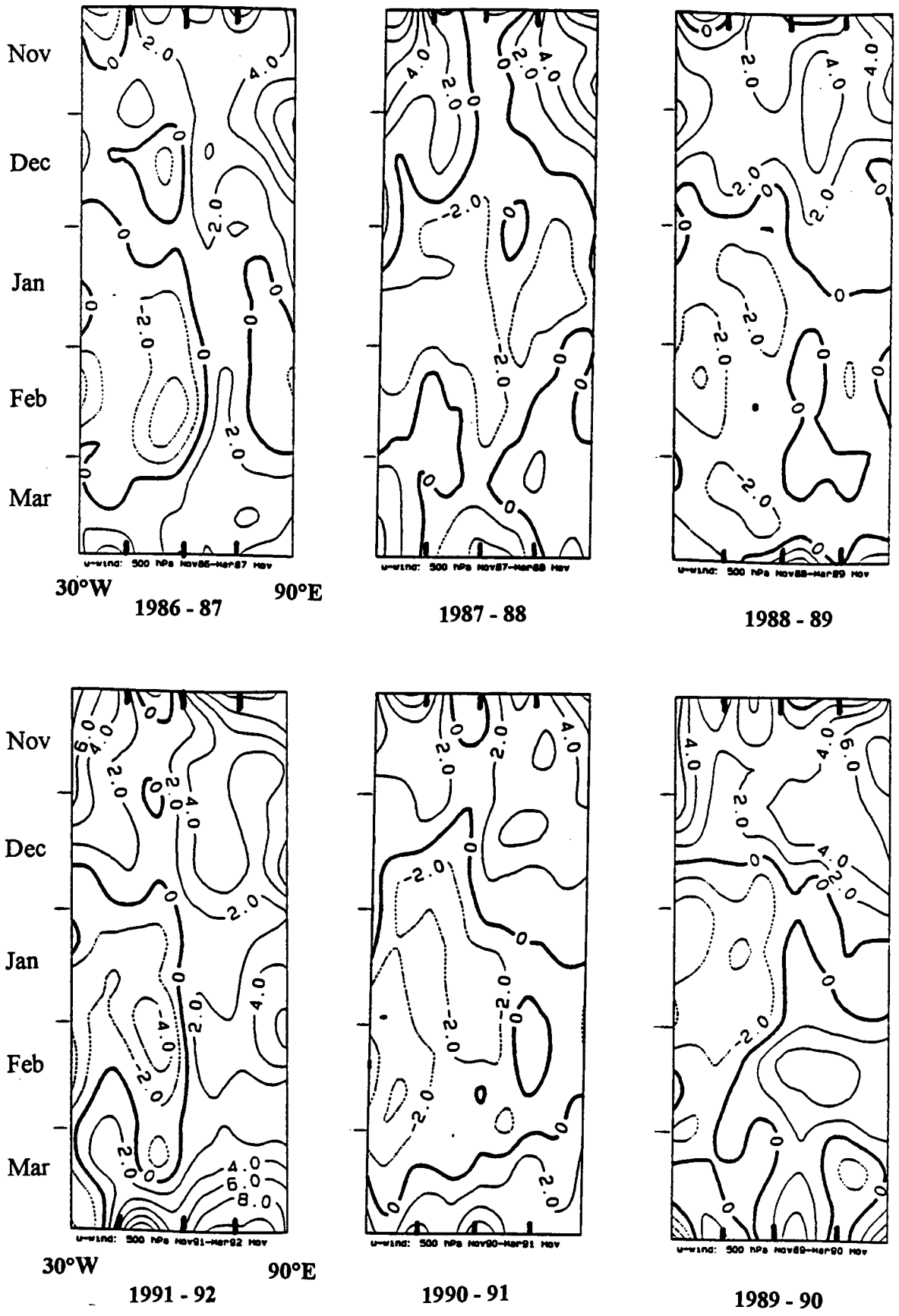

Figure 9.2 : As in Figure 9.1 but for zonal winds. Contours are at every 2 m s^{-1}

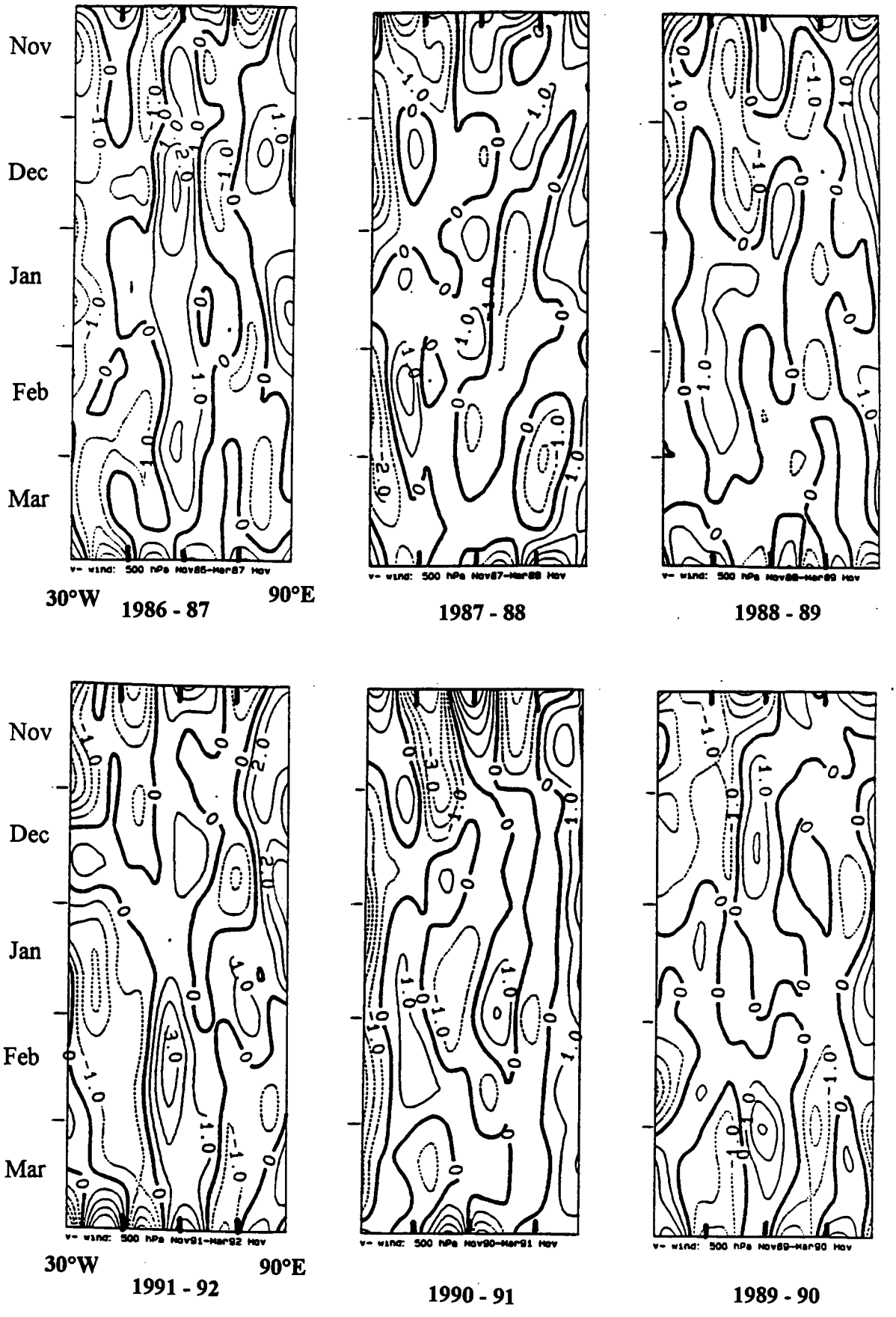

Figure 9.3 : As in Figure 9.1 but for meridional winds. Contour interval is 1 m s^{-1}

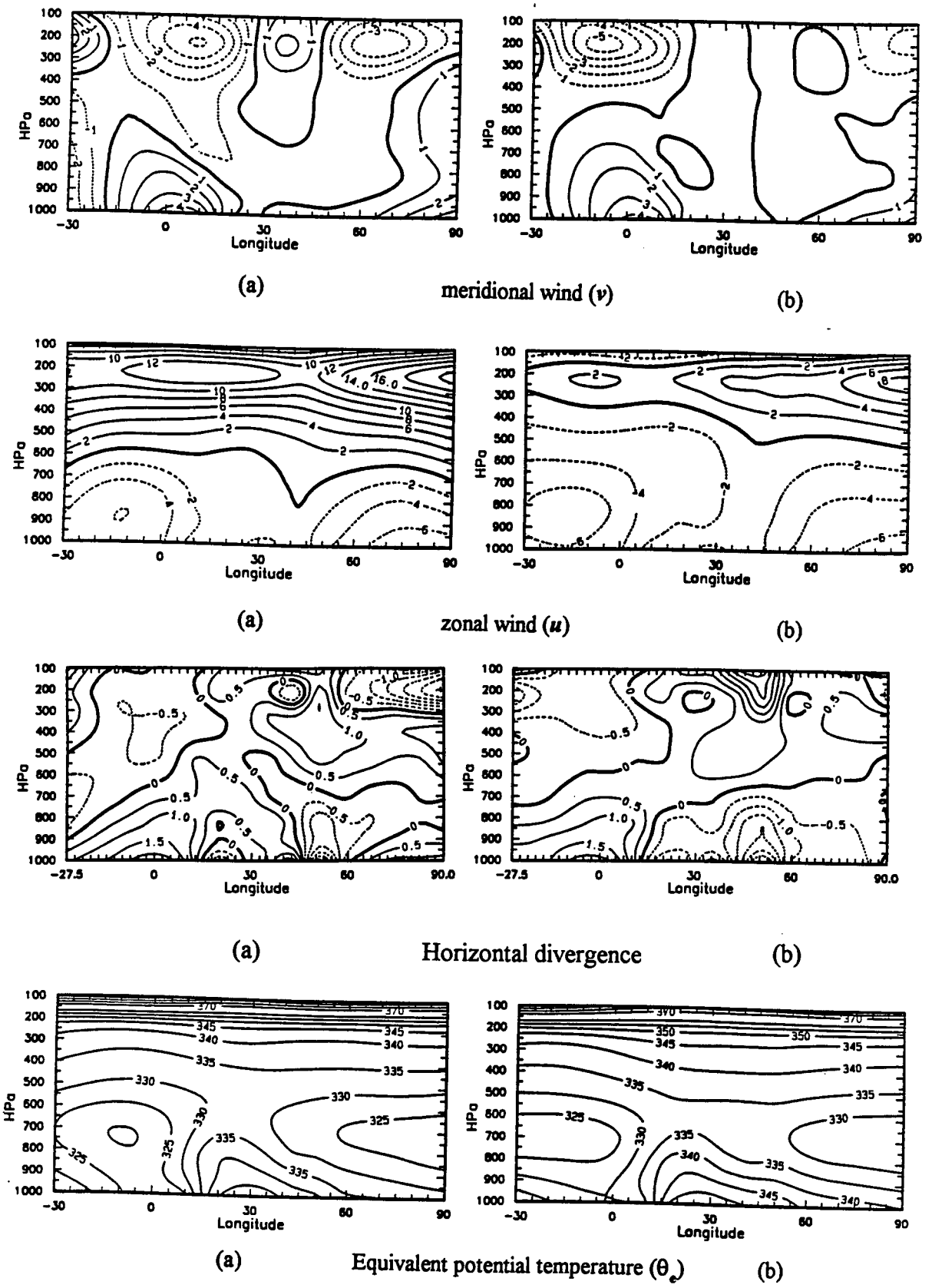

Figure 9.4 : Vertical profiles along 20°S of mean meridional wind (m s^{-1}), zonal wind (m s^{-1}), divergence (x $10^{-6}s^{-1}$) and equivalent potential temperature (°K) for EFW (a) and LSFW (b) phases.

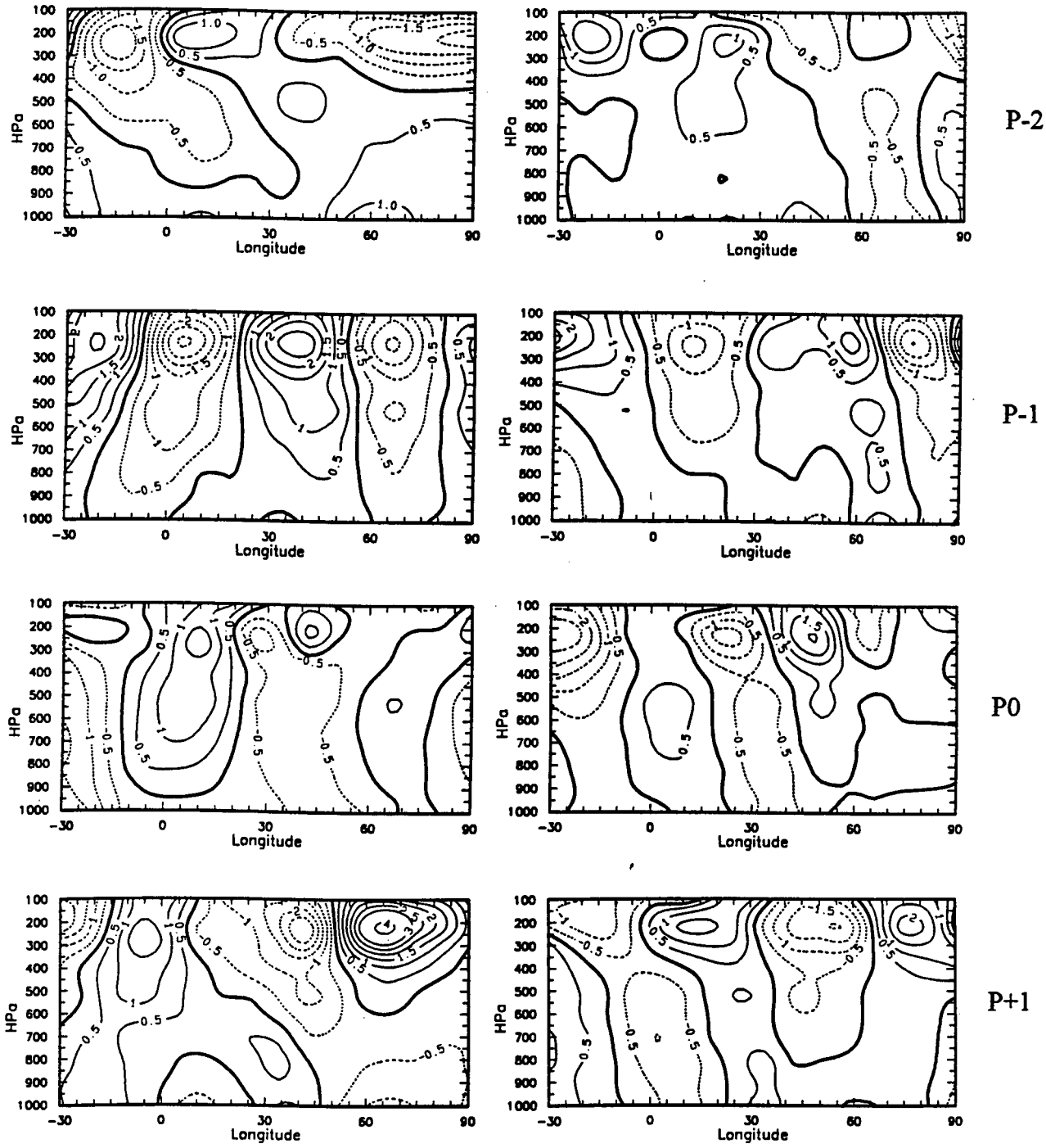

Figure 9.5 : Vertical sections of meridional wind anomalies (v') for EFW (a) and LSFW (b). Contour interval is 0.5 m s^{-1}.

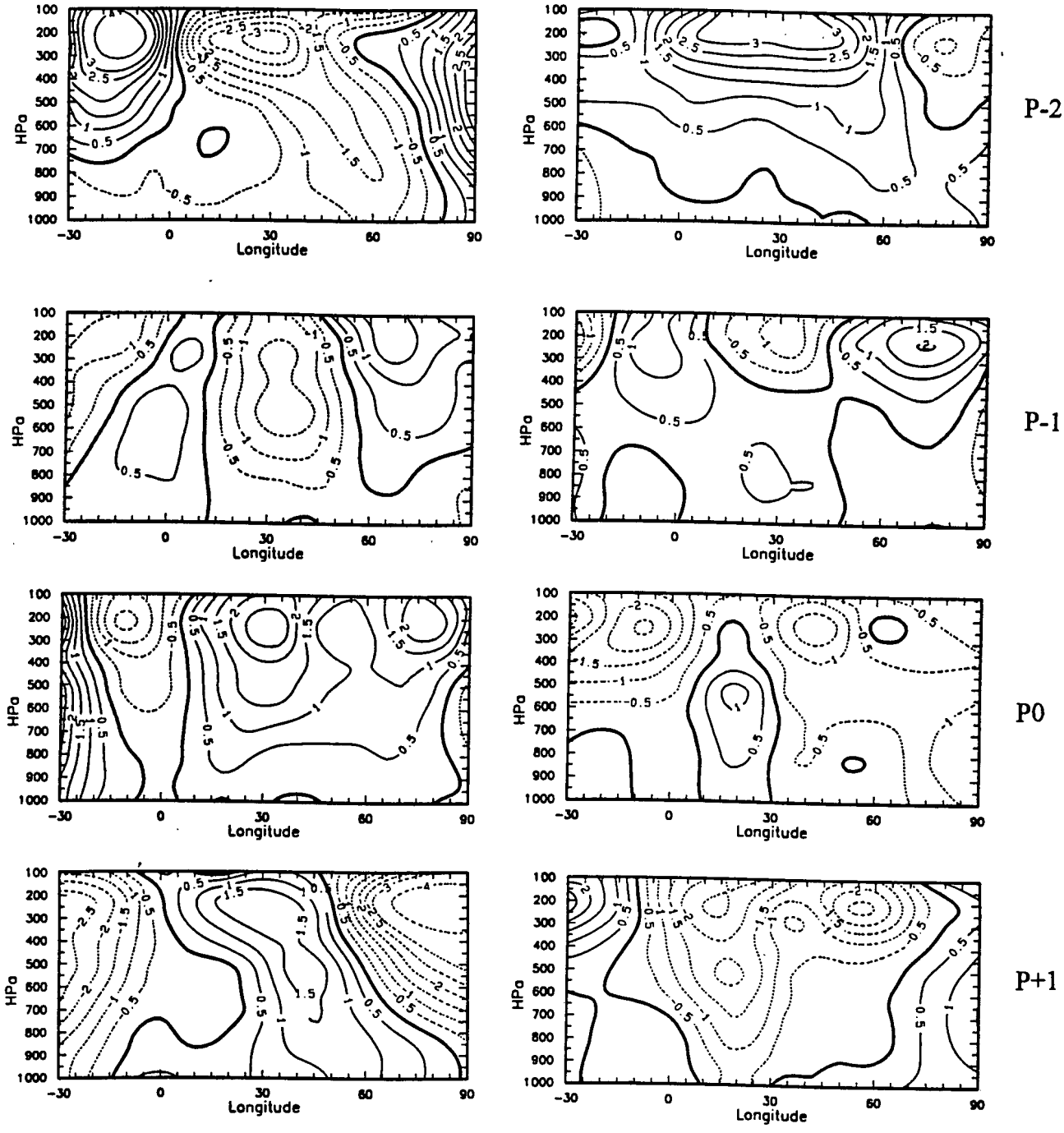

Figure 9.6 : As in Figure 9.5, but for zonal wind anomalies (u').

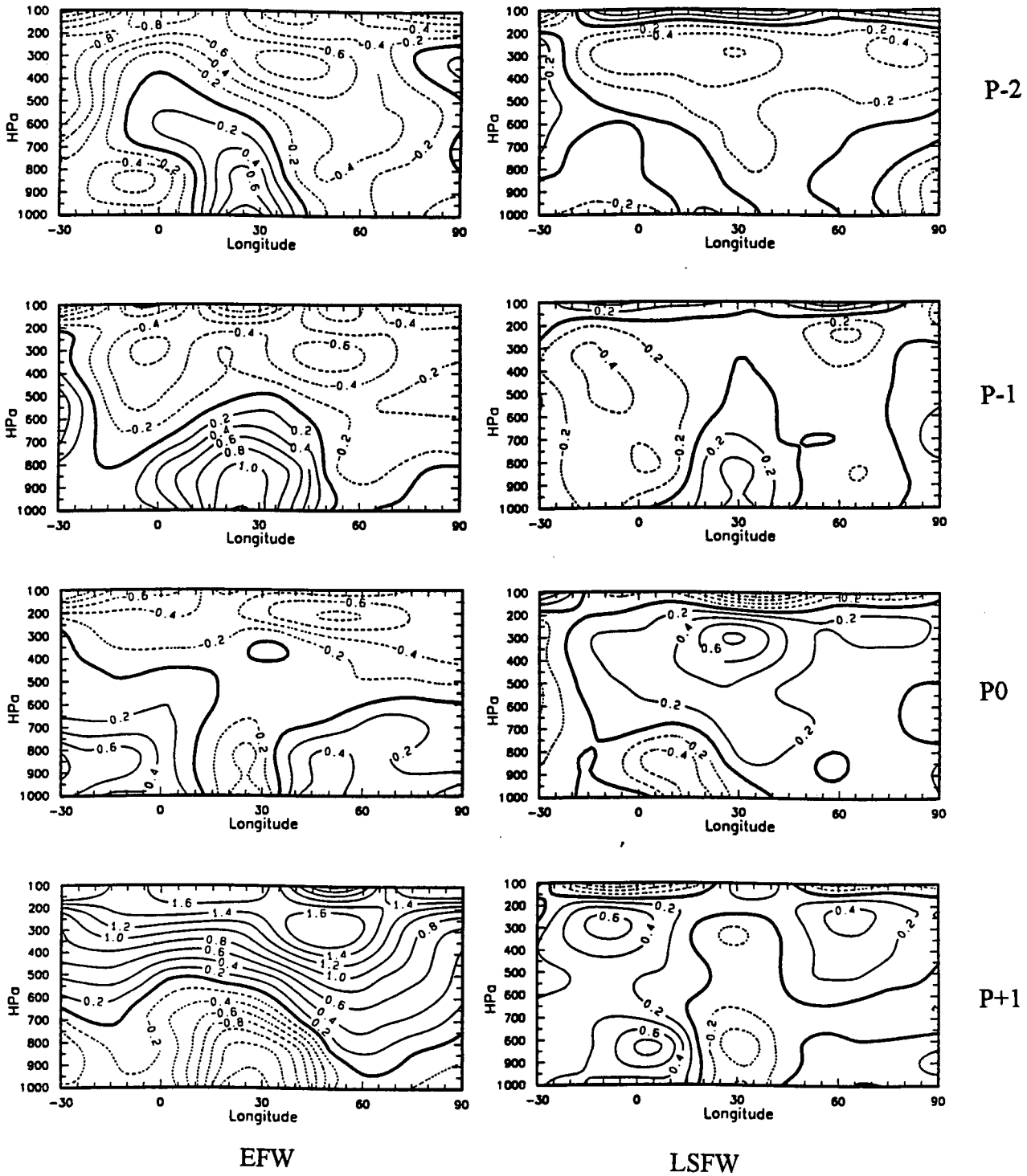

Figure 9.7 : As in Figure 9.5, but for temperatures (T'). Contours are at every 0.2° C.

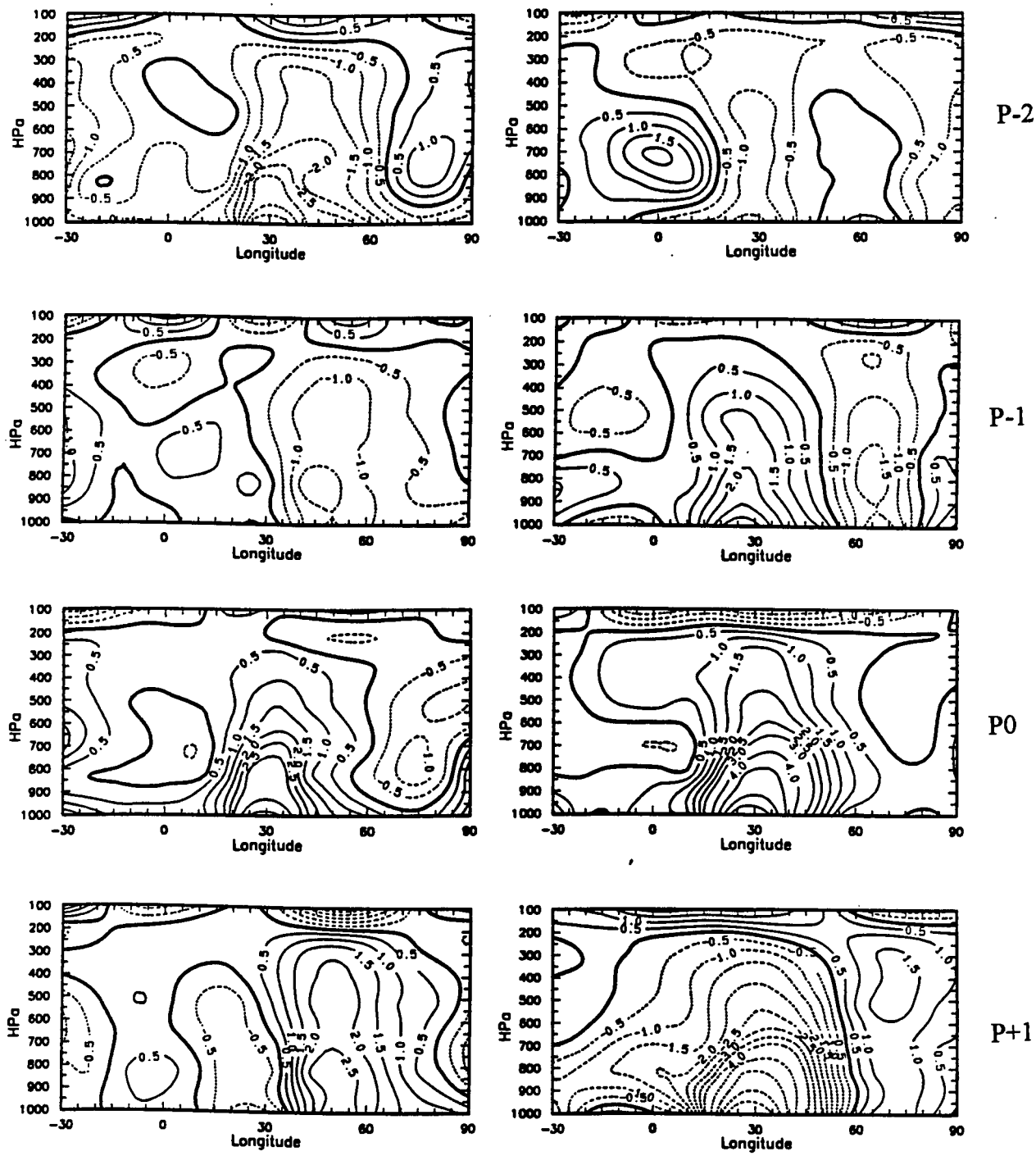

Figure 9.8 : As in Figure 9.5, but for equivalent potential temperature (EPT) anomalies (θ_e').

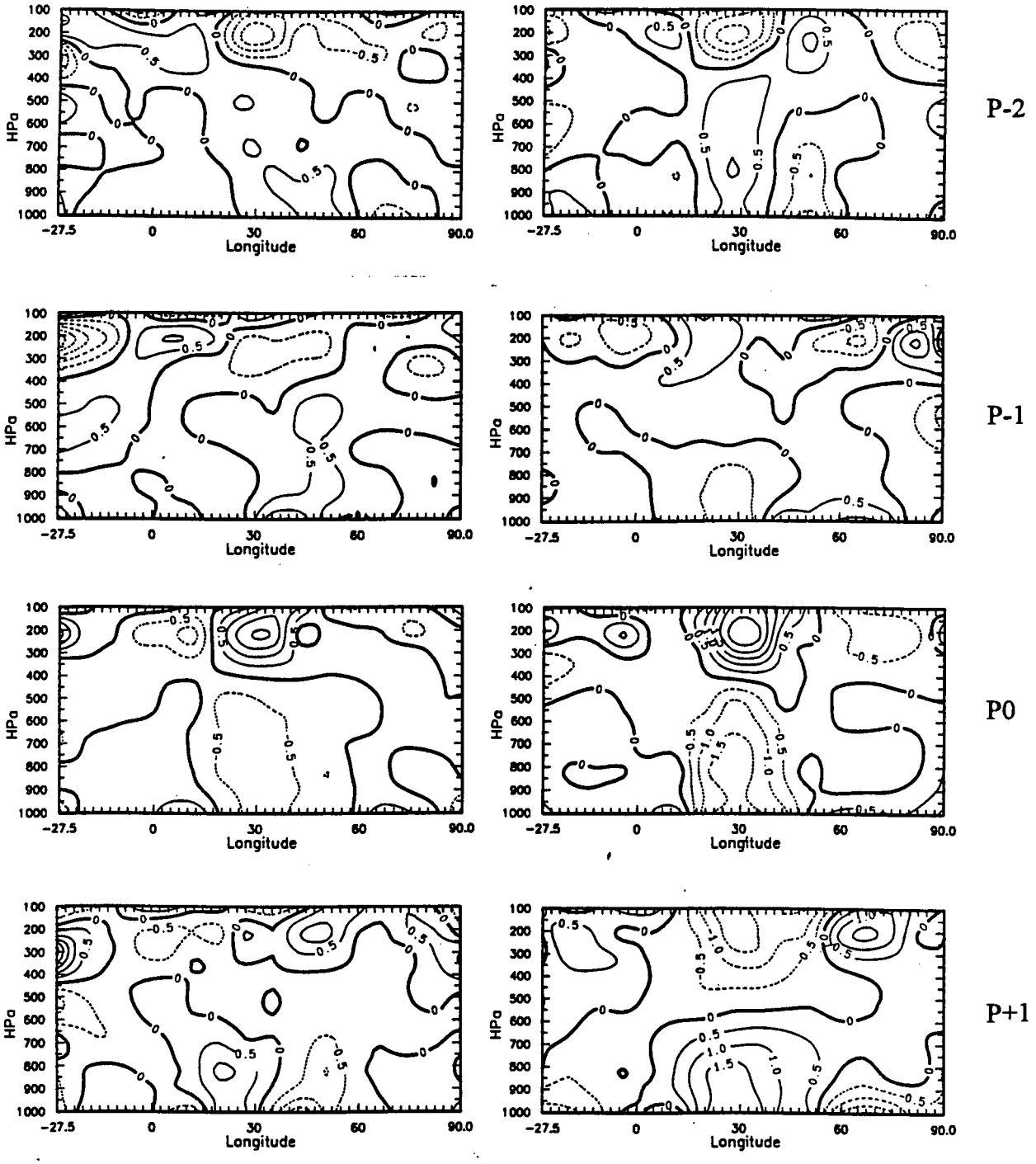

Figure 9.9 : As in Figure 9.5, but for horizontal divergence.
Contour interval is 0.5 x10^{-6} s^{-1}

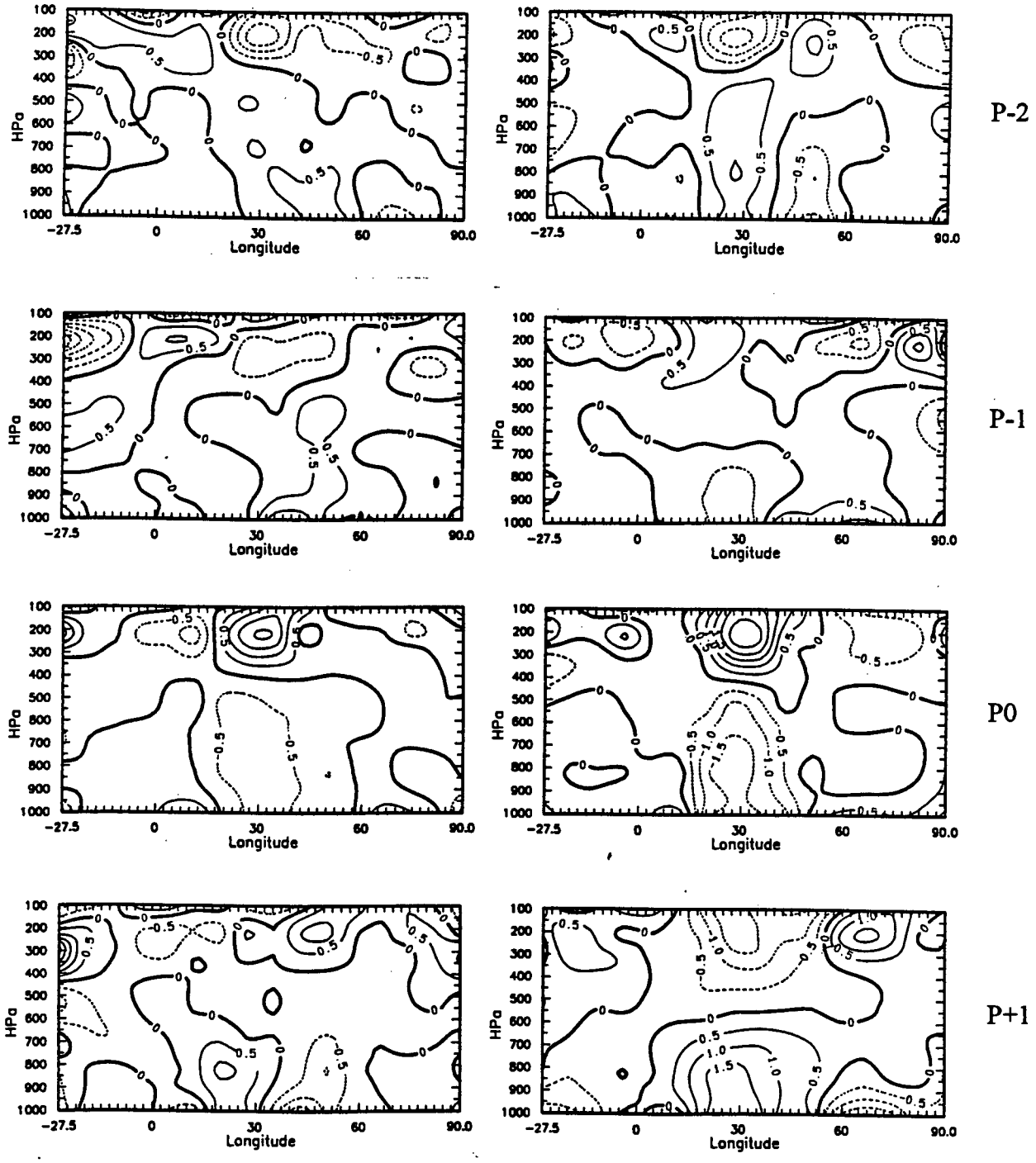

Figure 9.9 : As in Figure 9.5, but for horizontal divergence.
Contour interval is 0.5 x10^{-6} s^{-1}

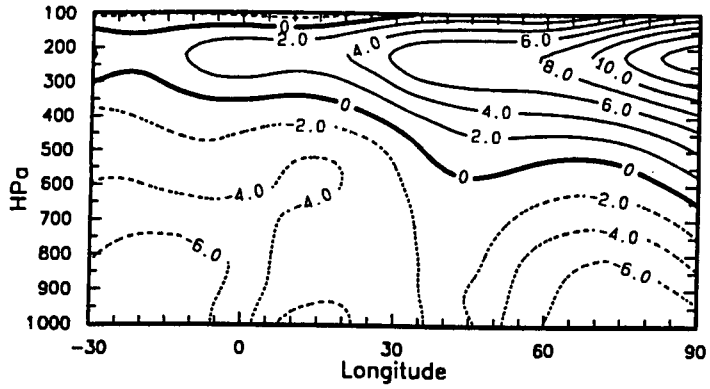

Figure 9.10 : Vertical sections of zonal wind for MSD. Contours are at every 2 m s^{-1}

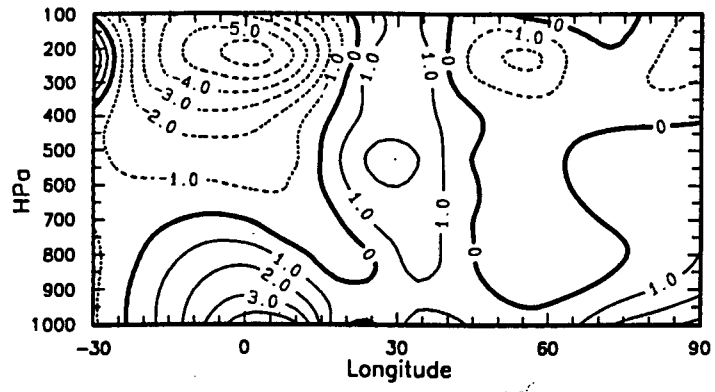

Figure 9.11 : As in Figure 9.10, but for meridional wind.

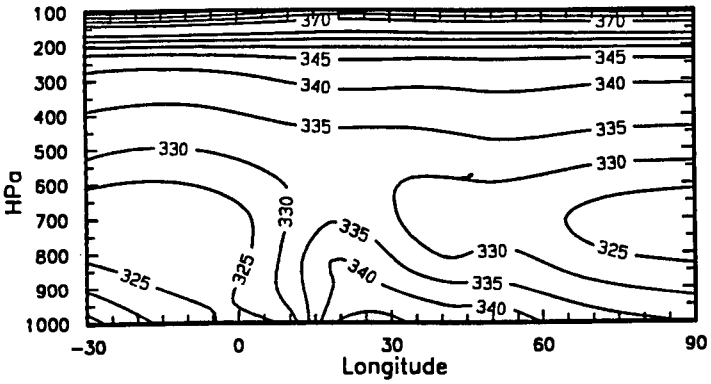

Figure 9.12 : As in Figure 9.10, but for EPT (θ_e). Contour intervals are 5° K to 250 and 10° K thereafter.

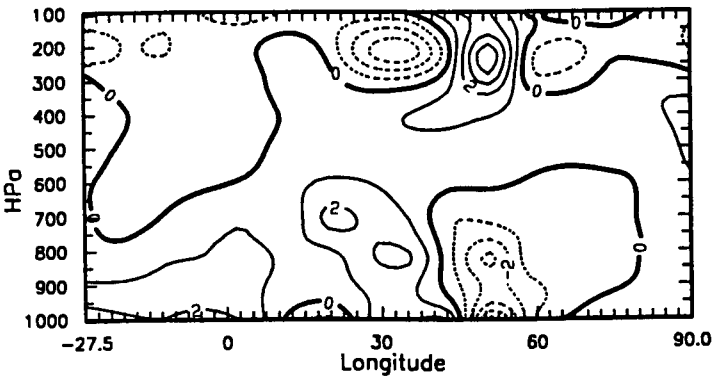

Figure 9.13 : As in Figure 9.10, but for horizontal divergence. Contour interval is 2 x 10^{-6} s^{-1}.

Chapter 10

Conclusions

Summer rainfall in southern Africa appears to be on the decline for a significant portion of southern Africa. Droughts are becoming more frequent and extreme. In the region, largely climate- driven agricultural variability is recognised as one of the major factors affecting economic development and needing urgent address. This thesis is intended to shed more light on characteristics of ensemble weather patterns during austral summer, with emphasis on the period November to March, the effective growing season for rain- fed agriculture.

The overall objective is to investigate the variability of southern African summer climate through analysis of Intra-Seasonal Oscillations (ISO) in a seasonal progression. Intercorrelation analyses reveal that the seasonal rainfall distribution among stations in South Africa, Botswana, Namibia and Zambia are similar. Correlation coefficients range from +0.68 to +0.92. While some progress has been made with South African rainfall, much more needs to be done for the rest of the region, since the countries are inter-dependent economically and experience similar vagaries of the weather. However, most research to date assumes that the climate variability over the whole region is homogeneous and weather responses to teleconnections are the same. For operational predictive purposes, unique relationships are needed, particularly for lags. Objective long- term (seasonal) forecasting techniques over the region have been less than satisfactory. The best tools have been statistical regression and involving teleconnections, which assume the climate over southern Africa is uniform. It is for this reason that the thesis has included a chapter (Chapter 3) to investigate exact relationships between rainfall and regional teleconnections. South African rainfall responses have been discussed already, most notably by Lindesay (1988) and Pathack (1993). The thesis has used Zimbabwe rainfall data to check the validity of the homogeneity assumption and has gone further to update previous findings which were non- unspecific. The following results, based upon Zimbabwe monthly data, present a basis and avenue for further understanding the climate of southern Africa and its relationships with regional teleconnections.

10.1 Zimbabwe summer rainfall characteristics

- The monthly distribution of summer seasonal rainfall is unimodal and generally centred on January. The length of the season and the skewness of the distribution are variable yearly as well as spatially across the region. The rainy season over southern Africa generally commences in late October and ends in early April of the following calendar year (approximately 220 days). Regarding agriculture, however, effective summer is from November to March (about 152 days). The rainfall is on a decreasing trend since 1901 and extreme years (droughts and floods) are getting more severe and frequent.

- The rainfall is cyclic with principal periodicities of 2.3, 18-20 and 3-5 years attributed to the QBO, luni- solar tidal activity and ENSO, respectively. Comparison with South Africa (Tyson, 1986; Lindesay, 1988) illustrates that the contribution of each cycle varies spatially. For example the 18-20- and 10-11- year cycles are more pronounced in South Africa than in Zimbabwe where the 2.3 year component is quite significant.

- On average, extreme (high and low) ENSO years recur every four years and only on six occasions since 1901 have they occurred consecutively. Extreme events (drought and flood) in Zimbabwe are not so regular and have coincided with extreme ENSO years in only 50% of cases. Extreme rainfall has been experienced independently of extreme ENSO episodes in only 14% of cases. Separately, droughts and excess rainfall years have occurred simultaneously with extreme ENSO years in 53% and 83% cases, respectively. Thus, the association between rainfall and ENSO is useful in extreme cases only. The problem is, as yet, there is no satisfactory procedure to predict ENSO intensity. Historical analogues are currently in use.

- Zimbabwe seasonal rainfall and SOI are best correlated when the SOI is a three-month average of August, September and October (ASO) values, two months prior to the onset of the main rains. The correlation is low, suggesting that other phenomena, collectively more important than the SOI should be employed to investigate the climatic variability of Zimbabwe rainfall. A dense rainfall station network in the country reveals highest correlations with ASO SOI located at stations in the north of Zimbabwe. This is in contrast to previous regional studies of Ropelewski and Halpert (1987), Lindesay (1988), Matarira (1990) and Rocha (1992) employing less rainfall data, which indicated that the strongest correlations were over the southern parts. In

addition, spatial and temporal patterns of the correlations show that the SOI fluctuations have a rippling effect across Zimbabwe with axes oriented SW-NE and moving from the southeast of the country to the northwest.

- Operationally, it is now possible to predict Zimbabwe summer rainfall as early as six months in advance (July). Prior to the onset of drought in Zimbabwe (and indeed most of Southern Africa), warm SST anomalies occur in the equatorial waters of the central Indian Ocean as early as July. The best correlations are with September-November average SSTs. Upper tropospheric zonal winds in the central equatorial Atlantic Ocean just south of the equator appear to be equally useful as predictors of the forthcoming rainfall season. Monthly correlations with Atlantic Ocean upper level zonal wind peak at lag -3 (around October) while that of the SST reaches its peak in November (lag -2). The winds are better correlated with Zimbabwe early summer rainfall, whereas SST is better for late summer. In terms of degrees of freedom, though, SST data has a longer record than the Atlantic Ocean wind data. The QBO has a significant influence on rainfall, especially when its cycle is in phase with the end of the season. It can enhance (suppress) the late summer precipitation when it is in a westerly (easterly) phase. Due to its periodic nature, the QBO is predictable, but with a cycle of about 28 months. It is, of course, non- stationary with respect to the southern African summer rainfall season.

Significant progress has already been made regarding prediction and understanding of the interannual variability of the climate of this region. It is still far from satisfactory, though. Caution is therefore needed when employing teleconnectivity to predict rainfall, especially for southern Africa. For credibility, forecasts should take cognisance of spatial and temporal variations of correlations across entire region (research of which is still in developmental stages), otherwise they remain subjective and prone to error. The statistical association (from correlation coefficients) between Zimbabwe rainfall and teleconnections has illustrated the need to explore other avenues for rainfall prediction. More importantly and particularly with agriculture, seasonal forecasts are inapplicable for operational short-term farming decisions. Lead times allowing implementation of appropriate contingency measures are sub- monthly, hence the study of intra- seasonal oscillations, the central theme of this thesis.

10.2 Sub- monthly climate variability over southern Africa

10.2.1 Intra- seasonal phases of summer

The second part of the thesis (from Chapter 4) investigates characteristics of a typical summer through analysis of daily data and 5- day averages. Pentad analysis is more ideal for day-to-day agricultural operations, especially on- farm decision making. The intra-seasonal time scale analysis of Zimbabwe, Zambia and Botswana rainfall (representing central southern Africa) has shown that the summer rainfall season is not entirely unimodal in its distribution, but pulsed with five main wet and two main dry periods, each lasting up to 3 pentads. Mean patterns show a sequence of alternating spells of wet and dry weather and have periodicities of 10-25 days and about 45 days, with a mean frequency of approximately 3-4 pentads (15-20 days). The major peak pentads for the wet periods are 27 November- 1 December (EFW), 17- 21 December (ESW), 21- 25 January (LSFW), 10- 14 February (LSSW) and 22-26 March (LSTW). The dry periods which are most important are those which extend from 27 December to 11 January (MSD) and from 25 February to 16 March (LSD). Another important result is that the climatology of southern Africa is complex in the early months of summer. EFW and ESW are well defined over eastern regions (NE Zimbabwe, Zambia and Mozambique) but not so clear- cut for the rest (Namibia, Botswana and central and NW South Africa). Late summer wet periods, apart from lags of 1- 2 pentads, are common to all. Finally, pentad analysis has identified the mean dates of onset, cessation and duration of wet and dry spells during a typical season, an important factor with practical implications, particularly medium- range weather forecasting.

The intra- seasonal nature of rainfall in southern Africa casts a totally different scenario compared to monthly data. Monthly rainfall, in the mean, is unimodal over most parts of the region. All indicate a monthly rainfall peak in January, with one wet spell triggered by mechanisms from outside the regional boundary. In other words, there is large- scale instability at the peak of summer, as will be evidenced elsewhere in the thesis, and also detected by Harrison (1986) and Harangozo (1989). The large- scale flow and the synoptically triggered instability mutually influence each other.

Chapters 5 through 9 have looked at wet and dry phases of summer based upon occurrences of peak activity and on the hypothesis that characteristics of summer convective systems change as the season progresses. In other words, weather variability is contributed by different factors during the season as outlined in Table 10.1 and

summarised in the following sections. ECMWF data have contributed by enabling the identification of meteorological factors associated with the wet and dry phases.

10.2.2 Wet spell phases of summer

Wet spells have been investigated from Chapter 5 to 7. Chapter 5 concentrated on mean phases based upon wet spell life cycles in the summer period 1986- 1991. Chapter 6 dwelt only on the peaks of these wet spells while Chapter 7 looked at life cycles (evolution) of two representative wet spells. Major features stood out, some of which are summarised below.

- From a dynamic and physical perspective, the period- mean analysis reveals the need to view summer as a series of phases, each with a different "mix" of meteorological factors and triggering mechanisms, but all modulated by 10-25 and 40- 50 day ISOs. The analysis is based upon daily (reduced to pentad) variability for the duration of each phase, results of which are more useful than monthly and seasonal mean analyses.

- Period mean analysis also indicates a relatively dry stable atmosphere over southern Africa, consisting of low- level anticyclonic ridging from the Atlantic Ocean, divergent and anti clockwise circulation with northerly (southerly) winds on the western (eastern) flank. There is more equator to poleward flow in late summer. A seasonal cycle is manifested in the low and mid- level equatorial westerly wind regime and vorticity circulation in the Indian Ocean (**Figure 5.2**). Upper tropospheric velocity potential patterns **(Figure 5.13)** portray the cycle translocating from central southern Africa in early summer to the western Indian Ocean in mid- summer before retreating to the continent in March.

- During wet phases, two troughs are pronounced over southern Africa. The first cuts across central southern Africa from Angola to the Mozambique Channel (MCAT) while the other is located along the west coast (**Figure 5.14**). Both are quasi-stationary and are low- tropospheric features. The west coast trough is most effective in early summer, by advecting moisture from Namibia/ Angola regions southeastwards across southern Africa. This determines the onset of summer convection over the sub-continent. The MCAT develops in December and dominate thereafter. Their shallowness implies that rainfall causation and enhancement in the vicinity of these troughs are primarily due to convergence of air masses and horizontal wind in the

zonal (MCAT) and meridional (west coast trough) axes. Poleward advection is due the energy and inertia of the ITCZ (the seasonal cycle) and results in convective build-up. Equatorward surges of the sub- tropical westerly waves also work in conjunction with tropical flows to ensure extended wet spells.

- Temporal convective regions of the ITCZ are readily delineated from wet spell analyses. Low- level divergence and vorticity patterns (**Figure 6.2**) indicate that the ITCZ is most active over southern Africa and the western Indian Ocean in January just north of the TSB (20°S). This partly explains the January peaks in both pentad and monthly rainfall data. Convergence is greatest over eastern regions of the sub-continent. Mid- level vertical velocity fields (**Figure 6.5**), however, show the whole region experiences uplift, particularly Madagascar.

- ISO controls during early summer are different from those in late summer. Troughs play a major role in early summer. There is little direct evidence of the monsoon over the region, either. The atmosphere is reluctant to precipitate due to stabilising influences of the Atlantic Ocean Anticyclone near the TSB. Rainfall triggering controls are from extra- tropical westerly wave incursions in southern Africa. In late summer, the Indian Ocean becomes more influential, facilitating a southward incursion of moisture and energy from the Equator. The monsoon is felt in NE southern Africa (northern Mozambique and Malawi). It is the MCAT which is a major role player then. The ITCZ is also important (Lindesay et al., 1986; Harangozo, 1989 and D'Abreton, 1992) and enhances the MCAT.

- Vertically integrated water vapour fluxes indicate that the circulation over the SE Atlantic Ocean plays a minor role as regards southern Africa. The Atlantic Ocean Anticyclone transports moisture towards the Equator mostly in low- level southeasterly trade winds. Some moisture accumulates on the west coast (mostly over northern Namibia). Passage of a family of frontal systems in the extra- tropics results in the transformation of a heat low into an elongated trough which deepens and extends down the western flank. Ridging behind the family of frontal systems enables the trough to propagate southeastwards by merging with the pre- frontal trough. In late summer, however, the South- West Indian Ocean and the Mozambique Channel are the major sources of water vapour in the southern parts of sub- region (South Africa, Zimbabwe and Mozambique). The westward advection is enhanced by a quasi-permanent low- tropospheric anticyclone along and off the east coast of South Africa.

This is in agreement with the findings of Tyson (1986) and Taljaard (1990). A significant amount of moisture from the Indian Ocean "destined" for southern Africa is blocked by and deposited over Madagascar, especially on its eastern escarpment. In late summer also, as supported by low- level meridional wind flow, there is a sympathetic poleward advection of moisture from the Congo, most of which is deposited along the MCAT. This is consistent with the findings of McNaughton and Wurzel (1972) and Harrison (1986).

- Anomaly patterns (Chapter 7) show contrasting features of early summer (represented by EFW) and late (LSFW) summer. For example, low - level wind patterns spread into southern Africa from higher latitudes. LSFW anomalies show eastward propagation across the region, particularly for zonal and meridional eddy temperature transports (**Figures 7.1 and 7.11**). More differences are apparent in the Indian Ocean. Firstly, low- level tropical equatorial westerlies are ill- defined throughout EFW, but are more pronounced during LSFW, located off east Africa at evolution and dominating the Indian Ocean by the time LSFW decays 20 days later. Low- level vorticity anomalies in the equatorial Indian Ocean propagate at 5-10° latitude per pentad southwestwards during EFW but remain quasi- stationary in late summer.

- Vertically integrated water vapour flux fields for life cycles reveal sources and sinks of moisture over southern Africa and the Indian Ocean. EFW fluxes over southern Africa are zonal and from the east via the northern Mozambique Channel. The bulk of moisture from the Indian Ocean is deposited over Madagascar and east Africa in the formative stages of EFW. In later stages, this moisture is re- directed to SE Africa (Northern Mozambique, Malawi and Zambia). In contrast, a meridional poleward flux occurs over tropical southern Africa, into the TSB during LSFW. At the peak of the wet spell, moisture is sourced from the Congo in the north and the South West Indian Ocean, via the south Mozambique Channel.

- Another important feature of anomaly analyses is the detection of short waves in the middle and upper levels of the troposphere over the Atlantic Ocean and southern Africa with a SW- NE propagation. The sub- tropical wave train reaches peak amplitude about five days before maturity of the wet spell as observed from geopotential height, zonal and meridional wind fields (for example, **Figure 7.7**). The anomalies are displaced equatorward, evidenced by the wave axis shifting from 20°S at P-1 to the Equator at P+1. The anomalies also show eastward propagation, slower for

EFW due to downstream blocking in the east Indian Ocean. Simultaneously, upper tropospheric meridional wind anomalies in the tropical Indian Ocean reveal a sympathetic northwestward movement, culminating in an anti clockwise circulation centred over tropical southern Africa.

- The anomaly patterns have highlighted major discrepancies between life cycles of early and late summer wet spells. The departures show organised low- and mid- level exchanges of moisture and energy between the Equator and the TSB in the build- up to wet spells in late summer. Low- level convergence, deep convection and upper outflow all point to an internal and self- sustaining rainfall triggering mechanism during LSFW, specifically convective and boundary-layer processes (as noted by Gutzler and Wood, 1990) In contrast, an upper northwesterly jet stream emanating from the equatorial Atlantic Ocean streaks through western South Africa during early summer. Thus, advection from outside the regional boundary plays a major role as regards rainfall over southern Africa in EFW.

Dry spell episodes over southern Africa have been dealt with in Chapter 8, with emphasis on the mid- summer (MSD) and late- summer (LSD) dry spells. A major feature of dry spells is the anticyclonic, subsident, divergent circulation over the region, centred over eastern South Africa in the low- levels and over northern Botswana (hence the Botswana Upper High, or BUH) at upper levels. In mid- levels, the zonal wind is tropical easterly and sub- tropical westerly. The MCAT, a semi- permanant feature of wet spell situations, is absent during dry spells.

The circulation over the central interior of southern Africa has also been looked at using a 9- grid point box centred at 20°S, 22.5°E (Botswana). The study has revealed the following:

- Area- averaged daily 500 hPa geopotential height displays a 26- 30 day oscillation in dry years (1987 and 1992) over southern Africa, 45 days in wet seasons (occur 3 times only for the entire season) and 60- day cycles for normal seasons. On average, there are approximately 5 major dry episodes during dry summers and 3 in wet years. Higher frequencies are notable and include 10- 25- day spectral peaks in rainfall indices over the region. This indicates that ISOs are influential throughout summer and "drive" synoptic scale weather patterns, be they wet or dry.

- 700 and 200 hPa divergence and vorticity patterns (**Figure 8.11**) over Botswana also confirm the existence of intra- seasonal oscillations. Using pentad means, the atmosphere exhibits a prominent 15- 17- day oscillation, with a secondary frequency at around 22 days. The oscillations of divergence and vorticity achieve greater spectral power than that of the 500 hPa geopotential height because they are more senstive to external forcing. Daily fluctuations of the two parameters brings out a 4- 8- day oscillation, also noticeable in frontal activity across South Africa (Preston- Whyte and Tyson, 1988).

- Lagged correlation analysis among pentad 500 hPa geopotential height, 700 and 200 hPa divergence and vorticity fields and rainfall in the vicinity of Botswana (**Table 8.3**) show that, firstly, low-level divergence occurs simulatneously with upper convergence, is inversely related to rainfall, leads vorticity fields by 1 pentad and is followed by mid-level geopotential height increase. There is good agreement between upper divergence and precipitation over Zimbabwe and Maun (Botswana). Rainfall at Maun precedes upper divergence which, in turn, leads rainfall over Zimbabwe by 3 pentads. The converse is found for dry spells.

Finally, time series of rainfall have illustrated that, at times, minor dry spells may extend to become intra- seasonal droughts. There are no precursors and the transition is subtle. While the cross- correlations indicate a definite linkage and potential for weather prediction, the correspondence over southern Africa is still too complex to be isolated and used effectively. Therefore, more research is imperative as dry spells are part and parcel of climate variability over southern Africa.

10.3 The tropical- subtropical Boundary (TSB)

The 20°S latitude is the mean low- tropospheric boundary over southern Africa, separating tropical from sub- tropical circulations. It is subsequently referred to as the Tropical- Subtropical Boundary (or TSB). Equatorward of this are easterlies (also noted by Harrison, 1986; D' Abreton, 1992) while a westerly regime prevails poleward of the TSB. More important, higher temperatures in the mean are experienced at or near the TSB. Dry convection (updrafts or thermals) usually starts over areas eperiencing higher temperatures. This, according to Harrison (1983) and Pathack (1993), provides suitable conditions for tropical- extratropical heat and moisture exchanges through eddy motions.

The resulting configuration is conducive for rain formation over the sub- region, provided there is ample low- level moisture. The TSB is also delineated as the area of minimum water vapour fluxes over central southern Africa. The 20°S latitude, the subject of Chapter 9, is, therefore, central to understanding dynamics and physics of circulations over southern Africa. Any cross- over between the tropics and sub- tropics is best viewed along this latitude in the middle and upper levels of the troposphere. This thesis has used time- longitude plots in the horizontal (hovmollers) and vertical space frames to examine patterns across the TSB.

10.3.1 Hovmoller analysis at 500 hPa

Hovmoller (time versus longitude) plots are useful in studying the horizontal north- south fluctations. The period in question is 1986- 1991, from November to March in each summer. The analysis, along the TSB from 30°W to 90°E, shows that, at 500 hPa, the Atlantic Ocean is a source of higher geopotentials over southern Africa, with principal surge at every 45 days (Madden Julian Oscillation). Minor cycles of 15- 20 days are more pronounced in the mid- level zonal winds. Meridional wind hovmollers display a standing short- wave pattern in the early (November) and final (March) stages of summer. There is little east- west propagation, except in the 1987 summer in the Indian Ocean. Most evident in all patterns are similarities for 1987 and 1992 (El Nino years). Both seasons are characterised by prolonged dry spells and attendant subsident southeasterly flow. It should be noted that this easterly flow does not emanate from the Indian Ocean as is the case during wet spells. When scrutinised even further, there is little interaction between the Atlantic and the Indian Oceans. This is most conspicuous in the geopotential height and meridional wind plots. Africa seems to act as a "barrier", with a demarcation in the proximity of the 30°E longitude (eastern escarpment). Ridging from the Atlantic ocean limits moisture advection from the SWIO. This observation has useful implications, particularly in investigating why southeastern and southernwest parts of Africa are sometimes under different weather regimes.

10.3.2 Vertical sections

Vertical sections have been included in this study to complete a 3- D perspective of tropospheric changes over southern Africa. For consistency and brevity, EFW, LSFW and MSD were analysed and can be assumed to be continuations of Chapters 7 and 8. Wet spells are discussed from formation to dissipation (life cycle) while total values were

utilised for the MSD. As with hovmollers, the vertical sections are along 20°S latitude, from the central Atlantic to the eastern Indian Oceans. Important features stand out, a summary of which is enunciated below;

- The upper- tropospheric jet stream is prominent at 200 hPa, moreso for EFW (**Figure 9.4**), with standing short- waves of about 45° longitude wavelength. The jet is weakest in late summer over Africa and Madagascar due to a combined influence of a homogeneously warm underlying surface, embedded deep convective entities of the ITCZ and the barotropic tendency of the atmosphere then.

- Precursor patterns of early and late summer wet spells show contrasting features. P-2 vertical sections of meridional wind anomalies show northerlies slanting from the Atlantic Ocean at upper levels to the Mozambique Channel at 850 hPa prior to the peak of EFW (**Figure 9.5**). The reverse is the case for LSFW, with southerlies dominant. At P-1, the anomalies are opposite, southerly for EFW and northerly during LSFW. The anomaly patterns are similar over southern Africa at P0. In addition, there is evidence of eastward propagation from development (P- 1) to decay, particularly in late summer.

- Low- level easterly anomalies predominate Africa in the formative and developmental phases of EFW, important for advecting moisture from the Indian Ocean. Thereafter, the flow becomes westerly. In the case of LSFW, pre- convective stages are characterised by westward fluxes accompanied by poleward water vapour fluxes showing advection from the Equator into the MCAT. At decay, westward wind anomalies dominate Africa, a reversal of anomalies with respect to EFW.

- Temperature anomalies show a maximum at the surface over Africa prior to peaks of wet spells. Differences exist at maturity when amonalies are negative (positive) for EFW (LSFW), indicating increased contribution of mid- tropspheric latent heating in late summer. At decay, the atmosphere rapidly becomes stable (potentially unstable) for EFW (LSFW).

- Equivalent potential temperature (EPT) anomalies clearly exhibit important features. Firstly, both EFW and LSFW patterns show eastward propagation during their cycles (15-20° longitude per pentad for EFW). Secondly, build- up of EFW is from the

middle levels over the Atlantic Ocean. As regards LSFW, the transition is internal and gradual.

- The vertical distribution of horizontal divergence displays eastward translation from the Atlantic Ocean to the western Indian Ocean, moreso during EFW. The atmosphere over Africa is less likely to experience overturning in early summer, attributed to the Atlantic Ocean influence. During LSFW, there is a tendency towards lower- level convergence.

10.4 Wet and dry spell comparisons

Mindful of the fact that a fair degree of research has already been carried out on wet and dry spells in southern Africa (references in Chapter 2), this thesis has minimised objective comparisons to avoid duplication of efforts. Mid- summer patterns are the most crucial as far as agriculture, especially crop yield, are concerned. The thesis has revealed significant climatic departures between wet and dry spells. **Figure 10.1** shows 500 hPa geopotential height differences between typical wet spell patterns at their peaks (in other words, P0) and dry spells. The patterns represent EFW- MSD and LSFW-MSD geopotential height anomalies, respectively. It is apparent that, with repect to the MSD, early and late summer patterns generally contrast each other. Sub- tropical mid- level geopotential heights in early summer are significantly lower than during the MSD. Of greater implication is the NW- SE "ridge" of negative anomalies across southern Africa stretching to higher latitudes of the SWIO. This configuration best illustrates the position of a trough over southern Africa during EFW acting as an "attractor" for poleward fluxes. Negative anomalies poleward of 15°S across the entire domain imply either a weak sub- tropical anticyclone or increased frontal activity, hence greater baroclinicity in early summer. The LSFW-MSD pattern presents an opposite pattern. Of immediate relevance to southern Africa is a reduction of the Botswana Upper High and the linking of the MCAT (along 20° S) and the ITCZ axis in the Indian Ocean as seen in **Figure 10.1**. Tropical- extratropical exchanges of moisture and energy are more critical in early than in late summer over southern Africa. The elongation of a trough over southern Africa in **Figure 10.1** a also substantiates earlier- mentioned inferences that the west coast trough is more efficient in early summer while the MCAT- ITCZ combination dominates late summer wet spell episodes. In late summer, mid- latitude geopotentials are increased relative to dry spells and monsoon acts as the "attractor" then.

Contrasts between wet and dry spells can also be noted in moisture fields. **Figure 10.2** shows water vapour flux differences between EFW (P0) and MSD (a) and LSFW (P0) and MSD. In both cases, the MSD fluxes are subtrated from wet spell fluxes. The patterns are contrasting over oceanic regions, moreso in the south Atlantic and equatorial Indian Oceans. Both patterns also show a cyclonic gyre over central sub- tropical southern Africa along 25°S with a confluent region between 10 and 20°S. The moisture convergence is greater in the LSFW- MSD pattern, due to equator- to poleward fluxes during LSFW. The large eastward vectors in the latitudes of the MCAT indicate that low- level subsident easterlies associated with the BUH are strong in dry spells and equatorial westerlies, which characteristic of wet spells at maturity, are significantly effective. The former is supported by **Figures 7.20, 7.21** and **8.3**. Greater poleward fluxes in the Mozambique Channel and over Madagascar in the LSFW- MSD difference pattern is due to greater monsoonal effect during LSFW and the equatorward fluxes during the MSD.

Other parameters have also clearly displayed differences between dry and wet spells. Divergence patterns over southern Africa and the western Indian Ocean are generally opposite (for example, **Figure 9.13**). Lower divergence is beneath upper convergence over tropical southern Africa. The opposite is the case in the western Indian Ocean. This "dipole" confirms assertions in Chapter 8 that, during dry spells over southern Africa opposing vertical motions occur between the two. The most plausible explanation is the failure of Atlantic troughs to penetrate the Botswana Upper High. Comparisons between MSD and wet spell structures reveal opposite patterns. For example, meridional and zonal flow and divergence patterns at wet- spell peaks reverse direction during dry spells. **Figure 10.3** is an algebraic difference between EPTs for mean LSFW and MSD (LSFW-MSD). It is evident that, in general, EPT values during the LSFW phase are higher than for MSD everywhere but upwards of 200 hPa. Positive departures decrease from the surface to a minimum near 650 in the east Atlantic Ocean and close to 500 hPa in the Indian Ocean. The water vapour content of the atmosphere is the main cause of the difference, with more moisture in the Indian Ocean than the Atlantic Ocean. In addition, the axis of greatest departures is in a vertical column over 30- 50°E, rather than over Africa. This is due to the presence of low- level moisture convergence in the western Indian Ocean during dry spells over Africa.

10.5 Concluding remarks

The composites, mean and consequent anomalies used in this thesis are based upon a limited set of ECMWF data in the 1986/87- 1991/92 period. The meteorological inferences in the thesis lie not so much in the absolute magnitudes of the basic parameters, but in their relative structure and temporal variability. Hence, reference to magnitudes has been kept to a minimum. It is hoped that, as quality data of a longer period is available, the understanding and prediction of climate variability over southern Africa will become more objective. In addition, scale interactions between intra- seasonal and inter- annual fluctuations can be studied.

In summary, this thesis has identified the most probable onset, cessation and duration of wet and dry spells during southern African summer. Intra- seasonal oscillations exist, the most frequent are 10- 25- and 40- 50- day modes. Tracking the season has revealed synoptic configurations associated with different phases of summer, particularly trajectory of air masses and sources and sinks of moisture and controlling mechanisms. Life cycle analysis has shown precursors and triggers of wet spell episodes from 10- 15 days prior to wet spell peaks, both horizontally and vertically. **Table 10.1** provides summarised scenarios of weather variability prevalent from initiation to maturity of typical early and late summer wet spells. All the above shed more light on the atmospheric physics and dynamics over southern Africa, most importantly the role of the Mozambique Channel-Angola Trough and the Botswana Upper High. These features alternatively dominate climatic variability over the region. Such information is not only useful academically, but assists in medium range (sub- monthly) weather forecasting for utilisation by the agricultural sector. This is a significant departure from most research to date on southern Africa, where investigations have been largely diagnostic and based upon teleconnections and monthly to seasonal time frames. Regional climate modeling can produce more realistic scenarios by incorporating variability at intra- seasonal time frames.

Early summer wet spell Evolution

Precursor stages

Initiation (P-2) and development (P-1)

Upper northerlies in the equatorial Atlantic Ocean propagate to middle levels.

Middle and upper northerlies extend from northern Hemispheric Atlantic through SW Africa.

Middle and upper easterlies across central southern Africa.

Westward water vapour flux across central southern Africa from central Indian Ocean.

Meridional low- level kinematic confluence across central interior immediately downstream of west coast trough.

Maturity stage (P0)

NW- SE oriented trough across central interior of southern Africa.

Mid- level zonal westerly flow originating from Namibia

Upper westerly (*u* component) and upper southerly (*v*) flow across southern Africa.

Table 10.1 : Typical evolution of early and late summer wet spells

Late summer wet spells

Precursor stages:
Initiation (P-2) and development (P-1)

westward water vapour flux into tropical
southern Africa from the equatorial Indian Ocean

westward moisture advection into sub- tropical
southern Africa from the SWIO and Mozambique Channel.

low- and mid- level wind veering from equatorial
regions towards the TSB.

increase in kinematic confluence (hence boundary layer convergence)
across the TSB (due to northerly flow from the Equator to MCATand
easterlies from the SWIO).- intensification of the MCAT

increase in boundary layer pumping along the MCAT

Upper divergence over central southern Africa

Maturity stage

Low- level convergence and maximum uplift along 15S
(equatorward edge of the MCAT)

Moisture advection from the Congo and
from the SWIO convergent over southern Africa.

mid- level latent heat release - CISK

stronger upper divergence- Deep convection.

Table 10.1 (continued)

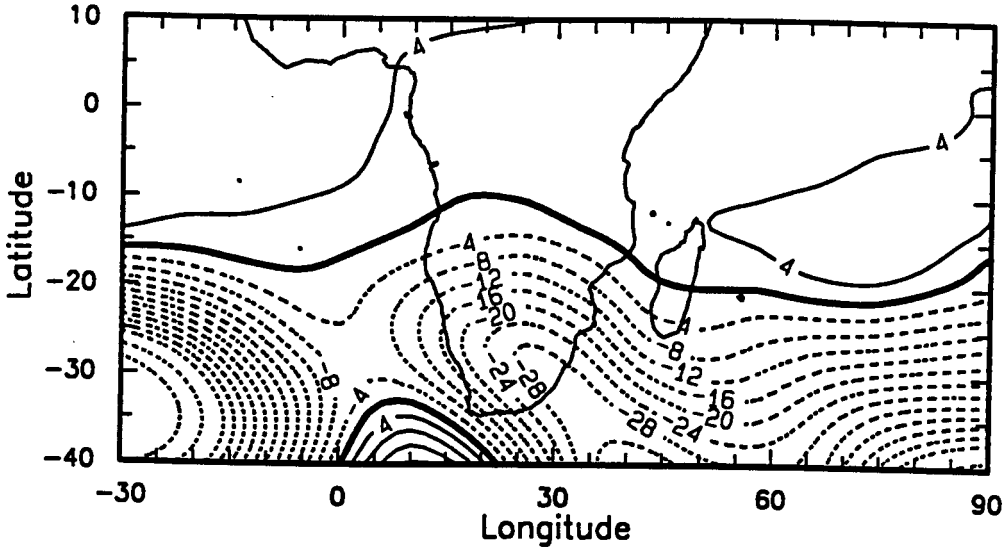

(a) EFW (P0)-MSD gpm anomaly

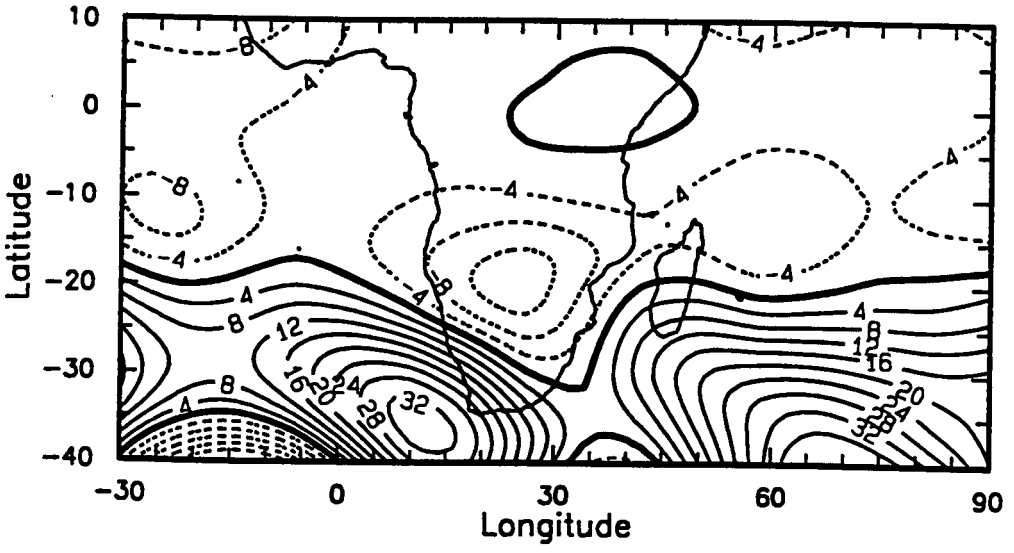

(b) LSFW (P0)-MSD gpm anomaly

Figure 10.1 : 500 hPa geopotential height departures (gpm) between wet spells at peak activity (P0) and the mid- summer dry spell. (a) shows EFW-MSD and (b) indicates LSFW-MSD anomalies.

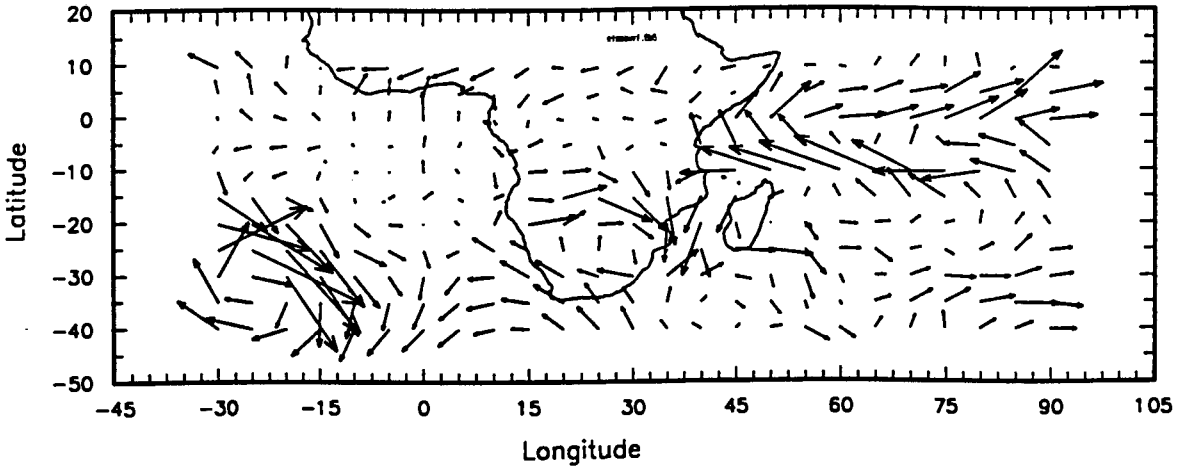

(a) EFW (P0)-MSD WVF anomaly. The longest vector corresponds to 181 g kg^{-1} m s^{-1}

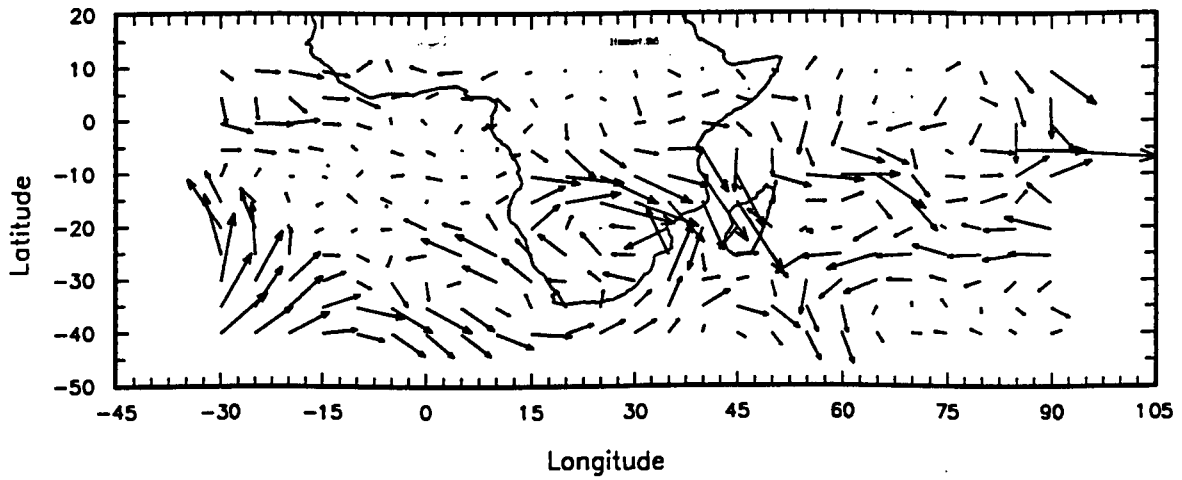

(b) LSFW (P0)-MSD WVF anomaly. The longest vector corresponds to 156 g kg^{-1} m s^{-1}

Figure 10.2 : Vertically integrated water vapour flux differences between wet spells at peak activity (P0) and the mid- summer dry spell. (a) shows EFW-MSD and (b) indicates LSFW-MSD anomalies.

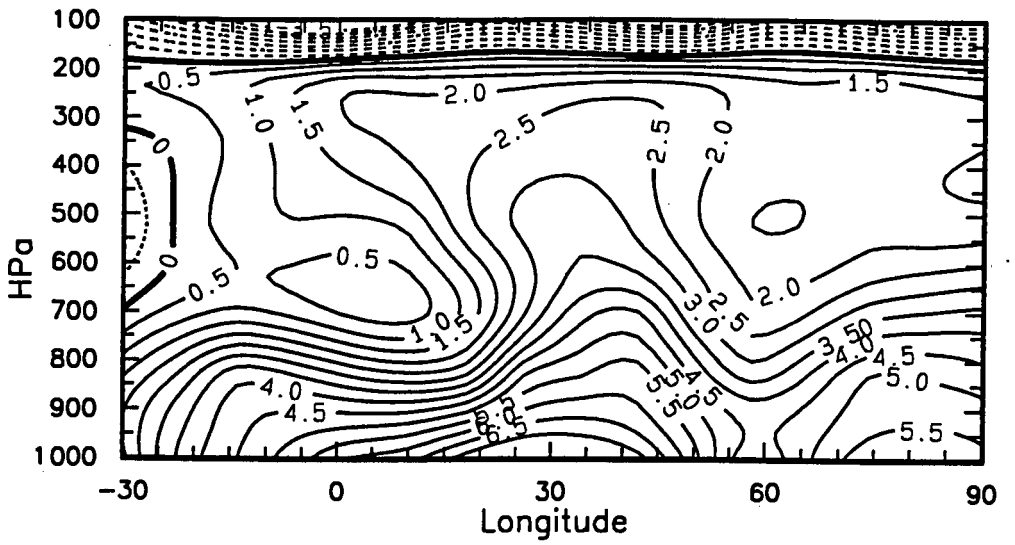

Figure 10.3 : Intercomparison: Mean LSFW- MSD Equivalent potential temperature from the surface to 100 hPa. Contour interval is 0.5°K.

Annexure 1

Composites used in Chapter 4

Annex 1(a) : Composition of pentads from October to March, the standard World Meteorological Organisation format and pentad numbers used in this thesis.

Pentad	WMO No.	Thesis No	Pentad	WMO No.	Thesis No
Oct 3 -7	56	1	Jan 1 - 5	1	19
8 -12	57	2	6 - 10	2	20
13 - 17	58	3	11 - 15	3	21
18 - 22	59	4	16 - 20	4	22
23 - 27	60	5	21 - 25	5	23
28 - Nov 1	61	6	26 - 30	6	24
Nov 2 - 6	62	7	31 - Feb 4	7	25
7 - 11	63	8	Feb 5 - 9	8	26
12 - 16	64	9	10 - 14	9	27
17 - 21	65	10	15 - 19	10	28
22 - 26	66	11	20 - 24	11	29
27 - Dec 1	67	12	25 - Mar 1	12	30
Dec 2 - 6	68	13	Mar 2 - 6	13	31
7 - 11	69	14	7 - 11	14	32
12 - 16	70	15	12 - 16	15	33
17 - 21	71	16	17 - 21	16	34
22 - 26	72	17	22 - 26	17	35
27 - 31	73	18	27 - 31	18	36

Annex 1 (b) : Thesis pentads (Annex 1 (a) above) used to construct composites of wet spells.

EFW	1986-87	1987-88	1988-89	1989-90	1990-91	1991-92
P - 2	12	10	10	10	9	8
P - 1	13	11	11	11	10	9
P0	14	12	12	12	11	10
P + 1	15	13	13	13	12	11
ESW						
P - 2	-	13	-	15	15, 18	15
P - 1	-	14	-	16	16, 19	16
P0	-	15	-	17	17, 20	17
P + 1	-	16	-	18	18, 21	18
LSFW						
P - 2	21	21	21	22	18	21
P - 1	22	22	22	23	19	22
P0	23	23	23, 25	24	20	23
P + 1	24	24	24, 26	25	21	24
LSSW						
P - 2	25	27	28	27	25	29
P - 1	26	28	29	28	26	30
P0	27	29	30	29	27	31
P + 1	28	30	31	30	28	32
LSTW						
P - 2	33	30	33	-	31	33
P - 1	34	31	34	-	32, 34	34
P0	35	32	35	-	33, 35	35
P + 1	36	33	36	-	34, 36	36

Annex 1 (c): Same as Annex 1 (b), but for peaks of dry spells

	1986-87	1987-88	1988-89	1989-90	1990-91	1991-92
MSD	16 - 17, 20	19	17	16	-	21
ESMD	-	-	14	-	12	12
LSMD	-	25 - 26	22	-	-	21
LSD	28 - 31 33 - 34	35 - 36	33 - 34	30 - 33	30 - 31	27 - 29

Abbreviations

Wet spells

EFW	: First wet spell of early summer
ESW	: Second wet spell of early summer
LSFW	: First wet spell of late summer
LSSW	: Second wet spell of late summer
LSTW	: Third wet spell of late summer

Dry spells

MSD	: Mid-Season Dry Spell
LSD	: Late Season Dry Spell
ESMD	: Early Summer Minor Dry Spell
LSMD	: Late summer Minor Dry Spell

Annexure 2

Basic equations, mathematical concepts and definitions

The following notation and list of symbols are generally universal.

t	Time
T	Temperature
q	specific humidity
p	pressure
p_O	standard pressure of 1000 hPa
ps	surface pressure
p_u	pressure at which water vapour amounts become negligible (taken as 300 hPa)
u	eastward (zonal) component of V
v	northward (meridional) component of V
V	horizontal wind velocity
w	vertical velocity
W	precipitable water
z	Geopotential height above sea level
x	arbitrary dependent variable
$\overline{x}$	time average of x
x'	deviation from time average
$[x]$	zonal average of x
x^*	deviation from zonal average
$\sigma(x)$	standard deviation of x
a	radius of the earth taken as a sphere, (6.371×10^6 m)
g	acceleration of gravity, (9.81 m s^{-2})
φ	latitude, positive northward
λ	longitude, positive eastward
ψ	stream function
χ	velocity potential
θ	potential temperature (°K)

Units and typical orders of magnitude of most common parameters

horizontal velocity	-	ms^{-1}
vertical velocity	-	$x\ 10^{-2}\ Pa\ s^{-1}$
divergence	-	$x\ 10^{-5}\ s^{-1}$
vorticity	-	$x\ 10^{-5}\ s^{-1}$
velocity potential	-	$x\ 10^{4}\ m^{2}\ s^{-1}$
stream function	-	$x\ 10^{5}\ m^{2}\ s^{-1}$
water vapour flux	-	$kg\ m^{-1}\ s^{-1}$
precipitable water	-	mm
Geopotential height	-	gpm

The velocity components of motions with respect to the earth's surface are given horizontally by u and v, and vertically by w

$$u = \cos\phi \frac{d\lambda}{dt}$$

$$v = a\frac{d\phi}{dt}$$

$$w = \rho\left(\frac{\partial\theta}{\partial t} + \frac{u}{a\cos\phi}\frac{\partial\theta}{\partial\lambda} + \frac{v}{a}\frac{\partial\theta}{\partial\phi} - g\omega\right) \text{ or } w = \frac{dp}{dt}$$

where ω is the geometrical vertical velocity. Generally, tropospheric tends to have the same sign. They reach a maximum value in the mid- troposphere, in the vicinity of the 600 hPa level, a level at which isobaric divergence must be zero (referred to commonly as the level of non divergence, or LND). While individual cases may depart from this mean position, the troposphere is usually consistent with the existence of only one NLD, with either divergence below and convergence above (subsidence) or with convergence below and divergence above (ascent). Thus, in this thesis, only middle tropospheric vertical motion is accorded due recognition.

Sign conventions : eastward (westward) flow is positive (negative)
: northward (southward) flow is positive (negative)
: subsidence (ascent) is positive (negative).

Time mean quantity calculations are carried out in the following format, eg. horizontal zonal wind

$$\bar{u} = \frac{1}{\Delta t}\int_{t}^{t+\Delta t} u(\lambda, \phi, p, t)dt$$

Chapter 5 of the thesis is based upon this type of equation.

Deviations from the temporal and zonal averages are derived using the form

$$u' = u - \bar{u}$$

They are merely departures from the long- term mean and are referred to as anomalies in Chapters 6, 7 and 9. The anomalies in Chapter 4 are further normalised with respect to the standard deviation $(\frac{u'}{\sigma})$ where σ is the standard deviation

Vector variables (eg. horizontal wind and water vapour flux) are obtained trigonometrically using the formulae

$$\sqrt{(xu)^2 + (xv)^2}$$

$$\arctan(\frac{xu}{xv})$$

for the magnitude (top) and direction (bottom), where ***x*** is an arbitrary parameter while ***u*** and ***v*** have the usual notation.

At present the ECMWF data consist of daily grid-point values of the meteorological parameters ***u, v, T, z, RH*** (RH is the relative humidity). Data is reduced into u', v', T', z', time-averaged values (for, example, $\overline{u}, \overline{v}, \overline{T}, \overline{q},$) and water vapour transports $(\overline{u'q'}, \overline{v'q'})$ as well as temperature transports $(\overline{T'u'}, \overline{T'v'})$, where the bar denotes a time average and the prime the deviation from it.

To determine the long- term mean, say ***u***, the formula to use is

$$\bar{u} = \frac{\sum_{m} N\bar{u}}{\sum_{m} N}$$

where $\bar{u}$ and N are values of the pentad means and the number of data points entering the respective means for all pentads for all years in a typical season, respectively.

Stream function

Consider the following Figure:

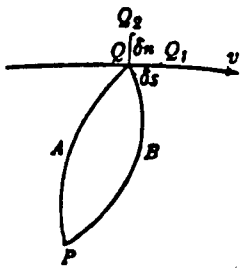

In a two- dimensional motion of a perfect fluid (say of unit thickness perpendicular to the paper), we can define the "flux" across any line **PQ** in the fluid as $\psi = \int_P^Q v_n ds$, where ds is an element of the line and v_n is the component velocity of the fluid perpendicular to ds. Thus, $\delta\psi = v_n\, \delta s$. Any line, therefore, through **P** and **Q** will have the same flux across it, as the flux across **PAQ** from left to right is the total volume entering the space **PAQBP** per second which must be equal to the volume leaving this space per second, i.e. the flux across **PBQ** from right to left. This is because the fluid is considered to be incompressible. If **Q** moves to Q_1, where $QQ_1 = \delta s$ is along a stream- line, $v_n = 0$; $\therefore\ \delta\psi = 0$. Thus, ψ is constant along a streamline and it is called the "stream function". One can imagine stream functions as a series of stream- lines at equal increments like contour lines on a map. If **Q** moves to Q_2, where $QQ_2 = \delta n$ and is perpendicular to a stream- line, $v_n = v$, $\delta\psi = v\, \delta n$, therefore $v = \frac{d\psi}{dn}$, or the closer the stream- lines the greater the velocity.

Velocity potential

Similarly, one can imagine the integral $\chi = \int_P^Q v_s ds$, where v_s is the component velocity of the fluid parallel to ds, in other words $\delta\chi = v_s\, ds$. When the vorticity (circulation per unit area) at all points in the fluid is zero, its motion is said to be "Irrotational". The integral becomes a quantity like ψ and is independent of the path between **P** and **Q** but dependent only on the position of **Q**.

$$\therefore \int_P^Q Bv_s ds = -\int_Q^P Bv_s ds = \int_P^Q Av_s ds$$

The integral is referred to as the "velocity potential" at **Q** with respect to **P**. If **Q** moves to $\mathbf{Q_1}$, where $\mathbf{QQ_1} = ds$, or $v = \frac{d\chi}{ds}$, i.e the velocity at Q is the "gradient" of χ along a stream- line, vs = 0; $\therefore\ \delta\chi = 0$, or χ is constant along lines which cut the stream- lines at right angles (equi- potential lines). The dimensions of χ are the same as those of ψ, viz. velocity x length.

The above concept can be applied to describe zonal and meridional circulations.
The horizontal wind field (V) can be resolved into two parts, namely the rotational ($V\psi$) and irrotational or divergent ($V\chi$) components such that

$$V = V\chi + V\psi \qquad \text{(from Helmholtz theorem)}$$

χ and ψ are the velocity potential and streamfunction, obtained through mathematical relaxation procedures using horizontal divergence and vorticity, respectively. The streamfunction and velocity potential can be defined as

$$\nabla^2\psi = \zeta$$
$$\nabla^2\chi = \delta$$

where ζ and δ are relative vorticity and divergence, respectively. These are in turn defined by the following :

$$\zeta = \frac{1}{r\cos\phi}\left[\frac{\partial v}{\partial\lambda} - \frac{\partial}{\partial\phi}(u\cos\phi)\right] \quad \textbf{or in cartesian coordinates } (\frac{\partial u}{\partial x} - \frac{\partial v}{\partial y})$$

$$\delta = \frac{1}{r\cos\phi}\left[\frac{\partial u}{\partial\lambda} + \frac{\partial}{\partial\phi}(v\cos\phi)\right] \quad \textbf{or} \quad \delta = \frac{\partial u}{\partial x} + \frac{\partial v}{\partial y}$$

ϕ and λ are latitude and longitude, respectively. The sign convention used is that winds travel cyclonically around a local ψ maximum (in other words, low geopotential heights) in the Southern Hemisphere. In the Northern Hemisphere, they move cyclonically around a local ψ minimum (inferred low heights). This notation has been used before (Knutson and Weickmann, 1987). The technique is not new (Holton, 1973; Krishnamurti et al., 1973; Pathack, 1993; Levey, 1993, for example) and the parameters are determined from taking the Laplacian of divergence and vorticity. To overcome boundary problems, the

domain of χ and ψ is smaller than that of the original windfield in this thesis by 5° on all sides.

sign convention: The divergent component of the total wind field flows from negative (or small) to positive (higher) values and the flow is perpendicular to the contours (Knutson and Weickmann, 1987). The speed of flow is proportional to the contour gradient. Thus the greater the curvature, the larger the divergence. The divergent component is useful in intra- seasonal oscillations of sources and sinks of atmospheric energetics, moisture and convection (Chen, 1985; Chen and Tzeng, 1990).

The water vapour content of moist air can be expressed by many variables utilised in meteorology, the most frequently being specific humidity (q), mixing ratio (r) and the relative humidity (RH). The specific humidity is defined as the ratio of the mass m_v of water vapour to the total mass, m. The mixing ratio is the ratio of m_v to the mass of dry air m_d, while RH is the ratio of the molar fraction of water to the molar fraction corresponding to saturation with respect to water or ice. In this thesis, tropospheric RH below 300 hPa is considered, on assumption the region experiences mainly warm rain, especially over all but the extreme south west of southern Africa. Mathematically, the variables can be represented by the following:

$$r = \frac{\varepsilon e}{p - e}, \qquad q = \frac{r}{1 + r}, \qquad RH(p) = \frac{q(p)}{q_s(p, T)}$$

where $\varepsilon = \frac{R_d}{R_v} = 0.622$ (ratio of molecular weights of water and dry air), e is water vapour pressure and the rest of the variables are according to the usual notation. In addition, r and q are always smaller than 0.04. Thus, without great error, $q \cong r$.

Precipitable water, W

This can be defined as the potential quantity of a water obtained if a column of air of uniform cross- sectional area were to condense onto a horizontal plane of unit area. It is determined from a unit mass of saturated air rising in the atmosphere. During the ascent, the water vapour will condense into water (or ice) by assuming that all the water precipitates as rain (convectively efficient). Taking into account that the density is 10^3 kg m^{-3}, 1 kg m^{-2} of precipitated water is equivalent to 1 mm. The common practice in

meteorology is to express it in mm h^{-1}. The equation for W is useful mainly for semi-quantitative prediction for a large area. It is not a satisfactory procedure as, in practice, precipitation amounts are seldom representative, more so in the tropics where the precipitation is chiefly of convective origin. A few rain gauges (for observed rates of precipitation) do not constitute an adequate sample of a large area for quantitative purposes. Mathematically, water vapour content of a unit column of air (**precipitable water**), ***W***,

$$= \frac{1}{g}\int_{p_u}^{p_s} q dp$$

In this thesis, p_s = 1000 hPa (sea level) or 850 hPa over land, while p_u remains at 300 hPa. The objective is to include the lowest troposheric levels where moisture is abundant (Newell, et al., 1972). W in the thesis is determined in mm.

Water vapour flux (Q)

Q can be defined as the advection of moisture through a deep tropospheric layer by horizontal wind. Thus, like precipitable water, Q is also obtained through vertical integration. In the tropics, the bulk of the horizontal transfer of water vapour takes place below 700 (Newell et al, 1972). The vapour transport can, therefore, be assumed to be largely determined by the low- tropospheric wind field. In this thesis, the integration is from the surface, p_s (1000 hPa over the ocean and 850 hPa over elevated land) to 500 hPa (p_u) levels.

$$Q = \frac{1}{g}\int_{p_u}^{p_s} qV dp$$

where q is the specific humidity and V the velocity at a particular level.

Internal Energy, U

In the mean, the earth as a whole is in a state of radiative equilibrium, in which the solar radiation absorbed is compensated by emission to space. However, between absorption and emission, the solar heating causes an increase in the specific internal energy of the atmospheric gas. As the gas expands due to the increase in temperature, it lifts the mass centre of any vertical column under consideration, implying an increase in potential

energy. The internal and potential energies may then be transformed into kinetic energy of motion of large air masses, then turbulence and finally into heat.

The approximate formula for U is

$$U = c_v T + l_v q + const \qquad \text{(Irbarne and Godson, 1981)}$$

The equation includes a term proportional, at every point, to the temperature, and another due to the vapourisation of its water vapour content. U can be referred to as sensible heat. This thesis concentrates only on terms proportional to the temperature ($c_v T$), to avoid more complex situations when there are water phase transitions. Besides, globally, sensible heat is by far greater in magnitude than latent heat (up to 25 times by Peixoto and Oort, 1992). In other words, the assumption is adiabatic atmospheric motion. Adiabatic motion (or process) is defined as motion (process) in which entropy, hence potential temperature, is conserved for every parcel of air. The above assumption is not truly valid. For example, atmospheric motion is not purely adiabatic since ground surface friction and the mixing of air are non- adiabatic, yet they alter the kinetic energy, destroying it and generating internal energy. Despite the above remarks, the advantage of considering adiabatic flows reside in that they represent a good approximation to large scale motions of the atmosphere (Irbarne and Godson, 1981). Solar heating increases the specific internal energy of the atmospheric gas. As the gas expands due to the increase in temperature, it raises the centre of mass of any vertical column that may be considered, implying an increase in potential energy.

The equation applied to determine U in this thesis is

$$= \frac{c_v}{g} \int_{ph}^{p0} T dp$$

where c_v, T, p, and R have the usual notations, while the integrations are performed from the surface (p_0 = 850 hPa) to a pressure surface (p_h = 500 hPa) and neglecting the small variations of c_v and R with humidity and of g with altitude.

Dew point

A mass of moist air cooling at consant pressure contracts. The relative humidity increases and if cooling continues the air can reach saturation. The temperature at which saturation is reached is called the dew point. It is thus a useful variable to characterise the humidity of the air. In this thesis, it is assumed the humidity of the atmosphere in the latitudes under study (from 10°N to 40°S) may change by incorporating water vapour through turbulent diffusion from the ocean surface and from water falling through the air mass. In this regard only the lower troposphere will be considered. The dew point values are extracted from ECMWF data via relative humidity.

Equivalent potential temperature (EPT)

The EPT can be defined as the temperature attained by a parcel of air at 1000 hPa after its moisture has condensed at a given level. The parcel then follows a dry adiabat from that level down to 1000 hPa. Useful references are Holton (1973), Bolton (1980) and Peixoto and Oort (1992). EPT eliminates problems associated with local temperature changes like cooling (warming) due to adiabatic expansion (compression), thereby enabling comparisons to be made at various atmospheric levels. As a quasi- conservative parameter, can be used for investigating the stability of the atmosphere.

Mathematically, in this thesis,

$$EPT = \theta_e \exp\left[\left(\frac{3.376}{T_L} - 0.00254\right) * r(1 + 0.81 * 10^{-3} r)\right]$$

where $_{e} = \mathrm{T}(\frac{\mathrm{p_o}}{\mathrm{p}})^{\kappa}$ and $\kappa = \frac{R_d}{C_p}$

T_L is the lifting condensation level, expressed as

$$T_L = \frac{2840}{3.5\ln(T + 273.15) - \ln(e) - 4.805} + 55$$

e is the water vapour pressure, T temperature and r the mixing ratio.

References

Abbreviation	Full name of Publication
Adv. Geophys.	: Advances in Geophysics
Agric. Met	: Agricultural Meteorology
Aus. Met. Mag.	: Australian Meteorological Magazine
Bul. Amer. Met. Soc.	: Bulletin of the American Meteorological Society
Climate Dyn.	: Climate Dynamics
Int. J. Climatol.	: International Journal of Climatology
J. Afr. Met. Soc.	: Journal of the African Meteorological Society
J. Appl. Meteor.	: Journal of Applied Meteorology
J. Atmos. Sci.	: Journal of the Atmospheric Sciences
J. Clim.	: Journal of Climate
J. Clim. Appl. Met.	: Journal of Climate and Applied Meteorology
J. Climatol.	: Journal of Climatology
J. Geophys. Res.	: Journal of Geophysical Research
J. Meteor.	: Journal of Meteorology
J. Met. Soc. Japan	: Journal of the Meteorological Society of Japan
Meteor. and Geophys.	: Meteorology and Geophysics
Meteor. Atmos. Phys.	: Meteorology and Atmospheric Physics
Met. Mag.	: Meteorological Magazine
Mon. Wea. Rev	: Monthly Weather Review
Quart. J. Roy. Met. Soc.	: Quarterly Journal of the Royal Meteorological Society
S. Afr. Geogr. Journ.	: South African Geographical Journal
Theor. Appl. Climatol.	: Theoretical and Applied Climatology
Rev. Geophys. Space Phys.	: Review of Geophysical Space Physics
S. Afr. J. Mar. Sci.	: South African Journal of Marine Science
S. Afr. J. Sci.	: South African Journal of Science
S. Afr. Wea. Bur. Tech. Paper	: South African Weather Bureau Technical Paper
Zim. Sci. News	: Zimbabwe Science News

Acharya, U.R., and N.S. Bhaskara Rao, 1981: Meteorology of Zambia: Part II. *Govt. Printers, Lusaka, Zambia.*49 pp.

Anyamba, E.K., 1992: Some properties of a 20-30 day oscillation in tropical convection. *J. Afr. Met. Soc.*, **1**, 1-19.

Anderson, J.R., and R.D. Rosen, 1983: The latitude height structure of the 40-50-day variations in atmospheric angular momentum. *J. Atmos. Sci.*, **40**, 1584- 1591.

Arkin, P.A., and P.E. Ardanuy, 1989: Estimating climatic- scale precipitation from space: A Review. *J. Clim.*, **2**, 229- 1238.

Asnani, G.C., 1993: Tropical Meterorology. *Noble Printers,* Pune- India, 1202 pp.

Bannon, P.R., 1981: Synoptic- scale forcing of coastal lows: forced double Kelvin waves in the atmosphere. *Quart. J. Roy. Met. Soc.*, **107**, 313- 327.

Barclay, J.J., 1992: Wet and Dry troughs over Southern Africa during early summer. *MSc thesis, University of Cape Town*, Cape Town, South Africa. Unpublished. 152 pp.

Barnett, T.P., 1984: Long- term trends in surface temperatures over the oceans. *Mon. Wea. Rev.*, **112**, 303- 312.

Barnett, T.P., N. Graham, M. Cane, S. Zebiak, S. Dolan, J. O'brien, and D. Legler, 1988: On the prediction of the El Nino of 1986- 87. *Science,* **241**, 192- 196.

Bell, I.D., 1986: The Northwest Australian Cloud Band. *Preprints of the 2nd International Conference on Southern Hemisphere Meteorology, Amer. Met. Soc.*, 42- 45.

Benedict, W.L., and R.L. Haney, 1988: Contribution of tropical winds to subseasonal fluctuations in atmospheric angular momentum and length of day. *J. Geophys. Res.*, **93**, 15973- 15978.

Bhalotra, Y.P.R., 1973: Disturbances of the summer season affecting Zambia. *Tech. Memorandum,* **3**, Zambia Met. Dept.

Bhanu, O., L.J. Ogallo, and P.M. Bundi, 1989: A comparative study of estimation of monthly precipitation over the tropical southern Indian Ocean from satellite data. *Proc. 3rd Conf. Southern Hem. Met., 229- 232, Amer. Met. Soc.*, Buenos Aires.

Blackmon, M.L., Y.-H. Lee, and J.M. Wallace, 1984a: Horizontal structure of 500-mb height fluctuations with long, intermediate and short time scales. *J. Atmos. Sci.*, **41**, 961-979.

Blackmon, M.L., Y.-H. Lee, and H.-H. Hsu, 1984b: Time variations of 500-mb height fluctuations with long, intermediate, and short time scale as deduced from lag-correlation statistics. *J. Atmos. Sci.*, **41**, 981-991.

Blackmon.,M., S. Mullen, and G. Bates, 1986: The climatology of blocking events in a perpetual January simulation of a spectral general circulation model. *J. Atmos. Sci.*, **43**, 1379- 1405.

Bjerknes, J., 1966: A possible response of the amospheric Hadley circulation to equatorial anomalies of ocean temperature. *Tellus*, **18**, 820- 829.

Bjerknes, J., 1969: Atmospheric teleconnections from the equatorial Pacific. *Mon. Wea. Rev.*, **97**, 163- 172.

Bjerknes, J., L.J. Allison, E.R. Kreins, F.A. Godshall, and G. Warnecke, 1969: Satellite mapping of the Pacific tropical cloudiness. *Bul. Amer. Met. Soc.*, **50**, 313- 322.

Boer, G.J., 1985: Modelling the atmospheric response to the 1982/83 El Nino. *Elsevier Oceanographic Series*, **40**.

Bolton, D., 1980: The computation of Equivalent Potential Temperature. *Mon. Wea. Rev.*, **108**, 1046- 1053.

Brier, G.W., 1978: The Quasi- Biennial Oscillation and feedback processes in the atmosphere- ocean- earth system. *Mon. Wea. Rev.*, **106**, 1890- 1897.

Chang, C-P., 1976: Forcing of stratospheric Kelvin waves by tropospheric heat sources. *J. Atmos. Sci.*, **33**, 740- 744.

Chang, C-P., and H. Lim, 1988: Kelvin wave- CISK: A possible mechanism for the 30-50 day oscillation. *J. Atmos. Sci.*, **45**, 1709- 1720.

Charney, J.G., 1966: Some remaining problems in numerical weather. Advances in Numerical Weather Prediction. *The Travelers Research Center, Inc.*, Hartford, CT., 61- 70.

Chelliah, M. and P. Arkin, 1992: Large- scale interannual variability of monthly outgoing longwave radiation anomalies over the global tropics. *J. Clim.*, **5**, 371-389.

Chen, T-C., and Murakami, M., 1988: The 30- 50 day variation of convective activity over the western Pacific Ocean with emphasis on the northwestern region. *Mon. Wea. Rev.*, **116**, 892- 906.

Chen, T-C., M-C. Yen, and M. Murakami, 1988a: The water vapour transport associated with the 30- 50 day oscillation over the Asian monsoon regions during the 1979 summer. *Mon. Wea. Rev.*, **116**, 1983- 2002.

Chen, T-C., R-Y. Tzeng and M-C. Yen, 1988b: Development and life cycle of the Indian monsoon: Effect of the 30- 60 day oscillation. *Mon. Wea. Rev.*, **116**, 2183- 2199.

Chen, T-C., and R-Y. Tzeng, 1990: Global scale Intra- seasonal and annual variation of divergent water vapour flux. *Meteorol. Atmos. Phys.*, **44**, 133- 151.

Chen, T-C., and M-C. Yen, 1990: A study of the maintenance of the 30- 60 day oscillation of the planetary- scale divergent circulation. *J. Geophys. Res.* Pending review.

Chen, T-C., and M-C. Yen, 1991: Intraseasonal variations of the tropical easterly jet during the 1979 northern summer. *Tellus*, **43a**, 213- 225.

Chen, W.Y., 1982: Assessment of Southern Oscillation sea level pressure indices. *Mon. Wea. Rev.*, **110**, 800- 807.

Chu, P.S., and R.W. Katz, 1985: Modeling and forecasting the Southern Oscillation: a time- domain approach. *Mon. Wea. Rev.*, **113**, 1876- 1888.

Cornejo- Garrido, A.G. and P.H. Stone, 1977: On the heat balance of the Walker Circulation. *J. Atmos. Sci.*, **34**, 1155- 1162.

Critchfield, H.J., 1974: General Climatology. *2nd Edition, Prentice- Hall Inc, NJ.* 420pp.

Currie, G.R., 1987: On bistable phasing of 18.6 year induced drought and flood in the Nile records since AD 650. *J. Climatol.*, 7, 373- 389.

Currie, G.R., 1993: Luni- solar 18.6- and 10- 11- year solar cycle signals in South African rainfall. *Int. J. Climatol.*, **13**, 237- 256.

Currie, G.R. and D.P. O'Brien, 1988: Periodic 18.6- year and cyclic 10 to 11 year signals in Northeastern United States Precipitation Data. *Mon. Wea. Rev.*, **8**, 255- 281.

D'Abreton, P., 1992: Water Vapour fluxes and kinematic forcing of South African summer rainfall. Department of Geography and Environmental Studies. *PhD thesis, University of Witwatersrand,* Johannesburg , S. Africa. 231pp

Daniels, J.M., and A.D. Vernekar, 1988: Influence of sea- surface temperature on intra- and inter- seasonal variations of the ITCZ. *Proc. 7th Conf. Ocean- Atmosphere Interaction, Anaheim Calif,* J61- 64.

Dartt, D.G., and A.D. Belmont, 1970: A global analysis of the variability of the Quasi-Biennial Oscillation. *Quart. J. Roy. Met. Soc.*, **96**, 186- 194.

Deser, C., and J.M. Wallace, 1987: El Nino events and their relation to the Southern Oscillation. *J. Geophys. Res.*, **92**, 14189- 14196

Diab, R.D., 1988: Rainfall- producing systems in Natal. *Final Report to FRD,* CSIR, Pretoria, 126pp.

Dickey, J.O., M. Ghil, and S.L. Marcus, 1991: Extratropical aspects of the 40- 50 day oscillation in length of day and atmospheric angular momentum. *J. Geophys. Res.*, **96**, 22634- 22658.

Doodson, A.T., and H.D. Warburg, 1941: Admiralty Manual of Tides. *Her Majesty's Stationary Office*, London. 270pp

Dole, R.M., 1982: Persistent anomalies of the extratropical Northern Hemisphere wintertime circulation. *PhD. thesis, Massachusetts Institute of Technology,* Cambridge, MA.

Dole, R.M., 1986: The life cycles of persistent anomalies and blocking over the North Pacific. *Adv. Geophys.*, **29**, *Academic Press*, 31- 69.

Dole, R.M., 1988: Life cycles of persistent anomalies. Part I: Evolution of 500mb- height fields. *Mon. Wea. Rev.*, **117**, 177- 211.

Dunn, P., 1985: An investigation into tropical cyclones in the SW Indian Ocean, Flood studies. *Tech. Note 1, Dept. Water Affairs*, Pretoria, South Africa. 33pp.

Dyer, T.G.J., 1975: The assignment of rainfall stations into homogeneous groups: An application of principal component analysis. *Quart. Jour. Roy. Met. Soc.*, **101**, 1005- 1013.

Ebdon, R.A., 1975: The Quasi- Biennial Oscillation and its association with tropospheric circulation patterns. *Met. Mag.*, **104**, 282- 297.

ECMWF, 1989: The Description of the ECMWF/ WMO global analysis data sets.

Eliot, J., 1895: A preliminary discussion of certain oscillatory changes of pressure of long period and short period in India. *Memoirs of the Indian Meteorological Department,* **6**, 89- 160.

Estie, K.E., 1984: Forecasting the formation and movement of coastal lows. *Abstracts and Summary of the coastal low workshop, Institute of Marine Technology,* Simonstown, Cape Town, 17-27.

Emanuel, K.A., 1987: An air- sea interaction model of intraseasonal oscillations in the tropics. *J. Atmos. Sci.*, **44**, 2324- 2340.

Fraedrich, K., 1988: El Nino/ Southern Oscillation predictability. *J. Atmos. Sci.*, **116**, 1001- 1002.

Frederiksen, J.S., and C.S. Frederiksen, 1993: Monsoon disturbances, intraseasonal oscillations, teleconnection patterns, blocking, and storm tracks of the global atmosphere during January 1979: Linear theory. *J. Atmos. Sci.*, **50**, 1349- 1372.

Frolow, S., 1942: On synchronous variation of pressure in the tropical regions. *Bul. Amer. Met. Soc.*, **23**, 239- 234.

Gadgil, S., P.V. Joseph, and P.H. Stone, 1984: Ocean- atmosphere coupling over monsoons regions. *Nature,* **312**, 141- 143.

Gadgil, S., A. Guruprasad, and J. Srinivasan, 1992: Systematic bias in the NOAA OLR Dataset. *J. Clim.*, **5**, 867- 875.

Gadgil, S., and A. Guruprasad, 1990: An objective method for the identification of the ITCZ. *J. Clim.*, **3**, 558- 567.

Gadgil, S., and J. Srinivasan, 1990: Low frequency variation of tropical convergence zone. *Meteor. Atmos. Phys.*, **44**, 119- 132.

Garanganga, B.J., 1989: The onset of 1982/83 summer monsoon over southern Africa: A diagnostic study. *M.Sc. thesis, University of Texas, A&M, Texas, USA. unpublished.* 74pp.

Ghil, M., and K. Mo, 1991: Intraseasonal oscillations in the global atmosphere, Part II: Southern Hemisphere. *J. Atmos. Sci.*, **48**, 780- 790.

Gill, A.E., 1977: Coastally trapped waves in the atmosphere. *Quart. J. Roy. Met. Soc.*, **103**, 431- 440.

Gill, A.E., 1980: Some simple solutions for heat- induced tropical Circulation. *Quart. J. Roy. Met. Soc.*, **106**, 447- 462.

Gill, A.E., 1982: Studies of moisture effects in simple atmospheric model: The stable case. *Geophys. Astrophys. Fluid Dyn.*, **19**, 119- 152.

Gill, A.E., and E.M. Rasmussen, 1983: The 1982- 83 climate anomaly in the equatorial Pacific. *Nature,* **306**, 229- 234.

Graham, N., and T. Barnett, 1987: Sea surface temperature, surface wind divergence and convection over tropical oceans. *Science,* **240**, 1293- 1302.

Graham, N., J. Michaelsen, and T. Barnett, 1986: An investigation of the El Nino-Southern Oscillation cycle with statistical models. *J. Geophys. Res.,* **92**, 14271-14289.

Gray, W.M., J.D. Sheaffer, and J.A. Knaff, 1991: Hypothesised mechanism for stratospheric QBO influence on ENSO variability. *5th Conference on Climate Variation,* Denver, Colorado, U.S.A.

Grimmer, M. 1963: The space filtering of monthly surface temperature data in terms of pattern using Empirical Orthogonal Functions. *Quart. J. Roy. Met. Soc.*, **39**, 395-408.

Gruber, A., 1990: A comparison of ERBE and AVHRR longwave flux estimates. *NOAA Tech. Rep., NESDIS*, **50**.

Gruber, A. and A.F. Krueger, 1984: The status of the NOAA outgoing longwave radiation. *Bul. Amer. Meteor. Soc.*, **65**, 958-962.

Gruber, A., M. Varnadore, P.A. Arkin, and J.S. Winston, 1986: Monthly and seasonal outgoing longwave radiation and anomalies. *NOAA Tech. Rep., NESDIS, 26,* Washington DC, USA.

Gutzler, D.S., and R.A. Madden, 1993: Seasonal Variations of the 40-50-day Oscillation in Atmospheric Angular Momentum. *J. Atmos. Sci.*, **50**, 850- 860.

Gutzler, D.S., and T.M. Wood, 1990: Structure of large- scale convective anomalies over tropical oceans. *J. Clim.*,**3**, 483- 496.

Halpert, M.S., and C.F. Ropelewski, 1992: Surface temperature patterns associated with the Southern Oscillation. *J. Clim.*, **5**, 577- 593.

Hamilton, K., 1990: A look at the recently proposed Solar- QBO- Weather Relationship. *J. Clim.*, **3**, 497- 503.

Hamilton, K. 1991: Mean wind evolution through the quasi- biennial cycle in the tropical lower stratosphere. *J. Atmos. Sci.*, **41**, 2113-2125.

Harangozo, S.A. and M.S.J. Harrison, 1983: On the use of synoptic data in indicating the presence of cloud bands over Southern Africa. *S. Afr. J. Sci.*, **79**, 413- 414.

Harangozo, S.A., 1989: Circulation characteristics of some South African rainfall systems. *Unpublished MSc Dissertation, Univ. Witwatersrand.*, S. Africa. 123pp.

Harrison, M.S.L., 1983:The Southern Oscillation, zonal equatorial circulation cells and South African rainfall. *Preprint of the 1st Int. Conf. on Southern Hemisphere Meteorology.* Amer. Met. Soc., 382- 385.

Harrison, M.S.J., 1984: A generalised classification of South African summer rain-bearing synoptic systems. *J. Clim.*, **4**, 567-560.

Harrison M.S.J., 1986: A synoptic climatology of South African rainfall variations. *PhD thesis, University of Witwatersrand,* Johannesburg, S. Africa. 341 pp.

Hartmann, D.L., M.L. Michelsen, and S.A. Klein, 1992: Seasonal variations of tropical intraseasonal oscillations: A 20- 25 day oscillation in the Western Pacific. *J. Atmos. Sci.*, **49**, 1277- 1289.

Hayashi. Y., and A. Sumi, 1986: The 30- 40 day oscilations simulated in an "Aqua Planet" model. *J. Met. Soc. Japan,* **64**, 451- 567.

Hayashi, Y., and D.G. Golder, 1993: Tropical 40- 50- and 25- 30- day oscillations appearing in realistic and idealized GFDL climate models and the ECMWF Dataset. *J. Atmos. Sci.*, **50**, 464- 494.

Heddinghaus, T.R. and A.F.Krueger, 1981: Annual and interannual variations of outgoing longwave radiation over the tropics. *Mon. Wea. Rev.*, **109**, 1208- 1218.

Hendon, H.H., 1988: A simple model of the 40- 50 day oscillation. *J. Amos. Sci.*, **45**, 569- 584.

Hendon, H.H., and B. Liebmann, 1990: The intraseasonal (30-50 day) oscillation of the Australian summer monsoon. *J. Atmos. Sci.*, **47**, 2909-2923.

Hess, P.G., D.S. Battisti, and P.J. Rasch, 1993: Maintenance of the intertropical convergence zones and the large- scale tropical circulation on a water-covered earth. *J. Atmos. Sci.*, **50**, 691- 713.

Holopainen, E., and C. Fortelius, 1988: High- frequency transient eddies and blocking. *J. Atmos. Sci.*, **44**, 1632- 1645.

Holton, J.R., 1973: An introduction to dynamic meteorology. *Academic Press,* 319pp.

Holton, J.R. and J. Austin, 1991: The influence of the Equatorial QBO on sudden stratospheric warmings. *J. Atmos. Sci.*, **48**, 607- 618.

Holton, J.R., and R.S. Lindsen, 1972: An updated theory for the Quasi- Biennial Oscillation of the tropical stratosphere. *J. Atmos. Sci.*, **29**, 1076- 1080.

Holton, J.R., and H.-C. Tan, 1980: The influence of the Equatorial Quasi- Biennial Oscillation on the global circulation at 50mb. *J. Atmos. Sci.*, **37**, 2200- 2208.

Horel, J.D., 1982: On the annual cycle of the tropical Pacific atmosphere and ocean. *Mon. Wea. Rev.*, **110**, 1863- 1878.

Horel, J.D., and J.M. Wallace, 1981: Planetary- scale atmospheric phenomena associated with the Southern Oscillation. *Mon. Wea. Rev.*, **109**, 813- 829.

Hoskins, B.J., A.J. Simmons, and D.G. Andrews, 1977: Energy dispersion in the barotropic atmosphere. *Quart. J. Roy. Met. Soc.*, **103**, 553- 567.

Hsu C-P.F. and J.M. Wallace, 1976: The global distribution of the annual and semi-annual cycles in precipitation. *Mon. Wea. Rev.*, **104**, 1093- 1101.

Hunt, B.G., and H.B. Gordon, 1988: The problem of "naturally" occurring drought. *Climate Dyn.*, **3**, 19- 33.

Hutchinson, P., 1992: The Southern Oscillation and Prediction of "Der" Season Rainfall in Somalia. *J. Clim.*, **5**, 525- 531.

Irbarne, J.V., and W.L. Godson, 1981: Atmospheric Dynamics. *Reidel Publishing Company.* 259 pp

Jackson, I.J., 1977: Climate, Water and Agriculture in the Tropics. *Longman*, 248pp.

Jackson, S.P., 1952: Atmospheric circulation over South Africa. *S. Afr. Geogr. Journ.*, **34**, 48- 60.

Janowiak, J.E., 1988: An investigation of interannual rainfall variability in Africa. *J. Clim.*, **1**, 240- 255.

Janowiak, J.A., A.F. Krueger, P.A. Arkin, and A. Gruber, 1985: Atlas of outgoing longwave radiation derived from NOAA satellite data. *NOAA Atlas, No. 6.*

Jones, P.D., 1991: Southern hemisphere sea level pressure dataset. *Int. J. Climatol.*, **11**, 585- 607.

Jones, P.D., T.M.L. Wigley, and P.B. Wright, 1986: Global temperature variations between 1861 and 1984. *Nature,* **322**, 430- 434.

Jury, M.R., 1993: A preliminary study of climatological associations and characteristics of tropical cyclones in the SW Indian Ocean. *Meteor. Atmos. Phys.*, **51**, 101- 115.

Jury, M.R., McQueen, C., and K. Levey, 1994: SOI and QBO signals in the African region. *Theor. Appl. Climatol.* (in press).

Jury, M.R., and B. Pathack, 1991: A study of climate and weather variability over the tropical Southwest Indian Ocean. *Meteorol. Atmos. Phys.*, **47**, 37- 48.

Jury, M.R., and B. Pathack, 1992: Climatic patterns associated with the 1992 drought over southern Africa: Observations and GCM results. *Proc. 1st. Conf. African Met. Soc.*, Nairobi, Kenya (in press).

Jury, M.R., B. Pathack, G. Campbell, B.Wang, and W. Landman., 1991: Transient convective waves in the Tropical SW Indian Ocean. *Meteorol. Atmos. Phys.*, **47**, 27- 36.

Jury, M.R., B. Pathack, and D.M. Legler, 1991: Structure and variability of surface atmospheric circulation anomalies over the tropical SW Indian Ocean in the Austral summer. *S. Afr. J. Mar. Sci.*, **11**, 1-14.

Jury, M.R., B. Pathack, and B.J. Sohn, 1992: Spatial structure and interannual variability of summer convection over southern Africa and the SW Indian Ocean. *S. Afr. J. Sci.*, 275- 280.

Jury, M.R., B. Pathack and D. Waliser, 1993: Satellite OLR and microwave data as a proxy for summer rainfall over subequatorial Africa and adjacent oceans. *Int. J. Climatol.*, **13**, 257- 269.

Jury, M.R., and D. Waliser, 1990: Satellite microwave measurements of atmospheric water vapour and marine wind speed: Case study application. *S. Afr. J. Marine Sci.*, **9**, 309- 316.

Katz, R.W., 1988: Use of cross correlations in the search for teleconnections. *J. Climatol.*, **8**, 241- 253.

Kelbe, B., 1988: Features of westerly waves propagating over southern Africa during summer. *Mon. Wea. Rev.*, **116**, 60- 70.

Keppene, C.L., and M. Ghil, 1992: Adaptive filtering and prediction of the Southern Oscillation Index. *J. Geophys. Res.*, **97**, 20449- 20454.

Kidson, J., 1975: Tropical eigenvector analysis and the Southern Oscillation. *Mon. Wea. Rev.*, **80**, 187- 196.

Kidson, J., 1977: African rainfall and its relation to the upper air circulation. *Quart. J. Roy. Met. Soc.*, **103**, 441- 456.

Kilonsky, B.J., and C.S. Ramage, 1976: A technique for estimating tropical ocean rainfall from satellite observations. *J. Appl. Meteor.*, **15**, 972- 975.

Knaff, J.A., W.M. Gray, and J.D. Sheaffer, 1991: Evidence for an association between the stratospheric QBO and ENSO. *5th Conference on Climate Variation,* Denver, Colorado., U.S.A.

Knutson, T.R., and K.M. Weickmann, 1987: 30- 60 day atmospheric circulations: Composite life cycles of convection and circulation anomalies. *Mon. Wea. Rev.*, **115**, 1407- 1436.

Knutson, T.R., K.M. Weickmann, and J.E. Kutzbach, 1986: Global- scale intraseasonal oscillation of outgoing longwave radiation and 200 zonal wind during northern Hemisphere summer. *Mon. Wea. Rev.*, **114**, 605- 623.

Kreft, J., 1972: Composition of Rhodesian (Zimbabwean) Rainfall. *Meteorological Series A. no. 34, Department of Meteorological Services,* Harare, Zimbabwe.

Krishnamurti, T.N., and P. Ardunay, 1980: The 10 to 20 day westward propagating mode and "breaks in monsoon". *Tellus*, **32**, 15- 26.

Krishnamurti, T.N., and H.N. Bhalme, 1976: Oscillations of the monsoon system : Part 1 : observational aspects. *J. Atmos. Sci.*, **33**, 1937- 1954.

Krishnamurti, T.N., P.K. Jayakumar, J. Shen, N. Surgi, and A. Kumar, 1985: Divergent circulations on the 30- 50 day time scale. *J. Atmos. Sci.*, **42**, 364- 375.

Krishnamurti, T.N., M. Kanamitsu, W.J. Koss, and J.D. Lee, 1973: Tropical east- west circulations during the northern winter. *J. Atmos. Sci.*, **30**, 780- 787.

Kuboto, S., and S. Lida, 1954: Statistical characteristics of the atmospheric disturbances. *Meteor. and Geophys.*, **5**, 22- 34.

Kuhnel, I., 1989: Tropical- extratropical cloudband climatology based on satellite data. *Int. J. Climatol.*, **9**, 441- 463.

Kuma, K., 1990: A quasi- biennial oscillation in the intensity of the intra- seasonal oscillation. *Int. J. Climatol.*, **10**, 263- 278.

Kumar, S., 1978: Interaction of upper westerly waves with the ITCZ and their effect on the weather over Zambia during the rainy season. *Govt. Printer,* Lusaka, Zambia.

Latif, M., J. Biecamp, H. Von Storch, M. McPhaden, and E. Kirk, 1990: Simulation of ENSO related surface wind anomalies with an atmospheric GCM forced by observed SST. *J. Clim.*, **3**, 509- 521.

Lau, K.-M., and P.H. Chan, 1983a: Short- term climate variability and atmospheric teleconnections from satellite- observed outgoing longwave radiation. Part I: Simultaneous relationships. *J. Atmos. Sci.*, **40**, 2735- 2750.

Lau, K.-M., and P.H. Chan, 1983b: Short-term climate variability and atmospheric teleconnections from satellite- observed outgoing lomgwave radiation. Part II: Lagged correlations. *J. Atmos. Sci.*, **40**, 2751- 2767.

Lau, K.-M., and P.H. Chan, 1985: Aspects of the 40-50 day oscillation during northern winter as inferred from outgoing longwave radiation. *Mon.Wea. Rev.* **113**, 1889-1909.

Lau, K.-M., and P.H. Chan, 1986: Aspects of the 40- 50 day oscillation during the northern summer as inferred from outgoing longwave radiation. *Mon. Wea. Rev.*, **114**, 1354- 1367.

Lau, K.-M., and P.H. Chan, 1988: Intra- seasonal and inter-annual variations of tropical convection: A possible link between the 40- 50 day oscillation and ENSO. *J. Atmos. Sci.*, **3**, 506- 521.

Lau, K.-M., and L. Peng, 1987: Origin of the low frequency (intraseasonal) oscillation in the tropical atmosphere. *J. Atmos. Sci.*, **44**, 950- 972.

Lau, K.-M., I.-S. Kang and P.J. Sheu, 1990: Principal modes of intra- seasonal variations in atmospheric angular momentum and tropical convection. *J. Geophys. Res. (Atmos)*, in press.

Lau, K.-M., and D.J. Shea, 1988: Annual cycle quasi-biennial oscillation on global precipitation. *J. Geophys. Res.*, **93**, 10975- 10988.

Lau, K.-M., and T. Phillips, 1986: Coherent fluctuations of extratropical geopotential height and tropical convection in intraseasonal time scale. *J. Atmos. Sci.*, **43**, 1164-1181.

Lau, N-C., 1979: The observed structure of the troposheric stationary waves and the local balances of vorticity and heat. *J. Atmos. Sci.*, **36**, 996- 1016.

Lau, N-C., 1981: A diagnostic study of recurrent meteorological anomalies appearing in a 15- year simulation with a GFDL general ciculation model. *Mon. Wea. Rev.*, **109**, 2287- 2311.

Lau, N-C., 1985: Modelling the seasonal dependence of the atmospheric response to observed El Ninos 1962- 76. *Mon. Wea. Rev.*, **113**, 1970- 1976.

Lau, N.-C., I.M. Held and J.D. Neelin, 1988: The Madden Julian- Oscillation in an idealised general circulation model. *J. Atmos. Sci.*, **45**, 3810-3932.

Lau, N-C. and K.M. Lau, 1986: The structure and propagation of intra-seasonal oscillations appearing in a GFDL general circulation model. *J. Atmos. Sci.*, **43**, 2023- 2047.

Lazante, J.R., 1990: The leading modes of 10-30-day variability in the extratropics of the Northern Hemisphere during the cold season. *J. Atmos. Sci.*, **47**, 2115-2140.

Legras, B., and M. Ghil., 1985: Persistent anomalies, blocking and variations in atmospheric predictability. *J. Atmos. Sci.*, **42**, 433- 471.

Levey, K.M., 1993: Intra-seasonal oscillations of convection over Southern Africa. *MSc. Thesis, University of Cape Town,* Cape Town, South Africa. 226 pp.

Liebmann, B., 1987: Observed relationships between large- scale tropical convection and the tropical circulation on subseasonal time scales during Northern Hemisphere winter. *J. Atmos. Sci.*, **44**, 2543- 2561.

Liebmann, B., and D.L. Hartmann, 1982: Interannual variations of outgoing IR associated with tropical circulation changes during 1974- 78. *J. Atmos. Sci.*, **39**, 1153-1162.

Lindesay J.A., 1988: The Southern Oscillation and atmospheric circulation changes over southern Africa. *PhD thesis, University of Witwatersrand,* Johannesburg, South Africa. 284pp.

Lindesay, J.A., 1992: Present climates of southern Africa, in *Southern Hemisphere Climates : Present, Past and Future, Belhaven Press,* London.

Lindesay, J.A. and M.R. Jury, 1991: Atmospheric circulation controls and characteristics of a flood event in Central South Africa. *Int. J. Climatol.*, **11**, 609-627.

Lorenc, A.C., 1984: The evolution of planetary scale 200 mb divergence during the FGGE year. *Quart. J. Roy. Met. Soc.*, **110**, 427- 442.

Lough, J.M., 1986: Tropical Atlantic sea surface temperatures and rainfall variations in sub- Saharan Africa. *Mon. Wea. Rev.*, **144**, 561- 570.

Lyons, S.W., 1990: Spatial and Temporal variability of monthly precipitation in Texas. *Mon. Wea. Rev.*, **118**, 2634- 2648.

Lyons, S.W., 1991: Origins of convective variability over equatorial southern Africa during Austral summer. *J. Clim.*, **4**, 23- 39.

Madden, R.A., 1978: Further evidence of travelling planetary waves. *J. Atmos. Sci.*, **35**, 1605- 1618.

Madden, R.A., 1979: Observations of large-scale travelling Rossby waves. *Rev. Geophys. Space Phys.*, **117**, 1935-1949.

Madden, R.A., 1986: Seasonal variation of the 40- 50 day oscillation in the tropics. *J. Atmos. Sci.*, **43**, 3138- 3158.

Madden, R.A., and P.R. Julian, 1971: Detection of a 40-50 day oscillation in the zonal wind in the tropical Pacific. *J. Atmos. Sci.*, **28,** 702- 708.

Madden, R.A., and P.R. Julian, 1972: Description of global- scale circulation cell in the tropics with a 40- 50 day period. *J. Atmos. Sci.*, **29**, 1109- 1123.

Magana, V., and Yanai, M., 1990: Tropical-midlatitude interaction on the time scale of 30 to 60 days during the northern summer of 1979. *J. Clim.*, **4**, 180-201.

Mason, S.J., 1992: Sea surface temperatures and South African rainfall variability. *PhD thesis, University of Witwatersrand,* Johannesburg, South Africa. 235pp

Mason, S.J., J.A. Lindesay, and P.D. Tyson, 1994: Simulating drought in southern Africa using sea surface temperature variations. *Water SA,* **20**, 15- 22.

Matarira, C.H., 1988: A diagnostic study of atmospheric circulation changes associated with rainfall anomalies over SE central Africa. *PhD thesis, University of Thessaloniki,* Greece. 183pp.

Matarira, C.H., 1990a: Drought over Zimbabwe in a regional and global context. *Int. J. Climatol.*, **10**, 609- 625.

Matarira, C.H., 1990b: Frequency and tracks of anticyclones and their effect on rainfall patterns over Zimbabwe. *Theor. Appl. Climatol.*, **42**, 53- 66.

Matarira, C.H., 1990c: Precipitation characteristics during Zimbabwe's rainy season. *Zim. Sci. News*, **4/6**, 36- 39.

Matarira, C.H., and A.A. Flocas, 1989: Spatial and temporal rainfall vriability over SE central Africa during extremely dry and wet years. *J. Meteor.*, **14**, (135), 3- 9.

Matarira, C.H., and M.R. Jury, 1990: Contrasting meteorological structure of intra-seasonal wet and dry spells in Zimbabwe. *Int. J. Climatol.*, **12**, 165- 176.

McNaughton, D.L., and P. Wurzel, 1972: Tritium in rain as an indicator of air mass source. *Tellus,* **24**, 255- 259.

Miron, O and P.D. Tyson, 1984: Wet and dry conditions and pressure anomaly fields over South Africa and the adjacent oceans, 1963- 1979. *Mon. Wea. Rev.*, **112**, 2127- 2132.

Mitra, K., and S.N. Dutta, 1992: Periodic 18.6 year luni- solar nodal and 11- year solar signal components in rainfall in India. *Int. J. Climatol.*, submitted.

Miyahara, S., 1987: A simple model of the tropical intraseasonal oscillation. *J. Met. Soc. Japan,* **65**, 341- 351.

Morrisey, M.L., 1986: A statistical analysis of the relationships among rainfall, outgoing longwave radiation and the moisture budget during January- March 1979. *Mon. Wea. Rev.*, **114**, 931- 942.

Murakami, M., 1976: Analysis of summer monsoon fluctuations over India. *J. Met. Soc. Japan,* **54**, 15-31.

Murakami, T., 1987: Intraseasonal atmospheric teleconnection patterns during northern hemisphere summer. *Mon. Wea.Rev.*, **115**, 2133- 2154.

Murakami, T., 1988: Intraseasonal atmospheric teleconnection patterns during Northern Hemisphere winter. *J. Clim.*, **1**, 117- 131.

Murakami, T., L.-X. Chen, A. Xie, and M.L. Shrestha, 1985: Eastward propagation of 30- 60 day perturbations as revealed from outgoing longwave radiation data. *J. Atmos. Sci.*, **43**, 961- 971.

Murakami, T., and T. Nakazawa, 1985: Tropical 40- 50- day oscillations during the 1979 Northern Hemisphere summer. *J. Atmos. Sci.*, **42**, 1107- 1122.

Murakami, T., T. Nakazawa, and H. Jinhai, 1983: 40- 50 day oscillations during 1979 Northern Hemisphere summer. *University of Hawaii, Dept. of Meteorology, UHMET 83- 02,* 133 pp.

Mysak, L.A., and G.J. Mertz, 1984: A 40- 60 day oscillation in the source region of the Somali Current during 1976. *J. Geophys. Res.*, **89**, 711- 715.

Namias, J., 1963: Interaction of circulation and weather between hemispheres. *Mon. Wea. Rev.*, **91**, 482- 486.

Nassor, A., 1994: Monsoon surges, tropical cyclones and extreme rainfall in NW Madagascar. *MSc. thesis, University of Cape Town,* Cape Town, S. Africa. (submitted). 183pp.

Naujokat, B. 1986: An update of the observed quasi- biennial oscillation of the stratospheric winds over the tropics. *J. Atmos. Sci.*, **43**, 1873- 1877.

Neelin, J.D. and I.M. Held 1987a: Modelling tropical convergence based on the moist static energy budget. *Mon. Wea. Rev.*, **115**, 3-12.

Neelin, J.D., I.M. Held, and K.M. Cook, 1987b: Evaporation- wind feedback and low-frequency variability in the tropical atmosphere. *J. Atmos. Sci.*, **44**, 2341-2348.

Newell, R.E., J.W. Kidson, D.G. Vincent and G.J. Boer, 1972: The general circulation of the tropical atmosphere and interactions with extratropical latitudes. Vol 1, *MIT Press,* Cambridge, MA, 258pp.

Ngara,T. and G.C. Asnani, 1978: Five- day oscillation in East African Low- Level Jet. *Nature,* **272**, 708- 709.

Ngara, T., S. Lineham and J.D. Torrance, 1983: Seasonal rainfall fluctuations in Zimbabwe. *Zim. Agric. Journ.*, **80**, 149- 150.

Nicholson, S.E. 1981: Rainfall and atmospheric circulation during drought and wetter periods in West Africa. *Mon. Wea. Rev.*, **109**, 2191- 2208.

Nicholson, S.E., 1986a :The nature of rainfall variability in Africa south of the Equator. *J. Climatol.*, **6**, 515- 530.

Nicholson, S.E., 1986b: The spatial coherence of African rainfall anomalies: Interhemispheric teleconnections. *J. Clim. Appl. Met.*, **25**, 1365- 1381.

Nicholson, S.E., 1989: African drought: Characteristics, causal theories and global teleconnections. in *Understanding Climate Change by* Berger, A., R. Dickenson, and J. Kidson : *J. Amer. Geophys. Union*, 79- 100.

Nicholson, S.E., and R.M. Chervin, 1983: Recent rainfall fluctuations in Africa- interhemispheric teleconnections. *Variations in the global water budget,* Street-Perrott et al., Eds., Reidel, 221- 238.

Nicholson, S.E., J. Kim, and J. Hoopingarner, 1988: Atlas of African rainfall and its interannual variability. *Florida State University,* Florida, USA.

Nihoul, J.C.J., 1985: Coupled Ocean- Atmosphere models. *Elsevier Oceanography Series*, **40**.

Ogallo, L.J., 1988: Relationship between seasonal rainfall in East Africa and Southern Oscillation. *J. Climatol.*, **8**, 31- 43.

Ogallo, L.J., J.E. Janowiak, and M.S. Halpert, 1988: Teleconnection between seasonal rainfall over East Africa and global sea surface temperature anomalies. *J. Meteor. Soc. Japan*, **66**, 807- 821.

Ogallo, L.J., R.E. Okoola, and D.N. Wanjohi, 1993: Characteristics of Quasi- Biennial Oscillation over Kenya and their predictability potential for the season. *J. Afr. Met. Soc.*, in press.

Okoola, R.E., 1989: Westwards moving disturbances in the Southwest Indian Ocean. *Meteorol. Atmos. Phys.*, **41**, 35- 44.

Padya, B.M., 1989: Weather and Climate of Mauritius. *Mauritius: M. Ghandi Institute.* 283 pp.

Palmer, C.E., 1954: The general circulation between 200 and 10 hPa over the equatorial Pacific. *Weather*, **9**, 341.

Pan, Y.H. and A.H. Oort, 1983: Global climate variations connected with SST anomalies in the Eastern Equatorial Pacific Ocean for the 1958- 73 period. *Mon. Wea. Rev.*, **111**, 1244- 1258.

Park, C.-K., D.M. Straus, and K.-M. Lau, 1990: An evaluation of the structure of tropical intraseasonal oscillation in three general circulation models. *J. Met. Soc. Japan*, **68**, 403- 417.

Park, C.-K., and S.D. Schubert, 1993: Remotely forced intraseasonal oscillations over the Tropical Atlantic. *J. Atmos. Sci.*, **50**, 89- 103.

Parker, D.E., 1973: Equatorial Kelvin waves at 100 millibars. *Quart. J. Roy. Met. Soc.*, **99**, 116- 129.

Pathack, B.M.R., 1993: Modulation of South African summer rainfall by global climatic processes. *PhD thesis, University of Cape Town,* Cape Town, South Africa. 261pp.

Peixoto, J.P and A.H. Oort, 1992: Physics of Climate. *American Institute of Physics, New York.* 520pp

Penman, 1972: The response of the upper ocean to meteorology forcing. *PhD thesis, Institute of Oceanography, Univ. of British Columbia,* Vancouver, Canada.

Pereira, A.R., 1982: Crop planning for different environments. *Agric. Met.*, **27**, 71- 77.

Philander, S.G., 1990: El Nino, La Nina and the Southern Oscillation. *Inter. Geoph. Series*, **46**.

Plumb, R.A., 1984: The Quasi- Biennial Oscillation. *In the "Dynamics of the Middle Atmosphere" edited by J.R. Holton and T. Matsuno: Terra Scientific Publishing Company.*

Pond, S., 1972: The exchanges of momentum, heat and moisture at the Ocean-Atmosphere interface: presented in Numerical Models of Ocean Circulation: *Proceedings of a symposium,* Durham, New Hampshire, 17- 20 October.

Pook, M.J., 1992: A note on the variability of the mid- tropospheric flow over the Southern Ocean in the Australian region. *Aust. Met. Mag.*, **40**, 169- 177.

Portman, D.A., W-C. Wang, and T.R. Karl, 1992: Comparison of GCM and Observed regional climates: Daily and seasonal variability. *J. Clim.*, **5**, 343- 353.

Preston- Whyte, R.A., and P.D. Tyson, 1973: Note on pressure oscillations over South Africa. *Mon. Wea. Rev.*, **101**, 650- 653.

Pugh, D.T., 1987: Tides, Surges and Mean Sea Level: A Handbook for Engineers and Scientists. *John Wiley & Sons.*

Quiroz, R.S., 1983: Relationships among stratospheric and tropospheric zonal flows and the Southern Oscillation. *Mon. Wea. Rev.*, **111**, 143- 154.

Ramage, C.S., 1977: Sea Surface Temperature and local weather. *Mon. Wea. Rev.*, **105**, 540- 544.

Rasmusson E.M. and T.H. Carpenter, 1982 : Variations in tropical SST and surface windfields associated with the Southern Oscillation/ El Nino. *Mon. Wea. Rev.*, **110**, 354- 384.

Reinhold, B.B., and R. Pierrehumbert, 1982: Dynamics of weather regimes: Quasi-stationary waves and blocking. *Mon. Wea. Rev.*, **110**, 1105- 1145.

Reinhold, B.B., and S. Yang, 1993: The role of transients in weather regimes and transitions. *J. Atmos. Sci.*, **50**, 1173-1180.

Richards, F., and P. Arkin, 1981: On the relationship between satellite observed cloud cover and precipitation. *Mon. Wea. Rev.*, **108**, 1840- 1853.

Riehl, H., 1979: Climate and Weather in the Tropics. *Academic press, London, 611pp.*

Risbey, J.S. and P.H. Stone, 1988: Observations of the 30-60 day oscillation in zonal mean atmospheric angular momentum and high cloud cover. *J. Atmos. Sci.*, **45**, 2026-2038.

Rocha A., 1992: The Influence of Global SSTs on the Southern African Summer Climate. *PhD thesis, University of Melbourne,* Melbourne, Victoria, Australia. 249pp.

Ropelewski, C.F. and M.S. Halpert, 1987: Global and regional scale precipitation patterns associated with the El Nino/ Southern Oscillation. *Mon. Wea. Rev.*, 115, 1606- 1626.

Ropelewski, C.F. and M.S. Halpert, 1989: Precipitation patterns associated with the high phase of the southern Oscillation. *J. Clim.*, **2**, 268-284.

Ropelewski, C.F., M.S. Halpert, and X. Wang, 1992: Observed tropospheric Biennial variability and its relationship to the Southern Oscillation. *J. Clim.*, **5**, 594- 616.

Ropelewski, C.F., and P.D. Jones, 1987: An extension of the Tahiti- Darwin SO Index. *Mon. Wea. Rev.*, **115**, 2161- 2165.

Rosen, R.D., and D.A. Salstein, 1983: Variations in atmospheric angular momentum on global and regional scales and length of day. *J. Geophys. Res.*, **88**, 5451- 5470.

Rui, H.and B. Wang, 1990: Development characteristics and dynamic structure of tropical intraseasonal convection anomalies. *J. Atmos. Sci.*, **47**, 357- 379.

Schubert, S.D., and Chung-Kyu Park, 1991: Low frequency intraseasonal tropical-extratropical interactions. *J. Atmos. Sci.*, **48**, 629- 650.

Shapiro, L.J., and S.B. Goldenberg, 1993: Intraseasonal oscillations over the Atlantic. *J. Clim.*, **6**, 677-699.

Sharon, D., 1981: The distribution in space of local rainfall in the Namib Desert. *J. Climatol.*, **1**, 69- 75.

Schulze, B.R., 1965: Climate of South Africa: Part 8. *General Survey, S. African Weather Bureau*, **WB28**, 330pp

Simmonds, I., G. Trigg, and R. Law, 1988: The Climatology of the Melbourne University General Circulation Model. *Department of Meteorology, Univ. of Melbourne, Australia.*

Slutz, R.J., S.J. Lubker, J.D. Hiscox, S.D. Woodruff, R.L. Jenne, D.H. Joseph, P.M. Steurer, and J.D. Elms, 1985: Comprehensive Ocean Atmosphere Data Set: Release 1. *NOAA Environmental Reserach Laboratories, Climate research Program, Boulder, Co.* 268 pp.

Smith, A.V., 1985: Studies of the effects of cold fronts during the rainy season in Zimbabwe. *Weather*, **40**, 198- 202.

Smith, I.N., and H.B. Gordon, 1992: Simulations of precipitation and atmospheric circulation changes associated with warm SSTs: Results from an ensemble of long- term integrations with idealised anomalies. *Climate Dyn.*, **7**, 141- 153.

Streten, N.A., 1973: Some characteristics of satellite- observed bands of persistent cloudiness over the southern hemisphere. *Mon. Wea. Rev.*, **101**, 486- 495.

Taljaard, J.J., 1972: Synoptic meteorology of the southern Hemisphere. *Commonwealth Met. Monographs, 139- 213.*

Taljaard, J.J., 1982: Upper- air circulation, temperature and humidity over southern Africa. *S. Afr. Wea. Bur. Tech. Paper*, **22**, 72pp.

Taljaard, J.J., 1985: Cut- off lows in the South African region. *S. Afr. Wea. Bureau Tech. Paper*, **4**, 153pp.

Taljaard, J.J., 1986a: Change in rainfall distribution and circulation patterns over southern Africa in summer. *J. Climatol.*, **6**, 579- 592.

Taljaard, J.J., 1986b: Contrasting atmospheric circulation during dry and wet summers in South Africa. *S. Afr. Wea. Bureau Newsletter*, **445**, 1- 5.

Taljaard, J.J., 1987: The anomalous climate and weather systems over South Africa during summer 1975- 1976. *S. Afr. Wea. Bur. Tech. Pap.*, **16**, 80pp.

Taljaard, J.J., 1990: The cloud bands of Southern Africa. *The S. African Weather Bureau Newsletter*, **43**, 6-8.

Taljaard, J.J, H. van Loon, H.L.Crutcher, and R.L. Jenne, 1969: Climate of the upper air : Southern Hemisphere. ***Vol 1**, NAVAIR 50- IC- 55, Chief of Naval Ops.*, Washington D.C., U.S.A., 135pp.

Tilbury, M.R.R., 1964: Trends in the Rainfall of Southern Rhodesia period 1901 to 1941. *Meteorological Notes, Series B, 3,* Zimbabwe Met. Sevices.

Torrance, J.D., 1979: Upper windflow patterns in relation to rainfall in south-east Central Africa. *Weather*, **34**, 106- 115.

Torrance, J.D., 1981: Climate Handbook of Zimbabwe. *Zimbabwe Met. Services,* Harare, Zimbabwe. 222p.

Torrance, J.D., 1990: The southern Oscillation and the rainy season in Zimbabwe. *Zim. Sci. News*, **24**, Nos. 4/6, 42.

Trenberth, K.E., 1980: Atmospheric Quasi- Biennial Oscillations. *Mon. Wea. Rev.*, **108,** 1370- 1377.

Trenberth, K.E., 1981: Observed Southern Hemispheric eddy statistics at 500 mb frequency and spatial distribution. *J. Atmos. Sci.*, **38**, 2585- 2605.

Trenberth, K.E., 1984: Signal versus noise in the Southern Oscillation. *Mon. Wea. Rev.*, **112**, 326- 332.

Trenberth, K.E., and G.W. Branstator, 1992: Issues in establishing causes of the 1988 drought over North Africa. *J. Clim.*, **5**, 159- 172.

Tsay, C.Y., 1974: Analysis of large-scale wave disturbances in the tropics simulated by the NCAR general circulation model. *J. Atmos. Sci.*, **31**, 330- 339.

Tyson, P.D., 1981: Atmospheric circulation variations and the occurrence of extended wet and dry spells over South Africa. *J. Climatol.*, **1**, 115- 130.

Tyson, P.D., 1984: The atmospheric modulation of extended wet and dry spells over South Africa, 1958- 1978. *J. Climatol.*, **4**, 621- 635.

Tyson, P.D., 1986: Climate Change and variability in southern Africa. *Oxford University Press,* Cape Town, 220pp.

Van Heerden, J., D.E. Terblanche and G.C. Shultze, 1988: The Southern Oscillation and South African summer rainfall. *J. Climatol.*, **8**, 577- 597.

Van Loon, H., and J. W. Kidson, 1993: The association between latitudinal temperature gradient and eddy transport. Part III: the Southern Hemisphere. *Aust. Met. Mag.*, **42**, 31- 37.

Van Loon, H and K. Labitzke, 1988: An association between the 11- year solar cycle, QBO, and the atmosphere. Part II: Surface and 700 mb in the Northern Hemisphere winter. *J. Clim.*, **1,** 905-920.

Vautard, R., and B. Legras, 1988: On the source of midlatitude low- frequency variance. Part II: Nonlinear equilibration of weather regimes. *J. Atmos. Sci.*, **45**, 2845- 2867.

Verma, R.K., 1993: Indian Ocean SST correlations with monsoon precipitation. *Toga Notes*, **10**, 5- 7.

Vermeulen, J.H., and M.R. Jury, 1992: Tropical cyclones in the south- west Indian Ocean : Track and verification, 1989- 91. *Met. Mag.*, **121**, 186- 192.

Vincent, D., T. Sperling, A. Fink, S. Zube, and P. Speth, 1990: Intraseasonal oscillation of convective activity in the tropical Southern Hemisphere: May1984- April 1986. *J. Clim.*, **4**, 40- 53.

Vines, R.G., and A.I. Tomlinson, 1985: The Southern Oscillation and rainfall patterns in the Southern Hemisphere. *S. Afr. J. Sci.*, **81**, 151- 156.

Vowinckel, E., 1956: The weather and climatology of the southern Mozambique Channel. *Misc. Geo. Pub. Serv. Met.* Angola, Luanda, 63- 86.

Walker, G.T., and E.W. Bliss, 1932: World weather V. *Mem. Roy. Met. Soc.*, **4**, 53- 84.

Walker, G.T., and E.W. Bliss, 1937: World weather VI. *Mem. Roy. Met. Soc.*, **4**, 119- 139.

Walker N.D., 1989: SST- Rainfall relationships and associated ocean- atmospheric coupling mechanisms in the Southern African region. *PhD thesis, University of Cape Town*, Cape Town, S. Africa. 171pp.

Wang, B., 1988a: Dynamics of tropical low- frequency waves.: An analysis of the moist Kelvin wave. *J. Atmos. Sci.*, **45**, 2051- 2065.

Wang, B., 1988b: Comments on "An air-sea interaction model of intraseasonal oscillation in the tropics." *J. Atmos. Sci.*, **45**, 3521-3525.

Wang, B, and J.-K. Chen, 1989: On the zonal scale selection and vertical structure of the equarorial intraseasonal waves. *Quart. J. Roy. Met. Soc.*, **115,** in press.

Wang, B. and T. Li, 1993: A simple tropical atmosphere model of relevence to short- term climate variation. *J. Atmos. Sci.*, **50**, 260- 284.

Wang, B., and H. Rui, 1990a: Synoptic climatology of transient tropical intraseasonal convection anomalies, 1975- 1985. *Meteorol. Atmos. Phys.*, **44**, 43- 61.

Wang, B.,and H. Rui, 1990b: Dynamics of the coupled moist Kelvin- Rossby wave on an equatorial beta- plane. *J. Atmos. Sci.*, **47**, 397- 413.

Wang, X-L., and T. Murakami, 1988: Intraseasonal disturbance activity before, during and after the 1982- 83 ENSO. *J. Atmos. Sci.*, **45**, 3754- 3770.

Webster, P.J., 1981: Mechanisms determining the atmospheric response to sea surface temperature anomalies. *J. Atmos. Sci.*, **38**, 554- 571.

Webster, P.J., 1982: Seasonality in the local and atmospheric responses to sea surface temperature anomalies. *J. Atmos. Sci.*, **39**, 41-52.

Webster, P.J., 1983: Large-scale structure of the tropical atmosphere. *Large- scale dynamic processes in the atmosphere. Academic Press,* London. 235- 275.

Webster, P.J., and D.G. Curtin, 1975: Interpretations of the EOLE experiment II. Spatial variation of transient and stationary modes. *J. Atmos. Sci.*, **32**, 1848- 1863.

Weickmann, K.M., 1983: Intraseasonal circulation and outgoing longwave radiation modes during Northern Hemisphere winter. *Mon. Wea. Rev.*, **111**, 1838-1858.

Weickmann, K.M., G.R. Lussky, and J.E. Kutzbach, 1985: Intraseasonal (30- 60) fluctuations of outgoing longwave radiation and 250 mb streamfunction during northern winter. *Mon. Wea. Rev.*, **113**, 941- 960.

Weickmann, K.M., and S.J.S. Khalsa, 1990: The shift of convection from the Indian Ocean to the Western Pacific Ocean during a 30- 60 day oscillation. *Mon. Wea. Rev.*, **118**, 964-978.

Whilhite, D.A. and W.E. Easterling, 1987: Planning for drought; precipitation patterns associated with the El Nino- Southern Oscillation. *Mon. Wea. Rev.*, **115**, 606- 626.

Woodruff, S.D., R.J. Slutz, R.J. Lenne, and P.M. Steurer, 1987: A comprehensive Ocean- Atmosphere Data Set. *Bul. Amer. Met. Soc.*, **68**, 1239- 1250.

Wright, P.B., 1986: Precursors of the Southern Oscillation. *J. Climatol.*, **6**, 17- 30.

Yamagata, T., 1987: A simple moist model relevant to the origin of intraseasonal disturbances in the tropics. *J. Met. Soc. Japan*, **65**, 153- 164.

Yasunari, T., 1981: Structure of the Indian summer monsoon system with a period around 40 days. *J. Met. Soc. Japan*, **59**, 336- 354.

Yoo, J.M., and J.A. Carton, 1988: Spatial dependence of the relationship between rainfall and outgoing longwave radiation in the tropical Atlantic. *J. Clim.*, **1**, 1047-1054.

Zebiak, S.E., 1982: A simple atmospheric model of relevance to the El Nino. *J. Atmos. Sci.*, **39**, 2017- 2027.

Zebiak, S.E., 1986: Atmospheric convergence feedback in a simple model for El Nino. *Mon. Wea. Rev.*, **114**, 1263- 1271.

Zhu, B., and B. Wang, 1993: The 30- 60- day convective seesaw between the Tropical Indian and Western Pacific Oceans. *J. Atmos. Sci.*, **50**, 184-199.